

Disorder Phenomena in Conjugated Oligomers and Polymers

From Single Chains to Crystalline Aggregates

Von der Universität Bayreuth
zur Erlangung des Grades eines
Doktors der Naturwissenschaften (Dr. rer. nat.)
genehmigte Abhandlung

von

Dominic Raithel

aus Münchberg

Erstgutachter: PD Dr. Richard Hildner

Zweitgutachter: Prof. Dr. Anna Köhler

Tag der Einreichung: 05.02.2018

Tag des Kolloquiums: 13.04.2018

Contents

1 Abstract	1
Zusammenfassung	5
2 Introduction	9
2.1 Motivation	9
2.2 Conjugation and conjugated polymers	12
2.2.1 π -electron models	13
2.2.2 Structural and electronic disorder in conjugated polymers	15
2.2.3 Recent theoretical models	23
2.3 Photophysics of isolated conjugated polymers	27
2.3.1 Electronic and vibronic transitions	27
2.3.2 Signatures of disorder in single-molecule spectra	29
2.3.3 Connection between coherence length and vibronic progression	31
2.4 Photophysics of electronically interacting conjugated polymers	33
2.4.1 Two-level systems	33
2.4.2 H- and J-type aggregation	34
2.4.3 Signatures of disorder in molecular aggregates	36
2.5 References	40
3 Overview of the publications	51
3.1 Connection	51
3.2 Individual Contribution	55
3.3 Key results	57
4 Publications	71
4.1 Publication 1: Emitting Species of P3HT: From Single, Isolated Chains to Bulk	71
4.2 Publication 2: Direct observation of backbone planarisation via side-chain alignment in single bulky-substituted polythiophenes	107
4.3 Publication 3: Signatures of Melting and Recrystallization of a Bulky Substituted Poly(thiophene) Identified by Optical Spectroscopy	123
4.4 Publication 4: Revealing order and disorder in films and single crystals of a thiophene-based oligomer by optical spectroscopy	151
Danksagung	179
Eidesstattliche Versicherung	182

List of Figures

2.1	Conjugation and conjugated polymers	13
2.2	Disorder in conjugated polymers	16
2.3	Excited state properties in conjugated polymers	19
2.4	Electronic and vibronic transitions	28
2.5	Inhomogeneous broadening mechanisms in single-molecule spectra	30
2.6	Vibrational modes of planar and non-planar polythiophenes	31
2.7	Davydov splitting in electronically interacting dimers	34
2.8	H-type and J-type aggregation	35
2.9	H-type molecular aggregates	37
3.1	Overview of the thesis	53
3.2	Low-temperature photoluminescence spectra of single P3HT	58
3.3	Bridging the gap between the single-chain ZPL distributions and the ensemble PL spectra	60
3.4	Low-temperature photoluminescence spectra of single polythiophenes	62
3.5	Simulations of the conformational, optical and electronic properties of PDOPT and P3HT	63
3.6	Anisotropic optical properties and spectra of spherulitic PDOPT crystals and the surrounding film	65
3.7	Temperature-dependent fitting parameter of PDOPT spherulites	66
3.8	Optical and spectroscopic properties of 3TBT single crystals	68
3.9	Photoluminescence spectra and peak ratios of 3TBT crystals	69

1 Abstract

During the last years, the performance of organic solar cells as well as of organic electronics has been continuously increasing. This stimulates further research in the field of organic semiconductors such as conjugated polymers. The active layer of these devices consists mostly of solution-processed conjugated polymer films or blends which additionally contain small molecules with opposite charge affinity. In contrast to inorganic semiconductors, the performance of organic devices is not mainly correlated with high crystallinity and long-range order. It rather depends on a finely tuned coexistence of ordered (crystalline) and disordered (amorphous) phases in the polymer films. However, the interplay between structural (dis)order and optoelectronic properties is still not well-addressed and understood. One of the reasons for this is the experimental difficulty to disentangle the respective contributions from ordered and disordered phases. Moreover, even the influence of structural disorder on the photophysical properties of *single* chains is still under debate and a challenging question for both theory as well as experiment.

A widely used class of conjugated polymers for this basic research are polythiophenes, including thiophene-based low-band gap co-polymers. The working horse of this class is the alkyl-substituted poly(3-hexylthiophene) (P3HT). Despite its importance, the degree of structural and electronic disorder in defect-free P3HT is debated controversially, as several conflicting reports exist. As the detailed conformation of single, isolated chains cannot be resolved in real space, a correlation between intra-chain disorder (e.g. distribution of dihedral angles between the monomers) and spectroscopic observables (e.g. transition energy, inhomogeneous linewidth, vibronic progression) is not established yet. Furthermore, the impact of intra-chain disorder on the excited state properties (e.g. charge-transfer character, conjugation length, electron-phonon coupling) is challenging for theoretical modelling due to the size of the system and its many degrees of freedom. A recent development in synthesis is the modification or replacement of side-chains to optimize the morphology and mutual orientation of the chains within polymer films. Apart from that, the influence of the side-chains on the intrinsic photophysical properties of isolated chains has not been clearly evaluated yet. But also when leaving the single-chain picture, the impact of intra-chain disorder on inter-chain interactions in crystalline aggregates is highly debated.

The main part of this thesis is devoted to reveal a clearer picture of intra-chain disorder and its influence on the photophysical properties of polythiophenes with single-molecule

spectroscopy. We use highly defined samples and a specific sample preparation technique to study the intrinsic properties of nearly defect-free polythiophenes on the single-chain level. The experiments are conducted at cryogenic temperatures ($T=1.5$ K) to resolve details of vibronic progression and to get insights into line-broadening mechanisms (dynamic disorder). In combination with molecular dynamics and excited state calculations, the impact of structural disorder and of side-chains on the excited state properties is evaluated. Based on the knowledge from single-molecule spectroscopy the focus shifts to crystalline structures to study the effects of intra-chain disorder on *inter*-chain interactions. Finally, we investigate the influence of the degree of crystallinity on the emission spectra in highly defined single crystals of a thiophene-based oligomer.

The first publication (section 4.1) characterises the properties of isolated, non-interacting P3HT chains with single-molecule spectroscopy. Surprisingly, P3HT chains possess a low degree of intrinsic electronic disorder on the length scale of the emitting site (< 10 repeating units), as shown by the narrow inhomogeneous distribution (< 300 cm^{-1}) of single-chain zero-phonon lines. The second central finding is that the average over many single-chain spectra does not reproduce the ensemble PL spectrum of an amorphous P3HT sample measured under essentially identical conditions. Supported by time-dependent density functional theory calculations, we ascribe this discrepancy to the formation of 'loose aggregates' in bulk samples leading to aggregation-induced partial planarisation and long-range electronic coupling between segments of adjacent P3HT chains. In conclusion, we develop a comprehensive picture of the photophysical properties of P3HT from single chains over amorphous, disordered samples to crystalline aggregates.

The second publication (section 4.2) deals with the question, how and whether the intra-chain disorder can be controlled by side-chain engineering. The results on P3HT from publication 1 are compared with poly(3-(2,5-dioctylphenyl)thiophene) (PDOPT), a second polythiophene, which has sterically very demanding side-chains but the same backbone. We find that the PDOPT single-chain spectra are strongly red-shifted by over 2000 cm^{-1} with respect to P3HT, which is not obvious from the corresponding ensemble spectra. Furthermore strong changes in electron-phonon coupling and dynamical disorder are observed. Quantum-classical atomistic simulations show that this substantial spectral shift is caused by a side-chain induced backbone planarisation in PDOPT which increases the electronic coupling between the repeating units. The bulky side-chains of PDOPT adopt a helical structure which enforces backbone planarity. Surprisingly, the conjugation length is unaffected by the planarisation in PDOPT. This stands in contrast to the common notion that a higher planarity leads to a longer conjugation. Instead, the stronger electronic coupling between the repeating units is reflected in the charge-transfer character. Our results suggest that this parameter is worth a closer look in theoretical studies, as in many models the charge-transfer character is treated as con-

stant. Furthermore we reveal an unexpected strategy to control intra-chain order by a substitution with bulky side-chains.

Based on the knowledge of the intra-molecular order in single PDOPT chains, the third publication (section 4.3) addresses the interplay between intra-chain and inter-chain electronic coupling in well defined crystalline PDOPT aggregates (spherulites). By heating these up to and beyond their melting temperature, intra- and inter-chain disorder are gradually increased. The spectral signatures in absorption and emission upon this order-disorder transition are interpreted in the context of the known crystal structure, differential scanning calorimetry measurements as well as the single-chain data. These results show nicely that a decrease in intra-chain coupling does not only lead to a rise transition energy (see publications 1 and 2) but also to an enhancement of inter-chain electronic coupling. Similar to publications 1 and 2, the essential degree of freedom is the dihedral angle between the monomers within the backbone. It determines the intra-chain coupling but as a consequence thereof it also influences the inter-chain interactions.

Highly defined single crystals of thiophene-benzene-thiophene (3TBT) oligomers are studied in publication 4 (section 4.4). They are compared with less ordered (spincoated) 3TBT films to investigate the impact of variable degree of order on the photophysical properties. Absorption and emission spectra are analysed in a framework for molecular H-aggregates and show the impact of structural disorder on the vibronic progressions. Spatially resolved emission spectra on both 3TBT crystals and films allow to reveal the high suppression of the pure electronic transition within the single crystals. Low-temperature emission spectra show the high electronic and structural homogeneity (narrow inhomogeneous linewidth) as well as the rich vibronic progression of the 3TBT crystals. These results emphasize the importance of optical spectroscopy for the characterisation of disorder in organic semiconductors.

Zusammenfassung

In den letzten Jahren ist die Effizienz organischer Solarzellen und organischer Elektronik deutlich gestiegen. Dies motiviert zur weiteren Grundlagenforschung im Gebiet der organischen Halbleiter, zu denen auch die konjugierten Polymere gehören. Die aktive Schicht der Bauelemente ist meist ein aus Lösungsmittel prozessierter, dünner Polymerfilm oder ein Blend, welcher zusätzlich kleine Moleküle mit gegenteiliger Ladungsaffinität enthält. Im Gegensatz zu inorganischen Halbleitern ist die Effizienz der organischen Bauelemente nicht hauptsächlich durch eine langreichweitige Ordnung und hohe Kristallinität bedingt. Vielmehr hängt sie von einer fein abgestimmten Koexistenz geordneter (kristalliner) und ungeordneter (amorpher) Phasen innerhalb des Polymerfilms ab. Allerdings ist der genaue Zusammenhang zwischen struktureller (Un-)Ordnung und den optoelektronischen Eigenschaften bisher kaum verstanden. Einer der Gründe dafür liegt in der experimentellen Schwierigkeit, die Beiträge der jeweiligen Phasen sauber zu trennen. Darüber hinaus ist sogar der Einfluss struktureller Unordnung auf die Photophysik *einzelner* Polymerketten nicht geklärt.

Eine weit verbreitete Klasse konjugierter Polymere im Bereich der Grundlagenforschung und Anwendung sind Polythiophene. Als Modellsystem dient dabei meist das alkyl-substituierte Poly(3-hexylthiophene) (P3HT). Trotz dessen Bedeutung sind die intrinsischen photophysikalischen Eigenschaften dieses Polymers bisher nicht eindeutig bestimmt und werden kontrovers diskutiert. Da die detaillierte Konformation einzelner Ketten nicht durch Strukturaufklärung ermittelt werden kann, ist es bisher nicht gelungen, eine fundierte Korrelation zwischen Intra-Ketten-Unordnung (z.B. Verteilung der Torsionswinkel zwischen den Monomeren) und spektroskopischen Observablen (z.B. Übergangsenergie, inhomogene Linienbreite, vibronische Progression) zu etablieren. Aufgrund der Größe der Moleküle und ihrer zahlreichen Freiheitsgrade ist es auch eine große Herausforderung für die theoretische Modellierung, die optischen und elektronischen Eigenschaften (z.B. Ladungstrennungs-Charakter, Konjugationslänge, Elektron-Phonon-Kopplung) als Funktion der Intra-Ketten-Unordnung zu beschreiben. Ein weiterer Einflussfaktor sind Seitenketten, welche es erlauben die Morphologie und Orientierung der Ketten innerhalb eines Polymerfilms oder Blends gezielt zu beeinflussen. Allerdings ist der Einfluss der Seitenketten auf die intrinsischen photophysikalischen Eigenschaften bisher noch nicht genauer untersucht worden. Noch komplexer wird es, wenn man das

Einzelmolekül-Bild verlässt. So ist beispielsweise der Einfluss intra-molekularer Unordnung auf die elektronische Wechselwirkung zwischen benachbarten Ketten nicht geklärt.

Der Hauptteil dieser Arbeit widmet sich der Aufgabe, mittels Einzelmolekülspektroskopie ein genaueres Bild der Intra-Ketten-Unordnung und deren Einfluss auf die photophysikalischen Eigenschaften von Polythiophenen zu erlangen. Mit Hilfe wohldefinierter Proben und einer speziellen Probenpräparation können wir die intrinsischen Eigenschaften nahezu defekt-freier Polythiophene auf Einzelmolekülebene untersuchen. Die Experimente finden bei kryogenen Temperaturen ($T=1.5\text{ K}$) statt, was einen detaillierten Einblick in die vibronische Progression und Linienverbreiterungsmechanismen (dynamische Unordnung) erlaubt. In Kombination mit Molekulardynamik-Simulationen, zeitabhängiger Dichtefunktionaltheorie und quanten-klassisch atomistischer Simulationen wird der Einfluss struktureller Unordnung sowie der von Seitenketten auf die strukturellen und photophysikalischen Eigenschaften untersucht. Basierend auf den Erkenntnissen der Wissen aus der Einzelmolekülspektroskopie, werden im Anschluss die Auswirkungen von Intra-Ketten-Unordnung auf die *Inter*-Ketten-Wechselwirkung studiert. Schließlich beschäftigen wir uns mit dem Einfluss der Kristallinität auf die Emissionsspektren in hochdefinierten Einkristallen eines thiophen-basierten Oligomers.

In der ersten Veröffentlichung (Abschnitt 4.1) werden die Eigenschaften isolierter, nicht-wechselwirkender P3HT-Ketten mittels Einzelmolekülspektroskopie genauer charakterisiert. Überraschenderweise besitzt P3HT einen niedrigen Grad intrinsischer elektronischer Unordnung auf der Längenskala der emittierenden Spezies (< 10 Wiederholeinheiten), was sich in der schmalen inhomogenen Verteilung ($< 300\text{ cm}^{-1}$) der Übergangsenergien widerspiegelt. Die zweite wichtige Erkenntnis ist die, dass der Mittelwert vieler Einzelmolekülspektren nicht dem Ensemblespektrum eines amorphen P3HT Films entspricht. Mit Hilfe von Dichtefunktionaltheorie können wir diese Diskrepanz der Bildung lockerer Aggregate (“loose aggregates”) zuordnen. Dies führt zu aggregations-induzierter Planarisierung und langreichweitiger elektronischer Wechselwirkung zwischen einzelnen Segmenten benachbarter P3HT-Ketten. Dadurch können wir ein zusammenhängendes Bild der photophysikalischen Eigenschaften von P3HT entwerfen, von der Einzelkette über amorphe, ungeordnete Proben bis hin zu kristallinen Aggregaten.

Die zweite Veröffentlichung, Abschnitt 4.2, beschäftigt sich mit der Frage, welchen Einfluss Seitenketten auf die Struktur und Photophysik einzelner Ketten besitzen. Dafür vergleichen wir die Einzelmolekülspektren von P3HT aus Veröffentlichung 1 mit Poly(3-(2,5-dioctylphenyl)thiophene) (PDOPT), einem zweiten Polythiophen, welches sterisch anspruchsvolle Seitenketten aber ein identisches Polymerrückgrat besitzt. Es zeigt sich, dass die PDOPT Einzelmolekülspektren im Vergleich zu P3HT über 2000 cm^{-1} rotverschoben sind. Darüber hinaus kann ein großer Unterschied in der Elektron-Phonon Kopplung und der Linienverbreiterung (dynamische Unordnung) festgestellt werden. Simulationen zeigen, dass die Rotverschiebung durch eine Planarisierung des Rückgrates

verursacht wird, welche die elektronische Kopplung zwischen den Wiederholeinheiten verstärkt. Die sperrigen Seitenketten von PDOPT legen sich in einer helikalen Struktur um das Rückgrat, welches dadurch planarisiert und stabilisiert wird. Überraschenderweise ist die Konjugationslänge unabhängig von der Torsion des Rückgrates. Dies steht im Gegensatz zur allgemeinen Interpretation, wonach die erhöhte Planarität in PDOPT eine größere Konjugationslänge zur Folge haben müsste. Interessanterweise ist es der Elektron-Loch Abstand (Ladungstrennungs-Charakter) des angeregten Zustandes, in dem sich die stärkere elektronische Kopplung zwischen den Wiederholeinheiten widerspiegelt. Unsere Resultate deuten darauf hin, dass dieser Parameter zukünftig genauer untersucht werden sollte, da er bisher in vielen Modellen als von der Unordnung unbeeinflusst angenommen wird. Darüber hinaus zeigen wir die unerwartete Möglichkeit auf, die Planarität des Polymerrückgrates mit Hilfe sperrige Seitenketten zu verbessern.

Basierend auf dem Wissen über Intra-Ketten-Unordnung in einzelnen PDOPT-Ketten wendet sich die dritte Publikation (Abschnitt 4.3) dem Zusammenwirken von Intra- und Inter-Ketten-Wechselwirkung in wohldefinierten kristallinen PDOPT Aggregaten (Spheruliten) zu. Durch Aufheizen dieser Strukturen bis zum Schmelzpunkt und darüber hinaus erhöhen wir schrittweise die Intra- und Inter-Ketten-Unordnung. Die Veränderungen in den Absorptions- und Emissionsspektren während des Ordnungs-Unordnungs-Übergangs wurden im Kontext bekannter Kristallstrukturanalysen, Differenzkalorimetrie-Messungen und der Einzelmoleküldaten interpretiert. Dabei zeigt sich, dass eine Abnahme der Intra-Ketten-Kopplung nicht nur zu einem Anstieg der Übergangsenergie führt, sondern auch zu einer Verstärkung der Inter-Ketten-Wechselwirkung. Ähnlich wie in den ersten beiden Publikationen ist der Torsionswinkel entlang des Polymerrückgrates der zentrale Parameter, da er direkt die Intra-Ketten-Kopplung aber in Folge davon auch die Inter-Ketten-Wechselwirkung beeinflusst.

Hochdefinierte Einkristalle aus Thiophen-Benzen-Thiophen Oligomeren (3TBT) werden in Publikation 4 (Abschnitt 4.4) näher untersucht. Die Kristalle werden dabei mit weniger geordneten 3TBT Filmen verglichen, um den Einfluss struktureller Unordnung zu untersuchen. Absorptions- und Emissionsspektren werden mit Hilfe eines Modells für molekulare H-Aggregate analysiert und verdeutlichen die Auswirkungen struktureller Unordnung auf die vibronische Progression. Ortsaufgelöste Emissionsspektren an 3TBT Kristallen als auch Filmen verdeutlichen die starke Unterdrückung des rein elektronischen Übergangs innerhalb der Kristalle, was auf einen hohen Ordnungsgrad schließen lässt. Tieftemperatur-Emissionsspektren an einzelnen Kristallen zeigen sowohl eine hohe elektronische und strukturelle Homogenität (schmale inhomogene Linienbreite) als auch eine strukturierte vibronische Progression.

2 Introduction

2.1 Motivation

The discovery of the conducting properties of conjugated polymers in 1977 [1] was awarded with the Nobel Prize in the year 2000 as it opened the door to a new class of materials with a broad range of potential applications. The research activity continuously increased, driven by the promise of cheap, flexible and efficient solar cells, lighting devices as well as field effect transistors [2–4]. Besides, conjugated polymers also facilitate new concepts like indoor light harvesting [5], wearable electronics [6] and inexpensive thermoelectrics [7]. Water-soluble conjugated polymers are attributed great potential in biological and medical applications like imaging, diagnostics and therapy [8–10].

The recent progress in device performance and the variety of applications stimulated fundamental research to understand the basic physical processes occurring within polymer films and single conjugated polymers. The active layer of these devices consists mostly of solution-processed conjugated polymer films or blends which contain additional small molecules with opposite charge affinity. The complexity of these polymer layers lies in the manifold of conformational degrees of freedom of the polymer chains, which results in complex morphologies and microstructures; Ordered, crystalline domains (aggregates) which are mostly formed by π - π -stacking of the chains are interrupted by disordered (amorphous) regions on the length scale of nanometres. Therefore, the research focussed on reducing the amount of disordered chains and promoting long-range crystalline order [11].

Recently, it was shown that mere crystallinity is not favourable for device performance. In contrast, the coexistence of ordered and disordered phases is beneficial as charge transport is maintained by disordered chains which connect the crystalline phases [12]. It is suggested to improve both the short-range order in crystalline regions as well as the interconnectivity between these domains by providing an accurate amount of disordered chains [13].

Quantifying, understanding and predicting disorder phenomena in conjugated polymers is thus a key element for further development. Due to the coexistence of ordered and disordered phases on the nanometre scale, it is challenging to separate both contributions with structure elucidation methods or optical spectroscopy. Furthermore, disorder can be separated in two categories: Firstly, intra-chain disorder (e.g. planarity of the

backbone, overall conformation), which defines the properties of the individual chains. Second, inter-chain disorder (e.g. relative distance and orientation of the chains), which accounts for differences in site energy and electronic coupling between the chains. Both contributions are mutually influencing each other [14, 15] making it difficult to establish clear structure-function properties in thin films on the molecular level. Nevertheless, experimental signatures are needed to characterise the crystalline regions as well as the amount and detailed properties of disordered chains.

For such a fundamental “bottom-up” understanding and modelling, the effects of intra-chain and inter-chain disorder on the optical and electronic properties have to be disentangled. The logical step is thus to shift the focus of research to the molecular level and examine the effects of disorder in single conjugated polymers. Above all, single-molecule spectroscopy has established as a widely used tool to characterize the photophysical properties of single molecules, since its first realisation around 1990 [16, 17]. The progress of this technique provided the basis of superresolution microscopy, which boosted the sensitivity and spatial resolution of optical microscopes [18] and was awarded with the Nobel Prize in Chemistry in 2015.

When applied to conjugated polymers, the technique is able to reveal many interesting features of single chains. By resolving the overall conformation of the chains (e.g. rod-like or coil-like), structure function relationships with excited state properties were established [19–21]. When conducted at liquid helium temperatures, insights into static and dynamic disorder are obtained from transition energies and line shapes [22–24].

However, especially in the important class of prototypical polythiophenes (including the thiophene-based donor-acceptor co-polymers), there is surprisingly little experimental consensus on the intrinsic properties of isolated chains. In particular, those of the important poly(3-hexylthiophene) (P3HT) are highly debated due to conflicting single molecule studies [21, 25–27]. But also from theoretical point of view, the description of conjugated polymers is challenging as long-range interactions prohibit simplified models in these large systems. Furthermore, not only the conjugated backbone but also the side-chains have a strong influence on the intra-chain disorder, which impedes the modelling even further. Nevertheless, a deeper understanding is needed here, as side-chain engineering has evolved as a versatile tool to tune the optical, electronic and structural properties of conjugated polymers [28].

The main part of this work aims at providing experimental data which allows a deeper understanding of the photophysical processes in single, isolated conjugated polymers. In a first step, single-molecule spectra of very defined samples of P3HT are acquired and characterised. These results are compared with a second polythiophene having bulky side-chains (poly(3-(2,5-dioctylphenyl)thiophene), PDOPT) to reveal the intrinsic influence of side-chains and how they can be used to control the intra-chain disorder in conjugated polymers. Both single-molecule studies are supported by theoretical simula-

tions to get a deeper understanding of excited state properties in conjugated polymers. Based on this, the influence of intra-chain disorder on inter-chain electronic interaction is investigated in crystalline PDOPT aggregates. Finally, single crystals of a thiophene-based oligomer serve as model system to study disorder in highly defined crystalline structures.

This thesis is organised as follows: in section 2.2, the basic properties of conjugated polymers and recent theories are presented. Section 2.3 first introduces basic photophysical principles and then focuses on the optical properties of single conjugated polymers and the signatures of disorder in single-chain spectra. In section 2.4, common models for describing inter-chain interactions are presented and spectroscopic signatures of order and disorder in aggregates are briefly explained. A short summary and the connection between the publications is given in chapter 3. The publications can be found in chapter 4.

2.2 Conjugation and conjugated polymers

The unique properties of conjugated polymers, e.g. semiconductivity and interaction with light in the visible range, derive from the sequence of alternating single and double carbon bonds which extends along the polymer backbone. In the elementary form, the four valence electrons of carbon occupy the $2s$ -orbitals and two of the three $2p$ -orbitals. Upon bonding, these four orbitals degenerate and mix, resulting in hybrid orbitals which are linear combinations of the initial orbitals. Depending on the number of mixing orbitals, different bonds form, ranging from the sp_3 -hybridisation with all four orbitals participating, over the sp_2 -hybridisation to the sp -configuration where only one p - mixes with the s -orbital. Each of the hybridised orbitals forms σ -bonds with the corresponding orbitals of the neighbouring atoms, whereas the remaining p -orbitals, which do not participate in the mixing, orient perpendicular to the sp - (or σ -) bonds [29].

In Figure 2.1a, the basic properties of the most prototypical conjugated polymer, polyacetylene, are shown on the example of its oligomer representative butadiene. The carbon atoms in the backbone are all sp_2 -hybridised. In consequence, each carbon has a free p_z -orbital sticking perpendicular out of the plane which is spanned by the σ -bonded carbon atoms, see Figure 2.1a. The neighbouring p_z -orbitals overlap slightly and it is energetically beneficial for them to mix and create a delocalised π -electron system along the backbone. In Figure 2.1b such a π -electron system, also called “conjugated path”, is illustrated on a thiophene oligomer. Crucial for the degree of delocalisation and coupling of π -electrons along the backbone is the overlap of the neighbouring p_z -orbitals. In real systems, it is weakened by torsions, chemical defects and alternations of the bond length along the conjugated path as discussed in detail below. The resulting semi-conductivity (and conductivity upon doping) of the delocalised electron system allows to design flexible electronics [3]. Furthermore, the resonance frequency of the electron system lies in the range of visible light, making conjugated polymers suitable for lighting applications [4] as well as photovoltaics [2].

Starting from simplest conjugated polymer polyacetylene (basic unit see Figure 2.1a), other conjugated polymers were synthesised such as the ladder-type poly(p -phenylene)s (PPs), the more flexible poly(p -phenylene vinylene)s (PPVs) and poly(thiophene)s (PTs, see Figure 2.1b). The conjugated backbones themselves are however not soluble which hinders defined synthesis (in terms of polydispersity and regioregularity) as well as processability. This problem was circumvented with solubilising side-chains such as linear or branched alkanes. These substituted polymers allow for solution processing and especially poly(3-hexylthiophene) (P3HT, see Figure 2.1c) established as a widely used model system for investigating the fundamental processes and to build devices with high efficiencies [30].

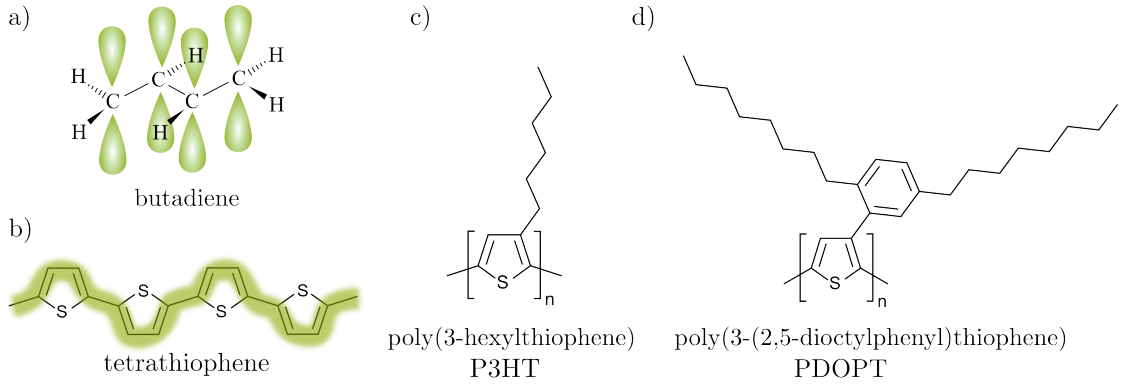


Figure 2.1: Conjugation and conjugated polymers. a) sp_2 -hybridisation in butadiene with the corresponding p_z -orbitals (green). b) The resulting conjugated path (green) illustrated on tetrathiophene, consists of alternating single and double bonds. The chemical structure of the monomers of c) poly(3-hexylthiophene) (P3HT) and d) poly(3-(2,5-dioctylphenyl)thiophene) (PDOPT) which are studied in this thesis. The number of repeating units of the polymers is denoted by n .

Over many years, the main research was focused on the tuning of the optoelectronic properties of the conjugated backbones, especially by optimizing the spectral overlap between absorption spectra and the black-body radiation of sunlight (e.g. low band-gap donor-acceptor polymers). However, in devices like solar cells, other conditions have to be fulfilled, for example the morphology of the polymer films and the orientation of the molecules at the (charge-separation) interfaces are of equal importance [31]. These factors depend mainly on the side-chains of the polymers which are modified via targeted side-chain engineering, a subject that gained recent attention in research [28]. A reliable prediction of the properties of conjugated polymers is however still not within reach, as the side-chains may also impact the backbone structure through sterical or non-bonding interactions. Publication 2 of this thesis will address this issue and focus on the change of the optical properties upon variation of the side-chains. The polymer analysed there is poly(3-(2,5-dioctylphenyl)thiophene) (PDOPT), its chemical structure is shown in Figure 2.1d.

2.2.1 π -electron models

As outlined in the motivation, the molecular understanding of photophysical and electronic processes in single conjugated polymers is the basis for further development of the corresponding devices. Accordingly, a brief overview over past and recent models to describe conjugated polymers is given in the following.

The optical and electronic properties of conjugated polymers are in general described by the many-body Hamiltonian

$$H = H_{nn}(\mathbf{R}_i) + H_{ee}(\mathbf{r}_i) + H_{en}(\mathbf{R}_i, \mathbf{r}_i), \quad (2.1)$$

where $\mathbf{R}_i(\mathbf{r}_i)$ is the set of nuclear (electron) coordinates [32]. The term H_{nn} (H_{ee}) on the right hand side of equation 2.1 describes the kinetic and mutual potential energy of the nuclei (electrons). H_{en} contains the potential energy arising from Coulomb interaction between nuclei and electrons and depends on both electron and nuclear coordinates. The Schrödinger equation with the full many-body Hamiltonian is only solvable exactly for simple systems like the hydrogen atom in free space. Therefore, approximation are made which simplify the many-body problem and allow the modelling of conjugated polymers [32].

A widely-used simplification to describe photophysical processes is the (adiabatic) Born-Oppenheimer approximation [33]. As the nuclei are much heavier than the electrons ($m_n/m_e \approx 10^4$), they are not able to follow their fast movements instantaneously. This allows to separate the time scales of electron and nuclear motion. The electronic part of the Hamiltonian includes therefore static or slowly changing fields generated by the nuclei. The Hamiltonian for the nuclei contains the averaged fields of the rapidly moving electrons [33].

One of the very first approaches to describe photophysics in conjugated polymers was the Hückel model which treats only the π -electron system along the conjugated backbone [34]. The σ -bonded electrons are fixed in time and space and define the geometry. Furthermore, the π -system is modelled in a one-electron picture, thus no electron-electron interaction is involved. This leads to an overestimation of the delocalisation of the π -electron system. Within this simple, particle-in-the-box-like, picture, the band gap should vanish for infinitely long chains [34]. This drastic oversimplification does not hold against experiment, as the optical gap saturates with increasing chain length [35].

Further early models like the Pariser-Parr-Pople (PPP) Hamiltonian included the electron-electron interaction under the assumption of fixed nuclear coordinates [32]. In contrast, the Su-Schrieffer-Heeger (SSH) model [36] drops the electron-electron interaction but takes the electron-phonon interaction into account. Subsequent semi-empirical methods combined both electron-electron interaction as well as electron-phonon coupling [32, 37]. They treated the excitations in conjugated polymers as bound electron-hole pairs which are dressed by local modes of the conjugated backbone [37–39]. In literature, these quasi-particles are referred to as excitons or sometimes exciton-polarons. The coupling to the normal modes as well as disorder lead to a localisation of the exciton wavefunction on a small subunit of the polymer, usually of the size of several repeating units [35, 40–43]. Therefore, not the whole conjugated chain interacts with light, but only parts of it. These parts are often called chromophores. The detailed mechanism behind the localisation are still up for debate, as there are several factors which have a strong impact; Apart from the coupling to normal modes, also long-ranging electron-electron interactions as well as electronic and conformational disorder have to be taken into account for a proper description of realistic systems [38, 39]. Due to the many conformational degrees

of freedom of polymer chains and the one-dimensionality of the system, disorder plays a particularly important role. Recent approaches that meet the challenge of modelling disorder in conjugated polymers will be presented at the end of this chapter.

2.2.2 Structural and electronic disorder in conjugated polymers

First it is reasonable to introduce the degrees of freedom and different types of disorder in single, conjugated polymers. In Figure 2.2, these are schematically illustrated on the example of a polythiophene backbone and will be discussed in the following step-by-step in the context of experimental and theoretical single-molecule studies.

Structural disorder

Bond-length alternation: As mentioned above, the backbone of conjugated polymers intrinsically consists of alternating single and double carbon bonds, which have slightly different equilibrium bond lengths. This causes an alternating p_z -overlap and therefore alternating coupling between the single carbon atoms. This basic disorder in conjugated polymers is sufficient for a disorder-induced localisation of the exciton wavefunction and a saturation of the optical gap with increasing chain length [35]. In real systems also other factors (see below) which weaken or disrupt the conjugation result in a disorder-induced localisation as well. Furthermore, the double (single) bonds lengthen (shorten) upon excitation and reduce the degree of bond-length alternation in the excited state [34]. This strong electron-phonon coupling plays an important role in the analysis of optical spectra, see below.

Torsion: A central degree of freedom in polythiophenes is the angle ϕ between subsequent repeating units, usually called dihedral angle or simply torsion (see Figure 2.2). This angle influences the π -overlap (and therefore the intra-chain coupling) between neighbouring repeating units. The coupling is maximised for a planar geometry (cis-planar with $\phi = 0^\circ$ or trans-planar with $\phi = 180^\circ$) and weakens upon deviation from planarity [44]. The torsional degree of freedom for a whole chain is characterised by the mean dihedral angle ϕ_0 and the variation σ_ϕ around this mean value. The width of the distribution of dihedral angles is termed as “torsional disorder” hereafter. The mean dihedral angle is also referred to as degree of planarity. From an experimental point of view, the dihedral angle of single chains is not accessible directly as structure elucidation methods are not sensitive enough. In single-molecule spectroscopy, the distribution of transition energies is depends on the torsional potential (see publication 2). However in many studies, especially when using long polymers, the intrinsic planarity of conjugated polymers is often hidden due to other effects such as planarisation upon back-folding or regioirregularities. Up to now, detailed studies on the influence of the dihedral angle on the photophysical properties were mostly restricted to oligomers [45, 46].

Chemical defects: Obviously, the chemical purity and quality of the polymers has a tremendous effect on the properties. Chemical defects which interrupt the conjugated path along the backbone alter the photophysical and conformational properties. Especially in poly(*p*-phenylene vinylene)- and poly(*p*-phenylene)-based polymers a significant number of defects along the backbone leads to changes in overall conformation and photophysics of single chains [19, 38, 47, 48]. For polythiophenes the problem of the disruption of the conjugated backbone due to synthesis is less pronounced. Nevertheless, such defects can be induced by photochemical effects [49, 50].

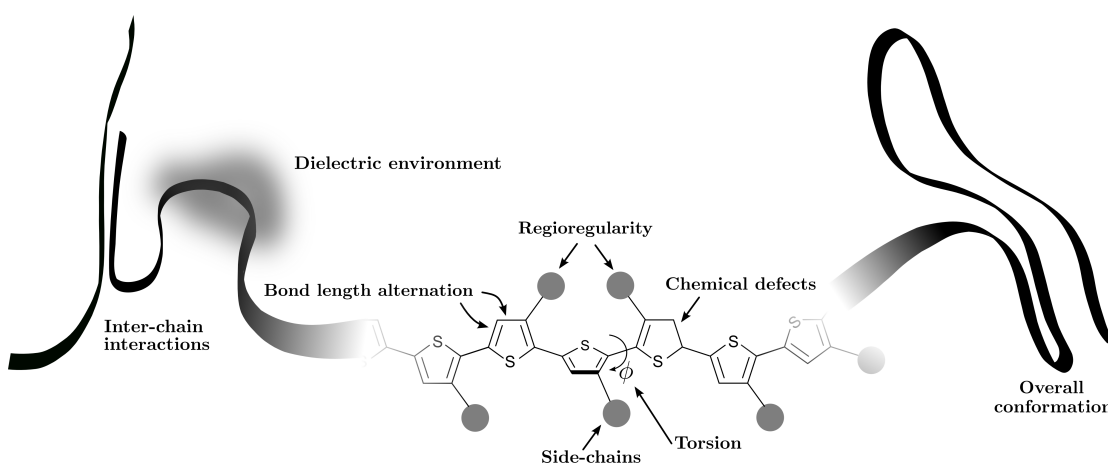


Figure 2.2: Origins of structural and electronic disorder in (single) conjugated polymers.

Side-chains: Originally introduced for a better solubility [30], side-chains are meanwhile extensively studied as they allow to influence backbone planarity and overall geometry [28, 51–55]. Also energy-transfer processes [56, 57] and the overall conformation [58] of single conjugated polymer chains are sensitive to the size of the side-chains. Incorporation of heteroatoms such as fluorine, nitrogen or oxygen introduce non-covalent interactions [59], which allow to tune the properties of isolated chains and bulk structures [60, 61]. Moreover, push-pull effects of atoms like fluorine with its high electro-negativity are further changing the electronic properties of the conjugated system. However, predicting the exact electronic and geometric changes is not straightforward, for details see references [62–64].

Regioregularity: Due to the side-chains, many monomers are asymmetric as for example in the case of P3HT and PDOPT. As a consequence, the monomers can bind in different orientations upon polymerisation. If the side-chains in the resulting polymer are all placed at the same ring-position, the polymer is referred to as 100% regioregular. Each deviation from this ideal case is called regioirregularity or regiodeflect. The grade of regioregularity is determined by the corresponding chemical shifts observed with nuclear magnetic resonance spectroscopy [65]. Regioirregular defects often lead to steric hindrance which often results in larger dihedral angles [28] and thus also effect the

overall conformation [66, 67], electron-nuclear coupling [68] and energy transfer [21] in single conjugated polymers. To reduce these undesired effects, much effort is spent on optimizing synthetic routes to gain highly regioregular conjugated polymers [28, 30, 69, 70].

Dielectric environment: The electrostatic dispersion interaction between the conjugated polymer and the local dielectric environment causes for example solvent-dependent shifts of the transition energies [71]. These arise due to differences in chain-solvent interaction in the electronic ground state and excited state [72]. Furthermore, dynamic changes within the direct dielectric environment impact the line-shape and evolution of single-molecule spectra [23, 73]. As these interactions vary from chain to chain, the degree of this static disorder is reflected in the width of ensemble spectra (inhomogeneous broadening), see also section 2.3.2.

Inter-chain interaction: Leaving the picture of the single, isolated chains for a moment, in dense bulk samples the photophysical properties are dominated by inter-chain interactions. These interactions can i) be of (non-resonant) dispersive nature leading for example to shifts in transition energies, ii) induce structural changes like mutual planarisation iii) and promote electronic coupling between transition dipole moments of chain segments. In the first publication we will show, that these interactions are also present in dilute systems, when attractive interactions between the backbones lead to formation of loose aggregates.

Overall conformation: The overall chain conformation of single, conjugated polymers is widely studied as it can be determined with polarisation resolved spectroscopy [20, 74, 75], often in combination with molecular dynamic simulations [19, 58]. Therefore, structure-function relationships connecting the overall conformation and the photophysical properties like transition energy and intra-chain energy transfer were established. It has been shown, that the conformation is strongly affected by the choice of the solvent: using a good solvent leads to (Gaussian) random-coil conformations, whereas bad solvents induce rod-like geometries, where the chain folds back upon itself due to strong π -attraction of the π -electron systems [19, 67, 76]. However, when chain segments of the same polymer get in close proximity to each other, a variety of interactions is possible (see inter-chain interactions above). Accordingly, it is non-trivial to interpret the results as numerous aspects influence the photophysical properties. One example is the red-site emission in single poly(2-methoxy-5-(2-ethylhexyloxy)-1,4-phenylenevinylene) (MEH-PPV) chains, which probably originates from back-folding and the resulting mutual planarisation of chain segments [48, 77].

In terms of classical polymer physics, conjugated polymers are described as semi-flexible polymers. This means they are rigid at length scales comparable to their persistence length and flexible at larger length scales [67, 78–80]. By using short chains in the scale of the persistence length, the effects of solvent and potentially backfolding

are reduced. As no chain-chain contacts are possible in a single short chain, its conformation is independent of the quality of the solvent and is only driven by entropy and intra-molecular degrees of freedom. The latter are given by regioregularity and side-chain chemistry [67], and one can refer to this as “intrinsic disorder”. In this regime of short, isolated chains, the overall conformation is of minor photophysical relevance as long as the intra-chain order (especially the degree of planarity) is not affected and no electronic coupling emerges between the transition dipole moments of chain segments.

Optical and electronic properties

As explained above, all these factors strongly impact the optical and electronic properties of conjugated polymers. Excitations in conjugated polymers are mostly described as weakly bound electron-hole pairs, which delocalise over several repeating units and are dressed by a lattice distortion (electron-phonon coupling), see Figure 2.3. All three properties, but also the observables which arise from them are affected by disorder, as discussed in the following.

Electron-phonon coupling: As mentioned above, the most prominent structural changes upon excitation are those of the alternating carbon single and double bonds: Upon excitation, the carbon double (single) bonds lengthen (shorten), reducing the degree of bond-length alternation [34]. These collective movements of the backbone are described by collective modes which have an energy around $\hbar\omega \approx 1400 \text{ cm}^{-1}$ for polythiophenes. This strong electron-phonon coupling emerges in absorption and emission spectra as a prominent vibronic progression, see section 2.3. The strength of this coupling also depends on the planarity of the backbone and is therefore sensitive to intra-chain disorder (see section 2.2.3). Also other vibrations of the backbone like torsional or ring-stretching modes may couple to the electronic transition. Especially low-energy torsional modes ($\hbar\omega < 200 \text{ cm}^{-1}$) seem to play an important role in the relaxation upon excitation and energy transfer rates [23, 39, 81–84]. Furthermore, coupling to low-energy environmental modes (phonons) is also observed [85]. The total dissipated energy upon geometric relaxation after excitation plays further a significant role for the energy transfer efficiency in conjugated polymer films [39].

Electron-hole distance: The mean distance between the electron and hole wavefunction (see Figure 2.3) quantifies the charge-transfer character of the excited state. It depends on detailed electron-electron interactions, which are sensitive to intra-chain disorder [86] as well as to doping [29]. In undoped conjugated polymers, the first excited state can usually be described as a Frenkel exciton with an electron-hole distance less than one repeating unit and a binding energy in the order of 8000 cm^{-1} (1 eV) [43]. Charge-transfer excitons, as they occur upon doping or at interfaces, have a larger electron-hole distance and a smaller binding energy 1600 cm^{-1} (0.2 eV) [43]. This thesis

however focuses alone on Frenkel-type excitons. In many models for describing conjugated polymers (e.g. in the frameworks of Barford, Spano and co-workers, see below), the electron-hole distance is separated from the excited state calculations and assumed to be constant for different realisations of disorder. In publication 2 (chapter 4.2) we will show that the charge-transfer character of the lowest excited state is sensitive to backbone disorder as well.

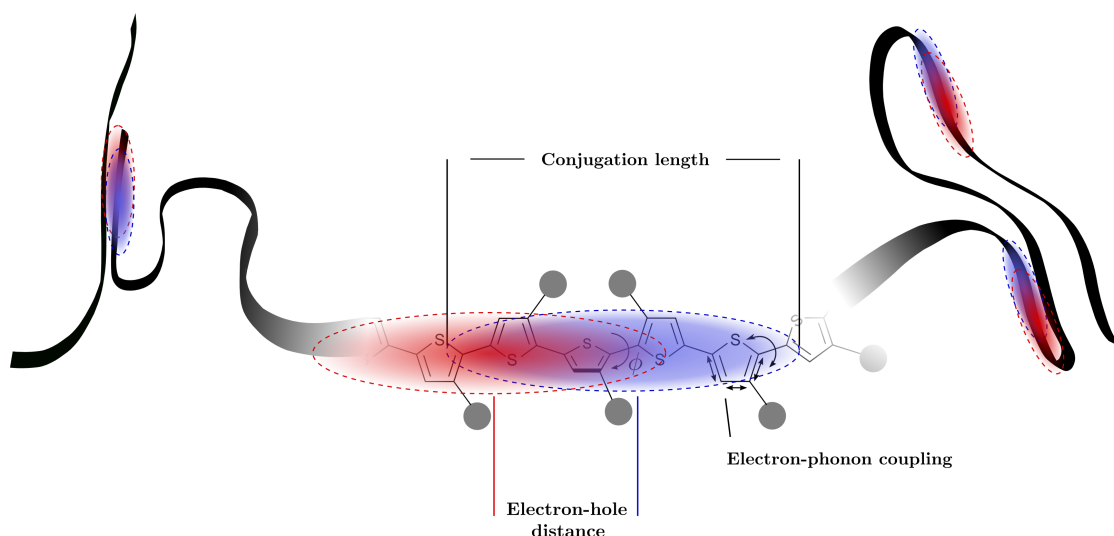


Figure 2.3: Excited states in conjugated polymers are generally described as weakly bound electron-hole pair, which localise on a part of the chain (“chromophore”). The localisation length of the electron (blue) and hole (red) wavefunctions is referred to as conjugation length. The distance between their centres is denoted as electron-hole distance or charge-transfer character. Furthermore, the exciton couples to normal modes of the backbone (electron-phonon coupling). Depending on the chain-length and nature of disorder, also several chromophores can exist within one chain.

Conjugation Length: As stated above, the excitation is only localised on a few repeating units. This “smallest unit within a polymer backbone which interacts with light” is also defined as “chromophore” [87]. Conformational and electronic disorder as well as electron-phonon coupling lead to a localisation of the exciton wavefunction. Usually, the size of these “chromophores” (also referred to as conjugation length¹) is taken as quantity for the degree of order in conjugated polymers. Large chromophores are associated with high intra-chain order while disorder results in shorter chromophores.

However, there is no possibility to measure the length of a chromophore directly up to now. As the excited state wavefunction delocalises only over a few repeating units, optical microscopy is not able to resolve chromophores in real space. Yet, two spectroscopic observables have shown dependencies on the conjugation length: The transition energy

¹Please note, that in the following the terms conjugation length, exciton (de-)localisation length, chromophore size and coherence length are used as synonyms.

between electronic ground state and first excited state and the shape of the vibronic progression.

Chromophores in conjugated polymers

The oligomer approach uses the transition energy between ground state and first excited state to estimate the conjugation length. This method is based on the comparison of the optical band gap (usually measured in solution) of a series of (mostly planar) oligomers with that of the corresponding polymer [35]. For small oligomers a particle in the box-model is applied which qualitatively describes the decrease in transition energy with increasing length of the molecules. As described above, the transition energy saturates with increasing chain length, usually at around 20 double bonds. The saturation behaviour is fitted by the Kuhn model [29, 35] which is a classical approach, taking the bond-length alternation into account. This is conceptually reasonable as on the quantum mechanical level, the bond-length alternation refers to changes in the π -overlap along the conjugated path. The saturation point of this fit² is then taken as an “effective conjugation length” of the polymer. In other words, the polymer behaves like an oligomer of a certain length with respect to its photophysical properties [35].

This model delivers reliable results if absorption and emission spectra are analysed carefully to extract the true value of the optical gap [35]. Yet, extrapolating the oligomer values to the polymer limit is only reasonable when there is no length-dependent change of the intra-chain disorder (e.g. mean dihedral angle or bond-length alternation). Otherwise the Kuhn model (assuming a constant disorder) breaks down. Moreover, for highly disordered polymers the saturation at the polymer limit may not be directly related to the conjugation length [64].

The oligomer approach inspired the picture of conjugated polymers as a sequence of stiff, planar chromophores, which are separated by strong kinks, twists or defects [75, 88]. Following a particle-in-the-box-like approach, the length of these chromophores determines their transition energy. Long segments are red-shifted in absorption and emission with respect to shorter segments. This picture is also in line with the observed multi-chromophoric emission in single conjugated polymers [24, 75, 89, 90].

The idea of planar segments which are separated by chemical or torsional defects is challenged by calculations which show that the electronic coupling is preserved also in the presence of large dihedral angles [91]. Even though the π -overlap is limited in these cases, the Coulomb-type through-space coupling J_{DD} between the transition dipole moments of the monomers is sufficient to retain strong coupling across the torsional defect [38]. Furthermore, classical polymer physics implies that the dihedral angles are rather continuously distributed around a mean value [41, 67, 78, 79]. In most defect-

²Please note that several definitions exist [64]

free polymers, large fluctuations like kinks and strong torsions are rather unlikely. The distribution and mean value are given by the torsional potential of the dihedral angle, see above. In the case of a rigid-rod like poly(*p*-phenylene vinylene) derivative (MEH-PPV) this abrupt flip model (i.e. conjugation is assumed to be broken above a specific threshold angle) did not fit with experimental results. The description of the excited state properties by random conformational disorder has been more successful [92].

Based on this picture of a rather smoothly disordered polymer chain (if free of defects and regioirregularities), the continuous disorder model [93] is more appropriate. The extend of the initial excitation is defined by electron-phonon coupling and by Anderson localisation via energetic and structural disorder. The latter one is a well known phenomenon, especially in low-dimensional materials [94]. Therefore, not the number of conjugation breaks is important but the detailed distribution of torsional angles, which defines the intra-chain disorder and electron-phonon coupling. However the dihedral angle is only measurable with structure elucidation methods for crystalline aggregates but not for disordered polymer films or even single chains. We show in publication 2, that the transition energy in single-molecule spectroscopy is quite sensitive to the distribution of dihedral angles. It should be noted that the conjugation length is not static. Experimental data suggest a dynamic localisation of the exciton wavefunction after initial excitation [84, 95]. This can happen along different vibrational modes or by disorder-induced Anderson localisation [82, 83, 94, 96].

The mechanism that determines the number of chromophores within a single conjugated polymer is still not fully understood. As stated above, the abrupt flip model, which cuts the polymer into planar segments, explains the multi-chromophoric emission in single chains but disagrees with other experimental results and polymer statistics. On the other hand, within the continuous disorder model, all neighbouring monomers are basically coherently connected in a defect-free chain. Despite the localisation of the wavefunction, the oscillator strength of long oligomers rises with chain length. This led to the picture of localised excitons which migrate coherently along the chain [35]. Indeed, in the case of well prepared polydiacetylene chains, a coherent coupling over several micrometre was observed at low temperatures [97]. In these experiments, the chains were polymerised in their monomer crystal, leading to ideally stretched chains with very low (torsional) disorder and a homogeneous dielectric environment. In contrast, in the case of highly disordered polymer conformations, the variation of intra-chain coupling and dielectric environment may lead to the segmentation of the chain to incoherently coupled chromophores [29].

An established technique to address this question is single-molecule spectroscopy as the number of emitters can be determined for example by blinking and anti-bunching experiments. Most of the studies observe several emitters [75, 98, 99] or absorbers [100] within a single conjugated polymer chain. Also single-chromophoric emission has been detected,

often explained by inter-chromophore energy transfer towards the lowest-energy site [20, 75, 100]. However, the experimental results depend strongly on the chemical quality of the sample (e.g. chemical defects or chain length) as well as on the sample preparation technique (e.g. environment or overall conformation). Unfortunately, in most cases the number of defects is not known and thus no correlations between the photophysical properties and the chemical quality of the samples can be given. It is an open question whether there is a lower threshold for torsional and environmental disorder below which a coherent coupling within a polymer chain is achieved. A step towards this are more defined samples and sample preparation techniques as used in publication 1 and 2 on PDOPT and P3HT. But also in these experiments, a discrepancy was observed as there are strong indications that P3HT is a single-chromophoric system, whereas for PDOPT multi-chromophoric emission was detected under otherwise identical conditions. Further chemical defects in the side-chains of PDOPT, or similar, yet unknown effects, which have a huge impact on the torsional disorder, may lead to the formation of several chromophores per chain.

The quantification of chromophores is also challenging from a theoretical point of view. This is reflected above all in the various notations and definitions of the size of a chromophore which are found in literature. One concept is to use the change in bond-length alternation upon excitation as a measure for the extend of the excitation [34, 101]. Others take the extend of frontier molecular orbitals (HOMO/LUMO) as measure for the delocalisation of electron and hole wavefunction [102]. However, the delocalisation of the excitation is not directly correlated with topologies of the frontier MOs when studying polymers with large dihedral angles (weak intra-chain coupling) [64]. Furthermore, if not carefully analysed, it may lead to false predictions about the charge-transfer character of the excitation if further orbital pairs contribute significantly [103]. Measuring the extend of the most dominant natural-transition orbital (NTO) pair circumvents these issues [42, 103, 104]. Other examples of definitions are the extend of the nodeless exciton ground states [105, 106] or the radius of gyration of the exciton wavefunction [86, 107]. The variety of definitions has its origin in the very different theoretical approaches and the definitions cannot be easily transferred to another model. Therefore, quantitative comparisons of conjugation lengths are only reasonable within one model.

Furthermore, using the conjugation length as a quality parameter for the degree of order or intra-molecular coupling can be misleading. As shown in publication 2 (section 4.2), the changes in intra-molecular coupling are not necessarily reflected in the conjugation length. For a proper description, the electron-hole displacement has to be taken into account as well.

2.2.3 Recent theoretical models

Due to the mere number of atoms as well as electron-electron interactions, electron-phonon coupling, conformational (structural) disorder and their mutual influence on each other, conjugated polymers are a challenging system for theoretical modelling. In the following, recent concepts to treat disorder and their results are briefly presented. The discussion focuses on those which are direct subject of research or discussion in the publications.

Absorption and emission spectra of conjugated polymers show a vibronic progression due to the coupling of the electronic transition to vibrational modes. In the last years Barford, Spano and co-workers derived expressions that connect the vibronic progression to the conjugation length. This connection of vibronic progression to intra-molecular disorder is interesting for spectroscopy as it provides a second observable apart from the transition energy. Both models are based on Frenkel-Holstein Hamiltonians and describe conjugated polymers as a linear chain of coupled monomers, with additional coupling to mostly a single effective vibrational carbon stretching mode.

Barford and co-workers use the Frenkel-Holstein model in the (adiabatic) Born-Oppenheimer limit to describe conjugated polymers as a linear arrangement of monomers which couple via the exciton transfer integral J . Furthermore, the total exciton wavefunction is split into a relative-electron-hole wavefunction, which describes the electron-hole separation, and into the centre-of-mass wavefunction [43, 44]. The latter one is used to describe the light-matter interaction and the delocalisation of the exciton over several repeating units and is studied as a function of disorder.

The coupling between the repeating units $J = J_{DD} + J_{SE} \cos^2(\phi)$ consists of two contributions: Firstly, the through-space dipole-dipole coupling J_{DD} between the transition dipole moments of neighbouring repeating units, which depend on their mutual orientation and distance. Secondly, the through bond (super-exchange) interaction $J_{SE} \cos^2(\phi)$, which is a function of the π -overlap of neighbouring monomer units. Accordingly, it depends on the dihedral angle ϕ between the monomers which allows to study the influence of torsional disorder and planarity on the transition energy and conjugation length. Generally, a more planar backbone leads to lower energies of the excited state. Furthermore enhancing the torsional disorder – in terms of fluctuations around a given mean value – shortens the conjugation length. Also an analytical expression connecting the vibronic progression of emission spectra with the coherence length is derived [87], see section 2.3.3.

Spano and co-workers initially developed a theory for molecular aggregates including exciton-phonon coupling and were able to relate the shape of the vibronic progression to the exciton delocalisation along the stack of molecules (see also section 2.4.3). By applying this theory to conjugated polymers, strong photophysical similarities with

molecular J-aggregates were highlighted [108, 109]. Similar to a molecular J-type aggregate, the monomer transition dipoles in conjugated polymers are arranged in-line, resulting in a negative excitonic coupling between them. Equivalent to Barford, an expression for the relation between the vibronic progression and the exciton coherence length was formulated (see section 2.3.3 for details). Furthermore, the model is able to explain the temperature dependence of the vibronic progression in single highly ordered polydiacetylene chains. Torsional disorder is however treated only indirectly via a variation of intra-chain coupling.

Although this model presents a tempting idea of thinking about conjugated polymers, some essential features are lacking. In contrast to the model of Barford, the exciton transfer between the molecules is based only on Coulomb-type dipole-dipole coupling. However, the through-bond coupling between the monomer units in conjugated polymers is much stronger than the through-space coupling as in the case of molecular aggregates. In addition, Spano uses the antiadiabatic regime (assuming that exciton motion is much slower than phonon motion) but in conjugated polymers the intra-chain coupling is stronger than the typical local normal mode energies. This leads to different predictions about the vibronic progression in absorption, for more details see the appendix of reference [44].

Density functional theory (DFT) is based on the Hohenberg-Kohn theorem [110] and relies on the particle density instead of the many-particle wavefunction. In the Kohn-Sham formulation [111], the interacting many-body problem is transferred to a non-interacting many-body problem in an effective potential. The effective potential is constructed such that the new system has (in principle) the same density as the real interacting one and includes the many-body interactions such as Coulomb-, exchange- and correlation-interaction. The observables of the system are then calculated from functionals of the particle density. Time-dependent density functional theory (TDDFT) additionally allows to calculate excited state properties [112, 113].

As a first principles method, DFT is formally exact, but in practice approximations have to be introduced, primarily for the exchange-correlation energy and potential [104]. These lead for example to a wrong description of charge-transfer excitations. The use of generalised Kohn-Sham theory and the development of a new class of (non-empirical) functionals, the optimally tuned range separated hybrid (RSH) functionals, surpass this limitation [114]. In a recent work, de Queiroz and Kümmel applied this formalism to non-substituted oligothiophenes with up to 24 repeating units. Realistic, disordered chain conformations were generated by a preceding molecular dynamics simulation. It was shown that the conformational distortions increase the transition energy of the first excited state by up to 4000 cm^{-1} (0.5 eV) [42, 104]. Besides, the localisation length (defined by the extent of the natural transition orbitals) decreases with increasing disorder. But also for a planar configuration, the extent is limited to around 10-12 repeating units.

Furthermore, for an accurate calculation of the optical gap, the solvent molecules have to be taken into account [104]. TDDFT calculations are used by our collaborators in publication 1 (section 4.1) to examine the role of structural disorder on the photophysical properties and to explore the long-range interactions between neighbouring P3HT chains.

Density functional theory is further used to calculate the torsional potential of the dihedral angle ϕ connecting the thiophene units, which is the central degree of freedom for modelling conformational and electronic disorder in conjugated polymers. This is particularly challenging when (non-covalent) interactions between the backbone and the side-chains are involved. Moreover, it was realised that dimers are not large enough to model the torsional potential and relaxed geometries for the corresponding polymer correctly [115]. Therefore, longer oligomers and polymers have to be modelled with their full side-chains to capture meaningful dihedral potentials and relaxed ground-state conformations [64, 102, 116, 117].

Quantum classical atomistic simulations belong to the class of semi-empirical methods which are a compromise as they allow to treat larger systems at acceptable computational costs. On the downside, the reliability of their results depends strongly on the accuracy of the experimental data and approximations that are put into the model. Recently, Simine and Rossky applied the quantum mechanical consistent force field for π -electrons (QCFF/PI) method to P3HT [86]. The thiophene π -electrons are treated quantum-mechanically, whereas the rest of the polymer is treated classically by force-fields which capture bonding and non-bonding interactions. This allowed to create disordered conformations of a 30-monomer P3HT for a broad range of temperatures (T=10 K to 298 K) including side-chains which were modelled fully atomistic. The potential for the dihedral angle ϕ was then calculated from the thermal population of dihedral angles by a Boltzmann inversion. At low temperatures, the potentials show a quasi-harmonic minimum around $\phi = 145^\circ$. As a result, the chains are uniformly twisted. At room temperature, the trans-planar configuration ($\phi = 180^\circ$) gets thermally accessible.

The absorption spectra of the corresponding thermal ensembles of P3HT were calculated with the semi-empirical Pariser-Parr-Pople Hamiltonian for π -electrons including electron-electron interaction at the level of configuration interaction singles (CIS). The conjugation length (localisation length) is defined here as the radius of gyration of the exciton wavefunction. The transition energies from electronic ground state to the first excited state slightly decrease upon heating, while the conjugation lengths get shorter at the same time. This seems contradicting first, as one would expect that a stronger delocalisation is connected to a red-shift (see above, particle-in-the-box picture). Here however, the chromophores at room temperature are shorter but more planar than their cooler counterparts which are in contrast uniformly, but relatively gently twisted. Thus the π -overlap is enhanced in the short chromophores as they are more planar. Interest-

ingly, this is also reflected in the electron-hole separation (or charge-transfer character) of the first excited state which increases with a more twisted backbone and increasing conjugation length. Our collaborators use this method in publication 2 to simulate the conformation and photophysical properties of a bulky-substituted polythiophene (PDOPT).

In general, this chapter about the basic concepts of single, isolated chains showed that the roles of electron-electron interaction, electron-phonon coupling, intra-chain disorder and their mutual influence on each other are highly debated. Recent models made it possible to take the role of intra-chain disorder into account with a special focus on torsional disorder and torsional potentials.

All these theoretical studies are performed on single, isolated chains. However, detailed experimental data which examines transition energy and electron-phonon coupling under the influence of torsional disorder is missing. Low-temperature single-molecule spectroscopy on conjugated polymers can give insights into transition energies, electron-phonon coupling and – with a proper choice of samples – the influence of structural and torsional disorder on these parameters. The aim of this thesis is thus to provide experimental data which, in combination with recent theoretical calculations, gives deeper insights into the photophysics of conjugated polymers.

2.3 Photophysics of isolated conjugated polymers

This chapter focuses on the photophysical properties of isolated conjugated polymers. After introducing the basic concepts of a chromophore interacting with light, the impact of disorder and its signatures on the emission spectra of single conjugated polymer chains are discussed [29, 33, 39].

2.3.1 Electronic and vibronic transitions

At first, a chromophore within a conjugated polymer, which consists of two electronic levels and corresponding vibrational levels is considered, see Figure 2.4. The solutions of the Schrödinger equation of the many-body Hamiltonian (equation 2.1) are wavefunctions which depend on both electron and nuclear coordinates (under the neglect of spin). Within the Born-Oppenheimer approximation, see section 2.2.1, the time scales of electron and nuclei dynamics can be separated. This allows to express the wavefunction as a product of electronic and vibrational contribution:

$$|\Psi\rangle = |\Psi_e(\mathbf{R}_i, \mathbf{r}_i)\rangle |\Psi_v(\mathbf{R}_i)\rangle. \quad (2.2)$$

Here, $|\Psi_e(\mathbf{R}_i, \mathbf{r}_i)\rangle$ denotes the electronic wavefunction which depends on the set of electron coordinates \mathbf{r}_i and parametrically on the set of nuclei coordinates \mathbf{R}_i . The vibrational wavefunction $|\Psi_v(\mathbf{R}_i)\rangle$ describes the dynamics and mutual interaction of the nuclei.

In the simplest case of a diatomic molecule, the potential energy term of the vibrational wavefunction is often approximated by a harmonic potential describing the movement around the equilibrium bond length. The energies of the vibrational levels $\nu = 1, 2, 3, \dots$ are then equally separated by $\hbar\omega$, where ω is the vibrational frequency of the bond. For larger molecules, the nuclear motions have to be regarded as a system of coupled oscillators and are usually described by their effective (eigen)modes or vibrations. The potential energy surface of a distinct mode i with frequency ω_i is then expressed in the normal mode coordinate Q_i , see Figure 2.4.

Due to the displacement of the charge densities upon excitation, the vibrational potentials differ in ground state and excited state. As illustrated in Figure 2.4 the potential energy surface shifts by ΔQ_i along the normal mode coordinate Q_i upon transition between electronic ground state $|\Psi^0\rangle$ and excited state $|\Psi^1\rangle$. The vibronic excitations which emerge in this potential are denoted by the vibrational quantum number ν , see Figure 2.4. A combination of an electronic and a vibrational wavefunction is usually referred to as vibronic state.

The strength of the optical transition between these vibronic states is given by the square of the transition dipole moment μ_{if} from, in general, initial state $|\Psi^i\rangle$ to final

state $|\Psi^f\rangle$, which is defined as

$$\mu_{if} = \langle \Psi^f | \mathbf{p} | \Psi^i \rangle = \langle \Psi_e^f | \mathbf{p} | \Psi_e^i \rangle \langle \Psi_v^f | \Psi_v^i \rangle \quad (2.3)$$

The integral is split up into the electronic and the vibrational part, which both have to be non-zero for an allowed transition. The transition dipole operator $\mathbf{p} = e\mathbf{r}$ with the set \mathbf{r} of electronic coordinates is an uneven function. Therefore, the pure electronic transition between the two states is only possible when they differ in parity. The Franck-Condon integral $\langle \Psi_v^f | \Psi_v^i \rangle$ is only non-zero if there is a significant overlap between the vibrational functions of initial and final states. As optical transitions occur vertical, the probability of a transition between two vibronic states depends on the shift ΔQ of the potential energy surface. Usually this overlap is expressed by the Huang-Rhys parameter $S \propto \Delta Q^2$. Thus a large Huang-Rhys parameter denotes an effective coupling of the respective vibration to the electronic transition (electron-phonon coupling). As already mentioned in section 2.2.2, in conjugated molecules this is especially the case for vibrations which promote a change in (carbon) bond-length alternation upon excitation. In conjugated polymers, the (effective) Huang-Rhys factor for the carbon-bond stretching modes ($\hbar\omega \approx 1400 \text{ cm}^{-1}$) is usually in the order of $S_{eff} \approx 1$.

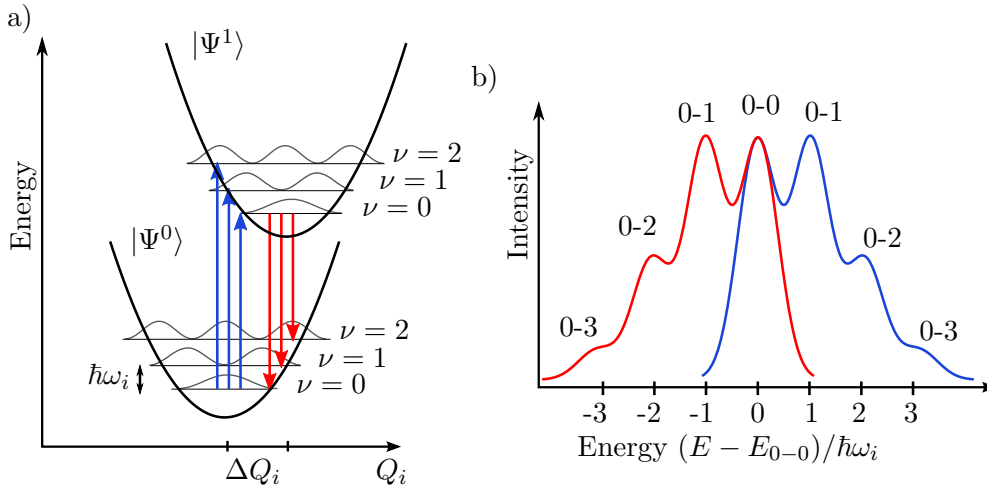


Figure 2.4: Absorption and emission processes: a) Ground state $|\Psi^0\rangle$ and excited state $|\Psi^1\rangle$ potential energy surfaces are shifted by ΔQ_i with respect to each other along the configurational coordinate Q_i of an effective mode. The wavefunctions of the vibronic excitations ν are sketched in grey. b) Vibronic (Franck-Condon) progressions in absorption (blue) and emission (red) for a Huang-Rhys parameter of $S = 1$. Please note that only a single mode Q_i is shown here, but usually several modes are coupling to the electronic transition. Adapted from [29].

A non-zero Huang-Rhys parameter allows absorption and emission into higher lying vibronic states (arrows in Figure 2.4a). The intensities of the distinct transitions in the corresponding spectra are determined by the so-called vibronic (Franck-Condon)

progression which follows a Poisson distribution. For emission, the peak ratios write as $I_{0-\nu} \propto |\langle \Psi_\nu^0 | \Psi_0^1 \rangle|^2 = e^{-S} \frac{S^\nu}{\nu!}$ as emission takes place from the vibration-less lowest excited state after non-radiative relaxation of the vibrational quanta. The formula for absorption is similar for this case, resulting in a mirror-symmetry of absorption and emission as displayed in Figure 2.4b. In conjugated polymers, this mirror symmetry may be broken, when different species contribute to absorption and emission due to structural relaxation upon excitation, inter-chromophore energy transfer or violation of the Born-Oppenheimer approximation [35, 44].

2.3.2 Signatures of disorder in single-molecule spectra

In this chapter, the low-temperature emission spectra of single molecules are discussed with focus on conjugated polymers. In short, such a spectrum is taken by exciting a single molecule with a focused laser beam and detecting the subsequent emitted fluorescence with a spectrograph and a CCD camera. The samples discussed in this thesis are cooled down to $T = 1.5$ K in a home-built helium-bath cryostat. For further experimental details see [118, 119] or the supporting information of publication 1 (section 4.1). In Figure 2.5b the main features of a low-temperature emission spectra of a single, isolated conjugated polymer chain are sketched. The highest energy peak, the so called zero phonon line (ZPL), corresponds to the pure electronic (0-0) transition from the vibration-less excited state to the ground state.

In general, the homogeneous linewidth (FWHM) of the ZPL is given by $\Gamma(T) = \frac{1}{2\pi T_1} + \frac{1}{\pi T_2(T)}$. Here T_1 is the excited state lifetime and $T_2(T)$ accounts for dephasing processes due to the scattering of phonons during the excited state lifetime which leads to a rapid and random shift in energy levels. The latter process freezes out at low temperatures. In this case the linewidth Γ_{hom}^{single} is only limited by the lifetime of the excited state (natural homogeneous line width) [22, 119–122].

However, the observed ZPL widths are usually inhomogeneously broadened due to averaging over dynamical processes. For amorphous environments, structural relaxation and subsequent changes in the local dielectric environment of the polymer chain happens on all time scales. The resulting fluctuations of the electrostatic dispersion interaction between the conjugated polymer and its environment lead to shifts of the transition energy [22, 23]. The spectral shifts, also called spectral diffusion, are averaged over the integration time of a single spectrum (typically around 1s) resulting in an inhomogeneously broadened observed line width Γ_{inhom}^{single} , see Figure 2.5a. Thus the dynamic disorder in direct vicinity of the emitting site is reflected in the ZPL width. In the case of substituted conjugated polymers, the side-chains contribute most to the dynamic disorder as they are directly attached to the backbone [23]. For an example of side-chain induced dynamic disorder, see publication 2 (chapter 4.2).

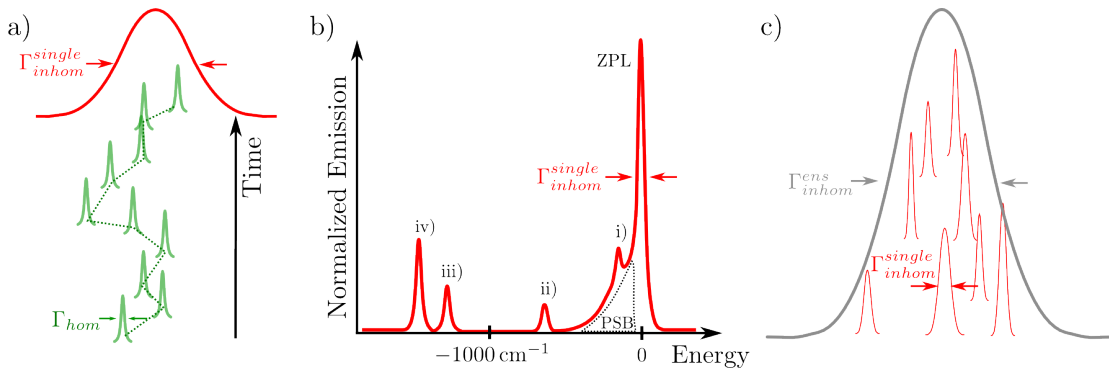


Figure 2.5: Inhomogeneous broadening mechanisms in low-temperature single-molecule spectra. a) Due to dynamic changes in the dielectric environment, the transition energy changes statistically during the acquisition time of an emission spectrum. This leads to an inhomogeneously broadened observed linewidth Γ_{inhom}^{single} . b) Sketched single-molecule spectrum with the characteristic zero-phonon line (ZPL), phonon-side band (PSB) and vibronic transitions (i-iv). The energy scale is set relative to the pure electronic transition (ZPL). c) The inhomogeneous distribution of transition energies leads to broadened ensemble statistics, described by the inhomogeneous linewidth Γ_{inhom}^{ens} .

Spectral diffusion occurring on time scales slower than the integration time of a single spectrum are recorded as a function of time, by taking sequences of spectra [22, 123]. The width and frequency of these spectral jumps contain detailed information about the dynamic disorder in the environment [23]. On the other hand, this slow diffusion leads also to an additional line broadening of the integrated signal of the entire sequence of spectra. This effect can be overcome by applying sorting algorithms to the stack of spectra [23, 124].

Apart from the pure electronic transition, the spectrum in Figure 2.5b shows features of electron-phonon coupling at lower energies with respect to the ZPL. The shoulder next to the ZPL arises due to the coupling to phonons of the surrounding matrix in which the molecule is embedded (phonon side band, PSB) [85, 118–120]. The distinct peaks i) to iv) at lower energies result from electron-phonon coupling to intra-molecular modes. Lines with vibrational energies smaller than $\hbar\omega \approx 250 \text{ cm}^{-1}$ (peak i)) are usually ascribed to collective stretching modes of the backbone. Intermediate peaks ($\hbar\omega \lesssim 1000 \text{ cm}^{-1}$, ii)) can for example arise due to ring-deformations of the monomer units [118].

Vibrational energies around $\hbar\omega = 1400 \text{ cm}^{-1}$ (peaks iii) and iv)) arise from electron-phonon coupling to carbon-bond stretching modes. Recent calculations in the context of Raman studies suggest that the energies and relative intensities of these modes are strongly connected to the conformation of the conjugated backbone [68, 125, 126]. Indeed, when comparing the single-molecule spectra of two conjugated polymers with different degrees of backbone planarity, a significant change in the vibrational signature can be observed as shown in Figure 2.6. This sensitivity of the vibrational modes gives thus a

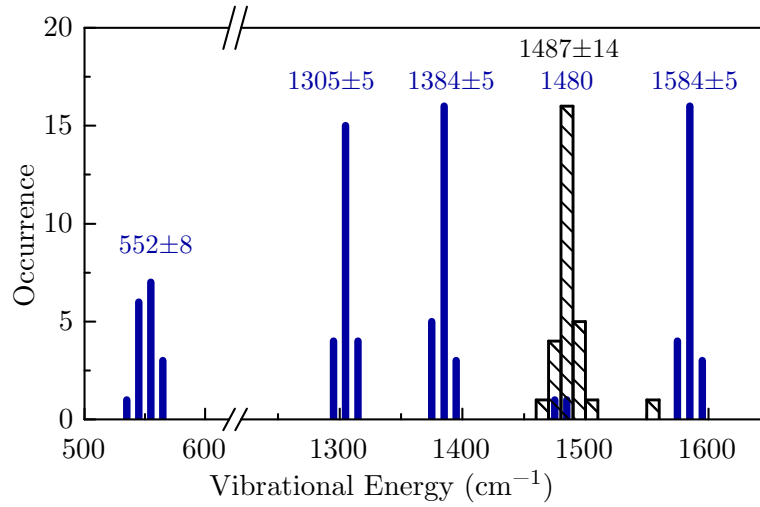


Figure 2.6: Histogram of vibrational energies for a planar (solid blue) and non-planar (hatched black) polythiophene between 500 cm^{-1} and 1650 cm^{-1} . The peak energies are given in the Figure, the error is the standard deviation.

further method to distinguish between different backbone conformations. In ensemble measurements, this dependence of vibrational energies and relative intensities on the backbone conformation is also known as missing mode effect [127], which can lead to misinterpretations of ensemble spectra.

The spectral distribution of transition energies of an ensemble of single molecules – the so-called inhomogeneous distribution function – is shown in Figure 2.5c. As outlined in section 2.2.3, recent calculations have shown that the dihedral angle ϕ has a profound effect on the transition energy [42, 86, 104, 117, 128]. In experiment, each chain experiences an individual distribution of dihedral angles leading to the inhomogeneous distribution of transition energies. The width Γ_{inhom}^{ens} of this distribution is a measure for the amount of static energetic disorder and is thus connected to the dihedral potential, see publication 2. Additionally to torsional disorder, each emitting site experiences a slightly different dielectric environment (see also section 2.2.2), leading to further broadening of the inhomogeneous distribution [120, 129–131]. As a note, the determination of the true inhomogeneous distribution function from ensemble spectra is not always straight forward, as the spectra can be substantially broadened by electron-phonon coupling to low-energy modes [118] or due to unintended inter-molecular coupling (see publication 1).

2.3.3 Connection between coherence length and vibronic progression

As already mentioned in chapter 2.2.3, the groups of Spano, Barford and co-workers recently developed frameworks which connect the shape of the vibronic progression to the conjugation length and to intra-molecular disorder. As a note, usually, only a single mode is used for the description of the vibronic progression (with $\hbar\omega \approx 1400\text{ cm}^{-1}$).

As illustrated in Figures 2.5b and 2.6, this is not necessarily the case for conjugated polymers. When analysing single-chain spectra within these frameworks, the modes have to be treated as effective modes with an effective Huang-Rhys parameter S_{eff} which is determined by numerical integration of the peak areas.

In Barfords treatment, the displacement ΔQ of this mode upon excitation is proportional to local exciton density. It can then be shown, that the corresponding Huang-Rhys factor S_{eff} decreases with increasing coherence length L . The integrated peak ratio in emission is connected to the exciton coherence length via

$$\frac{I_{0-1}}{I_{0-0}} = S_{eff} = \frac{S_{mon}}{\sum |\Psi(n)|^4} = 2 \frac{S_{mon}}{L}. \quad (2.4)$$

Here, $|\Psi(n)\rangle$ is the Frenkel exciton centre-of-mass wavefunction, S_{mon} is the Huang-Rhys factor of a single repeating unit (for polythiophenes $S_{mon} \approx 1.4 - 1.9$ [132]) and L denotes the conjugation length [44, 87].

Spano and co-workers formulated a similar relationship in their framework which treats conjugated polymers as molecular J-aggregates with exciton-vibrational coupling:

$$\frac{I_{0-1}}{I_{0-0}} = S_{eff} = \kappa \frac{S_{mon}}{L}. \quad (2.5)$$

Here, κ is a measure of the electron-hole distance which approaches unity for Frenkel excitons in conjugated polymers and decreases with increasing charge-transfer character [133, 134].

In both models, an increase in the observed peak ratio and thus Huang-Rhys parameter S_{eff} implies a decrease in conjugation length. In publication 2 (chapter 4.2) we compare two polythiophenes with different degree of backbone planarity and thus different strength in intra-chain coupling. We observe a change in the I_{0-1}/I_{0-0} peak ratio which suggests a change in coherence length according to the usual interpretation of the equations 2.4 and 2.5. In combination with direct quantum-classical atomistic simulations we can show that the conjugated length does not change, but the electron-hole distance does. Thus, the peak ratio is not necessarily a good measure for the extend of delocalisation along the backbone. For a proper description also a possible change in the charge-transfer character has to be taken into account (e.g. via κ).

In this thesis, electronic and structural disorder is investigated by careful analysis of the line-shape, spectral position and intensity ratios of single-molecule spectra. Furthermore it is shown that these details are only visible at the single-molecule level as the electronic coupling in amorphous and crystalline domains brings up new phenomena, which are introduced in the next section.

2.4 Photophysics of electronically interacting conjugated polymers

In this section, the concept of electronic coupling between the transition dipole moments of chromophores in adjacent polymer chains is introduced. Understanding the underlying mechanism helps to separate intra-chain effects from inter-chain interactions and connect single-chain and bulk experiments. [29, 33, 135]

2.4.1 Two-level systems

In the following, two chromophores on adjacent polymer chains are approximated as a pair of electronically interacting two level systems. Vibrational levels are neglected for simplicity first and will be introduced again later. Therefore, the systems consist of the electronic ground states $|0_1\rangle$ and $|0_2\rangle$ (with corresponding energy $E_g = 0$) as well as the excited states $|1_1\rangle$ and $|1_2\rangle$. Energetic disorder leads to slightly differing excited state energies E_1 and E_2 , separated by $2\Delta = |E_1 - E_2|$, see Figure 2.7a. The transition between ground and excited state of each molecule is described by the transition dipole moments μ_1 and μ_2 . The excitation of one of the molecules writes as the states $|1\rangle \equiv |1_1\rangle|0_2\rangle$ and $|2\rangle \equiv |0_1\rangle|1_2\rangle$, for excitation in molecule 1 or 2, respectively. With these as eigenstates, the Hamiltonian of the total system $H = H_1 + H_2$ is diagonal. This changes as a coupling V between the molecules is introduced³

$$H' = H_1 + H_2 + V, \quad (2.6)$$

where the new off-diagonal matrix elements describe a coupling between the transition dipole moments of the chromophores.

Diagonalisation gives the new eigenstates $|k_+\rangle$ and $|k_-\rangle$ which are a superposition of the initial eigenstates $|1\rangle$ and $|2\rangle$ [135]. These are called exciton states and describe a delocalisation of the excitation over both molecules. The corresponding eigenvalues write as

$$E_{\pm} = \frac{E_1 + E_2}{2} \pm \sqrt{\frac{1}{4}(E_1 - E_2)^2 + |V|^2} = E_m \pm \sqrt{\Delta^2 + |V|^2}. \quad (2.7)$$

This splitting of the energy levels, called Davydov splitting, depends on the strength of coupling V as well as the energy difference Δ of the two initial energy levels, see Figure 2.7b. This basic principle of electronic interaction can easily be expanded to a linear chain of N interacting molecules with the similar consequences. An exciton band containing N eigenstates emerges with an energy level splitting of $\Delta E = 4V$ in the absence of disorder ($\Delta = 0$).

³in the limit $V \ll E_1, E_2$, i.e the molecules preserve their individuality

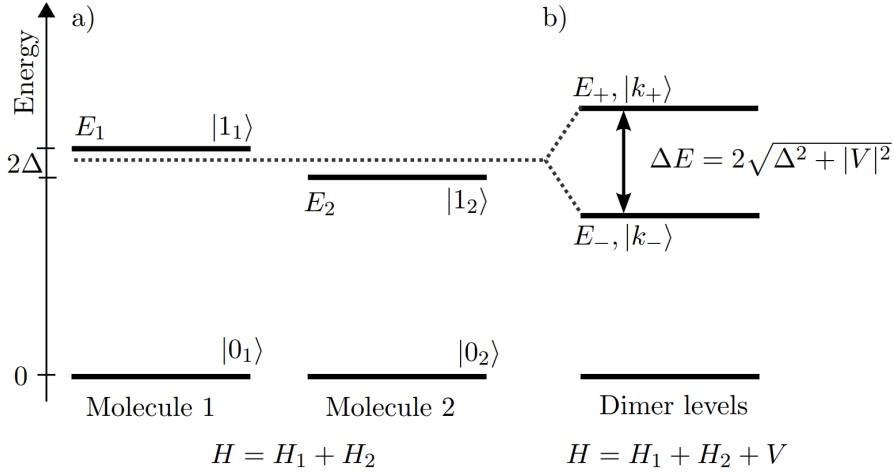


Figure 2.7: Davydov splitting in electronically interacting dimers: Energy level diagrams for a) isolated molecules and b) strongly coupled molecules showing excited-state splitting ΔE (Davydov splitting). Shifts due to non-resonant intermolecular interactions are neglected for simplification, adapted from [135].

To describe realistic systems, static and dynamic fluctuations of the energy levels and of the electronic coupling have to be taken into account. Static electronic (diagonal) disorder (Δ), arises due to different polarizabilities of the environment and intra-chain fluctuations of the energy levels. Changes in mutual orientation and distance between the molecules lead to deviations in the electronic coupling V (off-diagonal disorder). In general, a distinction is made between two coupling limits by comparing coupling strength with the amount of static electronic disorder. In the strong coupling regime ($|V| \gg \Delta$), the new eigenstates are delocalised over both molecules, i.e. the exciton delocalises over the whole system. In the case of weak coupling ($|V| \ll \Delta$) the eigenstates approximately represent the initial states $|1\rangle$ and $|2\rangle$. In this case, the excitation is localised by disorder on one of the molecules with a remaining weak splitting of the excited state energy levels.

2.4.2 H- and J-type aggregation

The oscillator strength of the excited states of the electronically interacting chromophores depends on the relative orientation of the transition dipole moments with respect to each other. As introduced by Kasha [135], the electronic coupling V between the transition dipole moments $\boldsymbol{\mu}_1$ and $\boldsymbol{\mu}_2$ can be approximated by the electrostatic Coulomb-type point-dipole interaction

$$V = \frac{1}{4\pi\epsilon\epsilon_0} \frac{\boldsymbol{\mu}_1 \cdot \boldsymbol{\mu}_2 - 3(\boldsymbol{\mu}_1 \cdot \hat{\mathbf{r}})(\boldsymbol{\mu}_2 \cdot \hat{\mathbf{r}})}{r^3}. \quad (2.8)$$

Here, $\hat{\mathbf{r}} = \mathbf{r}/r$ denotes the unit vector connecting the two dipoles and $\epsilon\epsilon_0$ reflects the dielectricity of the surrounding. Depending on the sign of the coupling V , a distinction between H-type aggregation ($V > 0$) and J-type aggregation ($V < 0$) is made. This is illustrated in Figure 2.8 on the example of a molecular dimer with arbitrary (but coplanar) mutual orientation. In a predominant parallel arrangement, the lowest excited state carries no oscillator strength as the transition dipole moments are interfering destructively. In these H-type aggregates, the highest excited state carries most of the oscillator strength, accordingly the absorption blue-shifts with respect to the non-interacting molecule. Due to Kasha's rule, emission occurs from the red-shifted lowest excited state, resulting in a large Stokes-shift. In ideal H-aggregates, this transition is optically forbidden. This rule is however weakened in real systems by several factors, see below.

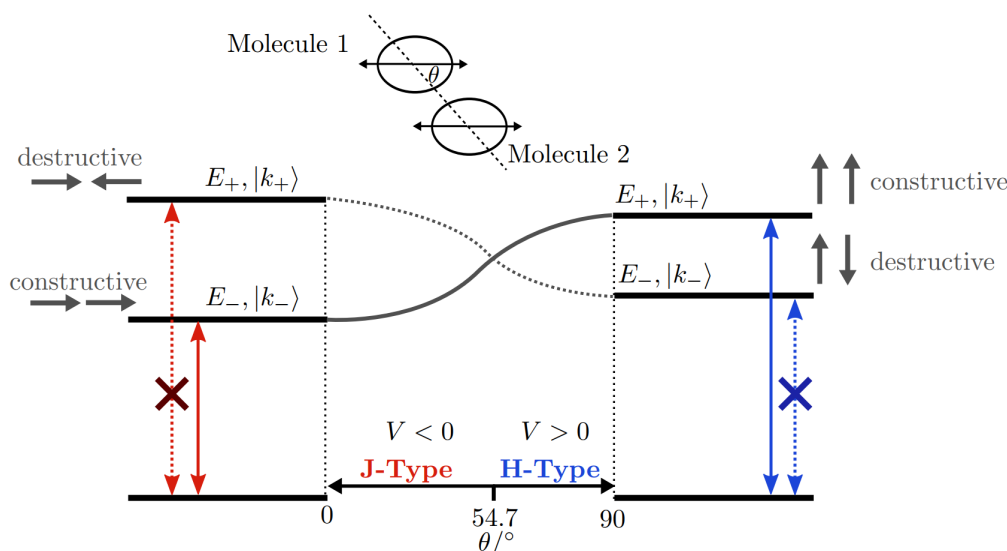


Figure 2.8: *Interacting Dimers: Electronic coupling of a molecular dimer with coplanar transition dipole moments as a function of the mutual orientation. Parallel oriented transition dipoles ($\theta = 90^\circ$) result in H-type coupling with a symmetry forbidden lowest excited state (no oscillator strength). J-type coupling is achieved by in-line arrangement of the transition dipole moments, where the lowest excited state carries all oscillator strength ($\theta = 0^\circ$). For arbitrary orientation angles θ in-between the two extreme cases, an intermediate situation arises with weakly allowed (solid grey line) or forbidden transitions (dotted grey line). The change point ($V = 0$) between H- and J-aggregation occurs at $\theta = 54.7^\circ$. Adapted from [135].*

In contrast, a negative coupling emerges ($V < 0$) when the molecules are primarily arranged in-line. Such systems are called J-type aggregates where the lowest excited state is optically allowed and carries most of the oscillator strength as the phases of the dipoles add up constructively. Absorption and emission are thus red-shifted and show a small Stokes-shift. As above, this basic principle of electronic interaction can easily be expanded to a chain of N interacting molecules.

The point-dipole approximation is quite useful to catch the basic photophysical consequences. In molecular aggregates, this approximation is too simplifying as the intermolecular distance is of the same order as the size of the molecules. The point-dipole approximation is not valid for these distances and quantum chemical methods give a more reliable output, see References [136, 137]. This has a qualitative impact as the red-shift for J-aggregates is less pronounced and the inversion point ($V = 0$) depends on the nature of the molecule, the intermolecular separation and non-nearest neighbor interactions.

Additionally, in real systems, structural disorder weakens the H- and J-type characteristics due to deviations from the perfect geometry. Moreover, the Kasha model gives only information about the oscillator strengths but not about efficiencies. Changes in non-radiative decay channels (i.e. internal conversion, inter-system crossing or quenching) are not included in this model as they rely on other parameters like the concentration of trap states, exciton diffusion length and Herzberg-Teller coupling to vibrational modes [137–139]. Defect-free H-type single crystals (see publication 4, section 4.4) can indeed have a high quantum yield [137].

The relative spectral shifts compared to the non-interacting molecule have to be analysed carefully, as they may additionally be superimposed by aggregation-induced changes in molecular structure and polarisability of the environment. Both are especially pronounced in π -stacking systems of conjugated molecules like P3HT [140], see also publication 1 (section 4.1). The shift alone is thus no indicator for H- or J-type aggregation and also the (non-)radiative rates, vibronic progression as well as the impact of structural and electronic disorder have to be taken into account.

2.4.3 Signatures of disorder in molecular aggregates

A more detailed picture which allows for a quantitative analysis of steady state absorption and emission spectra of molecular aggregates was developed in the last decade by Spano and co-workers [133, 141–145]. In addition to the Kasha-Model, electron-phonon (“exciton-phonon”) coupling to a collective carbon-bond stretching mode ($\hbar\omega_{eff} \approx 1400 \text{ cm}^{-1}$) is considered. Furthermore, the effect of disorder can be modelled and analytical expressions are derived which allow a quantitative analysis of absorption and emission spectra. The key concept of this framework is to include vibronic/vibrational pairs in the modelling of excitations. These consist of an electronically and vibrationally excited molecule (vibronic excitation) and a neighbouring molecule which is only vibrationally excited in the electronic ground state. The numerical evaluation with a Frenkel-Holstein-type Hamiltonian contains excitonic coupling, exciton-phonon coupling as well as site-correlated energy disorder. Furthermore, analytical formulas are derived, where disorder is treated perturbatively. Within the definition of Kasha (see above), the cou-

pling between the molecules is assigned to the strong to intermediate coupling regime as $V > \Delta$. Spano further distinguishes between weak and strong “excitonic coupling regimes” by comparing the inter-chain coupling, i.e. the free exciton bandwidth $W = 4V$, with the nuclear relaxation energy $S\hbar\omega_{eff}$ [141, 145]. The weak excitonic coupling regime is therefore valid for $W < S\hbar\omega_{eff}$. Alternatively, this limit is also referred to as strong “exciton-phonon coupling regime” [141].

Within this regime, each vibrational level of the excited state splits up into an exciton band upon aggregation (see Figure 2.9a). In the case of H-type interaction, the absorption takes place into the highest excited state $|A_i\rangle$ of each band which carry most of the oscillator strength. According to Kasha’s rule, the emission stems only from the lowest excited state $|em\rangle$, whereas the pure electronic transition (I_{0-0}) is forbidden by symmetry in ideal H-type aggregates (see above). The resulting vibronic progressions in absorption and emission are thus distorted with respect to the progression of non-interacting chains as discussed in the following.

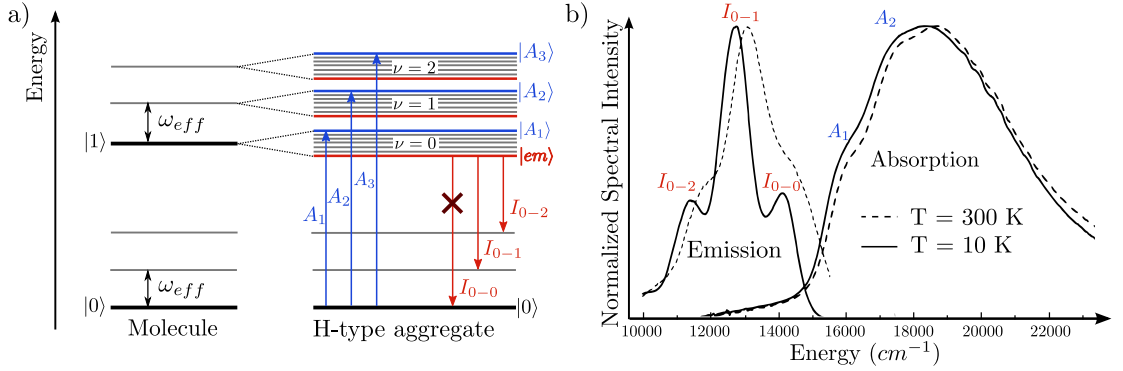


Figure 2.9: Energy level diagram and vibronic signatures in H-type aggregates. a) Energy level structure for a H-type aggregate in the weak exciton phonon coupling regime in comparison to the isolated molecule. The coupling results in a splitting of the vibrational levels ν into exciton bands with the width $We^{-S}S^\nu/\nu!$. In absorption (blue) the bulk of oscillator strength resides in the highest energy level $|A_\nu\rangle$, whereas emission (red) takes place from the lowest excited state $|em\rangle$. b) In absorption and emission spectra the coupling results in distorted vibronic progressions with suppressed A_1 and I_{0-0} peaks, respectively, as illustrated on the example of aggregated P3HT. Data taken from [144].

Absorption As a result of the inter-chain interactions (expressed by the bandwidth W), the A_1 peak intensity decreases with respect to A_2 while that of A_3 increases. To analyse the full absorption spectrum quantitatively, the modified Franck-Condon progression

$$\frac{A(\hbar\omega)}{\hbar\omega n} \propto \sum_{\nu=0} \frac{e^{-S}S^\nu}{\nu!} \left(1 - \frac{We^{-S}}{2\hbar\omega_{eff}}G_\nu\right)^2 \times \exp\left(\frac{(\hbar\omega - E_{A1} - \nu\hbar\omega_{eff})^2}{2\sigma^2}\right) \quad (2.9)$$

was derived [144, 146]. Additional to the peak energy E_{A1} and peak width σ , the exciton bandwidth W is determined by fitting this formula to the experimental data. The vibrational levels are denoted by ν . The factor $G_\nu = \sum_{n \neq \nu} S^n / n!(n - \nu)$ is a sum over the vibrational quantum number n [146]. In the fitting process, the Huang-Rhys parameter S and the vibrational energy $\hbar\omega_{eff}$ are usually kept fixed. They are extracted with a standard Franck-Condon progression from an emission spectrum taken in solution. This is based on the assumption that the Huang-Rhys factor obtained from the solution spectrum is identical to that of the non-interacting building block of the aggregate. However, there is no fixed Huang-Rhys parameter S for a given conjugated polymer, as it strongly depends on the planarity of the backbone (see chapter 2.2 or publication 2). Depending on the flexibility of the backbone, conjugated polymers may planarise upon aggregation, leading to a change in the Huang-Rhys factor of the isolated polymer. This has to be taken into account in the interpretation and analysis of aggregate spectra.

The strength of inter-chain interaction or exciton bandwidth W does not only rely on the orientation and distance of the chains as in the simple model by Kasha. In aggregates of conjugated polymers, the excitation can delocalise in two directions: Along the chains (intra-molecular) and between chains (inter-molecular). Which of these two dominates is the result of a subtle interplay between intra- and inter-chain coupling. It has been shown that an increasing intra-chain delocalisation reduces the inter-chain coupling [15, 37, 147] when the separation between the chains is smaller than the chain length, what is usually the case here. Therefore, intra-chain degrees of freedom like the dihedral angle ϕ which determines the intra-chain coupling have in consequence also a strong impact on the inter-chain interaction and the free exciton bandwidth W . The shape of absorption thus gives insights into the intra-chain coupling strength and disorder as well. The absorption spectrum of P3HT in Figure 2.9b shows only a weak dependence on the temperature. The blue-shift upon cooling is mainly due to thermal expansion of the lattice and the corresponding change in dielectric environment.

Emission The peak ratio I_{0-0}/I_{0-1} in emission is sensitive to the exciton coherence length (along the stacking direction) as well as to disorder. At $T = 0$ and in absence of any intra-aggregate disorder, the I_{0-0} emission is forbidden due to the perfect destructive interference in $|em\rangle$ (coherent origin of I_{0-0}). This rule is weakened by thermal, structural and energetic disorder. As shown in Fig 2.9b on the example of P3HT, the I_{0-0} peak intensity increases with temperature. Thermal excitation allows to access excited states with higher oscillator strength close to the bottom of the lowest vibronic band (with respect to $|em\rangle$). Furthermore, symmetry rules are softened and torsional angles are thermally excited and introduce a stronger site energy disorder. As a consequence of all, the I_{0-0} peak increases in (relative) intensity and broadens (inter-aggregate disorder) upon heating.

In contrast, the relative peak intensities of the vibronic transitions $I_{0-\nu}$ ($\nu > 0$) are not sensitive to disorder and coherence. Accordingly, the total emission spectrum can be fitted by a modified Franck-Condon progression with a suppressed I_{0-0} peak intensity:

$$\frac{I(\hbar\omega)}{(\hbar\omega)^{3n}} \propto \alpha \exp\left(\frac{(\hbar\omega - E_{0-0})^2}{2\sigma^2}\right) + \sum_{\nu=1} \frac{S^\nu}{\nu!} \exp\left(\frac{(\hbar\omega - E_{0-0} - \nu\hbar\omega_{eff})^2}{2\sigma^2}\right). \quad (2.10)$$

Here α denotes the suppression of the I_{0-0} peak with respect to the unperturbed Franck-Condon progression (solution spectrum).

The emission spectrum is very sensitive to the nature of the disordered landscape. Emission may stem from trap states which are populated via intra- and inter-aggregate energy transfer. Not only intra-chain and intra-aggregate disorder but also inter-aggregate energetic disorder has to be taken into account for the interpretation of emission spectra. Thus, there is no simple relationship which connects the exciton coherence length to the shape of the emission spectrum, as it is a complex function of exciton bandwidth, the nature of disorder and the vibronic coupling. The correlation with other data as for example absorption spectra or structure elucidation is useful to differentiate between the individual contributions.

In Publication 3 we show that this framework can also be applied to non- π -stacking conjugated polymers with bulky side-chains. Spano and co-workers extended this framework to describe conjugated polymers as molecular J-type aggregates (see section 2.2.3). Based on that, the two-dimensional exciton delocalisation in aggregates of conjugated polymers can be described as a ‘‘H/J-aggregate’’ [133]. Nevertheless, one has to keep the simplifications of this model in mind. As already mentioned, the assumption that the Huang-Rhys parameter in solution is identical to that of a non-interacting planar chain can be misleading in systems where different conformations exist in solution and crystalline aggregates, for example due to effects like planarisation upon aggregation (see publication 1). Furthermore, Gierschner and co-workers showed the importance of non-nearest neighbour interactions in molecular aggregates, which are largely neglected in the framework of Spano [35].

Also in many studies within this framework, a single (effective) mode is assumed to couple to the optical transition. As already shown for single molecules, usually several modes are coupling to the electronic transition. These and especially low-energy modes are neglected in this framework (an exception is Reference [148]). In low-temperature spectra of single oligomer crystals (see publication 4) these modes are visible. The rich vibronic features of such oligomer crystals cannot be reproduced by this model and a more sophisticated approach is needed [149].

2.5 References

1. Chiang, C. K. *et al.* Electrical Conductivity in Doped Polyacetylene. *Phys. Rev. Lett.* **39**, 1098–1101 (17 1977).
2. Heeger, A. J. 25th Anniversary Article: Bulk Heterojunction Solar Cells: Understanding the Mechanism of Operation. *Adv. Mater.* **26**, 10–27 (1 2014).
3. Sirringhaus, H. 25th Anniversary Article: Organic Field-Effect Transistors: The Path Beyond Amorphous Silicon. *Adv. Mater.* **26**, 1319–1335 (9 2014).
4. Friend, R. H. *et al.* Electroluminescence in conjugated polymers. *Nature* **397**, 121–128 (6715 1999).
5. Lee, H. K. H., Li, Z., Durrant, J. R. & Tsoi, W. C. Is organic photovoltaics promising for indoor applications? *Appl. Phys. Lett.* **108**, 253301 (25 2016).
6. Hamedi, M., Forchheimer, R. & Inganäs, O. Towards woven logic from organic electronic fibres. *Nat. Mater.* **6**, 357–362 (5 2007).
7. Russ, B., Glaudell, A., Urban, J. J., Chabinyk, M. L. & Segalman, R. A. Organic thermoelectric materials for energy harvesting and temperature control. *Nat. Rev. Mater.* **1**, 16050 (10 2016).
8. Klingstedt, T. & Nilsson, K Peter R. Conjugated polymers for enhanced bioimaging. *Biochim. Biophys. Acta* **1810**, 286–296 (3 2011).
9. Liao, C. *et al.* Flexible Organic Electronics in Biology: Materials and Devices. *Adv. Mater.* **27**, 7493–7527 (46 2015).
10. Zhu, C., Liu, L., Yang, Q., Lv, F. & Wang, S. Water-soluble conjugated polymers for imaging, diagnosis, and therapy. *Chem. Rev.* **112**, 4687–4735 (8 2012).
11. Brinkmann, M. Structure and morphology control in thin films of regioregular poly(3-hexylthiophene). *J. Polym. Sci. B* **49**, 1218–1233 (17 2011).
12. Noriega, R. *et al.* A general relationship between disorder, aggregation and charge transport in conjugated polymers. *Nat. Mater.* **12**, 1038–1044 (11 2013).
13. Wang, S. *et al.* Experimental evidence that short-range intermolecular aggregation is sufficient for efficient charge transport in conjugated polymers. *Proc. Natl. Acad. Sci. U. S. A.* **112**, 10599–10604 (34 2015).
14. Yamagata, H. & Spano, F. C. Interplay between intrachain and interchain interactions in semiconducting polymer assemblies: the HJ-aggregate model. *J. Chem. Phys.* **136**, 184901 (18 2012).
15. Gierschner, J. *et al.* Excitonic versus electronic couplings in molecular assemblies: The importance of non-nearest neighbor interactions. *J. Chem. Phys.* **130**, 044105 (4 2009).

16. Moerner, W. E. & Kador, L. Optical detection and spectroscopy of single molecules in a solid. *Phys. Rev. Lett.* **62**, 2535–2538 (21 1989).
17. Orrit & Bernard. Single pentacene molecules detected by fluorescence excitation in a p-terphenyl crystal. *Phys. Rev. Lett.* **65**, 2716–2719 (21 1990).
18. Moerner, W. E. & Fromm, D. P. Methods of single-molecule fluorescence spectroscopy and microscopy. *Rev. Sci. Instrum.* **74**, 3597 (8 2003).
19. Hu *et al.* Collapse of stiff conjugated polymers with chemical defects into ordered, cylindrical conformations. *Nature* **405**, 1030–1033 (6790 2000).
20. Vacha, M. & Habuchi, S. Conformation and physics of polymer chains: a single-molecule perspective. *NPG Asia Mater.* **2**, 134–142 (4 2010).
21. Adachi, T. *et al.* Conformational Effect on Energy Transfer in Single Polythiophene Chains. *J. Phys. Chem. B* **116**, 9866–9872 (32 2012).
22. Tamarat, P., Maali, A., Lounis, B. & Orrit, M. Ten Years of Single-Molecule Spectroscopy. *J. Phys. Chem. A* **104**, 1–16 (1 2000).
23. Hildner, R., Winterling, L., Lemmer, U., Scherf, U. & Köhler, J. Single-molecule spectroscopy on a ladder-type conjugated polymer: electron-phonon coupling and spectral diffusion. *ChemPhysChem* **10**, 2524–2534 (14 2009).
24. Feist, F. A. & Basché, T. Fluorescence excitation and emission spectroscopy on single MEH-PPV chains at low temperature. *J. Phys. Chem. B* **112**, 9700–9708 (32 2008).
25. Chen, P.-Y., Rassamesard, A., Chen, H.-L. & Chen, S.-A. Conformation and Fluorescence Property of Poly(3-hexylthiophene) Isolated Chains Studied by Single Molecule Spectroscopy: Effects of Solvent Quality and Regioregularity. *Macromolecules* **46**, 5657–5663 (14 2013).
26. Thiessen, A. *et al.* Unraveling the chromophoric disorder of poly(3-hexylthiophene). *Proc. Natl. Acad. Sci. U. S. A.* **110**, E3550–6 (38 2013).
27. Hu, Z., Zou, J., Deibel, C., Gesquiere, A. J. & Zhai, L. Single-Molecule Spectroscopy and AFM Morphology Studies of a Diblock Copolymer Consisting of Poly(3-hexylthiophene) and Fullerene. *Macromol. Chem. Phys.* **211**, 2416–2424 (22 2010).
28. Mei, J. & Bao, Z. Side Chain Engineering in Solution-Processable Conjugated Polymers. *Chem. Mater.* **26**, 604–615 (1 2014).
29. Köhler, A. & Bässler, H. *Electronic processes in organic semiconductors* (Wiley-VCH, Weinheim, 2015).
30. Ludwigs, S. *P3HT revisited - from molecular scale to solar cell devices* (Springer, Heidelberg, 2014).

31. Huang, Y., Kramer, E. J., Heeger, A. J. & Bazan, G. C. Bulk heterojunction solar cells: morphology and performance relationships. *Chem. Rev.* **114**, 7006–7043 (14 2014).
32. Barford, W. *Electronic and optical properties of conjugated polymers* 2nd ed. (Oxford University Press, Oxford, 2013).
33. Parson, W. W. *Modern optical spectroscopy* (Springer, Berlin, 2006).
34. Milián-Medina, B. & Gierschner, J. π -Conjugation. *Wiley Interdiscip. Rev. Comput. Mol. Sci.* **2**, 513–524 (4 2012).
35. Gierschner, J., Cornil, J. & Egelhaaf, H.-J. Optical Bandgaps of π -Conjugated Organic Materials at the Polymer Limit: Experiment and Theory. *Adv. Mater.* **19**, 173–191 (2 2007).
36. Su, W. P., Schrieffer, J. R. & Heeger, A. J. Solitons in Polyacetylene. *Phys. Rev. Lett.* **42**, 1698–1701 (25 1979).
37. Cornil, J., dos Santos, D. A., Crispin, X., Silbey, R. & Brédas, J. L. Influence of Interchain Interactions on the Absorption and Luminescence of Conjugated Oligomers and Polymers. A Quantum-Chemical Characterization. *J. Am. Chem. Soc.* **120**, 1289–1299 (6 1998).
38. Hennebicq, E., Deleener, C., Brédas, J.-L., Scholes, G. D. & Beljonne, D. Chromophores in phenylenevinylene-based conjugated polymers. Role of conformational kinks and chemical defects. *J. Chem. Phys.* **125**, 054901 (5 2006).
39. Brédas, J.-L., Beljonne, D., Coropceanu, V. & Cornil, J. Charge-transfer and energy-transfer processes in π -conjugated oligomers and polymers: a molecular picture. *Chem. Rev.* **104**, 4971–5004 (11 2004).
40. Becker, R. S., Seixas de Melo, J., Maçanita, A. L. & Elisei, F. Comprehensive Evaluation of the Absorption, Photophysical, Energy Transfer, Structural, and Theoretical Properties of α -Oligothiophenes with One to Seven Rings. *J. Phys. Chem.* **100**, 18683–18695 (48 1996).
41. Rossi, G., Chance, R. R. & Silbey, R. Conformational disorder in conjugated polymers. *J. Chem. Phys.* **90**, 7594 (12 1989).
42. de Queiroz, Thiago B & Kümmel, S. Charge-transfer excitations in low-gap systems under the influence of solvation and conformational disorder: exploring range-separation tuning. *J. Chem. Phys.* **141**, 084303 (8 2014).
43. Barford, W. Excitons in conjugated polymers: a tale of two particles. *J. Phys. Chem. A* **117**, 2665–2671 (13 2013).

44. Barford, W. & Marcus, M. Perspective: Optical spectroscopy in π -conjugated polymers and how it can be used to determine multiscale polymer structures. *J. Chem. Phys.* **146**, 130902 (13 2017).
45. Kobayashi, H., Tsuchiya, K., Ogino, K. & Vacha, M. Spectral multitude and spectral dynamics reflect changing conjugation length in single molecules of oligo-phenylenevinylenes. *Phys. Chem. Chem. Phys.* **14**, 10114–10118 (29 2012).
46. Yang, J. *et al.* Inhomogeneity in the excited-state torsional disorder of a conjugated macrocycle. *J. Phys. Chem. B* **119**, 4116–4126 (10 2015).
47. Romaner, L. *et al.* Ketonic Defects in Ladder-type Poly(p-phenylene)s. *Chem. Mater.* **16**, 4667–4674 (23 2004).
48. De Leener, C., Hennebicq, E., Sancho-Garcia, J.-C. & Beljonne, D. Modeling the dynamics of chromophores in conjugated polymers: the case of poly(2-methoxy-5-(2'-ethylhexyl)oxy 1,4-phenylene vinylene) (MEH-PPV). *J. Phys. Chem. B* **113**, 1311–1322 (5 2009).
49. Northrup, J. E. Radiation Induced Hydrogen Rearrangement in Poly(3-alkylthiophene). *Appl. Phys. Express* **6**, 121601 (12 2013).
50. Cook, S., Furube, A. & Katoh, R. Matter of minutes degradation of poly(3-hexylthiophene) under illumination in air. *J. Mater. Chem.* **22**, 4282–4289 (10 2012).
51. Zhang, Z.-G. & Li, Y. Side-chain engineering of high-efficiency conjugated polymer photovoltaic materials. *Sci. China Chem.* **58**, 192–209 (2 2015).
52. Shao, B., Zhu, X., Plunkett, K. N. & Vanden Bout, David A. Controlling the folding of conjugated polymers at the single molecule level via hydrogen bonding. *Polym. Chem.* (2017).
53. Sharber, S. A. *et al.* Substituent Effects That Control Conjugated Oligomer Conformation through Non-covalent Interactions. *J. Am. Chem. Soc.* (2017).
54. Do, K. *et al.* Impact of Fluorine Substituents on π -Conjugated Polymer Main-Chain Conformations, Packing, and Electronic Couplings. *Adv. Mater.* **28**, 8197–8205 (37 2016).
55. Lombeck, F. *et al.* PCDTBT: From Polymer Photovoltaics to Light-Emitting Diodes by Side-Chain-Controlled Luminescence. *Macromolecules* **49**, 9382–9387 (24 2016).
56. Hu, Z. *et al.* Excitonic energy migration in conjugated polymers: the critical role of interchain morphology. *J. Am. Chem. Soc.* **136**, 16023–16031 (45 2014).

57. Sugimoto, T., Habuchi, S., Ogino, K. & Vacha, M. Conformation-related exciton localization and charge-pair formation in polythiophenes: ensemble and single-molecule study. *J. Phys. Chem. B* **113**, 12220–12226 (36 2009).
58. Hu, Z. *et al.* Effect of the side-chain-distribution density on the single-conjugated-polymer-chain conformation. *ChemPhysChem* **14**, 4143–4148 (18 2013).
59. Jackson, N. E. *et al.* Controlling conformations of conjugated polymers and small molecules: the role of nonbonding interactions. *J. Am. Chem. Soc.* **135**, 10475–10483 (28 2013).
60. Mueller, C. J., Gann, E., Singh, C. R., Thelakkat, M. & McNeill, C. R. Control of Molecular Orientation in Polydiketopyrrolopyrrole Copolymers via Diffusive Noncovalent Interactions. *Chem. Mater.* **28**, 7088–7097 (19 2016).
61. Mueller, C. J., Singh, C. R., Fried, M., Huettner, S. & Thelakkat, M. High Bulk Electron Mobility Diketopyrrolopyrrole Copolymers with Perfluorothiophene. *Adv. Funct. Mater.* **25**, 2725–2736 (18 2015).
62. Milian-Medina, B. & Gierschner, J. Though It Be but Little, It Is Fierce: Excited State Engineering of Conjugated Organic Materials by Fluorination. *J. Phys. Chem. Lett.* **8**, 91–101 (1 2017).
63. Hu, Z. *et al.* Impact of backbone fluorination on nanoscale morphology and excitonic coupling in polythiophenes. *Proc. Natl. Acad. Sci. U. S. A.* **114**, 5113–5118 (20 2017).
64. Milad, R. *et al.* Effective conjugation in conjugated polymers with strongly twisted backbones. A case study on fluorinated MEHPPV. *J. Mater. Chem. C* **4**, 6900–6906 (28 2016).
65. Barbarella, G., Bongini, A. & Zambianchi, M. Regiochemistry and Conformation of Poly(3-hexylthiophene) via the Synthesis and the Spectroscopic Characterization of the Model Configurational Triads. *Macromolecules* **27**, 3039–3045 (11 1994).
66. Adachi, T. *et al.* Regioregularity and Single Polythiophene Chain Conformation. *J. Phys. Chem. Lett.* **2**, 1400–1404 (12 2011).
67. McCulloch, B. *et al.* Polymer Chain Shape of Poly(3-alkylthiophenes) in Solution Using Small-Angle Neutron Scattering. *Macromolecules* **46**, 1899–1907 (5 2013).
68. Brambilla, L. *et al.* Regio-Regular Oligo and Poly(3-hexyl thiophene): Precise Structural Markers from the Vibrational Spectra of Oligomer Single Crystals. *Macromolecules* **47**, 6730–6739 (19 2014).

69. Lohwasser, R. H. & Thelakkat, M. Toward Perfect Control of End Groups and Polydispersity in Poly(3-hexylthiophene) via Catalyst Transfer Polymerization. *Macromolecules* **44**, 3388–3397 (9 2011).
70. Schiefer, D. *et al.* Poly(3-(2,5-dioctylphenyl)thiophene) Synthesized by Direct Arylation Polycondensation. End Groups, Defects, and Crystallinity. *Macromolecules* **49**, 7230–7237 (19 2016).
71. Renge, I. Mechanisms of Solvent Shifts, Pressure Shifts, and Inhomogeneous Broadening of the Optical Spectra of Dyes in Liquids and Low-Temperature Glasses. *J. Phys. Chem. A* **104**, 7452–7463 (32 2000).
72. Renger, T., Grundkotter, B., Madjet, M. E.-A. & Muh, F. Theory of solvatochromic shifts in nonpolar solvents reveals a new spectroscopic rule. *Proc. Natl. Acad. Sci. U. S. A.* **105**, 13235–13240 (36 2008).
73. Wilma, K. *et al.* Tracing Single Electrons in a Disordered Polymer Film at Room Temperature. *J. Phys. Chem. Lett.* **7**, 1478–1483 (8 2016).
74. Huser, T., Yan, M. & Rothberg, L. J. Single chain spectroscopy of conformational dependence of conjugated polymer photophysics. *Proc. Natl. Acad. Sci. U. S. A.* **97**, 11187–11191 (21 2000).
75. Lupton, J. M. Single-molecule spectroscopy for plastic electronics: materials analysis from the bottom-up. *Adv. Mater.* **22**, 1689–1721 (15 2010).
76. Kolinski, A., Skolnick, J. & Yaris, R. The collapse transition of semiflexible polymers. A Monte Carlo simulation of a model system. *J. Chem. Phys.* **85**, 3585 (6 1986).
77. Feist, F. A., Zickler, M. F. & Basché, T. Origin of the red sites and energy transfer rates in single MEH-PPV chains at low temperature. *ChemPhysChem* **12**, 1499–1508 (8 2011).
78. Rubinstein, M. & Colby, R. H. *Polymer Physics* (Oxford University Press, Oxford and NY, 2003).
79. Strobl, G. R. *The Physics of Polymers. Concepts for Understanding Their Structures and Behavior* 3rd revised and expanded ed. (Springer, Berlin, 2007).
80. Kuei, B. & Gomez, E. D. Chain conformations and phase behavior of conjugated polymers. *Soft Matter* **13**, 49–67 (1 2016).
81. Westenhoff, S. *et al.* Anomalous Energy Transfer Dynamics due to Torsional Relaxation in a Conjugated Polymer. *Phys. Rev. Lett.* **97**, 166804 (16 2006).
82. Wells, N. P. & Blank, D. A. Correlated Exciton Relaxation in Poly(3-hexylthiophene). *Phys. Rev. Lett.* **100**, 086403 (8 2008).

83. Parkinson, P., Müller, C., Stingelin, N., Johnston, M. B. & Herz, L. M. Role of Ultrafast Torsional Relaxation in the Emission from Polythiophene Aggregates. *J. Phys. Chem. Lett.* **1**, 2788–2792 (19 2010).
84. Collini, E. & Scholes, G. D. Coherent intrachain energy migration in a conjugated polymer at room temperature. *Science* **323**, 369–373 (5912 2009).
85. Hildner, R., Lemmer, U., Scherf, U., van Heel, M. & Köhler, J. Revealing the Electron–Phonon Coupling in a Conjugated Polymer by Single-Molecule Spectroscopy. *Adv. Mater.* **19**, 1978–1982 (15 2007).
86. Simine, L. & Rossky, P. J. Relating Chromophoric and Structural Disorder in Conjugated Polymers. *J. Phys. Chem. Lett.* 1752–1756 (2017).
87. Marcus, M., Tozer, O. R. & Barford, W. Theory of optical transitions in conjugated polymers. II. Real systems. *J. Chem. Phys.* **141**, 164102 (16 2014).
88. Schwartz, B. J. Conjugated polymers as molecular materials: how chain conformation and film morphology influence energy transfer and interchain interactions. *Annu. Rev. Phys. Chem.* **54**, 141–172 (2003).
89. Hollars, C. W., Lane, S. M. & Huser, T. Controlled non-classical photon emission from single conjugated polymer molecules. *Chem. Phys. Lett.* **370**, 393–398 (3-4 2003).
90. Barbara, P. F., Gesquiere, A. J., Park, S.-J. & Lee, Y. J. Single-molecule spectroscopy of conjugated polymers. *Acc. Chem. Res.* **38**, 602–610 (7 2005).
91. Beenken, Wichard J. D. Excitons in conjugated polymers. Do we need a paradigm change? *Phys. Status Solidi A* **12**, 2750–2756 (2009).
92. Chang, R. *et al.* Experimental and theoretical investigations of absorption and emission spectra of the light-emitting polymer MEH-PPV in solution. *Chem. Phys. Lett.* **317**, 142–152 (1-2 2000).
93. Tilgner, A., Trommsdorff, H. P., Zeigler, J. M. & Hochstrasser, R. M. Poly(di-n-hexyl-silane) in solid solutions: Experimental and theoretical studies of electronic excitations of a disordered linear chain. *J. Chem. Phys.* **96**, 781 (1 1992).
94. Barford, W., Marcus, M. & Tozer, O. R. Polarons in π -Conjugated Polymers: Anderson or Landau? *J. Phys. Chem. A* **120**, 615–620 (4 2016).
95. Ruseckas, A. *et al.* Ultrafast depolarization of the fluorescence in a conjugated polymer. *Phys. Rev. B* **72**, 474 (11 2005).
96. Kim, P. *et al.* Relationship between Dynamic Planarization Processes and Exciton Delocalization in Cyclic Oligothiophenes. *J. Phys. Chem. Lett.* **6**, 451–456 (3 2015).

-
97. Dubin, F. *et al.* Macroscopic coherence of a single exciton state in an organic quantum wire. *Nat. Phys.* **2**, 32–35 (1 2005).
 98. Schindler, F. *et al.* Counting Chromophores in Conjugated Polymers. *Angew. Chem.* **117**, 1544–1549 (10 2005).
 99. Lin, H. *et al.* Fluorescence blinking, exciton dynamics, and energy transfer domains in single conjugated polymer chains. *J. Am. Chem. Soc.* **130**, 7042–7051 (22 2008).
 100. Zickler, M. F., Feist, F. A., Jacob, J., Müllen, K. & Basché, T. Single molecule studies of a ladder type conjugated polymer: vibronic spectra, line widths, and energy transfer. *Macromol. Rapid Commun.* **36**, 1096–1102 (11 2015).
 101. Beljonne, D., Cornil, J., Friend, R. H., Janssen, R. A. J. & Brédas, J.-L. Influence of Chain Length and Derivatization on the Lowest Singlet and Triplet States and Intersystem Crossing in Oligothiophenes. *J. Am. Chem. Soc.* **118**, 6453–6461 (27 1996).
 102. Zade, S. S. & Bendikov, M. Twisting of conjugated oligomers and polymers: case study of oligo- and polythiophene. *Chem. Eur. J.* **13**, 3688–3700 (13 2007).
 103. Karolewski, A., Neubig, A., Thelakkat, M. & Kümmel, S. Optical absorption in donor-acceptor polymers—alternating vs. random. *Phys. Chem. Chem. Phys.* **15**, 20016–20025 (46 2013).
 104. de Queiroz, Thiago B & Kümmel, S. Tuned range separated hybrid functionals for solvated low bandgap oligomers. *J. Chem. Phys.* **143**, 034101 (3 2015).
 105. Barford, W. & Marcus, M. Theory of optical transitions in conjugated polymers. I. Ideal systems. *J. Chem. Phys.* **141**, 164101 (16 2014).
 106. Barford, W. & Tozer, O. R. Theory of exciton transfer and diffusion in conjugated polymers. *J. Chem. Phys.* **141**, 164103 (16 2014).
 107. Barford, W., Lidzey, D. G., Makhov, D. V. & Meijer, Anthony J H. Exciton localization in disordered poly(3-hexylthiophene). *J. Chem. Phys.* **133**, 044504 (4 2010).
 108. Yamagata, H. & Spano, F. C. Strong Photophysical Similarities between Conjugated Polymers and J-aggregates. *J. Phys. Chem. Lett.* **5**, 622–632 (3 2014).
 109. Yamagata, H. & Spano, F. C. Vibronic coupling in quantum wires: applications to polydiacetylene. *J. Chem. Phys.* **135**, 054906 (5 2011).
 110. Hohenberg, P. & Kohn, W. Inhomogeneous Electron Gas. *Phys. Rev.* **136**, B864–B871 (3B 1964).
 111. Kohn, W. & Sham, L. J. Self-Consistent Equations Including Exchange and Correlation Effects. *Phys. Rev.* **140**, A1133–A1138 (4A 1965).

112. Becke, A. D. Perspective. Fifty years of density-functional theory in chemical physics. *J. Chem. Phys.* **140**, 18A301 (18 2014).
113. Maitra, N. T. Perspective. Fundamental aspects of time-dependent density functional theory. *J. Chem. Phys.* **144**, 220901 (22 2016).
114. Kümmel, S. Charge-Transfer Excitations: A Challenge for Time-Dependent Density Functional Theory That Has Been Met. *Adv. Energy Mater.* **42**, 1700440 (2017).
115. Darling, S. B. & Sternberg, M. Importance of side chains and backbone length in defect modeling of poly(3-alkylthiophenes). *J. Phys. Chem. B* **113**, 6215–6218 (18 2009).
116. Bhatta, R. S., Yimer, Y. Y., Tsige, M. & Perry, D. S. Conformations and torsional potentials of poly(3-hexylthiophene) oligomers: Density functional calculations up to the dodecamer. *Comput. Theor. Chem.* **995**, 36–42 (2012).
117. Bhatta, R. S., Tsige, M. & Perry, D. S. Torsionally-Induced Blue Shift of the Band Gap in Poly(3-Hexylthiophene). *J. Comput. Theor. Nanosci.* **11**, 2157–2164 (10 2014).
118. Baderschneider, S., Scherf, U., Köhler, J. & Hildner, R. Influence of the Conjugation Length on the Optical Spectra of Single Ladder-Type (p-Phenylene) Dimers and Polymers. *J. Phys. Chem. A* **120**, 233–240 (2 2016).
119. Hildner, R. *Investigation of the photophysical properties of π -conjugated polymers. a study by non-linear, time-resolved, and single-molecule spectroscopy* Dissertation (Universität Bayreuth, Bayreuth, 2008).
120. Rebane, L. A., Gorokhovskii, A. A. & Kikas, J. V. Low-temperature spectroscopy of organic molecules in solids by photochemical hole burning. *Appl. Phys. B* **29**, 235–250 (4 1982).
121. Orrit, M., Bernard, J. & Personov, R. I. High-resolution spectroscopy of organic molecules in solids. From fluorescence line narrowing and hole burning to single molecule spectroscopy. *J. Phys. Chem.* **97**, 10256–10268 (40 1993).
122. Naumov, A. V. Low-temperature spectroscopy of organic molecules in solid matrices: from the Shpol'skii effect to laser luminescent spectromicroscopy for all effectively emitting single molecules. *Phys.-Usp.* **56**, 605–622 (6 2013).
123. Hofmann, C., Michel, H., van Heel, M. & Köhler, J. Multivariate analysis of single-molecule spectra: surpassing spectral diffusion. *Phys. Rev. Lett.* **94**, 195501 (19 2005).

-
124. Baier, J., Richter, M., Cogdell, R. J., Oellerich, S. & Köhler, J. Determination of the Spectral Diffusion Kernel of a Protein by Single-Molecule Spectroscopy. *Phys. Rev. Lett.* **100**, 018108 (1 2008).
 125. Donohoo-Vallett, P. J. & Bragg, A. E. π -Delocalization and the vibrational spectroscopy of conjugated materials: computational insights on Raman frequency dispersion in thiophene, furan, and pyrrole oligomers. *J. Phys. Chem. B* **119**, 3583–3594 (8 2015).
 126. Khlaifia, D. *et al.* Unraveling the real structures of solution-based and surface-bound poly(3-hexylthiophene) (P3HT) oligomers. A combined theoretical and experimental study. *RSC Adv.* **6**, 56174–56182 (61 2016).
 127. Wise, A. & Grey, J. Understanding the Structural Evolution of Single Conjugated Polymer Chain Conformers. *Polymers* **8**, 388 (11 2016).
 128. Bjorgaard, J. A. & Köse, M. E. Theoretical study of torsional disorder in poly(3-alkylthiophene) single chains: intramolecular charge-transfer character and implications for photovoltaic properties. *J. Phys. Chem. A* **117**, 3869–3876 (18 2013).
 129. Moerner, W. E. A Dozen Years of Single-Molecule Spectroscopy in Physics, Chemistry, and Biophysics. *J. Phys. Chem. B* **106**, 910–927 (5 2002).
 130. Friedrich, J. & Haarer, D. Photochemical Hole Burning: A Spectroscopic Study of Relaxation Processes in Polymers and Glasses. *Angew. Chem. Int. Ed.* **23**, 113–140 (2 1984).
 131. Kador, L. Stochastic theory of inhomogeneous spectroscopic line shapes reinvestigated. *J. Chem. Phys.* **95**, 5574 (8 1991).
 132. Negri, F. & Zgierski, M. Z. The vibronic structure of the $S_0 \leftrightarrow S_1$ and $S_0 \leftrightarrow S_2$ transitions in simple oligomers of thiophene. *J. Chem. Phys.* **100**, 2571–2587 (4 1994).
 133. Spano, F. C. & Silva, C. H- and J-aggregate behavior in polymeric semiconductors. *Annu. Rev. Phys. Chem.* **65**, 477–500 (2014).
 134. Hestand, N. J. & Spano, F. C. Determining the spatial coherence of excitons from the photoluminescence spectrum in charge-transfer J-aggregates. *Chem. Phys.* **481**, 262–271 (2016).
 135. Kasha, M., Rawls, H. R. & Ashraf El-Bayoumi, M. The exciton model in molecular spectroscopy. *Pure Appl. Chem.* **11** (3-4 1965).
 136. Beljonne, D., Curutchet, C., Scholes, G. D. & Silbey, R. J. Beyond Förster resonance energy transfer in biological and nanoscale systems. *J. Phys. Chem. B* **113**, 6583–6599 (19 2009).

137. Gierschner, J. & Park, S. Y. Luminescent distyrylbenzenes: Tailoring molecular structure and crystalline morphology. *J. Mater. Chem. C* **1**, 5818 (37 2013).
138. Gierschner, J., Lüer, L., Milián-Medina, B., Oelkrug, D. & Egelhaaf, H.-J. Highly Emissive H-Aggregates or Aggregation-Induced Emission Quenching? The Photophysics of All-Trans para-Distyrylbenzene. *J. Phys. Chem. Lett.* **4**, 2686–2697 (16 2013).
139. Shi, J. *et al.* Solid State Luminescence Enhancement in π -Conjugated Materials. Unraveling the Mechanism beyond the Framework of AIE/AIEE. *J. Phys. Chem. C* **121**, 23166–23183 (41 2017).
140. Brown, P. J. *et al.* Effect of interchain interactions on the absorption and emission of poly(3-hexylthiophene). *Phys. Rev. B* **67**, 064203 (6 2003).
141. Spano, F. C. Modeling disorder in polymer aggregates: The optical spectroscopy of regioregular poly(3-hexylthiophene) thin films. *J. Chem. Phys.* **122**, 234701 (23 2005).
142. Spano, F. C. Absorption in regio-regular poly(3-hexyl)thiophene thin films. Fermi resonances, interband coupling and disorder. *Chem. Phys.* **325**, 22–35 (1 2006).
143. Clark, J., Silva, C., Friend, R. H. & Spano, F. C. Role of Intermolecular Coupling in the Photophysics of Disordered Organic Semiconductors: Aggregate Emission in Regioregular Polythiophene. *Phys. Rev. Lett.* **98**, 206406 (20 2007).
144. Spano, F. C., Clark, J., Silva, C. & Friend, R. H. Determining exciton coherence from the photoluminescence spectral line shape in poly(3-hexylthiophene) thin films. *J. Chem. Phys.* **130**, 074904 (7 2009).
145. Spano, F. C. The spectral signatures of Frenkel polarons in H- and J-aggregates. *Acc. Chem. Res.* **43**, 429–439 (3 2010).
146. Clark, J., Chang, J.-F., Spano, F. C., Friend, R. H. & Silva, C. Determining exciton bandwidth and film microstructure in polythiophene films using linear absorption spectroscopy. *Appl. Phys. Lett.* **94**, 163306 (16 2009).
147. Barford, W. Exciton transfer integrals between polymer chains. *J. Chem. Phys.* **126**, 134905 (13 2007).
148. Spano, F. C. & Silvestri, L. Multiple mode exciton-vibrational coupling in H-aggregates. Synergistic enhancement of the quantum yield. *J. Chem. Phys.* **132**, 094704 (9 2010).
149. Wykes, M., Parambil, R., Beljonne, D. & Gierschner, J. Vibronic coupling in molecular crystals: A Franck-Condon Herzberg-Teller model of H-aggregate fluorescence based on quantum chemical cluster calculations. *J. Chem. Phys.* **143**, 114116 (11 2015).

3 Overview of the publications

3.1 Connection

Understanding, quantifying and predicting disorder phenomena in conjugated polymers is an important step towards higher device efficiencies in the field of organic semiconductors. Disorder does not only influence the morphology of the polymer films and blends but has fundamental impact on the photophysical properties of single conjugated polymers and aggregates.

Despite this importance, systematic studies on the impact of disorder on the molecular level are scarce. One reason is the complexity and the numerous degrees of freedom of conjugated polymers even at the level of single chains. As shown in Figure 3.1, the polymers can adopt various overall conformations and explore a set of dihedral angles ϕ between the repeating units given by the torsional potential. Both degrees of freedom are influenced by artefacts from synthesis like regioirregularities or chemical defects which disrupt the conjugated path. In addition, there are non-covalent interactions introduced by side-chains as well as structural disorder within the dielectric environment. All these factors influence the photophysical and excited state properties like electron-phonon coupling, conjugation length or electron-hole separation. Complexity and disorder rise even more upon including inter-chain interactions. Electronic coupling between the chains as well as potential changes in the conformation and the dielectric environment depend strongly on the distance and mutual orientation of neighbouring chains.

As a consequence, the approach of this thesis was to start at the molecular level and develop a comprehensive picture of the influence of disorder on single chains (publications 1 and 2). Based on these studies, inter-chain disorder in larger, crystalline aggregates was investigated (publications 3 and 4), see Figure 3.1. As a model system we chose polythiophenes, which are widely used for organic photovoltaics and electronics. In particular poly(3-hexylthiophene) (P3HT) is both used as a benchmark system for device engineering and fundamental research on electronic processes in organic semiconductors. However, from experimental as well as theoretical point of view there is still no general consensus about the intrinsic properties of this important polymer. Especially the degree of (inhomogeneous) intra-chain electronic disorder, the influence of the side-chains on the torsional potential and the impact of the chain length on the photophysical properties are up for debate.

Single-molecule spectroscopy allowed us to exclude the various effects of inter-chain interactions. Furthermore, we use defined samples of high chemical quality, i.e. low polydispersity and high regioregularity (Ruth Lohwasser & Mukundan Thelakkat, Daniel Schiefer & Michael Sommer, Bayreuth and Freiburg). The influence of the overall conformation (and thus potential intra-chain inter-chromophoric interactions) was excluded by the choice of short chains in which the possibility of back-folding and the influence of the solvent on the conformation is negligible. Cryogenic temperatures ($T = 1.5$ K) gave detailed insights into line broadening mechanism (dynamic disorder) and vibronic signatures which are not resolvable at room temperature. The static energetic disorder (inhomogeneous distribution) further allowed us to estimate the intrinsic electronic disorder of a given sample. The measurements were further supported by time-dependent density functional theory (Thiago de Queiroz & Stephan Kümmel, Bayreuth) and quantum-classical atomistic simulation (Lena Simine & Peter Rossky, Rice University Houston). By this combination of single-molecule experiments and simulations, a deeper understanding of the influence of disorder on exciton delocalisation lengths and charge-transfer character of the excitations was developed.

In the first publication (section 4.1) we studied single, isolated regioregular P3HT chains with different, but well-defined molecular weights, to reveal intra-chain properties of their emitting sites. It turns out that the emitting species in P3HT is surprisingly well-defined and furthermore strongly blue-shifted with respect to disordered ensemble spectra. We ascribe this differences to planarisation upon aggregation as well as long-range electronic interactions between polymer segments in disordered films. Importantly, such loose aggregates are also the dominant emitting species in (dilute) solutions of good solvents. By comparing the results to amorphous and crystalline films as well as concentration-dependent measurements, we developed a comprehensive picture of P3HT, ranging from single, isolated chains to bulk structures. Thus, this publication provides important reference parameters for theoretical modelling (i.e. position and width of the inhomogeneous distribution of transition energies) as well as valuable input for the interpretation of ensemble spectra.

Based on these results, the second publication (section 4.2) is devoted to the influence of side-chains on the photophysical properties of a given conjugated backbone. Therefore, we examined a second polythiophene, poly(3-(2,5-dioctylphenyl)thiophene) (PDOPT) which, in contrast to P3HT, has very bulky side-chains, see Figure 3.1. Again, we selected defined samples of high regioregularity, low polydispersity and controlled chain lengths and performed the experiments under identical conditions as for P3HT. Surprisingly, the single-chain spectra showed strong differences in transition energy, vibronic signatures (electron-phonon coupling) as well as static and dynamic disorder. Quantum-classical atomistic simulations confirmed the shift in transition energy which originates in a side-chain induced backbone planarisation in PDOPT. At the same time, the conjugation

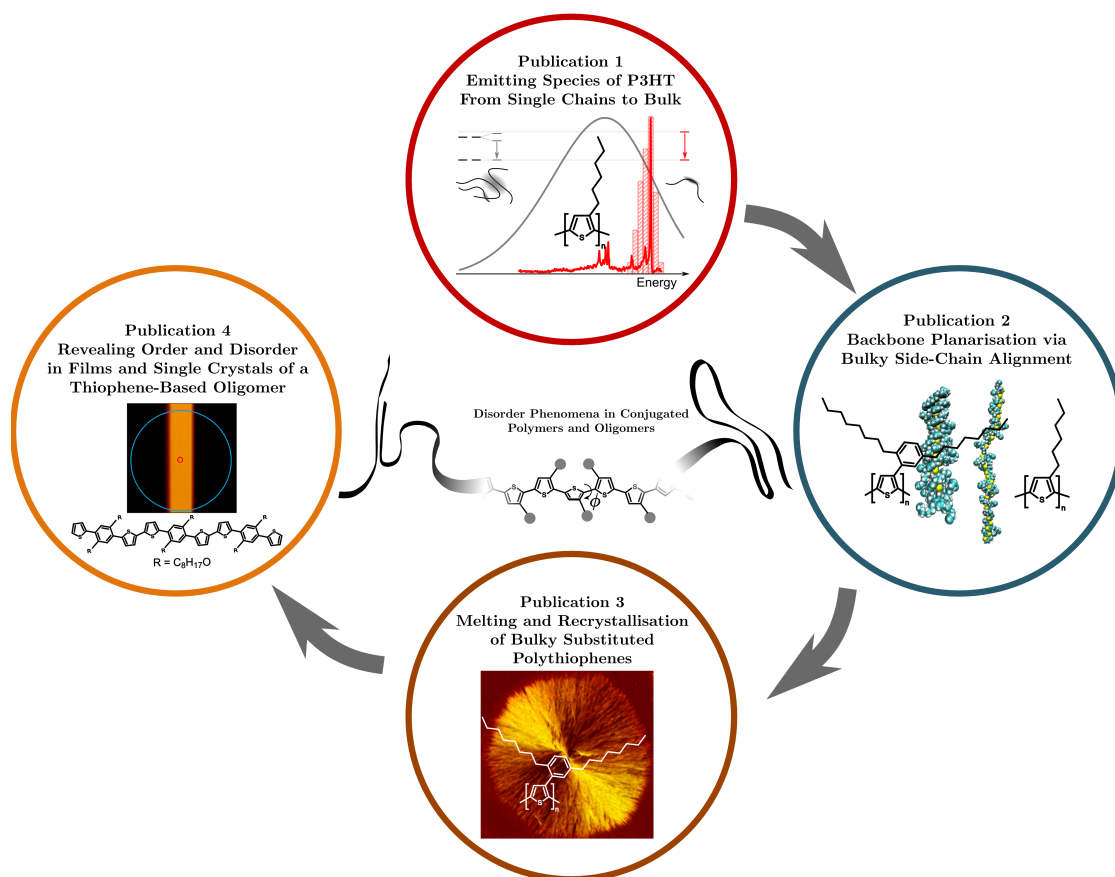


Figure 3.1: Overview of the thesis. The effects of disorder in conjugated polymers were studied at the single-chain level as well as in macroscopic bulk structures. First, well defined P3HT chains were studied with single-molecule spectroscopy. These results were compared with PDOPT, an equally defined thiophene with a bulkier side-chain. Based on that, the spectral characteristics of PDOPT spherulites were examined in publication 3 as a function of thermally induced disorder. Finally, highly defined single crystals of a thiophene-based oligomer were investigated in publication 4.

length is unaffected by the enhanced planarity. However, a reduction of the electron-hole separation in PDOPT in comparison to P3HT was observed. Furthermore we showed a new possibility to control the dihedral angle in conjugated polymers, which is of central importance for the photophysical properties. In the absence of other contributions (like aggregation induced planarisation) the inhomogeneous distribution function is strongly connected to the torsional potential of the dihedral angle. Up to now, this quantity is not measurable with other techniques in the case of isolated, non-interacting chains and thus emphasizes the importance of single-molecule spectroscopy on conjugated polymers.

In the third publication (section 4.3) we departed from the single-molecule perspective and transferred our knowledge of single PDOPT chains to defined crystalline films. By isothermal crystallisation of PDOPT, spherulitic crystals (spherulites) with a diameter of several 100 μm and a well-defined molecular order were grown (Fanuel Keheze

& Günter Reiter, Freiburg). We gradually increased intra- and inter-chain disorder by heating this structure up to and beyond its melting temperature. The spectral signatures in absorption and emission upon this order-disorder transition were correlated with the known crystal structure, with differential scanning calorimetry measurements as well as with single-chain properties. Although the PDOPT chains do not aggregate by direct π - π -stacking, they can nevertheless be described as H-type aggregates since the transition dipole moments of neighbouring chromophores are oriented parallel with respect to each other. This allowed us to quantify the order-disorder transition by analysing absorption and emission with the distorted vibronic progressions for molecular H-aggregates introduced by Spano and co-workers. The thermal induced increase in torsional disorder dominates the changes in absorption and emission spectra; The reduced intra-chain does not only lead to a rise in transition energy (see papers 1 and 2) but in consequence also to an enhancement of the inter-chain electronic coupling. Therefore, also in crystalline structures, the exact knowledge about the distribution of dihedral angles is of central importance for modelling and understanding inter-chain interactions.

In publication 4 (chapter 4.4), we focused on highly defined, macroscopic crystals of a thiophene-based oligomer (Sajedeh Motamen & Günter Reiter, Freiburg). By changing the processing conditions (slowly crystallised vs. spin-coated), we investigated the impact of variable degree of structural order on the electronic coupling between the chains. The macroscopic dimensions and the high quality of the single crystals allowed us to address differently processed crystallites separately. Both crystalline phases show the spectral characteristics of H-type aggregates in absorption as well as emission. The single crystal exhibits a higher excitonic coupling and a stronger suppression of the I_{0-0} peak in emission with respect to the more disordered film, which consists of smaller crystallites with potential non-interacting chains in-between. Low-temperature emission spectra of single crystals show, similar as observed for P3HT single chains, that not only vibronic carbon-bond stretching modes ($\hbar\omega \approx 1400 \text{ cm}^{-1}$) but also vibrations with intermediate energy ($\hbar\omega \approx 200 - 1000 \text{ cm}^{-1}$) are coupling significantly to the electronic transition.

The main results of the publications are shortly summarised in the following. More details about the samples, experiments and analysis can be found in the respective sections 4.1 - 4.4.

3.2 Individual Contribution

Publication 1: **D. Raithel**, S. Baderschneider, T. B. de Queiroz, R. Lohwasser, J. Köhler, M. Thelakkat, S. Kümmel, R. Hildner

Emitting Species of Poly(3-hexylthiophene): From Single, Isolated Chains to Bulk
Macromolecules 49 (2016) 9553.

Contribution: I performed all described measurements, including low-temperature single-chain spectra of P3HT and low-temperature concentration dependent measurements. I analysed the experimental data and interpreted it in the context of the simulations by Thiago B. de Queiroz. Furthermore I wrote the paper together with Richard Hildner.

Publication 2: **D. Raithel**, L. Simine, S. Pickel, K. Schötz, F. Panzer, S. Baderschneider, D. Schiefer, R. Lohwasser, J. Köhler, M. Thelakkat, M. Sommer, A. Köhler, P.J. Rossky, R. Hildner

Direct observation of backbone planarisation via side-chain alignment in single bulky-substituted polythiophenes

Proc. Nat. Acad. Sci. U.S.A. 115 (2018) 2699.

Contribution: I measured the low-temperature single-chain spectra of PDOPT together with Sebastian Pickel. I assisted in the Franck-Condon analysis of the temperature dependent solution spectra. I analysed all experimental data, compared it with our recent results on P3HT (see above) and interpreted it in the context of the simulations by Lena Simine. Furthermore I wrote the paper together with Lena Simine and Richard Hildner.

Publication 3: F. M. Keheze, **D. Raithel**, T. Wu, D. Schiefer, M. Sommer, R. Hildner, G. Reiter

Signatures of Melting and Recrystallization of a Bulky Substituted Poly(thiophene) Identified by Optical Spectroscopy

Macromolecules 50 (2017) 6829.

Contribution: I supported Fanuel Keheze in practical aspects of spectroscopy. Furthermore I performed the whole quantitative analysis of absorption and photoluminescence spectra with a home-written python script based on modified Franck-Condon progressions. I interpreted the results of the fits, wrote the corresponding part of the manuscript together with Richard Hildner and reviewed the paper.

Publication 4: S. Motamen, **D. Raithel**, R. Hildner, R. Khosrow, T. Jarrosson, F. Serein-Spirau, L. Simon, G. Reiter

Revealing Order and Disorder in Films and Single Crystals of a Thiophene-Based Oligomer by Optical Spectroscopy

ACS Photonics 3 (2016) 2315.

Contribution: I performed and analysed low-temperature measurements on the single crystals together with Sebastian Pickel. I interpreted the spectra together with Richard Hildner and reviewed the paper.

Additional publication which is not part of this thesis:

S. Motamen, C. Schörner, **D. Raithel**, J.-P. Malval, T. Jarrosson, F. Serein-Spirau, L. Simon, R. Hildner, G. Reiter

Low loss optical waveguiding in large single crystals of a thiophene-based oligomer

Phys. Chem. Chem. Phys. 19 (2017) 15980.

3.3 Key results

Publication 1: Emitting Species of P3HT: From Single, Isolated Chains to Bulk

The polythiophene P3HT established as working horse for research in the field of conjugated polymers. It is not only used to design prototypical organic solar cells and field effect transistors but also for fundamental studies regarding the photo-physical and electronic properties of conjugated polymers. Despite the broad research, the intrinsic properties of P3HT are still under debate from theoretical as well experimental point of view. Several single-molecule studies ascribe contradicting properties to the emitting species in single P3HT chains.

The first publication (section 4.1) of this thesis aims at resolving these conflicting reports by using defined samples and a controlled preparation technique. As samples we chose short P3HT chains with a length of about 16 repeating units (P3HT16, $M_n = 2.6$ kDa) and long chains with 144 repeating units (P3HT144, $M_n = 24$ kDa) with both high regioregularity (a single defect at the end of each chain) and low polydispersity (< 1.17). The two chain lengths were selected to study spectral features from non-folding (P3HT16) and potentially folding chains (P3HT144). The high regioregularity reduces structural defects, which would otherwise have a strong impact on the torsional disorder of the backbone. The goal is to get insights into the intrinsic, “defect-free” structural and energetic disorder in poly(3-hexylthiophene).

Figure 3.2a,b show two representative low temperature photoluminescence (PL) spectra of a single P3HT16 and P3HT144 chain, respectively (both embedded in shock-frozen *n*-hexadecane). Interestingly, the spectra of short and long chain look nearly identical, apart from a more pronounced phonon side band in the case of the long chains. Various intra-molecular vibrational modes accompany the ZPL, interestingly there are also modes below 1000 cm^{-1} which are coupling to the electronic transition. Furthermore we observe only a single ZPL for all chains, indicating that there is only a single emitter in P3HT.

The following discussion focuses on the ZPL which was analysed for about 100 molecules for each chain length. For both samples the mean ZPL width (FWHM) of about 30 cm^{-1} (see Figure 3.2c,d) gives insights into the conformation of the emitting site. The lines are broadened in comparison to the lifetime-limited natural line width by unresolved spectral diffusion processes, which is characteristic for a disordered guest-host system. The random, entropic conformation of isolated P3HT chains is therefore transferred to and frozen in the *n*-hexadecane solution.

The distribution of ZPL energies (Figure 3.2e,f) are centred around $18\,800\text{ cm}^{-1}$ and $18\,900\text{ cm}^{-1}$ for the short and long chains, respectively. Furthermore, the histograms

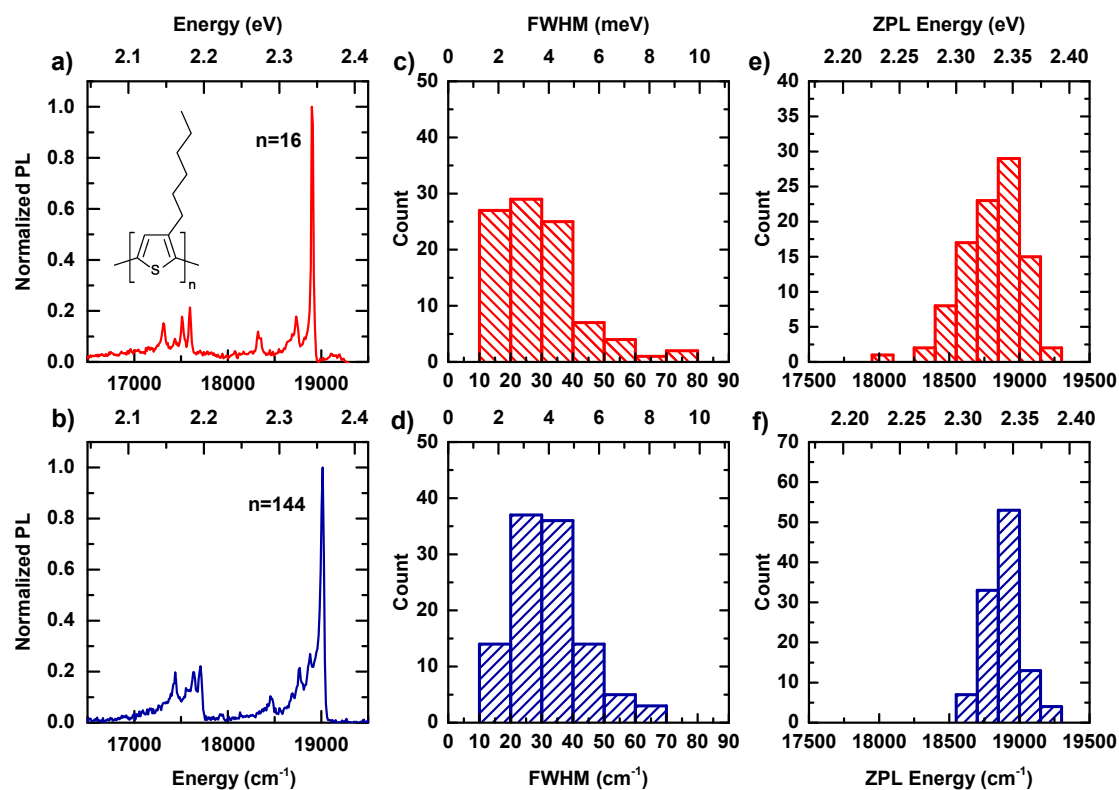


Figure 3.2: Low-temperature photoluminescence (PL) spectra of single poly(3-hexylthiophene), P3HT. a,b) Single-chain PL spectra of P3HT in *n*-hexadecane, c,d) distributions of line widths (FWHM) of the zero phonon lines (ZPL), and e,f) distributions of spectral positions of the ZPLs for P3HT with a molecular weight of 2.6 kDa, i.e., about 16 repeating units (P3HT16, red), and 24 kDa, i.e., about 144 repeating units (P3HT144, blue), respectively. The spectra in a) and b) have been obtained after partial temporal averaging using a pattern recognition algorithm. The chemical structure of P3HT is shown as an inset in a).

feature a surprisingly narrow width (FWHM) of only 480 cm^{-1} for the short chains and 300 cm^{-1} for the long chains. These inhomogeneous distributions are directly connected to the energetic disorder of the emitting sites. The narrow distribution indicates that dispersive interactions as well as torsional disorder (i.e. variation around the mean dihedral angle) along the backbone are surprisingly defined in single, isolated P3HT chains. Various quantum-chemical calculations suggest a mean dihedral angle around $\phi = 130\text{-}145^\circ$.

Of central interest is the spectral position of the ZPLs (Figure 3.2e,f) in comparison to the corresponding low-temperature PL spectrum of a disordered P3HT16 film as shown in Figure 3.3. Remarkably, the ZPL distribution is not only much narrower but also substantially blue-shifted by over 1200 cm^{-1} with respect to the transition of the disordered film. This is an unexpected observation as the PL from disordered ensembles is usually attributed to highly amorphous regions, i.e. the conformation of the emitting sites in disordered films and in our single-chain experiments is thought to be very similar.

Consequently, the line shape of the amorphous film spectrum should be identical to the spectral distribution of ZPL positions (i.e. the inhomogeneous distribution function).

This apparent contradiction can be resolved by the assumption that the emitting sites in disordered films and solution are predominantly species that are formed by chain-chain contacts due to high (local) concentrations. These close contacts induce on one hand a partial planarisation of the thiophene backbone and at the same time they allow electronic Coulomb coupling between their transition dipole moments. Both effects lead to a red-shift and strong broadening of the bulk spectra. The affinity of P3HT to form loose aggregates in solution was also demonstrated by concentration-dependent measurements. Even for the short chains (P3HT16) which should be less prone to aggregation, isolated chains exist only at the very lowest concentration. A slight increase in concentration leads to formation of aggregates, which are identified by their strong red-shift (see Figure 2 in section 4.1).

Further support for this hypothesis stems from time-dependent density functional theory (TDDFT) calculations on polythiophenes using long-range separated hybrid functionals (Thiago B. de Queiroz, Bayreuth). These simulations highlight the strong impact of (partial) planarisation and long-range inter-molecular electronic coupling in polythiophenes. The transition energy of a planar chain is red-shifted by up to 4800 cm^{-1} in comparison to a torsionally disordered chain (obtained by molecular dynamics simulations prior to the excited state calculations). This value is of course an upper boundary for the planarisation-induced red-shift. Additionally, calculations on a H-type coupled thiophene dimer reveal that even for chain-chain distances of about 8 \AA the lowest excited state of the dimer is shifted by 900 cm^{-1} . As this are realistic distances for loose aggregates in solution and amorphous films, the resulting electronic coupling will also have a strong impact on the spectral shifts and the photophysics in general in these systems.

In conclusion, the common interpretation of disordered P3HT bulk spectra as non-interacting chains does not hold against experiment. The disordered ensemble PL spectra are strongly red-shifted and broadened in comparison to the narrowly distributed ZPLs of single, isolated chains. Based on TDDFT calculations we account this to partial backbone planarisation and concomitant electronic coupling between transition dipole moments upon formation of loose aggregates in bulk samples. The degree of (partial) planarisation and electronic coupling is both ill-defined in disordered films, due to the random mutual arrangement of the P3HT chain segments. This strong variation leads to a broadening of the disordered film spectra with respect to the distribution of single molecules.

In π -stacked H-aggregates, planarisation and electronic coupling are both stronger but more defined, leading to a red-shift and a narrowing of the inhomogeneous linewidth in comparison to the disordered bulk spectra. Interestingly, even low-temperature aggregate spectra are broader than the distribution of single, isolated chains, emphasizing the low

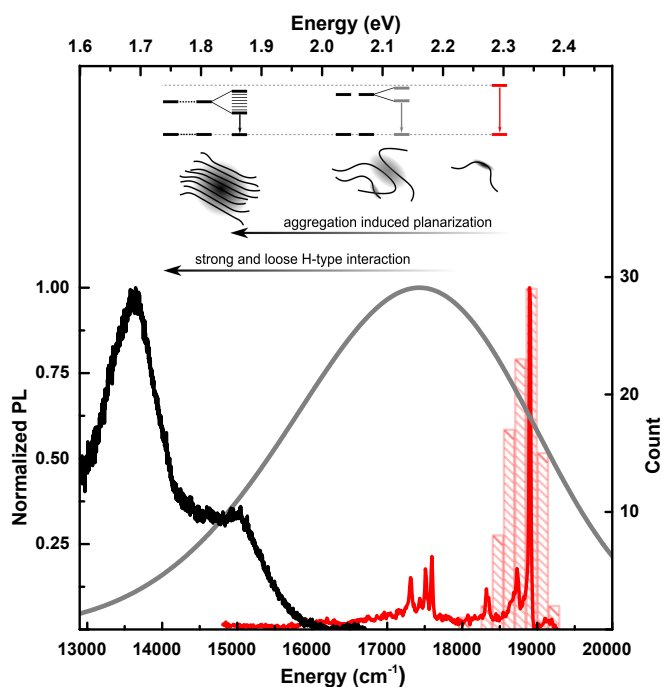


Figure 3.3: Bridging the gap between the single-chain ZPL distributions and the ensemble PL spectra. The single-chain spectrum (red line) and the corresponding histogram of ZPL positions at around $19\,000\text{ cm}^{-1}$ (red bars) result from PL of single sites on isolated, disordered P3HT16 chains. The ensemble PL spectrum from disordered regions of a thin P3HT16 film (gray line) is red-shifted due to the formation of loose aggregates with concomitant planarisation of P3HT segments and inter-chain electronic interaction. Finally, in ordered regions of P3HT films PL below $16\,000\text{ cm}^{-1}$ is observed (black), which results from π -stacked H-type aggregates with strong inter-chain electronic interaction. This situation is shown at the top with the illustration of an isolated chain (right), a loose aggregate prevailing in disordered films (centre), and a π -stacked H-aggregate (left). The grey shaded areas indicate the spatial extend of the excited state of the emitting species. The corresponding energy level schemes demonstrate that aggregation-induced planarisation and the concomitant electronic coupling of neighbouring chains leads to the formation of exciton bands, which results in red-shifted emission for both loose and π -stacked aggregates.

intrinsic disorder of P3HT. The impact of loose and strong aggregation on the bulk spectra in comparison to single, isolated chain is again depicted in Figure 3.3. This study shows, that single, spatially isolated P3HT chains appear to be a remarkably well-defined system independent of the molecular weight. The narrow ZPL distributions demonstrate the low degree of energetic (and thus torsional) disorder at least on length scales of the emitting sites.

Publication 2: Direct observation of backbone planarisation via side-chain alignment in single bulky-substituted polythiophenes

In the last years it was realised, that not only the structure of the electronic backbone can be tuned, but the side-chains have to be chosen in an appropriate way as well to achieve high-performance devices. Therefore, side-chain engineering has evolved as a versatile tool-kit for manipulating and optimising the relevant structural and electronic properties as it allows to influence the backbone planarity as well as mutual orientations of the molecules in bulk film. In most cases, non-covalent interactions introduced by heteroatoms (like fluorine or oxygen) within the side-chains are used to control the backbone disorder. However, the experimental studies to investigate the structural changes are restricted to bulk structure elucidation (X-Ray or electron diffraction) of crystalline domains, often in combination with density functional theory calculations.

Based on the results from publication 1 on P3HT, we investigate the impact of side-chains on the optical, electronic and structural properties directly on the level of single, isolated molecules. Therefore, after studying the influence of backbone disorder in conjugated polymers, we shift the focus to the question how this disorder can be controlled. Under identical experimental conditions as for P3HT, we examined a second polythiophene, poly(3-(2,5-dioctylphenyl)thiophene) (PDOPT) with sterically very demanding side-chains but identical chemical backbone.

For the single-chain experiments we used again defined samples with low polydispersity, high regioregularity and selected two different chain lengths of 16 repeating units ($M_n = 6.1$ kDa, PDOPT16) and 89 repeating units ($M_n = 33.7$ kDa, PDOPT89). Figure 3.4a,b shows two representative single-chain PL spectra of PDOPT16 and PDOPT89. Both have a prominent ZPL at $17\,022\text{ cm}^{-1}$ and $16\,777\text{ cm}^{-1}$ with line widths (FWHM) of 33 cm^{-1} and 64 cm^{-1} for PDOPT16 and PDOPT89, respectively. The ZPLs are accompanied by a broad phonon side-band (PSB) as well as a distinct vibronic transition around 1480 cm^{-1} , which is attributed to a carbon-bond stretching mode. The single-chain PL spectra for short and long chains of PDOPT are almost independent of the chain length with respect to shape and transition energy. However, in contrast to P3HT, PDOPT is a multi-chromophoric system. In polarisation resolved measurements we observed downhill energy transfer between different chromophores (see Figure S2 in section 4.2).

The ZPL widths (Figure 3.4d,e) are unaffected by the chain length, but with an average value of around 70 cm^{-1} twice as broad as those of P3HT (Figure 3.4f). This difference arises due to librational motions of the phenyl ring within the side-chains. The resulting fluctuations of the local dielectric environment of the emitting site causes strong spectral diffusion which broadens the ZPLs. Furthermore, the change in the vibronic signature (e.g. one carbon-bond stretching mode in the case of PDOPT, several for

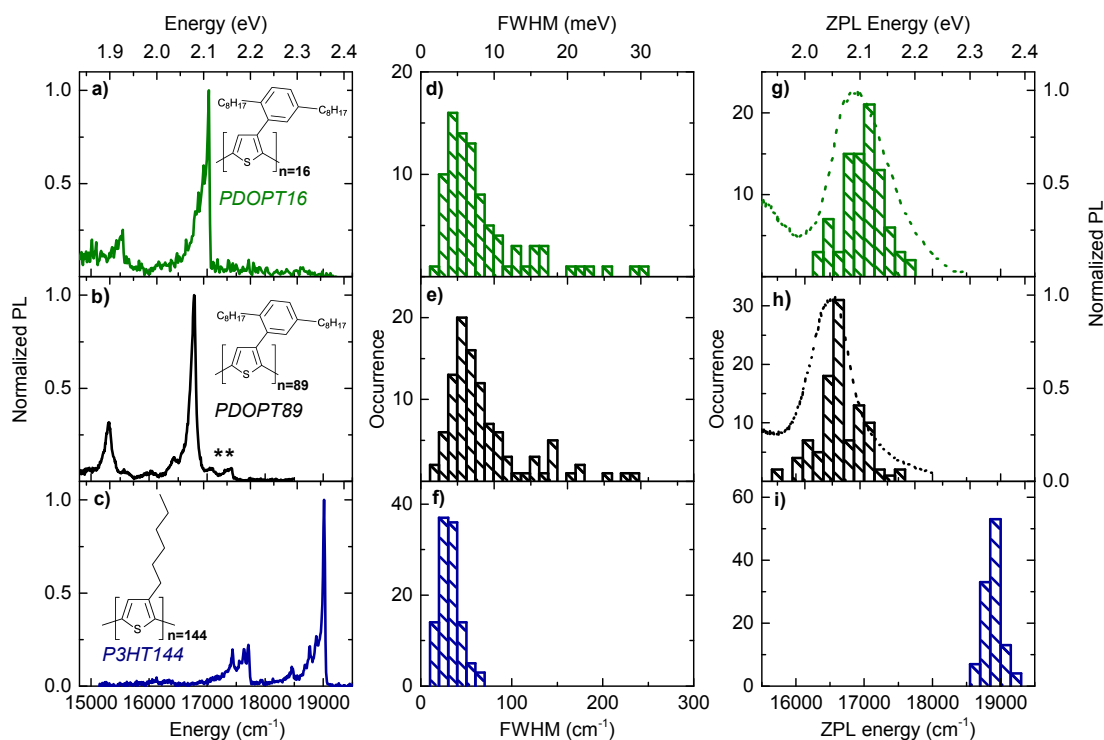


Figure 3.4: Low-temperature single-chain (PL) spectroscopy on single polythiophene chains. *a,b*) Single-chain PL spectra of poly(3-(2,5-dioctylphenyl)thiophene) (PDOPT) for two different chain lengths embedded in *n*-hexadecane. *c*) Single-chain PL spectrum of poly(3-hexylthiophene), P3HT, in *n*-hexadecane. *d,e,f*) Distribution of line widths (FWHM) of the zero phonon lines (ZPL). *g,h,i*) Distributions of spectral positions of the ZPLs. The dashed lines in *g*) and *h*) are low-temperature ensemble PL spectra of the corresponding matrix-isolated PDOPT sample (in *n*-hexadecane). In *a-c*) the chemical structures are shown as insets, *n* denotes the mean number of repeating units. The peaks in *b*) marked with asterisks denote additional weak ZPLs from the same single PDOPT-chain. The data in *c*), *f*) and *i*) have been taken from publication 1.

P3HT) indicates a different backbone geometry, as these modes are known to be sensitive to the conformation of the π -conjugated backbone, see section 2.3.2.

In the following, the focus is drawn to the comparison of the ZPL distributions (Figure 3.4g-i) of P3HT and PDOPT. The first observation is that the transition energies of the PDOPT chains are spread over a significant wider range. This larger inhomogeneous broadening is also reflected in PDOPT ensemble spectra, dashed lines in Figure 3.4g,h and is explained by a higher static energetic disorder in comparison to P3HT. The most interesting result is the red-shift of the absolute transition energies of PDOPT by around 2200 cm^{-1} in comparison to P3HT. This is not obvious from the ensemble solution spectra alone, mainly because the solution spectra of P3HT does not represent isolated molecules. Based on the calculations from publication 1, we propose that the PDOPT chains are more planar but less defined (larger inhomogeneous broadening)

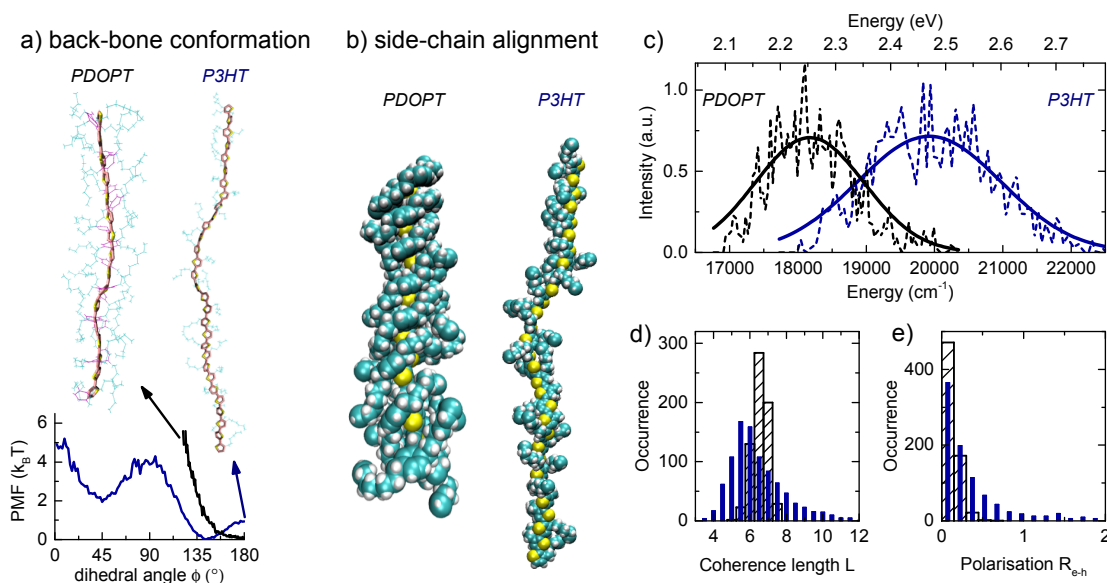


Figure 3.5: Quantum-classical atomistic simulations of the conformational, optical, and electronic properties of single PDOPT and P3HT chains. a) Top: Snapshots from trajectories of PDOPT16 and P3HT30 chains highlighting the backbone conformation. Bottom: Corresponding potential of mean force (PMF) as a function of the dihedral angle ϕ (blue: P3HT, black: PDOPT). b) Snapshots showing the side-chain alignment of the two polythiophenes. c) Dashed Lines: Calculated absorption spectra from thermal ensembles of PDOPT (black) and P3HT (blue). Solid lines: Gaussian fits to the calculated spectra. d) Distribution of coherence lengths L and e) distribution of electron-hole separation distances R_{e-h} (both in number of repeating units) for P3HT (solid blue) and PDOPT (hatched black).

with respect to P3HT. In line with this assumption, temperature dependent PL solution spectra also showed a stronger planarisation preceding aggregation in P3HT as compared to PDOPT (Figure 2 in section 4.2).

To gain further insights into the structural and optical properties of PDOPT, Lena Simine (Rice University, Houston) performed quantum-classical atomistic simulations on single PDOPT16 chains. The simulations showed that PDOPT chains adopt a stable, trans-planar conformation at room temperature, with the side-chain phenyl rings oriented perpendicular to the backbone and the octyl chains wrapped around the backbone, see Figure 3.5a,b. This unusual configuration results overall in a dihedral potential with a minimum at trans-planarity ($\phi = 180^\circ$).

The results are compared to recent, equivalent simulations on P3HT (see also section 2.2.3). Here, the side-chains do not adopt a structural motif. In contrast, the repulsive $S \cdots H$ interaction between the sulphur of the thiophene and the side-chain of the neighbouring monomer lead to a minimum in the torsional potential at around $\phi = 145^\circ$. Using a Pariser-Parr-Pople (PPP) Hamiltonian with configuration-interaction-singles (CIS), the optical and electronic properties of a thermal ensemble were calculated for

both PDOPT and P3HT. This includes the transition energy between electronic ground state and excited state, the coherence length L (defined as the radius of gyration of the exciton wavefunction) as well as the electron-hole displacement R_{e-h} . The absorption spectra show a red-shift of 2000 cm^{-1} for PDOPT in comparison to P3HT, which is in agreement with the experimental value (2200 cm^{-1}). Interestingly, the calculated coherence lengths are similar for both systems around $L = 6.5$ repeating units. This finding is rather surprising as the spectral red-shift, in line with the higher planarity of the PDOPT backbone, would conventionally be associated with an increase in coherence length L . In contrast, the stronger coupling along the backbone (in the sense of stronger π -overlap) in PDOPT is reflected in the magnitude of the electron-hole displacement R_{e-h} , which is reduced in PDOPT (0.11 repeating units) in comparison to P3HT (0.45 repeating units), see Figure 3.5e.

In this context it is worth to note, that in the common interpretation of the I_{0-1}/I_{0-0} ratio in the frameworks of Spano and Barford, the electron-hole displacement (i.e the charge transfer character of the exciton) is assumed to be constant. Accordingly, a change in the peak ratio is usually interpreted as a change in coherence length of the emitting site. Our results suggest that the electron-hole distance is worth a closer look in future research, especially as it is sensible to the intra-chain disorder of conjugated polymers.

This paper furthermore presented a new, unexpected possibility to control disorder in isolated conjugated polymers with bulky side-chains which adopt a shielding conformation and support the planarity of the backbone. This might stimulate new ideas for synthesis.

Publication 3: Signatures of Melting and Recrystallization of a Bulky Substituted Poly(thiophene) Identified by Optical Spectroscopy

In the first two publications we studied the effects of structural (torsional) disorder on the intra-molecular photophysical properties of single polythiophenes in both experiment and theory. Based on this, we turn to crystalline PDOPT aggregates in publication 3 and study *inter*-molecular interactions as a function of structural disorder.

Spherulitic crystals were grown in a melt of PDOPT chains ($M_w = 28$ kDa, $D = 1.86$) via isothermal crystallisation at 100°C for 50 hours (Fanuel Keheze & Günter Reiter, Freiburg). The spherulites have a diameter of several $100\ \mu\text{m}$, show a high birefringence and anisotropic absorption and photoluminescence, see Figure 3.6a-c. This is a result of the orientation of the thiophene backbones, which are aligned perpendicular to the radial growth direction of the spherulite.

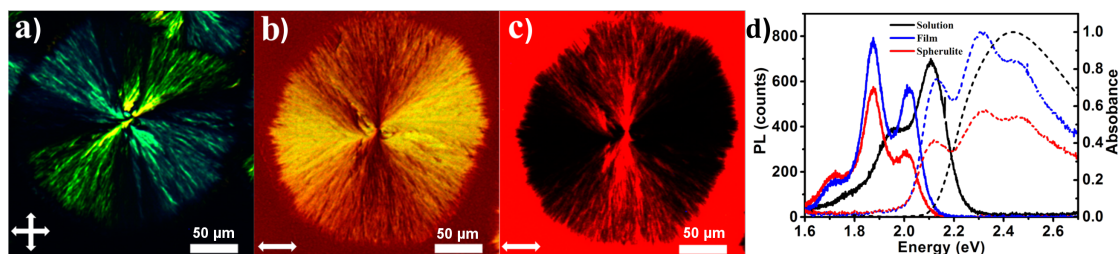


Figure 3.6: Anisotropic optical properties and spectra of spherulitic PDOPT crystals and the surrounding film. Polarised optical microscopy images a) under crossed polarisers (arrows) showing strong birefringence, b) of absorption and c) of emission upon excitation with polarised light for a spherulitic crystal surrounded by a rapidly crystallised film. The polarisation direction is indicated by the horizontal white arrows. d) Absorption (dashed) and PL spectra (solid) of PDOPT spherulites (red), disordered crystalline film (blue) and solution (black).

The spectral shape in absorption and PL of the PDOPT spherulites and the surrounding disordered, crystalline film (Figure 3.6d) resemble the spectral signatures of H-type aggregates, as the A_1 peak in absorption and I_{0-0} peak in emission are suppressed with respect to the solution spectrum. Yet, in contrast to usual π -stacked H-type aggregates, the bulky side-chains of PDOPT impede direct π - π -stacking of the backbones. This weakens the electronic coupling between the transition dipole moments along the π - π -stacking direction (backbone-backbone distance $1.45\ \text{nm}$). Perpendicular to the π -stacking direction however, the chains are also aligned parallel to each other at a distance of $0.55\ \text{nm}$, resulting in a H-type coupling as well. The amorphous, solution-like contribution to the absorption spectrum of spherulites (Figure 3.6, red) is a signature of remaining disordered regions between the lamellae of the radially growing spherulitic crystal.

The knowledge about the type of the electronic coupling and different contributions of the spectra allowed a quantitative analysis of absorption and emission spectra with the formalism developed by Spano and co-workers. The influence of structural disorder was

studied by heating the sample above the melting point at around 120 °C up to 150 °C at a rate of 2 °C/min. The melt was subsequently cooled down to room temperature at the same rate. The aggregate spectra in both absorption and PL blue-shift continuously until the melting temperature is reached, where they change to solution-like spectra as expected for a disordered, molten film. During the cooling cycle, this shape remains until recrystallisation around 75 °C, where the structured aggregate peaks rise again. However, no birefringence is observed any more, as the rapid cooling and recrystallisation process did not allow the re-formation of the spherulitic crystal, resulting in a crystalline film without long-range order.

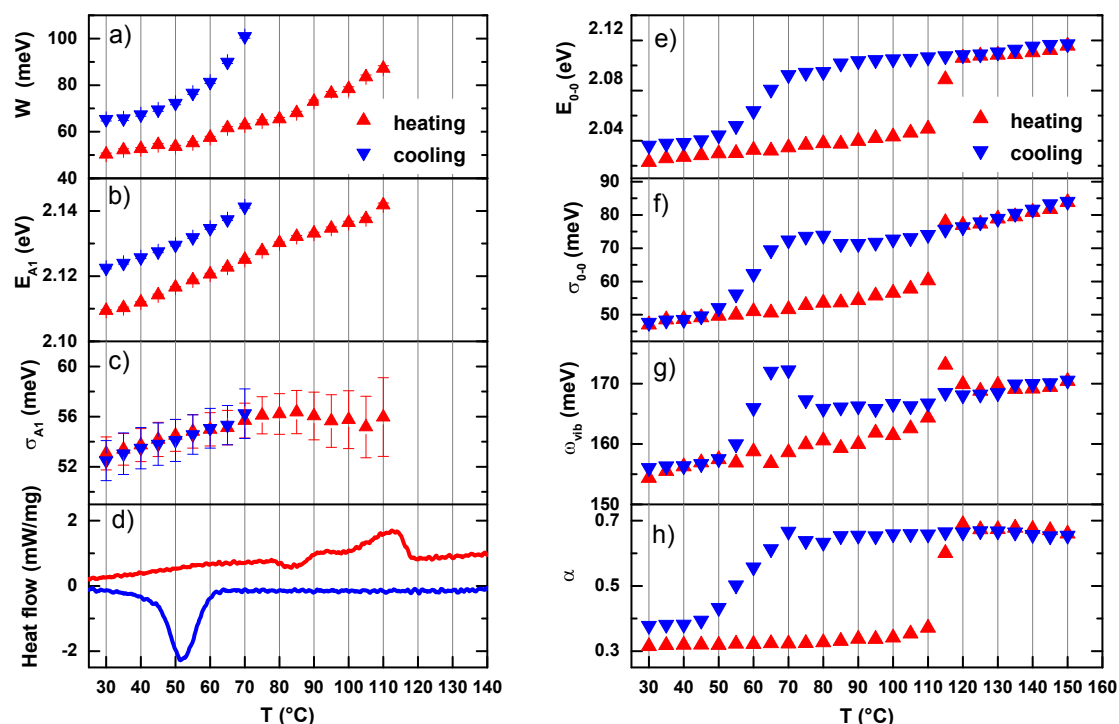


Figure 3.7: Results of the fits to the temperature-dependent contribution of crystalline domains to the absorption spectra (left) as well as to the PL spectra (right). Absorption: a) Free exciton bandwidth W , b) energy E_{A1} and c) linewidth σ_{A1} of the A_1 peak, evaluated for 30 °C to 120 °C for heating (red symbols) and cooling (75 °C to 30 °C, blue). Photoluminescence: e) Peak position E_{0-0} and f) linewidth σ_{0-0} of the I_{0-0} peak, g) vibronic energy ω_{vib} , h) relative amplitude α of the peak I_{0-0} for the heating (red) and cooling (blue) cycle, respectively. d) Differential scanning calorimetry heat flow curve for heating and cooling spherulitic crystals at a rate of 2 °C/min.

The results from the quantitative analysis of the absorption spectra are shown in Figure 3.7a-c. Scattering experiments have demonstrated that the thiophene backbones of PDOPT are perfectly planar in the spherulitic crystals at room temperature. Upon heating, thermally activated torsional disorder in the backbone should reduce the π -overlap leading in a first step to a weaker intra-chain coupling and as a consequence

to an enhanced inter-chain interaction. Indeed, the inter-chain interaction and thus the bandwidth W increases from 50 meV to 87 meV upon heating. The absolute value for W is smaller than the usual values for P3HT owing to the larger backbone-backbone distance (0.38 nm for P3HT and 0.55 nm for PDOPT). This is also in line with the blue-shifting peak energy E_{A1} which stems from the increase in bandwidth as well as from the decreased intra-chain coupling. Similarly, the linewidth σ_{A1} reflects the thermally increased backbone disorder, which saturates due to a cold crystallisation peak around 85 °C, see DSC curve in Figure 3.7d.

In emission, the peak energy E_{0-0} , the line width σ_{0-0} , the relative I_{0-0} amplitude α as well as the effective vibronic mode energy ω_{vib} increase continuously with temperature up to the melting point, indicating a gradual growth of backbone disorder (Figure 3.7e-h, red). The phase transition from crystal to melt becomes noticeable by a sudden rise in the fitting parameters (E_{0-0} , σ_{0-0} , ω_{vib} , α). Finally above 120 °C, the inter-chain coupling weakens as the crystalline structure is lost in the melt. This is consistent with the absorption spectra, where the crystalline vibronic progression vanishes at the same time. Nevertheless, the emitting chain segments in the melt experience weak H-type coupling as the I_{0-0} peak is still slightly suppressed ($\alpha = 0.7$) in comparison to the solution spectra. Please note in this context, that a strong increase in torsional disorder would result in a larger effective Huang-Rhys parameter for the I_{0-n} ($n > 0$) progression. However, the peak ratios within this low-energy part of the PL spectrum are well described by the initial Huang-Rhys parameter $S = 0.7$ for the planar chain. In the context of the molecular dynamics simulations in publication 2 we suggest therefore, that the side-chains of PDOPT stabilize the backbone planarity even in the melt.

Upon cooling and recrystallisation (around 75 °C), all trends show a reverse behaviour (Figure 3.7e-h, blue). The final saturation values at 30 °C are in most cases however slightly higher than the initial starting parameters. This indicates, that the resulting crystalline domains have a higher structural disorder in comparison to the slowly crystallised spherulites as the side-chains could not rearrange perfectly during the fast recrystallisation process. Furthermore, this study showed that the intra-chain torsional disorder is not only important for the interpretation of single-molecule data. The distribution of dihedral angles is also a central parameter for the description of inter-chain coupling in crystalline films of polythiophenes.

Publication 4: Revealing order and disorder in films and single crystals of a thiophene-based oligomer by optical spectroscopy

In the third publication, the order-disorder transition upon the melting process in PDOPT spherulites was examined. However, due to the remaining dispersity and regioirregularity of the polymer chains and the nature of radial growth of the spherulites, the crystallinity is limited by lattice disorder and grain boundaries. In publication 4 we study highly defined single crystals with optical spectroscopy. The comparison to disordered, spincoated films allows to examine the effect of structural disorder on the photophysical properties of crystalline aggregates.

Highly defined (100% regioregularity) thiophene-benzene-thiophene oligomers (3TBT, see Figure 3.8a), were used to grow millimetre-long needle-like single crystals in solution with a width of several micrometres (Sajedeh Motamen & Günter Reiter, Freiburg). The well-defined molecular order results in a high optical anisotropy which was characterised with polarised light microscopy and spectroscopy. In Figure 3.8b the transmission of a 3TBT single crystal under crossed polarisers is shown, demonstrating the high birefringence. Similarly, in Figure 3.8c the PL microscopy image of the same crystal shows a homogeneous PL intensity. The anisotropic absorption and PL (not shown) indicate that the transition dipole moment (and thus the backbone of the oligomer) is oriented perpendicular to the long axis of the crystal.

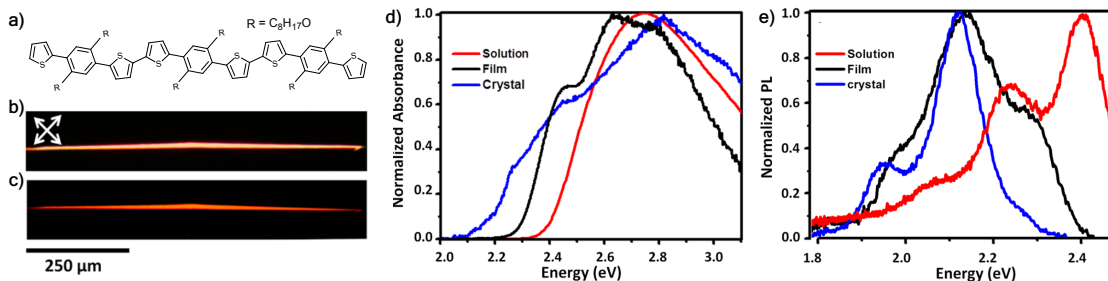


Figure 3.8: Optical and spectroscopic properties of 3TBT single crystals. a) Structural formula of the 3TBT oligomer. b) Optical microscopy image ($800\ \mu\text{m} \times 600\ \mu\text{m}$) under crossed polarisers of a 3TBT single crystal. c) PL microscopy image ($800\ \mu\text{m} \times 600\ \mu\text{m}$) of the same crystal as in b), excited between 450 nm to 490 nm. Normalised d) absorption and e) PL spectra of a homogeneous 3TBT solution (red), a spin-coated film (black) and a single crystal (blue).

A less ordered sample was obtained by spincoating a 3TBT solution, resulting in a disordered film which consists of both fiber-like crystalline aggregates and probably also non-interacting chains. The spectral properties of both crystalline film and single crystal 3TBT are measured individually. Compared to solution spectrum, the absorption (Figure 3.8d) in film and single crystal shows a strong red-shift and a distinct vibronic progression, with a suppressed A_1 peak. Both effects are more pronounced in the single crystal than in film and were further quantified by applying the H-aggregate model

developed by Spano and co-workers. The extracted excitonic coupling J between the oligothiophene chains of $J = 11$ meV (89 cm $^{-1}$) for the film and $J = 41$ meV (330 cm $^{-1}$) for the single crystal reveals that the chains are more densely and ordered packed in the single crystal in comparison to the film.

In the PL spectra, see Figure 3.8e, the I_{0-0} peak is suppressed in film and even stronger in the crystal in comparison to the solution spectrum. This is in line with the absorption data, indicating a higher H-type interaction within the crystal. Interestingly, the crystal PL spectrum cannot be fitted by a corresponding vibronic progression with a peak spacing of 1400 cm $^{-1}$. Therefore, low-temperature ($T = 1.5$ K) PL spectra of 3TBT single crystals were acquired. The reduction of the homogeneous line width and the low structural and electronic disorder result in a narrow highest energy transition ($\text{FWHM} < 300$ cm $^{-1}$) and allows to resolve the rich vibronic structure of the single crystal (Figure 3.9b). Similar to the room temperature spectra, the most prominent peaks are assigned to the vibronic progression of the carbon-bond stretching modes with an energy of around $\hbar\omega \approx 1400$ cm $^{-1}$. The other peaks and shoulders result from various low-energy intra-molecular modes which couple to the optical transition. Due to thermal broadening, these vibrational peaks are not resolvable individually any more at room temperature and merge into effective modes. As consequence, the room-temperature crystal is fitted with three peaks for the vibronic progression of the carbon-stretching modes and two additional effective modes which account for the coupling of probably several modes with energies in between the main peaks, see Figure 3.9a.

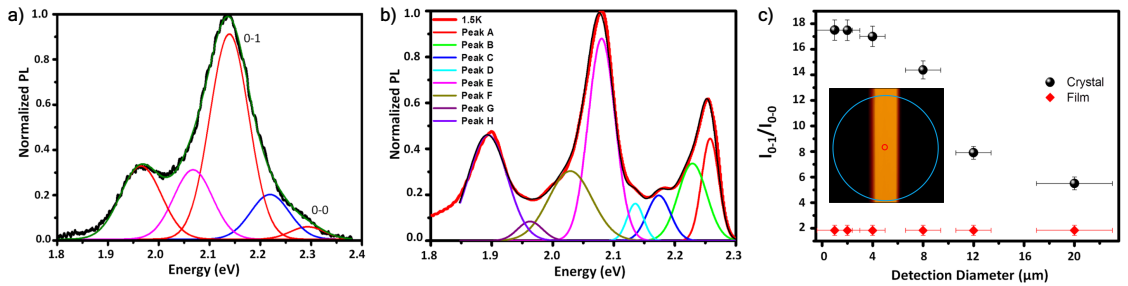


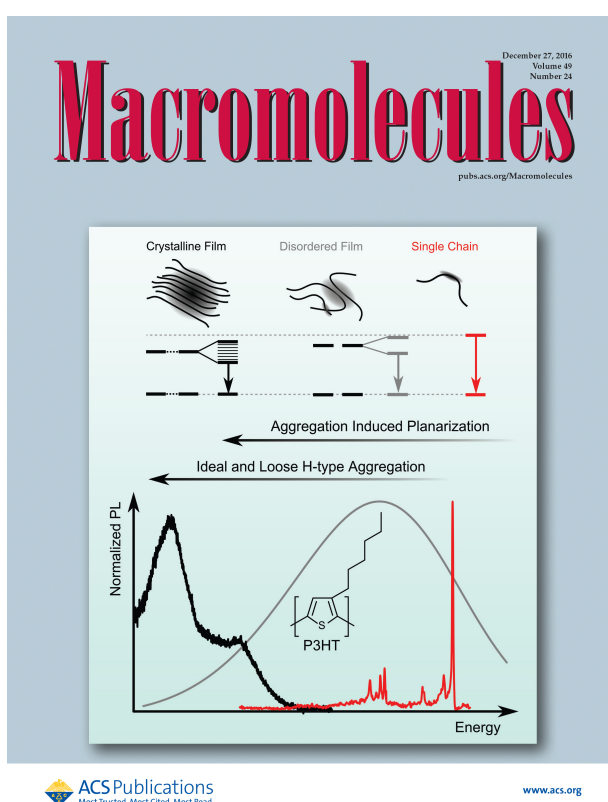
Figure 3.9: Photoluminescence spectra and peak ratios of 3TBT crystals. a) Normalised PL spectrum of a 3TBT crystal at room temperature (black), together with a fit of five Gaussian peaks to reproduce the vibronic structure (green). b) Normalised PL spectrum of a 3TBT crystal at 1.5 K (red), together with a fit of eight Gaussian peaks to reproduce the vibronic structure (black). c) I_{0-1}/I_{0-0} intensity ratio of the room-temperature PL spectrum as a function of the detection diameter (black), together with the corresponding values measured for a spin-coated film (red). Inset: Superposed on an AFM topography image (size 16.5×16.5 μm^2), schematic representation of the change in detection area centred on the crystal measured in c). The PL spectrum in a) (b) was acquired from a single crystal with a width of 4 μm (1 μm) using a detection area of 1 μm (600 nm). The width of the crystal in c) is 4 μm .

The knowledge about the vibrational structure of 3TBT allows the quantitative analysis of the I_{0-1}/I_{0-0} peak ratio as a function of disorder. This was realised by centring the detection focus on a single crystal whose width is around 4 μm . By expanding the detection diameter from 1 μm to 20 μm , the contribution of the small disordered crystallites lying on the substrate next to crystal is gradually increased. As a result, the I_{0-1}/I_{0-0} peak ratio decreases with increasing contribution from disordered areas, as expected for less ordered H-aggregates, see Figure 3.8c. Thus, 3TBT single crystals serve as nice model system to study the impact of structural disorder on the photophysical properties on conjugated oligomers.

However, a more detailed analysis is needed to understand all spectroscopic features of 3TBT. According to the model of Spano and co-workers, in such defined systems the I_{0-0} transition should loose intensity upon cooling as the H-type symmetry strengthens and no thermally activated transitions from the lowest-energy exciton band would be possible. In contrast, I_{0-0} peak intensity increases with decreasing temperature in 3TBT single crystals, see Figure 3.9b. Please note in this context, that this model includes strong simplifications as for example non-nearest neighbour interactions are not included in the framework of Spano and co-workers but may play a role in 3TBT crystals due to strong coupling of $J = 41 \text{ meV}$ (330 cm^{-1}). Furthermore, the rich vibronic structure and the temperature dependence of the low-energy modes cannot be modelled with the corresponding Hamiltonian. Temperature-dependent absorption, emission and lifetime measurements of single crystals have been measured and are currently analysed to get detailed insights into the inter-molecular coupling in 3TBT.

4 Publications

4.1 Publication 1: Emitting Species of P3HT: From Single, Isolated Chains to Bulk



Dominic Raithel, Sebastian Baderschneider, Thiago Branquinho de Queiroz, Ruth Lohwasser, Jürgen Köhler, Mukundan Thelakkat, Stephan Kümmel, Richard Hildner

Published in
Macromolecules

DOI: 10.1021/acs.macromol.6b02077

Reproduced with permission from Macromolecules 49 (2016) 9553

Copyright © 2016 American Chemical Society



Emitting Species of Poly(3-hexylthiophene): From Single, Isolated Chains to Bulk

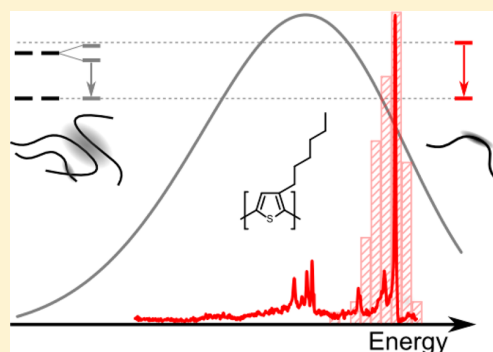
Dominic Raithel,[†] Sebastian Baderschneider,[†] Thiago B. de Queiroz,^{‡,||} Ruth Lohwasser,[§] Jürgen Köhler,[†] Mukundan Thelakkat,[§] Stephan Kümmel,[‡] and Richard Hildner^{*,†,||}

[†]Experimental Physics IV and Bayreuth Institute for Macromolecular Research (BIMF), [‡]Theoretical Physics IV, and [§]Applied Functional Polymers, University of Bayreuth, 95440 Bayreuth, Germany

^{||}Centro de Ciências Naturais e Humanas, Universidade Federal do ABC, 09510-580, Santo André-SP, Brazil

Supporting Information

ABSTRACT: The photophysical properties of films of alkyl-substituted polythiophenes are governed by a subtle interplay between intra- and interchain electronic couplings. The intramolecular properties, however, are still not entirely clear because polythiophenes possess a strong tendency to form π -stacked aggregate structures with appreciable interchain couplings. Here we employ low-temperature single-molecule photoluminescence spectroscopy on isolated regioregular poly(3-hexylthiophene), P3HT, chains with different, but well-defined molecular weights to reveal the intrachain properties of their emitting sites. We find that the inhomogeneous distribution function of the zero-phonon lines (ZPL) is very narrow ($<480\text{ cm}^{-1}$, 60 meV), which indicates a low degree of torsional disorder of the P3HT backbone on length scales of the emitting sites (despite a large mean dihedral angle). Moreover, the single-chain ZPLs are exclusively located in the high energy tail of the corresponding spectrum of a disordered ensemble. Using concentration-dependent measurements in combination with time-dependent density functional theory, we show that this spectral shift stems from aggregation-induced partial planarization and concomitant electronic coupling between segments of neighboring P3HT chains.



INTRODUCTION

The prototypical conjugated polymer poly(3-hexylthiophene) (P3HT) is widely used in organic electronics and photovoltaic applications.^{1,2} For the optimization of such devices, it is of key importance to understand the electronic structure of the excited states in films and nanostructures as well as the relation between electronic structure and sample morphology. Generally, in condensed phase the nature of excited states in P3HT is determined by an interplay between intrachain and interchain coupling, which strongly depends on processing conditions, molecular weight, and regioregularity, among other factors.^{3–6} For instance, neat P3HT films usually exhibit H-type behavior with excitations possessing predominantly interchain character, whereas P3HT nanofibers were shown to exhibit H-type or J-type behavior (excitations with predominant intrachain character) depending on molecular weight and experimental conditions (pressure, temperature).^{7–10}

To precisely predict and model the nature of excited states of P3HT in condensed phase, a clear discrimination of intra- and interchain effects is therefore required. Often this discrimination is based on changes of optical spectra of films and nanostructures with respect to the spectra from disordered ensembles (usually dilute solutions).^{3,6,11} This approach, however, should be taken with care: There are in many cases discrepancies between disordered ensemble and single-chain

photoluminescence (PL) spectra of P3HT, even if measured under essentially identical conditions.^{12–14} Since single-chain spectra should represent the properties of isolated (non-interacting) chains, this observation indicates some influence of interchain effects in disordered ensembles. Yet, there are also strong discrepancies between different single-molecule studies on alkyl-substituted polythiophenes, and essentially all studies suggest PL at different photon energies (often simultaneously).^{12–17} In general, PL at energies below $16\,500\text{ cm}^{-1}$ (2.06 eV) is ascribed to originate either from sites with planar backbone and thus large conjugation length (“red sites”) or from ordered π -stacked aggregates.^{12–17} PL around $17\,500\text{ cm}^{-1}$ (2.19 eV) is attributed to single polythiophene chains that possess what is usually called solution conformation (“solution sites”).^{12,15–17} Rarely PL between $18\,400$ and $19\,300\text{ cm}^{-1}$ (2.28–2.38 eV) was observed (“blue sites”); that is thought to stem from sites with particularly short conjugation length.^{13–15} An extraordinary case was the observation of PL spectra that are continuously spread over an extremely wide range ($20\,650$ – $12\,800\text{ cm}^{-1}$; 2.58–1.60 eV).¹² Also, the degree of regioregularity strongly influences PL spectra:¹³ The fraction of “blue

Received: September 27, 2016

Revised: November 21, 2016

Published: December 12, 2016

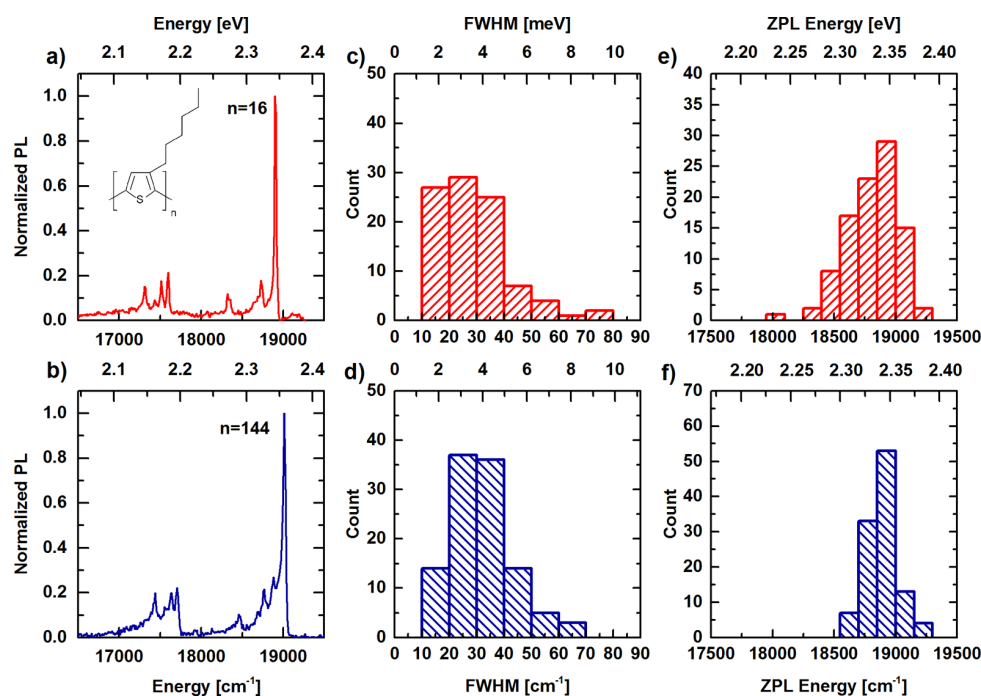


Figure 1. Low-temperature photoluminescence (PL) spectra of single poly(3-hexylthiophene), P3HT. (a, b) Single-chain PL spectra of P3HT in *n*-hexadecane, (c, d) distributions of line widths (fwhm) of the zero phonon lines (ZPL), and (e, f) distributions of spectral positions of the ZPLs for P3HT with a molecular weight of 2.6 kDa, i.e., ~16 repeating units (P3HT16, red), and 24 kDa, i.e., ~144 repeating units (P3HT144, blue), respectively. The spectra in (a) and (b) have been obtained after partial temporal averaging using a pattern recognition algorithm; see Methods section in [Supporting Information](#). The chemical structure of P3HT is shown as an inset in (a).

site” PL is higher for single regiorandom chains, whereas highly regioregular chains feature predominantly “solution” and “red site” PL, which was related to their more ordered and folded conformation and enhanced intrachain energy transfer.¹⁷ These discrepancies arise from the fact that both ensemble and single-molecule studies were often performed on chains with high molecular weight (>50 kDa, sometimes >150 kDa), which are prone to formation of π -stacked aggregates even in “good” solvents, such as *o*-DCB or THF.^{18,19} Furthermore, chains with molecular weight larger than ~10 kDa may exhibit back-folding of the backbone, which is another factor for aggregate formation.^{20–23}

Here we aim at resolving these conflicting observations and at unravelling the intrinsic properties of the emitting species of P3HT chains by employing low-temperature single-molecule PL spectroscopy (see [Supporting Information](#) for technical details). On the basis of these data, we develop a comprehensive picture of the spectral changes observed from isolated chains to disordered ensembles and finally ordered π - π -stacked structures. We investigate P3HT samples with 16 and 144 repeating units (P3HT16, $M_n = 2.6$ kDa and P3HT144, $M_n = 24$ kDa), respectively, low polydispersity (<1.17), and high regioregularity, that were synthesized via catalyst transfer polymerization²⁴ (see [Supporting Information](#), Figure S1, for details and room temperature solution spectra). The two extreme examples of very low and high molecular weight samples were selected to study spectral features from nonfolding (stretched chains) and possibly folded chains.²² For single-molecule spectroscopy the P3HT samples were diluted in the good solvent chloroform down to nearly single-chain level (15 nM). To ensure that we exclusively observe isolated chains and to provide a matrix, we further diluted this solution

by a factor of 50 (v/v) using *n*-hexadecane, a common host in single-molecule studies.^{25–27} A drop of the P3HT/*n*-hexadecane solution was then pipetted onto a quartz substrate, shock frozen in liquid nitrogen, and cooled to 1.5 K. From each single chain we recorded sequentially up to 500 individual spectra with an integration time of 1 s using a home-built confocal microscope. A single-chain spectrum is created by partial temporal averaging of these 500 spectra using a pattern recognition algorithm to improve the signal-to-noise ratio (see [Figures S2 and S3](#)).

RESULTS AND DISCUSSION

Two representative single-chain spectra of P3HT16 and P3HT144 are depicted in [Figures 1a](#) and [1b](#). Both spectra show a prominent and narrow zero-phonon line (ZPL) due to the purely electronic transition, which is located at $18\,97\text{ cm}^{-1}$ (2.34 eV) for P3HT16 and at $19\,03\text{ cm}^{-1}$ (2.36 eV) for P3HT144; the corresponding ZPL widths are 32 cm^{-1} (4 meV) and 40 cm^{-1} (5 meV, full width at half-maximum, fwhm), respectively. At lower energies the ZPLs are accompanied by broad, structureless phonon side-bands (PSB), which indicate only weak electron–phonon coupling to low-energy vibrations of the host material.²⁸ Moreover, up to seven less intense sharp lines appear that can be attributed to various intramolecular vibrational modes of P3HT ([Figures S2 and S3](#)). This vibronic structure is independent of the chain length and highly reproducible from chain to chain. The only significant differences between the single-chain spectra of P3HT16 and P3HT144 are the more pronounced PSB and the typically brighter emission signal of the longer P3HT144. Interestingly, for both P3HTs we very often find only a single ZPL in the spectra. Hence, there exists only a single emitting site per chain,

which is further supported by the observation of digital on–off blinking and bleaching of the PL signal (Figure S2) as well as by polarization-resolved measurements (Figure S3).

ZPL Widths: Conformation of the Emitting Site. In the following we focus on a quantitative analysis of the line widths (fwhm) and spectral positions of the ZPLs by fitting a Gaussian or Lorentzian function to their high-energy tails.²⁹ The resulting histograms are shown in Figures 1c–f for in total 97 (110) single P3HT16 (P3HT144) chains. The distributions of ZPL widths are essentially indistinguishable and centered around mean values of 28 cm⁻¹ (3.5 meV) for P3HT16 and 32 cm⁻¹ (4.0 meV) for P3HT144 (Figure 1c,d). In both histograms the widths of the narrowest ZPLs are determined by the spectral resolution of our setup of ~10 cm⁻¹. The ZPL widths are about 3 orders of magnitude broader than the corresponding lifetime-limited value of about 0.01 cm⁻¹ given an excited state lifetime of ~0.5 ns.^{13,30} The additional line broadening is likely to be caused by fast unresolved spectral diffusion processes, i.e., by random spectral jumps of the emission line due to structural fluctuations in the local environment of the emitting site (see Figure S2). Because these processes occur on all time scales, they give rise to a substantial broadening of the recorded ZPLs as shown recently.^{29,31,32} Such pronounced spectral diffusion is characteristic for a disordered guest–host system.^{29,31–34} Therefore, these data suggest that the random entropic conformation of isolated P3HT chains in chloroform solution is transferred to and frozen in the *n*-hexadecane host at 1.5 K, which is forced to form (at least locally) a disordered matrix around the P3HT chains. In this context, we stress that the solvent quality does not influence the conformation of a polymer chain on length scales of the persistence length.^{35,36} For P3HT the persistence length is ~8 repeating units,³⁷ which approximately corresponds to the effective conjugation length of the emitting sites.^{38–43} Hence, for both P3HT16 and P3HT144 it can be expected that the emitting sites adopt a similar, random entropic conformation both in the good solvent chloroform and in the bad solvent *n*-hexadecane.

Distributions of ZPL Positions: Torsional Disorder of the Emitting Sites. The distributions of the spectral positions of the ZPLs, plotted in Figures 1e,f, are virtually independent of chain length as well. The histograms are centered at 18 806 cm⁻¹ (2.33 eV) and 18 888 cm⁻¹ (2.34 eV) for the short and long chains, respectively. Furthermore, these distributions feature a remarkably narrow width (fwhm) of only 480 cm⁻¹ (60 meV) for P3HT16 and 300 cm⁻¹ (37.5 meV) for P3HT144, which is substantially narrower than the inhomogeneous line width of bulk PL spectra (see Figure 2a, Figures S1 and S4). We exclude preferential excitation of subensembles of P3HT chains because we employed different excitation wavelengths (see Supporting Information, Methods section). These defined ZPL distributions indicate, on the one hand, very small variations of dispersive interactions with the local environment from chain to chain.⁴⁴ On the other hand, they imply only small variations of the dihedral angle between thiophene rings around a mean angle, i.e., a small degree of torsional disorder of the emitting site.^{45–48} Here, the mean dihedral angle is rather large with 35°–50°^{49,50} because we have frozen in the ground state conformation that single P3HT chains adopt in solution (see above). The slightly broader ZPL histogram for P3HT16 compared to P3HT144 may be related to the single regiodefect per chain introduced by our synthetic route, which influences the torsional disorder of the emitting

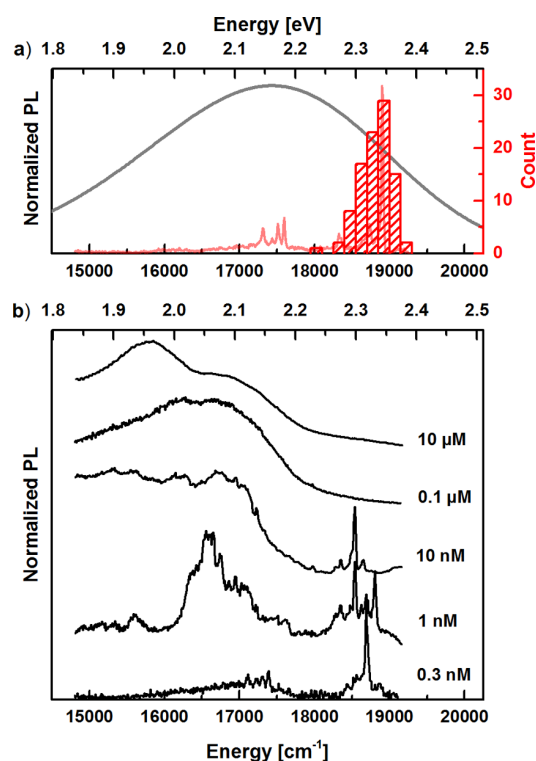


Figure 2. Concentration-dependent PL spectra of P3HT at low temperatures. (a) PL spectrum from a disordered (amorphous) region of a thin P3HT16 film (gray line) and the ZPL distribution of isolated P3HT16 chains (red bars). The PL spectrum of a single P3HT16 chain is shown as light red line. (b) PL spectra of P3HT16 at different concentrations in *n*-hexadecane. The concentration increases from 0.3 nM up to 10 μM (from bottom to top curve). Upon increasing the concentration, the sharp ZPLs of isolated chains disappear and broad, unstructured bands below ~17 000 cm⁻¹ appear, which are characteristic for the emission of π -stacked aggregates with moderate order. Notably, at energies between 17 300 and 18 000 cm⁻¹ no transitions are observed at any concentration.

site of a short chain to a greater extent with respect to a longer chain.^{47,49,51,52} Our interpretation of only small torsional disorder in P3HT is supported by our recent observation of comparably narrow (<390 cm⁻¹ or 49 meV) ZPL distributions for ladder-type oligomers and polymers, for which torsion is inhibited by synthesis.³²

When comparing the single-chain ZPL distribution with the corresponding low-temperature PL spectrum of a disordered (amorphous) film (both P3HT16, Figure 2a), we find that the ZPL distribution is not only much narrower but also significantly shifted by about 1200 cm⁻¹ (~150 meV) to higher energies with respect to the bulk data. This discrepancy is rather remarkable because the amorphous film PL is usually associated with largely noninteracting chain segments (sites) with disordered conformations that are transferred from solution by drop- or spin-casting. Because the conformation of the emitting sites does not depend on solvent, the conformation should be similar in both bulk and single-chain experiments (see also Supporting Information, section 4). Moreover, the electron–phonon coupling to low-energy phonon modes is only weak as shown by our single-chain spectra (Figure 1a,b). Consequently, the inhomogeneously broadened electronic line shape of the film spectrum in Figure

2a should be identical to the spectral distribution of ZPL positions, the so-called inhomogeneous distribution function.^{44,53–56} Obviously, this is not the case for P3HT, in contrast to e.g. ladder-type (*p*-phenylenes).³²

Bridging the Gap between Single-Chain and Ensemble Level. To resolve this discrepancy between bulk and single-chain data, we propose that in disordered ensembles (films and solutions) the emitting sites are predominantly species that are formed by chain–chain contacts due to the high concentrations involved (with respect to single-molecule experiments). Such chain–chain contacts tend to partially planarize the P3HT backbone, and at the same time the close proximity between chain segments gives rise to electronic Coulomb coupling between their transition dipole moments (importantly, this does not imply perfect π – π -stacking of chains). Both effects cause the noticeable red-shift and line broadening of (disordered) bulk spectra (see below). In contrast, we attribute the envelopes of the histograms of the single-chain ZPLs to the intrinsic inhomogeneous line shape of the emitting species of P3HT chains without chain–chain interactions. Notably, the nearly identical ZPL distributions for P3HT16 and P3HT144 (Figure 1e,f) indicate that even the long P3HT144 ($M_n \sim 24$ kDa) does not form low-energy emitting sites at the single-chain level due to e.g. back-folding of the backbone on itself.

The strong tendency of P3HT to form chain–chain contacts is demonstrated by concentration-dependent measurements specifically on the short P3HT16 embedded in *n*-hexadecane (Figure 2b) because P3HT16 is usually less prone to aggregation and back-folding does not occur.²² At the lowest concentration (0.3 nM) only a single ZPL is observed; i.e., only spatially isolated chains exist. Upon slightly increasing the concentration (1–10 nM), several P3HT16 chains, each with a single ZPL between 18 500 and 19 000 cm^{-1} (2.25 and 2.35 eV, cf. Figures 1e,f), are in the confocal excitation spot. At the same time an additional broad and red-shifted feature appears around 16 500 cm^{-1} (2.05 eV), which is characteristic for π -stacked aggregates with moderate order.⁶ For higher concentrations (≥ 100 nM) exclusively aggregate emission prevails.

It is very intriguing, though in line with recent work by vanden Bout et al.,⁵⁷ to find aggregates already at concentrations of ~ 1 nM in the P3HT16/*n*-hexadecane samples. This corresponds to ~ 50 nM in the P3HT16/chloroform solution, prior to the last dilution step into *n*-hexadecane and shock-freezing. Hence, even in the good solvent chloroform at such low concentration a significant fraction of chains must exist that interact by van der Waals forces between their π -electron systems. In chloroform solution, these interactions do not force the chains into ordered π -stacks; they rather lead to bundling of short segments of neighboring P3HT chains (“loose” aggregation), which is in dynamic equilibrium with spatially isolated chains. Upon adding *n*-hexadecane, the bundled segments will rearrange into more ordered π -stacked H-type structures to avoid this bad solvent. The presence of loose P3HT aggregates with a hydrodynamic radius of 50–60 nm in good solvents was verified in light-scattering experiments.^{19,58} In amorphous regions of rr-P3HT films, Russell et al. have recently identified domains with very short-range order,⁵⁹ which should be characteristic for loose aggregates. In fact, comparing Figures 2a and 2b suggests that the PL of an amorphous film is a superposition of emission from disordered, noninteracting sites and predominantly from loose aggregates that emit probably in

the range between 16 500 and 18 500 cm^{-1} (between π -stacked structures and isolated chains). As shown above, both species already exist in (dilute) solution using good solvents and are then transferred to films.

TDDFT Calculations: Impact of Torsional Disorder and Long-Range Electronic Coupling. To gain quantitative insights into the magnitudes of the spectral red-shifts due to partial planarization and electronic coupling associated with the formation of loose aggregates, we performed time-dependent density functional theory (TDDFT) simulations. These calculations are based on a nonempirical optimally tuned range separated hybrid,^{60–62} in which excited states are obtained in excellent agreement with experimental results⁴³ and with self-consistent many-body BSE-GW.⁶³

The influence of planarization is estimated by comparing the transition energy between the ground state and the lowest-energy optically allowed excited state of an isolated planar thiophene chain with that of a torsionally disordered chain obtained by MD simulations prior to the TDDFT calculations (P3HT with 16 repeating units; for details see Figures S5–S7). The results show that the effective conjugation length increases from about 6 to 10 repeating units with a concomitant decrease of the transition energy of up to about 4800 cm^{-1} (0.6 eV) when going from a torsionally disordered to a planar backbone. The effect of planarization on the transition energies in our experiments can be expected to be much smaller because planarization is certainly not complete upon loose aggregation.⁶ Hence, our calculations yield an upper bound for the shift between single-chain and ensemble PL, and our experimental findings are well within that bound.

In the next step we calculated the spectral shift of the lowest energy transition for an electronically coupled H-type dimer with two planar cofacially arranged oligothiophenes with 6 or 12 repeating units as a function of distance between the chains (Figure S8). We find that already at distances of 4.9 Å, larger than the typical π -stacking distance of ~ 3.8 Å,⁶⁴ the lowest energy transition of the dimer is red-shifted by about 1750 cm^{-1} (~ 0.22 eV) with respect to that of an isolated, planar chain. Notably, this electronic coupling in the dimer is rather long range, and even for chain–chain distances of ~ 8 Å the dimer's lowest-energy transition is still red-shifted by ~ 900 cm^{-1} (0.11 eV), in agreement with previous calculations.⁶⁵ In ensembles the geometric arrangement of interacting chain segments (in loose aggregates) as well as their torsional disorder will vary strongly. Orientations distinct from perfect cofacial arrangements tend to reduce the Coulomb coupling, i.e., reduce the red-shift, whereas higher intrachain disorder (for a given mutual arrangement) localizes electronic excitations and enhances electronic chain–chain couplings,^{11,65} which increases the red-shift.

CONCLUDING DISCUSSION

For the prototypical conjugated polymer P3HT, we investigated the discrepancies between the PL spectra of single chains and of amorphous films, in which disordered P3HT chains are usually thought of as noninteracting in the sense that spectral shifts due to Coulomb coupling between transition dipole moments do not play a role. We found that the single-chain ZPL distributions are blue-shifted by about 1200 cm^{-1} (~ 150 meV) in comparison to the electronic transition in the amorphous film PL spectrum; moreover, the inhomogeneous line width in the film is significantly broadened. Based on TDDFT calculations, this spectral shift can be accounted for by

partial backbone planarization and concomitant electronic coupling between transition dipole moments upon bundling of P3HT chain segments, i.e., by the formation of loose aggregates in bulk samples as illustrated in Figure 3. The precise

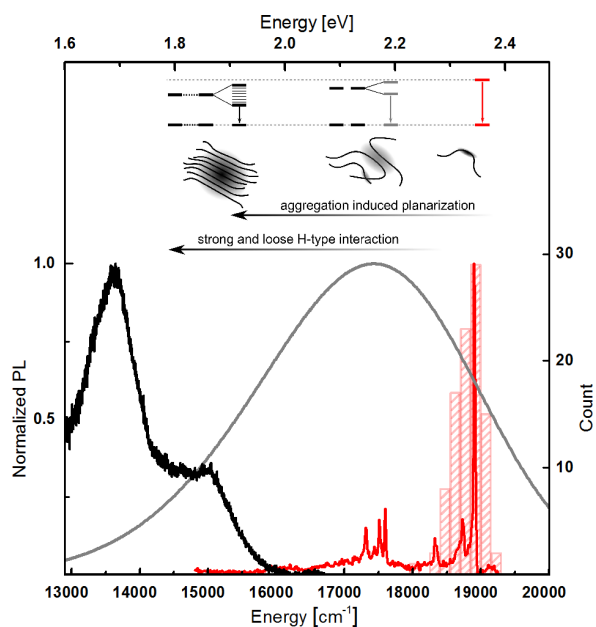


Figure 3. Bridging the gap between the single-chain ZPL distributions and the ensemble PL spectra. The single-chain spectrum (red line) and the corresponding histogram of ZPL positions at $\sim 19\,000\text{ cm}^{-1}$ (red bars) result from PL of single sites on isolated, disordered P3HT16 chains. The ensemble PL spectrum from disordered regions of a thin P3HT16 film (gray line) is red-shifted due to the formation of loose aggregates with concomitant planarization of P3HT segments and interchain electronic interaction. Finally, in ordered regions of P3HT films PL below $16\,000\text{ cm}^{-1}$ is observed (black), which results from π -stacked H-type aggregates with strong interchain electronic interaction. This situation is shown at the top with the illustration of an isolated chain (right), a loose aggregate prevailing in disordered films (and solutions, center), and a π -stacked H-aggregate (left). The gray shaded areas indicate the spatial extend of the excited state of the emitting species. The corresponding energy level schemes demonstrate that aggregation-induced planarization and the concomitant electronic coupling of neighboring chains leads to the formation of exciton bands, which results in red-shifted emission for both loose and π -stacked aggregates.

value for the red-shift is determined by the interplay between the mutual spatial arrangement of P3HT chain segments, their degree of planarization, and π -electron delocalization; the strong variations of these parameters in a disordered ensemble gives rise to the broad inhomogeneous line width of bulk spectra.

Importantly, in concentration-dependent measurements we provided evidence that loose aggregates are the dominating emitting species also in (dilute) P3HT solutions using good solvents, such as chloroform. Although one should be careful comparing low and room temperature data, we find that in the latter (P3HT in chloroform solution, Figure S1) the relative intensity of the (effective) carbon-bond stretch modes with respect to the electronic transition appears to be higher than in the single-chain PL spectra (Figure 1a,b). Because the Huang–Rhys factor for these high-energy modes ($\sim 1400\text{ cm}^{-1}$ or 175 meV) is rather independent of temperature,⁶⁶ this change in

relative intensity indicates H-type electronic interactions between chain segments in loose aggregates^{3,11,67} that exist in solution. Hence, while planarization is probably the dominating contribution to the observed red-shift from single chains to bulk, the influence of electronic coupling between chain segments is certainly not negligible.

Ultimately, loose aggregates can be forced to rearrange into ordered π -stacked H-aggregates by annealing of films or by reducing solvent quality (e.g., decrease of temperature, admixture of a bad solvent^{4,6,68}). Such H-aggregated P3HT chains feature a characteristic spectrum (Figure 3, thick solid line) with the further red-shifted electronic transition at $15\,500\text{ cm}^{-1}$ (1.9 eV), a distorted vibrational progression due to strong electronic Coulomb coupling (of up to 1600 cm^{-1} or 200 meV) between chains,^{3,4,65} and an inhomogeneous line width of only 760 cm^{-1} (95 meV)⁶⁸ reflecting a higher degree of order compared to solutions and disordered films. It is noteworthy that in another prototypical conjugated polymer, MEH-PPV, a similar spectral red-shift from single chains to solutions and films was observed.⁶⁹ However, in contrast to P3HT, for MEH-PPV this red-shift was shown to be exclusively caused by chain planarization, i.e., reduced conformational disorder, and not by interchain coupling.^{69–71} This is probably related to a different packing with larger center-of-mass distance between neighboring chains in MEH-PPV aggregates because, for instance, distyrylbenzenes, substituted with methoxy groups at the central ring, form only weakly coupled H-type aggregates.⁷²

In contrast to ensembles with their broad inhomogeneous line widths, single spatially isolated P3HT chains appear to be a remarkably well-defined system independent of the molecular weight. The very narrow ($<480\text{ cm}^{-1}$) ZPL distributions demonstrate that the degree of (torsional) disorder is very small, at least on length scales of the emitting sites, which is about 5–6 repeating units based on our TDDFT calculations. This length scale is in good agreement with the coherence length of the emitting site defined by Spano, Barford, and co-workers,^{45,73,74} who describe isolated conjugated polymer chains as J-type aggregates with the repeating units as building blocks (see Supporting Information, section 6). A conjugated polymer with a similar low degree of disorder as P3HT is e.g. represented by ladder-type (*p*-phenylene), LPP,³² in which the backbone is forced into a rigid, ordered structure by synthesis. The prototypical example for an ordered system is a defect-free single polydiacetylene (PDA) chain embedded in its own monomer crystal as extensively investigated by Schott et al.^{75–77} The common motif in the PL spectra of P3HT, LPP, and PDA is that the ZPLs are the most intense transitions, with the relative ZPL intensity showing an increasing trend in the order P3HT, LPP, PDA. Within the framework of the J-aggregate theory by Spano et al., this trend implies an increase in the coherence length in the same order. In particular, in PDA the ZPL intensity is strongly enhanced at low temperatures (about 100 times stronger than the intensities of the carbon-bond stretch modes), which yields a coherence length of several micrometers,⁷⁸ as indeed observed.^{76,79}

Although our single-chain P3HT spectra are reminiscent of the high-energy “blue-site” emission,^{13–15} which was attributed to stem from sites with exceptionally short effective conjugation length, we provided evidence that those “blue sites” are the emitting species of isolated poly(3-alkylthiophenes) without chain–chain interactions. We note that the ZPL energies measured here are also in good quantitative agreement with recent calculations on isolated P3HT chains at low temper-

atures.⁵⁰ “Solution” and “red site” emission (as defined above in the Introduction) often found in single-chain experiments are thus already a result of (loose) aggregation, which is difficult to avoid even at very low concentrations in good solvents.

Our results on single P3HT chains have strong implications for theoretical concepts that aim at describing the nature of electronic excitations in ordered P3HT films and nanostructures, such as H or HJ models put forward by Spano and co-workers.^{3,11,80} In such models, solution spectra are usually the starting point and are assumed to represent the PL/absorption of isolated, noninteracting chains. However, our data clearly show that this “solution approach” has several shortcomings: First, this approach strongly underestimates the spectral redshift from isolated chains to densely π -stacked aggregates in films and nanostructures. Second, the single-chain Huang–Rhys parameter for the carbon-stretching modes is usually retrieved from solution spectra (and is thus about unity). However, our data clearly show that emission from loosely aggregated chains dominates the solution PL, and hence this approach overestimates the single-chain Huang–Rhys factor (although we note that the Huang–Rhys factor determined from our PL spectra varies from chain to chain due to variations of the conjugation or coherence length of the emitting site; in this sense there is no well-defined Huang–Rhys parameter for a single chain). Finally, the “solution approach” strongly overestimates energy disorder of isolated chains because the inhomogeneous width of the electronic transition in solution spectra is much larger than that of the single-chain ZPL distributions. Hence, our data may help to improve the modeling and prediction of the properties of electronically excited states in device relevant P3HT films.

■ ASSOCIATED CONTENT

📄 Supporting Information

The Supporting Information is available free of charge on the ACS Publications website at DOI: [10.1021/acs.macromol.6b02077](https://doi.org/10.1021/acs.macromol.6b02077).

Materials, methods, single-chain spectra, Franck–Condon analysis of a disordered P3HT film at 1.5 K, TDDFT simulations on oligothiophenes, and coherence length of the emitting sites (PDF)

■ AUTHOR INFORMATION

Corresponding Author

*Phone +49 921 554040; e-mail richard.hildner@uni-bayreuth.de (R.H.).

ORCID

Richard Hildner: [0000-0002-7282-3730](https://orcid.org/0000-0002-7282-3730)

Notes

The authors declare no competing financial interest.

■ ACKNOWLEDGMENTS

This work was financially supported by the German Research Foundation DFG within projects HI1508/2 (D.R., S.B., R.H.) and GRK1640 (D.R., S.B., J.K., M.T., S.K., R.H.). Additional funding came from the Bavarian State Ministry of Science, Research and the Arts for the collaborative research network Solar Technologies Go Hybrid (J.K., M.T., S.K.). R.H. acknowledges the Elite Network of Bavaria (ENB) Macromolecular Sciences for funding his position. We thank Marin

van Heel (University of Leiden, NL) for providing the MSA algorithm for data analysis.

■ REFERENCES

- (1) Huang, Y.; Kramer, E. J.; Heeger, A. J.; Bazan, G. C. Bulk heterojunction solar cells: morphology and performance relationships. *Chem. Rev.* **2014**, *114* (14), 7006–7043.
- (2) Sirringhaus, H. 25th anniversary article: organic field-effect transistors: the path beyond amorphous silicon. *Adv. Mater.* **2014**, *26* (9), 1319–1335.
- (3) Clark, J.; Silva, C.; Friend, R. H.; Spano, F. C. Role of Intermolecular Coupling in the Photophysics of Disordered Organic Semiconductors: Aggregate Emission in Regioregular Polythiophene. *Phys. Rev. Lett.* **2007**, *98* (20), 206406.
- (4) Scharsich, C.; Lohwasser, R. H.; Sommer, M.; Asawapirom, U.; Scherf, U.; Thelakkat, M.; Neher, D.; Köhler, A. Control of aggregate formation in poly(3-hexylthiophene) by solvent, molecular weight, and synthetic method. *J. Polym. Sci., Part B: Polym. Phys.* **2012**, *50* (6), 442–453.
- (5) Paquin, F.; Yamagata, H.; Hestand, N. J.; Sakowicz, M.; Bérubé, N.; Côté, M.; Reynolds, L. X.; Haque, S. A.; Stingelin, N.; Spano, F. C.; Silva, C. Two-dimensional spatial coherence of excitons in semicrystalline polymeric semiconductors: Effect of molecular weight. *Phys. Rev. B: Condens. Matter Mater. Phys.* **2013**, *88* (15), 155202.
- (6) Panzer, F.; Bäessler, H.; Lohwasser, R. H.; Thelakkat, M.; Köhler, A. The Impact of Polydispersity and Molecular Weight on the Order–Disorder Transition in Poly(3-hexylthiophene). *J. Phys. Chem. Lett.* **2014**, *5* (15), 2742–2747.
- (7) Niles, E. T.; Roehling, J. D.; Yamagata, H.; Wise, A. J.; Spano, F. C.; Moulé, A. J.; Grey, J. K. J-Aggregate Behavior in Poly-3-hexylthiophene Nanofibers. *J. Phys. Chem. Lett.* **2012**, *3* (2), 259–263.
- (8) Baghgar, M.; Labastide, J.; Bokel, F.; Dujovne, I.; McKenna, A.; Barnes, A. M.; Pentzer, E.; Emrick, T.; Hayward, R.; Barnes, M. D. Probing Inter- and Intrachain Exciton Coupling in Isolated Poly(3-hexylthiophene) Nanofibers: Effect of Solvation and Regioregularity. *J. Phys. Chem. Lett.* **2012**, *3* (12), 1674–1679.
- (9) Martin, T. P.; Wise, A. J.; Busby, E.; Gao, J.; Roehling, J. D.; Ford, M. J.; Larsen, D. S.; Moulé, A. J.; Grey, J. K. Packing dependent electronic coupling in single poly(3-hexylthiophene) H- and J-aggregate nanofibers. *J. Phys. Chem. B* **2013**, *117* (16), 4478–4487.
- (10) Baghgar, M.; Labastide, J. A.; Bokel, F.; Hayward, R. C.; Barnes, M. D. Effect of Polymer Chain Folding on the Transition from H- to J-Aggregate Behavior in P3HT Nanofibers. *J. Phys. Chem. C* **2014**, *118* (4), 2229–2235.
- (11) Spano, F. C.; Silva, C. H- and J-aggregate behavior in polymeric semiconductors. *Annu. Rev. Phys. Chem.* **2014**, *65*, 477–500.
- (12) Thiessen, A.; Vogelsang, J.; Adachi, T.; Steiner, F.; Vanden Bout, D. A.; Lupton, J. M. Unraveling the chromophoric disorder of poly(3-hexylthiophene). *Proc. Natl. Acad. Sci. U. S. A.* **2013**, *110* (38), E3550.
- (13) Chen, P.-Y.; Rassamesard, A.; Chen, H.-L.; Chen, S.-A. Conformation and Fluorescence Property of Poly(3-hexylthiophene) Isolated Chains Studied by Single Molecule Spectroscopy: Effects of Solvent Quality and Regioregularity. *Macromolecules* **2013**, *46* (14), 5657–5663.
- (14) Palacios, R. E.; Barbara, P. F. Single molecule spectroscopy of poly 3-octyl-thiophene (P3OT). *J. Fluoresc.* **2007**, *17* (6), 749–757.
- (15) Hu, Z.; Zou, J.; Deibel, C.; Gesquiere, A. J.; Zhai, L. Single-Molecule Spectroscopy and AFM Morphology Studies of a Diblock Copolymer Consisting of Poly(3-hexylthiophene) and Fullerene. *Macromol. Chem. Phys.* **2010**, *211* (22), 2416–2424.
- (16) Hu, Z.; Liu, J.; Simón-Bower, L.; Zhai, L.; Gesquiere, A. J. Influence of backbone rigidity on single chain conformation of thiophene-based conjugated polymers. *J. Phys. Chem. B* **2013**, *117* (16), 4461–4467.
- (17) Adachi, T.; Lakhwani, G.; Traub, M. C.; Ono, R. J.; Bielawski, C. W.; Barbara, P. F.; Vanden Bout, D. A. Conformational Effect on Energy Transfer in Single Polythiophene Chains. *J. Phys. Chem. B* **2012**, *116* (32), 9866–9872.

- (18) Liu, Y.-C.; Liang, R.; Fu, L.-M.; Ren, F.; Zhang, J.-P. A critical temperature regime for poly(3-hexylthiophene) dissolution in concentrated solutions of ortho-dichlorobenzene. *Chem. Phys. Lett.* **2015**, *631*–632, 78–82.
- (19) Huang, Y.; Cheng, H.; Han, C. C. Unimer–Aggregate Equilibrium to Large Scale Association of Regioregular Poly(3-hexylthiophene) in THF Solution. *Macromolecules* **2011**, *44* (12), 5020–5026.
- (20) Liu, J.; Arif, M.; Zou, J.; Khondaker, S. I.; Zhai, L. Controlling Poly(3-hexylthiophene) Crystal Dimension: Nanowhiskers and Nanoribbons. *Macromolecules* **2009**, *42* (24), 9390–9393.
- (21) Balko, J.; Lohwasser, R. H.; Sommer, M.; Thelakkat, M.; Thurn-Albrecht, T. Determination of the Crystallinity of Semicrystalline Poly(3-hexylthiophene) by Means of Wide-Angle X-ray Scattering. *Macromolecules* **2013**, *46* (24), 9642–9651.
- (22) Singh, C. R.; Gupta, G.; Lohwasser, R. H.; Engmann, S.; Balko, J.; Thelakkat, M.; Thurn-Albrecht, T.; Hoppe, H. Correlation of charge transport with structural order in highly ordered melt-crystallized poly(3-hexylthiophene) thin films. *J. Polym. Sci., Part B: Polym. Phys.* **2013**, *51* (12), 943–951.
- (23) Brinkmann, M.; Rannou, P. Effect of Molecular Weight on the Structure and Morphology of Oriented Thin Films of Regioregular Poly(3-hexylthiophene) Grown by Directional Epitaxial Solidification. *Adv. Funct. Mater.* **2007**, *17* (1), 101–108.
- (24) Lohwasser, R. H.; Thelakkat, M. Toward Perfect Control of End Groups and Polydispersity in Poly(3-hexylthiophene) via Catalyst Transfer Polymerization. *Macromolecules* **2011**, *44* (9), 3388–3397.
- (25) Moerner, W. E.; Plakhotnik, T.; Irngartinger, T.; Croci, M.; Palm, V.; Wild, U. P. Optical Probing of Single Molecules of Terrylene in a Shpol'kii Matrix: A Two-State Single-Molecule Switch. *J. Phys. Chem.* **1994**, *98* (30), 7382–7389.
- (26) Lang, E.; Würthner, F.; Köhler, J. Photophysical properties of a tetraphenoxy-substituted perylene bisimide derivative characterized by single-molecule spectroscopy. *ChemPhysChem* **2005**, *6* (5), 935–941.
- (27) Mais, S.; Tittel, J.; Basché, T.; Bräuchle, C.; Göhde, W.; Fuchs, H.; Müller, G.; Müllen, K. Terrylenediimide: A Novel Fluorophore for Single-Molecule Spectroscopy and Microscopy from 1.4 K to Room Temperature. *J. Phys. Chem. A* **1997**, *101* (45), 8435–8440.
- (28) Hildner, R.; Lemmer, U.; Scherf, U.; van Heel, M.; Köhler, J. Revealing the Electron–Phonon Coupling in a Conjugated Polymer by Single-Molecule Spectroscopy. *Adv. Mater.* **2007**, *19* (15), 1978–1982.
- (29) Hildner, R.; Winterling, L.; Lemmer, U.; Scherf, U.; Köhler, J. Single-molecule spectroscopy on a ladder-type conjugated polymer: electron-phonon coupling and spectral diffusion. *ChemPhysChem* **2009**, *10* (14), 2524–2534.
- (30) Ferreira, B.; da Silva, P. F.; Seixas de Melo, J. S.; Pina, J.; Maçanita, A. Excited-state dynamics and self-organization of poly(3-hexylthiophene) (P3HT) in solution and thin films. *J. Phys. Chem. B* **2012**, *116* (8), 2347–2355.
- (31) Feist, F. A.; Basché, T. Fluorescence excitation and emission spectroscopy on single MEH-PPV chains at low temperature. *J. Phys. Chem. B* **2008**, *112* (32), 9700–9708.
- (32) Baderschneider, S.; Scherf, U.; Köhler, J.; Hildner, R. Influence of the Conjugation Length on the Optical Spectra of Single Ladder-Type (p-Phenylene) Dimers and Polymers. *J. Phys. Chem. A* **2016**, *120* (2), 233–240.
- (33) Pullerits, T.; Mirzov, O.; Scheblykin, I. G. Conformational fluctuations and large fluorescence spectral diffusion in conjugated polymer single chains at low temperatures. *J. Phys. Chem. B* **2005**, *109* (41), 19099–19107.
- (34) Schindler, F.; Lupton, J. M.; Feldmann, J.; Scherf, U. A universal picture of chromophores in pi-conjugated polymers derived from single-molecule spectroscopy. *Proc. Natl. Acad. Sci. U. S. A.* **2004**, *101* (41), 14695–14700.
- (35) Rubinstein, M.; Colby, R. H. *Polymer Physics*; Oxford University Press: Oxford, NY, 2003.
- (36) Strobl, G. R. *The Physics of Polymers: Concepts for Understanding Their Structures and Behavior*, 3rd revised and expanded ed.; Springer: Berlin, 2007.
- (37) McCulloch, B.; Ho, V.; Hoarfrost, M.; Stanley, C.; Do, C.; Heller, W. T.; Segalman, R. A. Polymer Chain Shape of Poly(3-alkylthiophenes) in Solution Using Small-Angle Neutron Scattering. *Macromolecules* **2013**, *46* (5), 1899–1907.
- (38) Becker, R. S.; Seixas de Melo, J.; Maçanita, A. L.; Elisei, F. Comprehensive Evaluation of the Absorption, Photophysical, Energy Transfer, Structural, and Theoretical Properties of α -Oligothiophenes with One to Seven Rings. *J. Phys. Chem.* **1996**, *100* (48), 18683–18695.
- (39) Gierschner, J.; Cornil, J.; Egelhaaf, H.-J. Optical Bandgaps of π -Conjugated Organic Materials at the Polymer Limit: Experiment and Theory. *Adv. Mater.* **2007**, *19* (2), 173–191.
- (40) Milián-Medina, B.; Gierschner, J. π -Conjugation. *WIREs Comput. Mol. Sci.* **2012**, *2* (4), 513–524.
- (41) Rossi, G.; Chance, R. R.; Silbey, R. Conformational disorder in conjugated polymers. *J. Chem. Phys.* **1989**, *90* (12), 7594.
- (42) de Queiroz, T. B.; Kümmel, S. Charge-transfer excitations in low-gap systems under the influence of solvation and conformational disorder: exploring range-separation tuning. *J. Chem. Phys.* **2014**, *141* (8), 084303.
- (43) de Queiroz, T. B.; Kümmel, S. Tuned range separated hybrid functionals for solvated low bandgap oligomers. *J. Chem. Phys.* **2015**, *143* (3), 034101.
- (44) Kador, L. Stochastic theory of inhomogeneous spectroscopic line shapes reinvestigated. *J. Chem. Phys.* **1991**, *95* (8), 5574.
- (45) Marcus, M.; Tozer, O. R.; Barford, W. Theory of optical transitions in conjugated polymers. II. Real systems. *J. Chem. Phys.* **2014**, *141* (16), 164102.
- (46) Hoffmann, S. T.; Bässler, H.; Köhler, A. What determines inhomogeneous broadening of electronic transitions in conjugated polymers? *J. Phys. Chem. B* **2010**, *114* (51), 17037–17048.
- (47) Kobayashi, H.; Tsuchiya, K.; Ogino, K.; Vacha, M. Spectral multitude and spectral dynamics reflect changing conjugation length in single molecules of oligophenylenevinylenes. *Phys. Chem. Chem. Phys.* **2012**, *14* (29), 10114–10118.
- (48) Habuchi, S.; Fujita, H.; Michinobu, T.; Vacha, M. Twist Angle Plays an Important Role in Photophysical Properties of a Donor–Acceptor-Type Conjugated Polymer: A Combined Ensemble and Single-Molecule Study. *J. Phys. Chem. B* **2011**, *115* (49), 14404–14415.
- (49) Bhatta, R. S.; Yimer, Y. Y.; Tsigie, M.; Perry, D. S. Conformations and torsional potentials of poly(3-hexylthiophene) oligomers: Density functional calculations up to the dodecamer. *Comput. Theor. Chem.* **2012**, *995*, 36–42.
- (50) Simine, L.; Rossky, P. J. Relating Chromophoric and Structural Disorder in Conjugated Polymers. *ArXiv e-prints* [Online] 2016; <https://arxiv.org/abs/1610.02604>.
- (51) Brambilla, L.; Tommasini, M.; Botiz, I.; Rahimi, K.; Agumba, J. O.; Stingelin, N.; Zerbi, G. Regio-Regular Oligo and Poly(3-hexyl thiophene): Precise Structural Markers from the Vibrational Spectra of Oligomer Single Crystals. *Macromolecules* **2014**, *47* (19), 6730–6739.
- (52) Zade, S. S.; Bendikov, M. Twisting of conjugated oligomers and polymers: case study of oligo- and polythiophene. *Chem. - Eur. J.* **2007**, *13* (13), 3688–3700.
- (53) Moerner, W. E. A Dozen Years of Single-Molecule Spectroscopy in Physics, Chemistry, and Biophysics. *J. Phys. Chem. B* **2002**, *106* (5), 910–927.
- (54) Friedrich, J.; Haarer, D. Photochemical Hole Burning: A Spectroscopic Study of Relaxation Processes in Polymers and Glasses. *Angew. Chem., Int. Ed. Engl.* **1984**, *23* (2), 113–140.
- (55) Tamarat, P.; Maali, A.; Lounis, B.; Orrit, M. Ten Years of Single-Molecule Spectroscopy. *J. Phys. Chem. A* **2000**, *104* (1), 1–16.
- (56) Rebane, L. A.; Gorokhovskii, A. A.; Kikas, J. V. Low-temperature spectroscopy of organic molecules in solids by photochemical hole burning. *Appl. Phys. B: Photophys. Laser Chem.* **1982**, *29* (4), 235–250.

- (57) Hu, Z.; Willard, A. P.; Ono, R. J.; Bielawski, C. W.; Rossky, P. J.; Vanden Bout, D. A. An insight into non-emissive excited states in conjugated polymers. *Nat. Commun.* **2015**, *6*, 8246.
- (58) Huang, Y.; Cheng, H.; Han, C. C. Temperature Induced Structure Evolution of Regioregular Poly(3-hexylthiophene) in Dilute Solution and its Influence on Thin Film Morphology. *Macromolecules* **2010**, *43* (23), 10031–10037.
- (59) Shen, X.; Hu, W.; Russell, T. P. Measuring the Degree of Crystallinity in Semicrystalline Regioregular Poly(3-hexylthiophene). *Macromolecules* **2016**, *49* (12), 4501–4509.
- (60) Stein, T.; Kronik, L.; Baer, R. Prediction of charge-transfer excitations in coumarin-based dyes using a range-separated functional tuned from first principles. *J. Chem. Phys.* **2009**, *131* (24), 244119.
- (61) Stein, T.; Kronik, L.; Baer, R. Reliable prediction of charge transfer excitations in molecular complexes using time-dependent density functional theory. *J. Am. Chem. Soc.* **2009**, *131* (8), 2818–2820.
- (62) Karolewski, A.; Neubig, A.; Thelakkat, M.; Kümmel, S. Optical absorption in donor-acceptor polymers—alternating vs. random. *Phys. Chem. Chem. Phys.* **2013**, *15* (46), 20016–20025.
- (63) Niedzialek, D.; Duchemin, I.; de Queiroz, T. B.; Osella, S.; Rao, A.; Friend, R. H.; Blase, X.; Kümmel, S.; Beljonne, D. First Principles Calculations of Charge Transfer Excitations in Polymer-Fullerene Complexes: Influence of Excess Energy. *Adv. Funct. Mater.* **2015**, *25* (13), 1972–1984.
- (64) Wirix, M. J. M.; Bomans, P. H. H.; Friedrich, H.; Sommerdijk, N. A. J. M.; de With, G. Three-dimensional structure of P3HT assemblies in organic solvents revealed by cryo-TEM. *Nano Lett.* **2014**, *14* (4), 2033–2038.
- (65) Gierschner, J.; Huang, Y.-S.; van Aeverbeke, B.; Cornil, J.; Friend, R. H.; Beljonne, D. Excitonic versus electronic couplings in molecular assemblies: The importance of non-nearest neighbor interactions. *J. Chem. Phys.* **2009**, *130* (4), 044105.
- (66) Richards, J. L. Study of Impurity–Host Coupling in Shpolskii Matrices. *J. Chem. Phys.* **1971**, *54* (5), 2014.
- (67) Spano, F. C. Modeling disorder in polymer aggregates: The optical spectroscopy of regioregular poly(3-hexylthiophene) thin films. *J. Chem. Phys.* **2005**, *122* (23), 234701.
- (68) Panzer, F.; Sommer, M.; Bäessler, H.; Thelakkat, M.; Köhler, A. Spectroscopic Signature of Two Distinct H-Aggregate Species in Poly(3-hexylthiophene). *Macromolecules* **2015**, *48* (5), 1543–1553.
- (69) Mirzov, O.; Scheblykin, I. G. Photoluminescence spectra of a conjugated polymer: from films and solutions to single molecules. *Phys. Chem. Chem. Phys.* **2006**, *8* (47), 5569–5576.
- (70) Köhler, A.; Hoffmann, S. T.; Bäessler, H. An order-disorder transition in the conjugated polymer MEH-PPV. *J. Am. Chem. Soc.* **2012**, *134* (28), 11594–11601.
- (71) De Leener, C.; Hennebicq, E.; Sancho-Garcia, J.-C.; Beljonne, D. Modeling the dynamics of chromophores in conjugated polymers: the case of poly(2-methoxy-5-(2'-ethylhexyl)oxy 1,4-phenylene vinylene) (MEH-PPV). *J. Phys. Chem. B* **2009**, *113* (5), 1311–1322.
- (72) Gierschner, J.; Park, S. Y. Luminescent distyrylbenzenes: Tailoring molecular structure and crystalline morphology. *J. Mater. Chem. C* **2013**, *1* (37), 5818.
- (73) Spano, F. C.; Yamagata, H. Vibronic coupling in J-aggregates and beyond: a direct means of determining the exciton coherence length from the photoluminescence spectrum. *J. Phys. Chem. B* **2011**, *115* (18), 5133–5143.
- (74) Yamagata, H.; Spano, F. C. Strong Photophysical Similarities between Conjugated Polymers and J-aggregates. *J. Phys. Chem. Lett.* **2014**, *5* (3), 622–632.
- (75) Lécuyer, R.; Berréhar, J.; Ganière, J. D.; Lapersonne-Meyer, C.; Lavallard, P.; Schott, M. Fluorescence yield and lifetime of isolated polydiacetylene chains: Evidence for a one-dimensional exciton band in a conjugated polymer. *Phys. Rev. B: Condens. Matter Mater. Phys.* **2002**, *66* (12), 125205.
- (76) Dubin, F.; Melet, R.; Barisien, T.; Grousson, R.; Legrand, L.; Schott, M.; Voliotis, V. Macroscopic coherence of a single exciton state in an organic quantum wire. *Nat. Phys.* **2006**, *2* (1), 32–35.
- (77) Legrand, L.; Choueiry, A. A.; Holcman, J.; Enderlin, A.; Melet, R.; Barisien, T.; Voliotis, V.; Grousson, R.; Schott, M. Excitons in a perfect quasi-1D organic quantum wire, an isolated polydiacetylene chain. *Phys. Status Solidi B* **2008**, *245* (12), 2702–2707.
- (78) Yamagata, H.; Spano, F. C. Vibronic coupling in quantum wires: applications to polydiacetylene. *J. Chem. Phys.* **2011**, *135* (5), 054906.
- (79) Holcman, J.; Al Choueiry, A.; Enderlin, A.; Hameau, S.; Barisien, T.; Legrand, L. Coherent control of the optical emission in a single organic quantum wire. *Nano Lett.* **2011**, *11* (10), 4496–4502.
- (80) Yamagata, H.; Hestand, N. J.; Spano, F. C.; Köhler, A.; Scharsich, C.; Hoffmann, S. T.; Bäessler, H. The red-phase of poly[2-methoxy-5-(2-ethylhexyloxy)-1,4-phenylenevinylene] (MEH-PPV): a disordered HJ-aggregate. *J. Chem. Phys.* **2013**, *139* (11), 114903.

**Supporting Information
to**

**Emitting Species of Poly(3-hexylthiophene):
From Single, Isolated Chains to Bulk**

Dominic Raithel¹, Sebastian Baderschneider¹, Thiago B. de Queiroz^{2,3}, Ruth Lohwasser⁴,
Jürgen Köhler¹, Mukundan Thelakkat⁴, Stephan Kümmel³, Richard Hildner^{1*}

¹ *Experimental Physics IV and Bayreuth Institute for Macromolecular Research (BIMF), University of
Bayreuth, 95440 Bayreuth, Germany*

² *Centro de Ciências Naturais e Humanas, Universidade Federal do ABC, 09510-580, Santo André-SP, Brazil*

³ *Theoretical Physics IV, University of Bayreuth, 95440 Bayreuth, Germany*

⁴ *Applied Functional Polymers, University of Bayreuth, 95440 Bayreuth, Germany*

1. Materials

2. Methods

3. Single-Chain Spectra

4. Frank-Condon analysis of PL spectra of a disordered P3HT film at 1.5 K

5. TDDFT simulations on oligothiophenes

6. Coherence length of the emitting sites

*Corresponding Author:

Phone.: +49 921 554040

E-Mail: richard.hildner@uni-bayreuth.de

1. Materials

Using catalyst transfer polymerization we synthesized P3HT with various chain lengths and low dispersity.¹ For our studies we used short chains with 16 repeating units (P3HT16: $M_n = 2.6$ kg/mol, regioregularity $\sim 93\%$ $\bar{D} = 1.17$, MALDI-TOF MS) and long chains with 144 repeating units (P3HT144: $M_n = 24.0$ kg/mol, regioregularity $> 98\%$, $\bar{D} = 1.15$, MALDI-TOF MS). Especially the short chains are a very defined system, as e.g. back-folding can be excluded; moreover, the number of repeating units is only slightly larger than the effective conjugation length of < 10 repeating units (see main text, SI section 5 and references 2–7).

The room temperature ensemble spectra of both P3HT samples in chloroform (Fluka, $\geq 99.8\%$) solution are depicted in Fig. S1 (P3HT16: red; P3HT144: blue). Prior to the measurements both samples have been heated up to about 60°C to dissolve P3HT and subsequently cooled down to room temperature. The absorption spectra (dashed lines) exhibit the well-known structureless shape with a peak at $\sim 22500\text{ cm}^{-1}$ (corresponding to 2.81 eV or 444 nm) for P3HT16 (red) and at $\sim 22000\text{ cm}^{-1}$ (corresponding to 2.73 eV or 455 nm) for P3HT144 (blue), respectively.

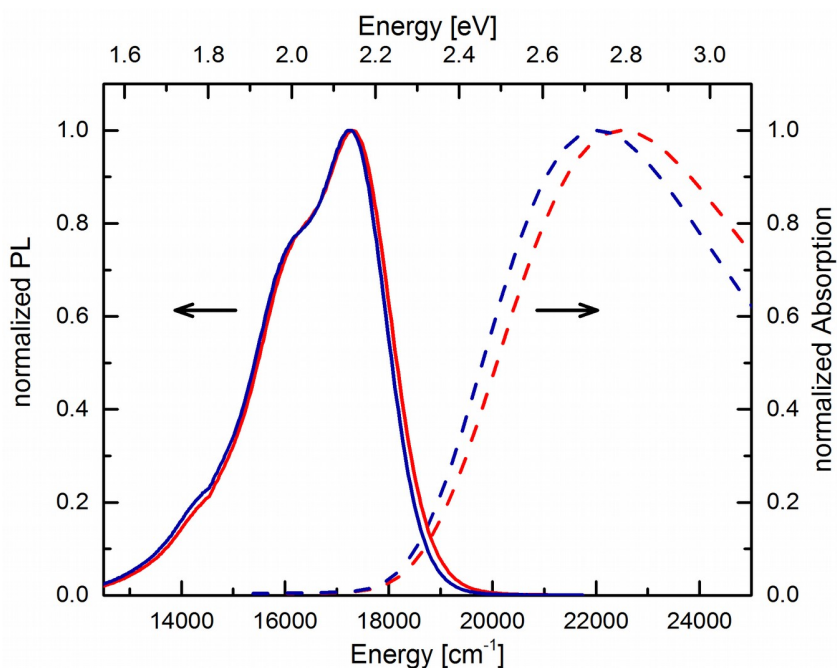


Figure S1: Normalized absorption (dashed lines) and photoluminescence spectra (solid) of P3HT16 (red) and P3HT144 (blue) dissolved in chloroform at room temperature. The concentrations were 5 μM for P3HT16 and 0.5 μM for P3HT144.

The PL spectra (solid lines) of the short (red) and long chains (blue) are virtually identical, which is reasonable given the effective conjugation length of < 10 repeating units for polythiophenes.²⁻⁷ Both spectra feature their maximum at around 17300 cm^{-1} (2.16 eV or 578 nm) and a vibrational progression due to electron-phonon coupling to aromatic carbon-bond stretch modes with energies of $\sim 1400\text{ cm}^{-1}$. The inhomogeneous line width of the electronic transition is $\sim 1500\text{ cm}^{-1}$ (full width at half maximum, FWHM).

2. Methods

Ensemble absorption and PL spectra were recorded using commercial spectrometers (Lambda 750 UV/VIS Spectrometer, Perkin Elmer and Cary Eclipse Fluorescence Spectrophotometer, Varian) using chloroform (Fluka, $\geq 99.8\%$) as solvent.

For the low-temperature single-chain and concentration-dependent experiments P3HT was dissolved and further diluted in chloroform (Fluka, $\geq 99.8\%$). Only the last dilution step (by a factor of 50, vol/vol) was carried out into *n*-hexadecane (Fluka, $\geq 98\%$). The final concentration for single-chain measurements on those samples was about 0.3 nM; for the concentration-dependent measurements the numbers are given in the main text (Fig. 2b). A drop of the top layer of this solution was sandwiched between a quartz substrate and a microscopy coverslip. The sample was then shock-frozen by inserting into liquid nitrogen and subsequently cooled down to liquid helium temperature (1.5 K). This procedure allows us to prepare samples in a very controlled way, because *n*-hexadecane is a bad solvent for P3HT and thus the chains can only exist in two states: truly isolated or in ordered π -stacked H-aggregates. First, at very low (single-molecule) concentration P3HT chains are largely spatially isolated already in the highly diluted chloroform solution, and hence isolated, non-interacting chains will also exist in the *n*-hexadecane solution after the last dilution step. In other words, true single-chain level is achieved. Second, at higher concentrations, chains in close proximity to each other (which eventually form loose aggregates) in chloroform solution, immediately start to form π -stacked aggregates upon adding *n*-hexadecane to avoid contact with this bad solvent (Fig. 2).

The low-temperature single-chain and concentration-dependent experiments were conducted on a home-built confocal microscope. In order to exclude preferential excitation of

specific sub-ensembles of P3HT chains, we excited P3HT with wavelength of 450 nm and 488 nm, using diode lasers (LDH-P-C-450B, PicoQuant with Clean-Up filter BP 440/40, AHF; Alphaslas Monopower 488-50-MM with Clean-Up filter BP488/6, AHF). The laser light was focused into the sample plane by an objective (NA=0.65, Laser2000; NA=0.85, Edmund Optics; NA=0.9, Microthek) that was mounted inside the cryostat and immersed in liquid helium. The emitted light was collected by the same objective and passed the beam splitter (z488RDC or 458DCR, both AHF) as well as long-pass filters (514LP, 496LP or 467LP, all AHF). Finally, it was focused onto the entrance slit of a spectrometer (SpectraPro-150, Acton Research Corporation, 300 lines/mm grating), equipped with a water-cooled electron-multiplying charge-coupled device (emCCD) camera (iXon DV-887, Andor). The total spectral resolution was 11 cm^{-1} (1.38 meV; corresponding to 0.3 nm at 530 nm). From each single chain we measured consecutively up to 500 individual spectra with an integration time of 1 s per spectrum. For polarization-resolved measurements we additionally inserted a motorized polarizer in the emission path in front of the spectrometer.

We performed data analysis with a home-written php-program which allowed to correct for background signals and the quantum efficiency of the detector as well as to fit the spectra. Furthermore we employed a multivariate statistical pattern recognition algorithm (MSA) for data analysis to overcome spectral diffusion on time scales slower than the integration time for an individual spectrum (1 s). The algorithm sorts each individual spectrum from a single chain into a predetermined number of classes (here: 4 – 14) according to their statistical similarity, such that the variance between the classes is maximized and the total intraclass variance is minimized. Subsequent averaging over spectra within the same class, i.e. over sufficiently similar spectra,

results in so called class averaged spectra (CAS). These CAS exhibit narrower ZPLs and allow to reveal more spectral details compared to the spectra that are temporally averaged over entire stacks of up to 500 individual spectra,⁸⁻¹⁰ see Section 3.

3. Single-chain spectra

In Figs. S2 and S3 the data analysis of single-chain PL spectra is illustrated on two examples. To demonstrate the power of the MSA algorithm we show in Fig. S2 (top left) a stack of 400 sequentially recorded PL spectra of a single P3HT144 chain.

Strong spectral diffusion as well as one-step blinking (e.g. around 200 s) and a photobleaching event (at ~ 340 s) are clearly visible. All these observations indicate that the long chain behaves as a single emitter. The time-averaged spectrum over all 400 individual spectra is displayed in the bottom panel and shows a ZPL at ~ 19000 cm^{-1} with a broad width of 180 cm^{-1} (FWHM). Applying the MSA algorithm to this stack of spectra, the 400 individual spectra are grouped into 8 classes, as described above. Fig. S2 (right) shows three examples of CAS that feature substantially reduced ZPL widths down to 36 cm^{-1} . Due to the narrow ZPLs, also the vibronic lines feature a smaller width, making it possible to resolve details that are otherwise hidden in the time-averaged spectrum (see below for an assignment of vibrational modes).

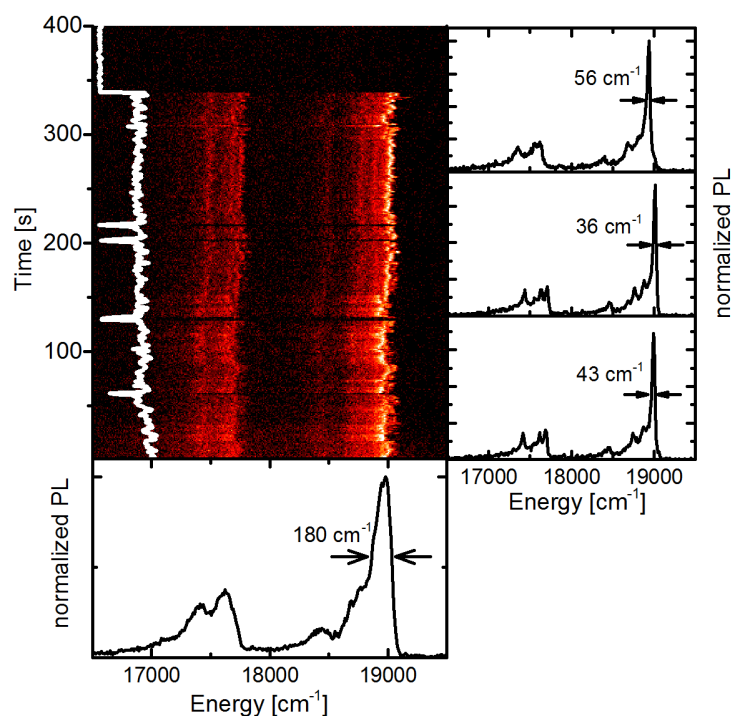


Figure S2: Low temperature PL spectrum of a single isolated P3HT144 chain embedded in *n*-hexadecane. Top left: 2-dimensional representation of a stack of 400 sequentially acquired spectra with an integration time of 1 s per spectrum. As vertical axis we display the measurement time, the horizontal axis is the photon energy and the PL intensity is colour-coded. The white line shows the spectrally integrated intensity for each spectrum as a function of time. Bottom: PL spectrum averaged over the full acquisition time of 400 s. The ZPL is located at 18980 cm^{-1} with a FWHM of 180 cm^{-1} . Top right: Three examples of class averaged spectra (out of a total of 8 classes) as obtained after applying the MSA algorithm. The ZPL widths (FWHM) are indicated at the spectra.

Fig. S3 (top left) displays a stack of 485 consecutively recorded spectra from a P3HT16 chain with an integration time of 1 s each. Between two successive spectra the polarizer in front of the spectrometer is rotated by 0.9° , which results in a clear modulation in the PL intensity from that chain. Integrating the emission intensity of the ZPL from 18865 to 18931 cm^{-1} (Fig. S3, top right) reveals a full modulation between maximum intensity and background signal as a function of the polarization angle. This observation is in good agreement with a \cos^2 -dependency (grey line) and is a strong indication for a single emitter. Notably, the emission of this P3HT chain is spectrally very stable, i.e. it features essentially no spectral diffusion on time scales slower than the acquisition time for an individual spectrum. Hence, applying the MSA algorithm is not necessary, and we directly analysed the time-averaged spectrum of this particular chain (i.e. the average over all 485 individual spectra, Fig. S3 bottom), which exhibits its ZPL at $\sim 18900 \text{ cm}^{-1}$ with a width of only 32 cm^{-1} (FWHM).

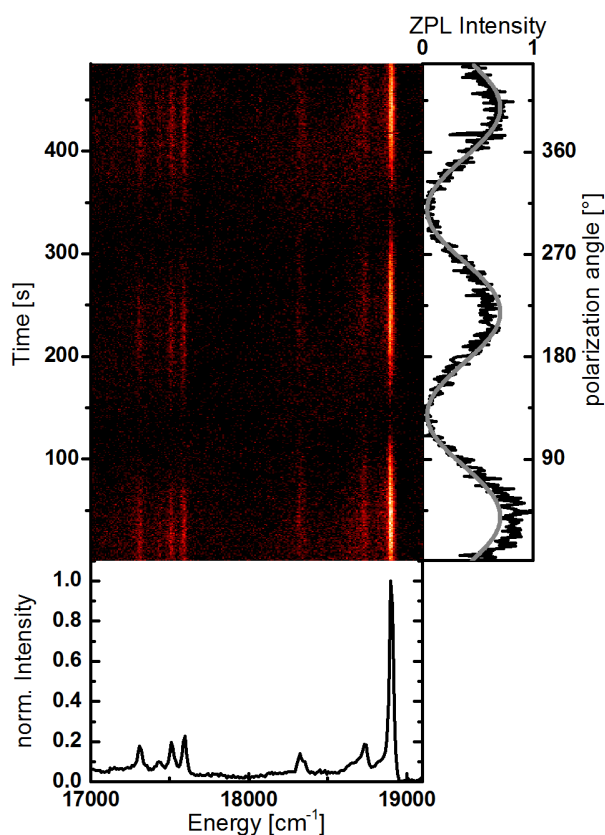


Figure S3: Low temperature PL spectrum of a single isolated P3HT16 chain embedded in *n*-hexadecane. Top left: 2-dimensional representation of a stack of 485 sequentially acquired spectra with an integration time of 1 s per spectrum. Between two successive spectra the polarizer in the emission path is rotated by 0.9° . As vertical axis we display the measurement time, the horizontal axis is the photon energy and the PL intensity is colour-coded. Bottom: PL spectrum averaged over the full acquisition time of 485 s. Top right: PL intensity of the ZPL, spectrally integrated from 18865 to 18931 cm^{-1} as a function of the polarization angle. The grey line is a \cos^2 -fit to the data.

There are several important points that we would like to comment on: First, as already mentioned in the main text, we very often find only one single ZPL in the spectra of both P3HT samples, i.e. there exists only a single emitting site per chain independent of the molecular weight. This observation is supported by the polarization dependency of the emission, the spectral diffusion and the one-step blinking and bleaching events shown in Figs. S2 and S3, which are all hallmarks for single-emitter detection. For the short P3HT16 chains emission from a single site only seems reasonable, given an effective conjugation length of < 10 repeating units for polythiophenes (see also Section 5 below).²⁻⁷ For the long P3HT144 chains, however, this finding is very surprising, because for other conjugated polymers, such as MeLPPP¹¹ and MEH-PPV,¹² the number of ZPLs (or emitting sites) observed per chain increases with chain length.

Second, the strong spectral diffusion processes observed in Fig. S2 occur on time scales slower than the acquisition time of 1 s for an individual spectrum. Since this integration time is arbitrarily chosen to obtain a reasonable signal-to-noise and signal-to-background ratio for data analysis, there is no reason why spectral diffusion should be limited to (this arbitrary) time scale of ≥ 1 s. In fact, it has been shown that these processes take place on *essentially all time scales* even at low temperatures.^{9,10,13-16} Fast (≤ 1 s) spectral diffusion gives rise to ZPL widths of single P3HT chains that are ~ 3 orders of magnitude broader than expected from their excited state lifetime. In other words, all ZPLs from P3HT chains in this work are inhomogeneously broadened by spectral diffusion. We stress that fast spectral diffusion is also the line broadening mechanism for the specific example shown in Fig. S3. Although there is apparently no spectral diffusion visible on time scales slower than 1 s in this case, the ZPL features typically a Gaussian line shape, which is a clear indication of inhomogeneous line broadening by spectral diffusion.

For a detailed discussion on spectral diffusion on different time scales and the corresponding line broadening mechanisms, we refer to our previous work in Ref. ¹⁰.

Finally, we note that the (up to seven) sharp vibronic peaks in the single-chain spectra (after application of the MSA algorithm) can be attributed to intra-molecular vibrational modes. The lines with vibrational energies of 1300 – 1600 cm^{-1} (i.e. at lower energies with respect to the corresponding ZPLs) are ascribed to aromatic carbon-bond stretch modes,¹⁷ lines with energies of 550 cm^{-1} originate from ring-deformations,¹⁸ and the peaks at with vibrational energies smaller than 250 cm^{-1} arise from collective stretching modes of the backbone or librational motions of the thiophene rings. Moreover, a rather broad and unstructured phonon side band (PSB) appears in the low-energy wing of the ZPLs. These PSBs result probably from electron-phonon coupling to low-energy ($< 100 \text{ cm}^{-1}$) phonon modes of the *n*-hexadecane matrix.^{9,10}

4. Frank-Condon analysis of PL spectra of a disordered P3HT film at 1.5 K

Usually, thin film PL spectra of P3HT at low temperatures exclusively feature emission from π -stacked aggregates, although the corresponding absorption spectra consistently yield a substantial fraction of non-aggregated (disordered) chains in the films.¹⁹ This observation means that the size of domains in the film with predominantly disordered chains (amorphous regions) is smaller than twice the exciton diffusion length of ca. 10 nm. Hence, to be able to record an “amorphous” PL spectrum of a P3HT film, the size of the amorphous domains has to be increased. We prepared such a film from our P3HT16 sample by dropping some 10 μ l from a P3HT16/chloroform solution (0.01 mg/ml) onto a cover slip. Because the cover slip was pre-heated to $\sim 90^\circ$ C, the solvent rapidly evaporated and an orange/brownish film immediately formed, indicating the presence of large amorphous domains. This sample was then cooled to 1.5 K and the resulting PL spectrum upon excitation at 450 nm is shown in Fig. S4a (orange line). The emission between about 13000 and 16000 cm^{-1} stems from the aggregated phase of the P3HT16 film,¹⁹ and the signal around 18000 cm^{-1} is ascribed to arise from amorphous regions of the film.

The PL spectrum of the amorphous part is extracted following an approach based on a Franck-Condon (FC) analysis, as described by several authors.¹⁹⁻²² In the first step a FC progression according to eq. (1)

$$I_{PL}(E) \propto E^3 \sum_{i=0}^{\infty} \frac{S^m}{m!} \exp\left(-\frac{1}{2} \left[\frac{E - (E_{0-0} - mE_{vib})}{\sigma} \right]^2\right) \quad (1)$$

is fitted to the film spectrum between 16000 and 21000 cm^{-1} . Here, E is the photon energy, E_{0-0} is the centre energy of the purely electronic (0-0) transition, E_{vib} represents the energy of an

effective carbon-stretching mode, S denotes the Huang-Rhys factor, m represents the vibrational quantum number, and σ is a Gaussian line width (disorder parameter). From the fit we obtained $E_{\text{vib}} = 1350 \text{ cm}^{-1}$ and $S = 0.84$; for the inhomogeneous line width we obtained a value of $\sigma = 1283 \text{ cm}^{-1}$ (corresponding to 3015 cm^{-1} FWHM) with a peak energy of $E_{0,0} = 17756 \text{ cm}^{-1}$ for the purely electronic transition. The resulting fit curve is shown as grey line in Fig. S4a. In a second step, this fit curve is subtracted from the film spectrum, which yields the pure aggregate phase emission (black curve) at energies between 12000 and 16000 cm^{-1} . Note that this aggregate PL exhibits a strongly suppressed high-energy peak at $\sim 15000 \text{ cm}^{-1}$ with respect to the peak at 13600 cm^{-1} , which indicates the formation of H-aggregates with a rather high degree of order.²³

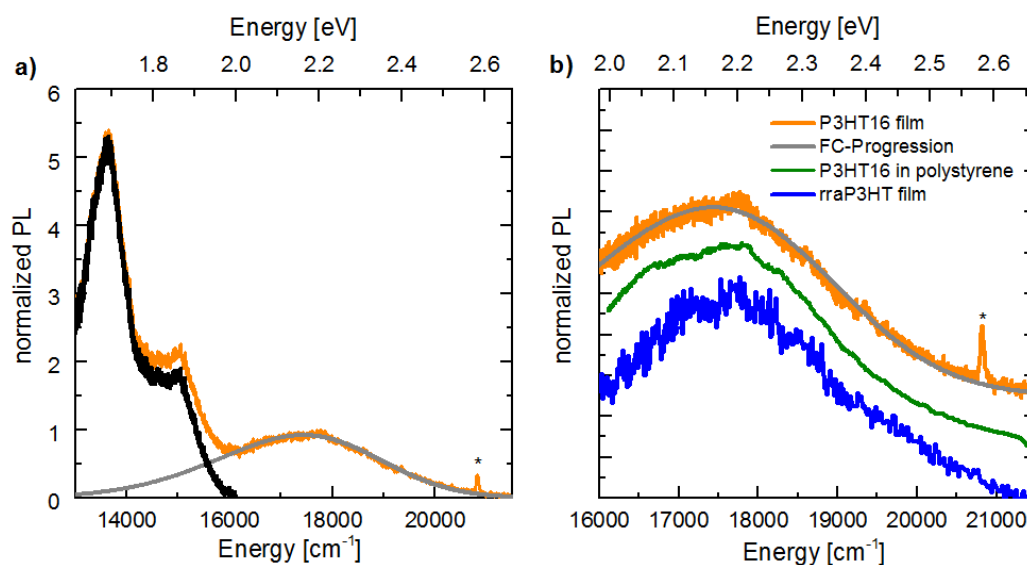


Figure S4: a) Low temperature PL spectrum of a thin P3HT16 film (orange). The Franck-Condon fit to the amorphous contribution to the film spectrum is shown in grey. The black curve corresponds to the aggregate emission from this film, obtained by subtracting the grey fit curve from the orange total spectrum. b) Comparison of low-temperature amorphous spectra of the P3HT16 film from part a (orange, together with the FC-fit in grey), of P3HT16 embedded at high concentration in polystyrene (green), and of a regio-random P3HT film (blue). The peak labelled by an asterisk in a and b is a Raman line.

To verify that the PL between 16000 and 21000 cm^{-1} in Fig. S4a indeed corresponds to PL from an amorphous region of the P3HT16 film, we also measured a film of P3HT16 embedded in polystyrene as well as of a regio-random P3HT, both at 1.5 K. The former sample was prepared by dissolving P3HT16 in chloroform at a concentration of 1 mg/ml, further diluting by a factor of 10^5 (vol/vol), adding a polystyrene/chloroform solution, and drop-casting. The rra-P3HT ($M_w = 40$ kDa, PDI = 2.4) was dissolved in chloroform at a concentration of 0.05 mg/ml and spin-coated. In particular, rra-P3HT is known to form large amorphous domains without long-range order, and only small aggregated regions.²⁴ Since all three PL spectra agree very well in the spectral range between 16000 and 21000 cm^{-1} , we can confidently attribute this signal to PL from amorphous regions with disordered P3HT chains. Note that the amorphous PL of P3HT exhibits a very peculiar, nearly triangular, line shape. According to Rebane *et al.* such line shapes can arise from an inhomogeneous distribution of line widths of the underlying zero-phonon lines that add up to yield such ensemble spectra.²⁵ Given the high degree of intra- and inter-chain disorder (both structurally and electronically) in amorphous P3HT film regions, such an observation is reasonable.

Based on the following reasons, the substantial energy difference of around 1200 cm^{-1} between the single-chain ZPL distributions and the electronic transition energy of the amorphous film PL spectrum (Fig. 2a) is rather surprising: First, the film PL is usually attributed to emission from highly amorphous regions,^{26,27} i.e., the conformation of the emitting sites in disordered films and in our single-chain experiments should be very similar (as mentioned in the main text, the conformation of polymer chains on scales of the persistence length – equivalent to the conjugation length for P3HT – is independent of the solvent, and this solution conformation is

transferred to films). Second, transient planarization of chains with concomitant transient spectral red-shift after photoexcitation is strongly inhibited in solid environments.²⁸ Third, this difference can not result from inter-chain energy transfer to energetically lower lying sites in densely packed films. Such inter-chain transfer usually gives rise to a red-shift and apparent narrowing of the inhomogeneous line in PL spectra. Yet, in the P3HT16/polystyrene film, in which P3HT16 exists in very low concentration, this inter-chain transfer should be largely suppressed. Because the PL spectrum of this P3HT16/polystyrene sample is identical to that of the neat P3HT16 film, we conclude that in neat P3HT16 films inter-chain energy transfer is also not important. Fourth, a spectral shift due to different dielectric constants for P3HT-films (P3HT in its own matrix) and for single P3HT chains (in *n*-hexadecane matrix) can be expected to be only minor, because the refractive indices of amorphous P3HT (≈ 1.7)²⁷ and frozen *n*-hexadecane (≈ 1.6)²⁹ are very similar in the relevant spectral region.

5. TDDFT simulations on oligothiophenes

We performed time-dependent density functional theory (TDDFT) calculations on isolated oligothiophenes with various chain lengths for both optimized planar geometries in vacuum and after molecular dynamics (MD) simulations either in vacuum or immersed in dioxane (see reference 6 for MD details). Additionally, dimers composed of a pair of oligothiophenes with 6 or 12 repeating units in a face-to-face configuration are investigated in vacuum as a function of the distance between the chains. The optimized geometries of the dimers are obtained using density functional theory (DFT) including dispersive forces as introduced by the semi-empirical dispersion correction DFT-D3.³⁰ From the inter-molecular equilibrium distances, the molecules are displaced in steps of 0.5 or 1.0 Å for further calculations. Excited states are calculated with TDDFT using the range separated hybrid functional ω PBE³¹ optimized for each particular system, enforcing that the first ionization energies and the Kohn-Sham frontier orbital eigenvalues agree as closely as possible.^{7,32} The functional optimizations are performed in vacuum and in dioxane by explicitly representing the solvent, as reported in reference 7.

5.1 Isolated oligothiophenes – The effect of torsional disorder

To investigate the influence of torsional disorder, we calculated the transition energies between the ground state and the first excited state of oligothiophenes with planar and torsionally distorted configurations. For this study we neglected the influence of the solvent, as the solvatochromic shifts are independent of the conjugation length.^{6,7} The calculations were performed for oligomers with lengths varying from 2 to 24 repeating units, such that the

transition energy saturation, i.e. the effective conjugation length in the polymer limit, can be estimated via a Kuhn plot.^{6,7}

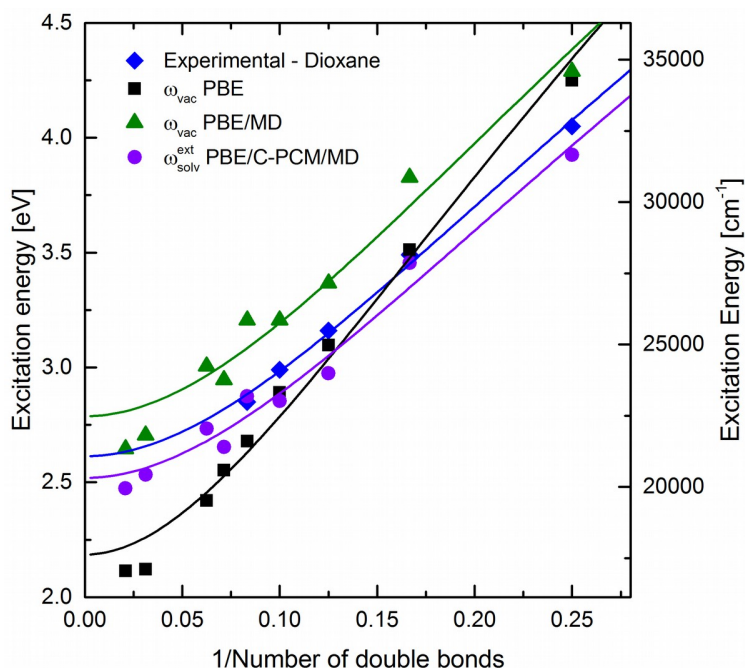


Figure S5: Comparison of the experimental optical gap of oligothiophenes in dioxane solution (blue diamond) with TDDFT calculations as function of the inverse number of double bonds. The TDDFT first excitation energies for vacuum-optimized geometries (ω_{vac} PBE) are denoted in black squares. The corresponding results for MD configurations calculated using the RSH functional optimized in vacuum (ω_{vac} PBE/MD) are shown in green triangles. The purple circles are the results for MD configurations calculated using the OT-RSH optimized in solvated systems and adding the implicit model C-PCM representing the dielectric medium (ω_{solv}^{ext} PBE/CPCM/MD). In case of the MD configurations, the optical gap is taken from a composed spectrum, averaged over 25 configurations. Solid lines are fits according to the Kuhn model. Data taken from reference 7.

As shown in Fig. S5, the P3HT chains with planar geometry (ω_{vac} PBE, black) exhibit a lower transition energy in comparison to the ones with distorted geometry (ω_{vac} PBE/MD, green). The fits according to the Kuhn model³ saturate at values of 17700 cm⁻¹ (2.19 eV, planar) and

22500 cm^{-1} (2.79 eV, distorted). This difference of 4800 cm^{-1} (0.6 eV) in transition energy stems solely from the enhanced disorder along the chain and gives an upper boundary for the energy shift which can be attributed to dihedral and conformational disorder (see main text).

Furthermore, we looked at the influence of torsional disorder on the spatial extend (conjugation length) of the first electronically excited state. In Fig. S6 the natural transition orbital (NTO) of the first excited state of a planar thiophene with 16 repeating units is shown. The NTO is not spread over the whole chain but restricted to about 10 repeating units. For a disordered chain with a conformation taken from a MD snapshot, the NTO of the dominant hole-electron pair of the first excited state for a thiophene with 16 repeating units is shown in Fig. S7a. For this particular conformation the spatial extend of the NTO is restricted to about 6 repeating units due to the dihedral disorder. In Fig. S7b the same is shown for a thiophene chain with 24 repeating units. Again, the spatial extend of the NTO is restricted to about 5 repeating units, emphasising the great effect of torsional disorder on the electronic structure of polythiophenes.

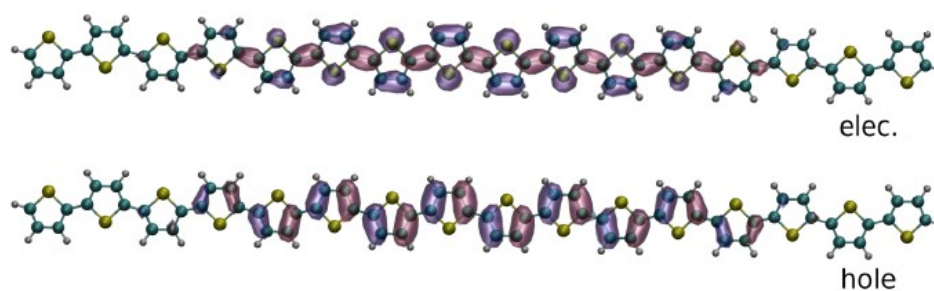


Figure S6: Natural transition orbital (NTO) of the dominant hole-electron pair of the first singlet excited state for thiophene with 16 repeating units with optimized structures (dihedral angles $\sim \pm 0.7^\circ$). The NTO is not delocalized over the whole chain but restricted to 10-12 repeating units with a transition energy of 17100 cm^{-1} (2.12 eV). Plots are generated with translucent surfaces and contour value of 0.015.

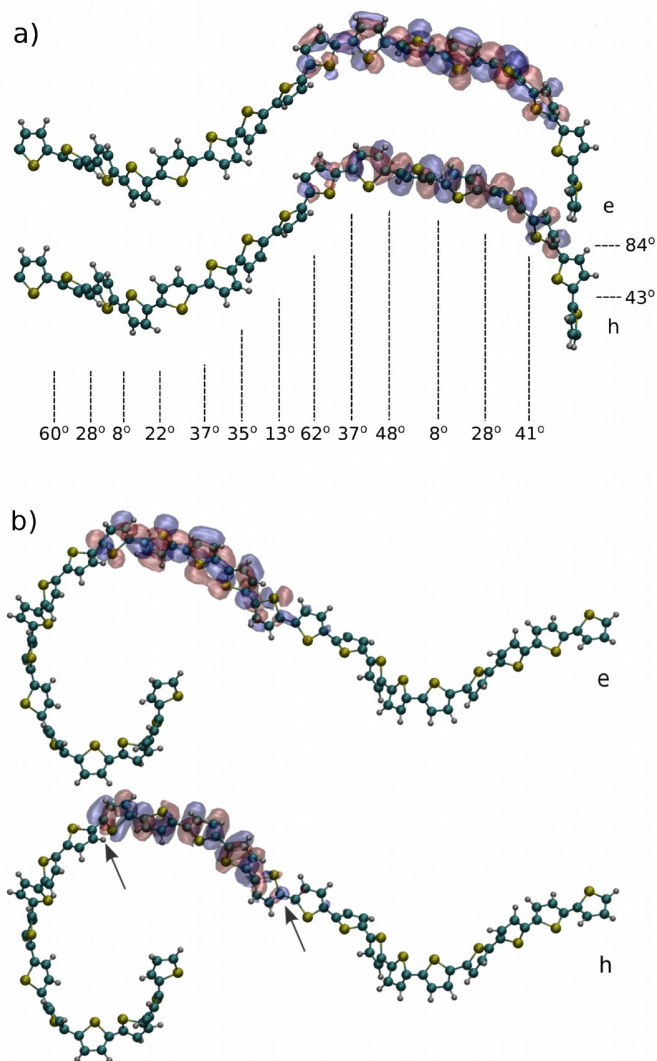


Figure S7: NTO of the dominant hole (h) – electron (e) pair of the first singlet excited state for a thiophene with a) 16 repeating units and b) 24 repeating units with a conformation taken from a MD snapshot. The NTO localizes on about 5-6 monomers for both disordered conformations. The transition energies from the ground state to the lowest excited state are a) 19900 cm^{-1} (2.47 eV) for 16 repeating units and b) 19400 cm^{-1} (2.40 eV) for 24 repeating units. In a) the dihedral angles between neighbouring thiophene rings are also displayed. Plots are generated with translucent surfaces and contour value of 0.015.

5.2. Oligothiophene dimers

In addition to the TDDFT simulations on isolated oligothiophenes we investigated dimers composed of oligothiophenes with 6 or 12 repeating units in a face-to-face configuration in vacuum as a function of the distance between the chains. This approach allows us to elucidate the influence of the electronic coupling between neighbouring chains with distances greater than the usual π - π -stacking distance of 3.8 Å³³ on the transition energy (from ground state to lowest excited state). Note that for perfect cofacially aligned H-type dimers, this lowest energy transition is usually optically forbidden and has no oscillator strength, if only electronic states are considered. However, due to electron-phonon coupling to e.g. carbon-bond stretch modes, transitions into excited states dressed with molecular vibrations satisfy the momentum conservation and make such transitions optically allowed.³⁴ Moreover, in real systems with disorder, such as in weakly ordered H-aggregates and especially in loose aggregates or disordered amorphous films, the symmetry is broken, making the transition from/to the lowest excited state optically active (weakly allowed).

We were able to observe a long-range interaction between the two parallel aligned polythiophenes (Fig. S8). For distances close to 5 Å, the transition into the lowest excited state is red-shifted by about 1700 cm⁻¹ (0.21 eV) compared to that into the excited state of an isolated chain with the same length. The red-shift decreases monotonously, yet, at about 8 Å, it is still about 900 cm⁻¹ (0.11eV). We note that Gierschner et al. found even for chain-chain distances of 12 Å electronic couplings exceeding 100 cm⁻¹.³⁵ This coupling is still comparable to the energy disorder of ~ 300 cm⁻¹ as estimated from the width of the ZPL distributions in Fig. 1e,f, and gives rise to a noticeable spectral red-shift. In our calculations, non-nearest neighbor interactions are

not included, which further enhance the inter-chain coupling as shown by Gierschner et al.³⁵ In amorphous films or in solution with loose aggregates this long-ranging dimerization is of huge importance and contributes to the differences in transition energies we observed between single, isolated chains and the corresponding ensemble spectra.

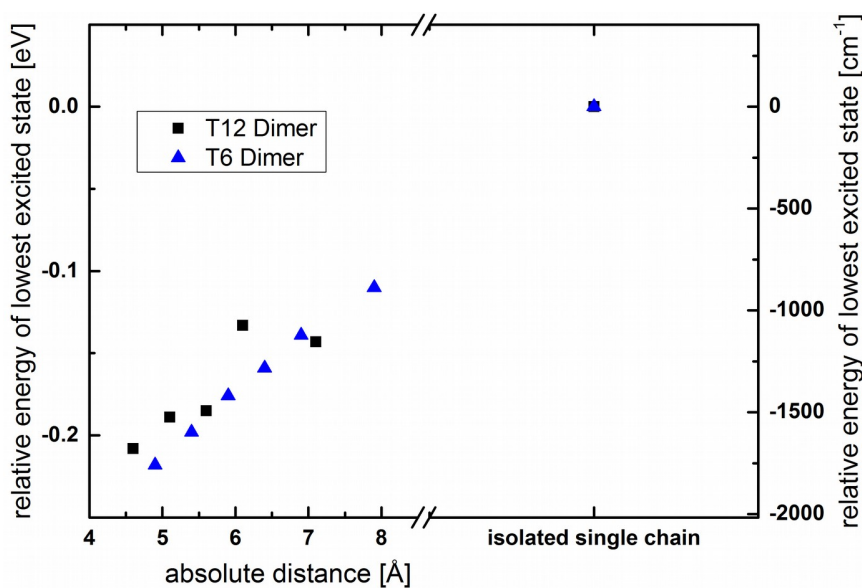


Figure S8: TDDFT calculated shifts in transition energy of H-type dimers at various intermolecular distances in comparison with the results from the corresponding isolated oligothiophene chain. T6 (T12) denotes a thiophene with 6 (12) repeating units.

In total, the spectral red-shift from isolated chains over loosely aggregated chains to π -stacked films contains several effects (see main text and Fig. 3). First, planarization (mediated by neighboring chains) takes an important role and leads to a shift in transition energy of the intra-chain excitations (see Section 5.1). The electronic coupling between neighboring chains (or segments of neighbouring chains) leads to a dimerization and thus an additional red-shift of the lowest energy transition due to electronic coupling between their transition dipole moments.

Finally, in H-aggregates strong inter-chain coupling gives again an additional redshift of the lowest excited state, resulting in total in an energy difference of more than 0.6 eV (4800 cm⁻¹) between the isolated chains and the bulk aggregate spectra (see Fig. 3 and reference 19). Note that in aggregated films, an additional factor for the red-shift is the so-called gas-to-crystal shift, i.e. the change of the dielectric constant that individual chains experience between gas phase (or solution) and crystal.

6. Coherence length of the emitting sites

According to a theoretical work by Yamagata and Spano, the photophysics of isolated, non-interacting conjugated polymer chains can be described in terms of a J-aggregate built up from thiophene monomers. The (de-)localisation of an excitation on an electronically disordered chain is quantified by the coherence length N_{coh} (number of monomers or repeating units), which can be determined from PL spectra using:^{36,37}

$$N_{\text{coh}} = R_{\text{em}} \cdot S_{\text{mon}}.$$

Here R_{em} is the 0-0/0-1 intensity ratio of the PL spectra, i.e. in our single-chain data the ratio between the relative area of the ZPL and the areas of the (four) lines at 1400 cm⁻¹ below the ZPL (~ 17600 cm⁻¹ in the data shown in Fig. 1a and b). From our data we find $R_{\text{em}} \sim 1.4 - 2$. S_{mon} represents an effective Huang-Rhys factor for a thiophene monomer for the several vibrational lines around 1400 cm⁻¹, which was determined to be $S_{\text{mon}} = 1.4 - 1.9$.²³ From these numbers we obtain $N_{\text{coh}} \sim 2 - 4$.

Barford and co-workers^{38,39} derived a slightly different expression for the mean spatial extend of the emitting site (in units of number of monomers)

$$N = 2 \cdot S_{\text{mon}} \cdot R_{\text{em}} (E_{01}/E_{00})^3,$$

with E_{01} (E_{00}) being the energy of the 0-1 (0-0) transition, which yields $(E_{01}/E_{00})^3 = 0.79$ from our single-chain spectra. We thus obtain values of $N \sim 3 - 6$. Given that real polymer chains also possess some degree of conformational disorder and can thus be curved, these values of N_{coh} and N are lower bounds only.^{40,41} Hence, there is good agreement with the conjugation length of 5 – 6 repeating units determined above from our TDDFT calculations on conformationally disordered chains.

References

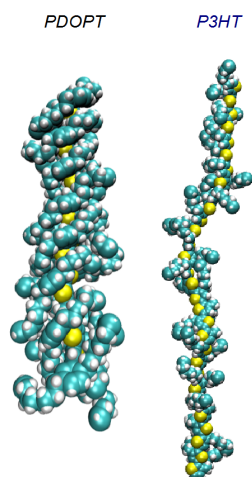
- (1) Lohwasser, R. H.; Thelakkat, M. Toward Perfect Control of End Groups and Polydispersity in Poly(3-hexylthiophene) via Catalyst Transfer Polymerization. *Macromolecules* **2011**, *44* (9), 3388–3397.
- (2) Becker, R. S.; Seixas de Melo, J.; Maçanita, A. L.; Elisei, F. Comprehensive Evaluation of the Absorption, Photophysical, Energy Transfer, Structural, and Theoretical Properties of α -Oligothiophenes with One to Seven Rings. *J. Phys. Chem.* **1996**, *100* (48), 18683–18695.
- (3) Gierschner, J.; Cornil, J.; Egelhaaf, H.-J. Optical Bandgaps of π -Conjugated Organic Materials at the Polymer Limit: Experiment and Theory. *Adv. Mater.* **2007**, *19* (2), 173–191.
- (4) Milián-Medina, B.; Gierschner, J. π -Conjugation. *WIREs Comput. Mol. Sci.* **2012**, *2* (4), 513–524.
- (5) Rossi, G.; Chance, R. R.; Silbey, R. Conformational disorder in conjugated polymers. *J. Chem. Phys.* **1989**, *90* (12), 7594.
- (6) de Queiroz, Thiago B; Kümmel, S. Charge-transfer excitations in low-gap systems under the influence of solvation and conformational disorder: exploring range-separation tuning. *J. Chem. Phys.* **2014**, *141* (8), 84303.
- (7) de Queiroz, Thiago B; Kümmel, S. Tuned range separated hybrid functionals for solvated low bandgap oligomers. *J. Chem. Phys.* **2015**, *143* (3), 34101.

- (8) Hofmann, C.; Michel, H.; van Heel, M.; Köhler, J. Multivariate Analysis of Single-Molecule Spectra: Surpassing Spectral Diffusion. *Phys. Rev. Lett.* **2005**, *94* (19), 195501.
- (9) Hildner, R.; Lemmer, U.; Scherf, U.; van Heel, M.; Köhler, J. Revealing the Electron–Phonon Coupling in a Conjugated Polymer by Single-Molecule Spectroscopy. *Adv. Mater.* **2007**, *19* (15), 1978–1982.
- (10) Hildner, R.; Winterling, L.; Lemmer, U.; Scherf, U.; Köhler, J. Single-molecule spectroscopy on a ladder-type conjugated polymer: electron-phonon coupling and spectral diffusion. *ChemPhysChem* **2009**, *10* (14), 2524–2534.
- (11) Schindler, F.; Jacob, J.; Grimsdale, A. C.; Scherf, U.; Müllen, K.; Lupton, J. M.; Feldmann, J. Counting Chromophores in Conjugated Polymers. *Angew. Chem.* **2005**, *117* (10), 1544–1549.
- (12) Feist, F. A.; Tommaseo, G.; Basché, T. Single-Molecule Spectroscopy of MEH-PPV Polymer Molecules in Different Host Matrices. *J. Phys. Chem. C* **2009**, *113* (27), 11484–11490.
- (13) Feist, F. A.; Basché, T. Fluorescence excitation and emission spectroscopy on single MEH-PPV chains at low temperature. *J. Phys. Chem. B* **2008**, *112* (32), 9700–9708.
- (14) Pullerits, T.; Mirzov, O.; Scheblykin, I. G. Conformational fluctuations and large fluorescence spectral diffusion in conjugated polymer single chains at low temperatures. *J. Phys. Chem. B* **2005**, *109* (41), 19099–19107.
- (15) Schindler, F.; Lupton, J. M.; Feldmann, J.; Scherf, U. A universal picture of chromophores in pi-conjugated polymers derived from single-molecule spectroscopy. *Proc. Natl. Acad. Sci. U.S.A.* **2004**, *101* (41), 14695–14700.
- (16) Baderschneider, S.; Scherf, U.; Köhler, J.; Hildner, R. Influence of the Conjugation Length on the Optical Spectra of Single Ladder-Type (p-Phenylene) Dimers and Polymers. *J. Phys. Chem. A* **2016**, *120* (2), 233–240.
- (17) Brambilla, L.; Tommasini, M.; Botiz, I.; Rahimi, K.; Agumba, J. O.; Stingelin, N.; Zerbi, G. Regio-Regular Oligo and Poly(3-hexyl thiophene): Precise Structural Markers from the Vibrational Spectra of Oligomer Single Crystals. *Macromolecules* **2014**, *47* (19), 6730–6739.
- (18) Baibarac, M.; Lapkowski, M.; Pron, A.; Lefrant, S.; Baltog, I. SERS spectra of poly(3-hexylthiophene) in oxidized and unoxidized states. *J. Raman Spectrosc.* **1998**, *29* (9), 825–832.
- (19) Panzer, F.; Sommer, M.; Bäessler, H.; Thelakkat, M.; Köhler, A. Spectroscopic Signature of Two Distinct H-Aggregate Species in Poly(3-hexylthiophene). *Macromolecules* **2015**, *48* (5), 1543–1553.
- (20) Panzer, F.; Bäessler, H.; Lohwasser, R. H.; Thelakkat, M.; Köhler, A. The Impact of Polydispersity and Molecular Weight on the Order–Disorder Transition in Poly(3-hexylthiophene). *J. Phys. Chem. Lett.* **2014**, *5* (15), 2742–2747.
- (21) Ho, Peter K. H.; Kim, J.-S.; Tessler, N.; Friend, R. H. Photoluminescence of poly(p-phenylenevinylene)–silica nanocomposites: Evidence for dual emission by Franck–Condon analysis. *J. Chem. Phys.* **2001**, *115* (6), 2709.

- (22) Scharsich, C.; Lohwasser, R. H.; Sommer, M.; Asawapirom, U.; Scherf, U.; Thelakkat, M.; Neher, D.; Köhler, A. Control of aggregate formation in poly(3-hexylthiophene) by solvent, molecular weight, and synthetic method. *J. Polym. Sci. Part B: Polym. Phys.* **2012**, *50* (6), 442–453.
- (23) Yamagata, H.; Spano, F. C. Interplay between intrachain and interchain interactions in semiconducting polymer assemblies: the HJ-aggregate model. *J. Chem. Phys.* **2012**, *136* (18), 184901.
- (24) Shen, X.; Hu, W.; Russell, T. P. Measuring the Degree of Crystallinity in Semicrystalline Regioregular Poly(3-hexylthiophene). *Macromolecules* **2016**, *49* (12), 4501–4509.
- (25) Rebane, L. A.; Gorokhovskii, A. A.; Kikas, J. V. Low-temperature spectroscopy of organic molecules in solids by photochemical hole burning. *Appl. Phys. B* **1982**, *29* (4), 235–250.
- (26) Thiessen, A.; Vogelsang, J.; Adachi, T.; Steiner, F.; Vanden Bout, D. A.; Lupton, J. M. Unraveling the chromophoric disorder of poly(3-hexylthiophene). *Proc. Natl. Acad. Sci. U.S.A.* **2013**, *110* (38), E3550-6.
- (27) Brown, P.; Thomas, D.; Köhler, A.; Wilson, J.; Kim, J.-S.; Ramsdale, C.; Sirringhaus, H.; Friend, R. H. Effect of interchain interactions on the absorption and emission of poly(3-hexylthiophene). *Phys. Rev. B* **2003**, *67* (6), 064203.
- (28) Westenhoff, S.; Beenken, Wichard J. D.; Friend, R. H.; Greenham, N. C.; Yartsev, A.; Sundström, V. Anomalous Energy Transfer Dynamics due to Torsional Relaxation in a Conjugated Polymer. *Phys. Rev. Lett.* **2006**, *97* (16), 166804.
- (29) Banasiewicz, M.; Deperasińska, I.; Kozankiewicz, B. Spectroscopic Characteristics of Pentacene In Shpol'skii Matrixes. *J. Phys. Chem. A* **2003**, *107* (5), 662–667.
- (30) Grimme, S.; Antony, J.; Ehrlich, S.; Krieg, H. A consistent and accurate ab initio parametrization of density functional dispersion correction (DFT-D) for the 94 elements H-Pu. *J. Chem. Phys.* **2010**, *132* (15), 154104.
- (31) Vydrov, O. A.; Scuseria, G. E. Assessment of a long-range corrected hybrid functional. *J. Chem. Phys.* **2006**, *125* (23), 234109.
- (32) Stein, T.; Kronik, L.; Baer, R. Reliable prediction of charge transfer excitations in molecular complexes using time-dependent density functional theory. *J. Am. Chem. Soc.* **2009**, *131* (8), 2818–2820.
- (33) Wirix, M. J. M.; Bomans, P. H. H.; Friedrich, H.; Sommerdijk, N. A. J. M.; With, G. de. Three-dimensional structure of P3HT assemblies in organic solvents revealed by cryo-TEM. *Nano Lett.* **2014**, *14* (4), 2033–2038.
- (34) Spano, F. C.; Silva, C. H- and J-aggregate behavior in polymeric semiconductors. *Annu. Rev. Phys. Chem.* **2014**, *65*, 477–500.
- (35) Gierschner, J.; Huang, Y.-S.; van Averbeke, B.; Cornil, J.; Friend, R. H.; Beljonne, D. Excitonic versus electronic couplings in molecular assemblies: The importance of non-nearest neighbor interactions. *J. Chem. Phys.* **2009**, *130* (4), 44105.

- (36) Spano, F. C.; Yamagata, H. Vibronic coupling in J-aggregates and beyond: a direct means of determining the exciton coherence length from the photoluminescence spectrum. *J. Phys. Chem. B* **2011**, *115* (18), 5133–5143.
- (37) Yamagata, H.; Spano, F. C. Strong Photophysical Similarities between Conjugated Polymers and J-aggregates. *J. Phys. Chem. Lett.* **2014**, *5* (3), 622–632.
- (38) Marcus, M.; Tozer, O. R.; Barford, W. Theory of optical transitions in conjugated polymers. II. Real systems. *J. Chem. Phys.* **2014**, *141* (16), 164102.
- (39) Barford, W.; Marcus, M. Theory of optical transitions in conjugated polymers. I. Ideal systems. *J. Chem. Phys.* **2014**, *141* (16), 164101.
- (40) Hestand, N. J.; Spano, F. C. The effect of chain bending on the photophysical properties of conjugated polymers. *J. Phys. Chem. B* **2014**, *118* (28), 8352–8363.
- (41) Barford, W.; Marcus, M. Theory of optical transitions in curved chromophores. *J. Chem. Phys.* **2016**, *145* (12), 124111.

4.2 Publication 2: Direct observation of backbone planarisation via side-chain alignment in single bulky-substituted polythiophenes



Dominic Raithel, Lena Simine, Sebastian Pickel, Konstantin Schötz, Fabian Panzer, Sebastian Baderschneider, Daniel Schiefer, Ruth Lohwasser, Jürgen Köhler, Mukundan Thelakkat, Michael Sommer, Anna Köhler, Peter J. Rossky, Richard Hildner

Published in
Proc. Nat. Acad. Sci. U.S.A.
DOI: 10.1073/pnas.1719303115

Reproduced with permission from Proc. Nat. Acad. Sci. U.S.A. 115 (2018) 2699
Copyright © 2018 National Academy of Sciences



Direct observation of backbone planarization via side-chain alignment in single bulky-substituted polythiophenes

Dominic Raithel^a, Lena Simine^b, Sebastian Pickel^a, Konstantin Schötz^c, Fabian Panzer^c, Sebastian Baderschneider^a, Daniel Schiefer^d, Ruth Lohwasser^e, Jürgen Köhler^{a,f}, Mukundan Thelakkat^e, Michael Sommer^{d,1}, Anna Köhler^{c,f}, Peter J. Rossky^b, and Richard Hildner^{a,2}

^aExperimental Physics IV, University of Bayreuth, 95440 Bayreuth, Germany; ^bDepartment of Chemistry, Rice University, Houston, TX 77005; ^cExperimental Physics II, University of Bayreuth, 95440 Bayreuth, Germany; ^dInstitute of Macromolecular Chemistry, University of Freiburg, 79104 Freiburg, Germany; ^eApplied Functional Polymers, University of Bayreuth, 95440 Bayreuth, Germany; and ^fBayreuth Institute of Macromolecular Research, University of Bayreuth, 95440 Bayreuth, Germany

Edited by Michael L. Klein, Temple University, Philadelphia, PA, and approved February 2, 2018 (received for review November 5, 2017)

The backbone conformation of conjugated polymers affects, to a large extent, their optical and electronic properties. The usually flexible substituents provide solubility and influence the packing behavior of conjugated polymers in films or in bad solvents. However, the role of the side chains in determining and potentially controlling the backbone conformation, and thus the optical and electronic properties on the single polymer level, is currently under debate. Here, we investigate directly the impact of the side chains by studying the bulky-substituted poly(3-(2,5-dioctylphenyl)thiophene) (PDOPT) and the common poly(3-hexylthiophene) (P3HT), both with a defined molecular weight and high regioregularity, using low-temperature single-chain photoluminescence (PL) spectroscopy and quantum-classical simulations. Surprisingly, the optical transition energy of PDOPT is significantly ($\sim 2,000\text{ cm}^{-1}$ or 0.25 eV) red-shifted relative to P3HT despite a higher static and dynamic disorder in the former. We ascribe this red shift to a side-chain induced backbone planarization in PDOPT, supported by temperature-dependent ensemble PL spectroscopy. Our atomistic simulations reveal that the bulkier 2,5-dioctylphenyl side chains of PDOPT adopt a clear secondary helical structural motif and thus protect conjugation, i.e., enforce backbone planarity, whereas, for P3HT, this is not the case. These different degrees of planarity in both thiophenes do not result in different conjugation lengths, which we found to be similar. It is rather the stronger electronic coupling between the repeating units in the more planar PDOPT which gives rise to the observed spectral red shift as well as to a reduced calculated electron-hole polarization.

conjugated polymers | single-molecule spectroscopy | quantum-classical atomistic simulations | side-chain engineering | organic electronics

Device applications of conjugated polymers are strongly determined by their structural, electronic, and optical properties. However, the design of new polymers is not straightforward, as often conflicting demands have to be satisfied simultaneously to achieve optimum device performance (1). For instance, application in organic light-emitting diodes requires strong and efficient emission as well as efficient transport of injected charges. The charge transport characteristics strongly depend on film morphology, orientation with respect to interfaces, and the strength of interchain interactions (2). However, dense packing of conjugated polymers into typically π - π -type arrangements reduces emission quantum yield. Hence, suppression of π stacking, while maintaining high intrachain and interchain order, is important for lighting applications (3).

To manipulate and optimize the relevant structural and electronic properties of conjugated polymers for specific applications, side-chain engineering has emerged as a versatile toolkit in recent years (note that “side-chain engineering” is to be understood here in its widest sense, i.e., direct backbone substitution with heteroatoms and modifying large side groups) (4–8). Noncovalent

interactions between backbone and substituents (e.g., CH \cdots S, CH \cdots F, CH \cdots O, or F \cdots S interactions) have a strong impact on the backbone conformation of isolated chains (9). In combination with interactions between chains, such as π - π - or hydrogen-bonding interactions, which direct self-assembly, the resulting film morphologies can be controlled (10). In particular, fluorination has attracted attention, because it can introduce steric interactions with neighboring groups and thus modify backbone conformation (10). Moreover, fluorine possesses the highest electronegativity, which was shown to stabilize the highest occupied molecular orbital (HOMO) and/or lowest unoccupied molecular orbital (LUMO; see e.g., ref. 5 for a recent review). However, disentangling structural and electronic effects of fluorination is very challenging (4). An alternative approach is to increase the density or bulkiness of side groups. For example, enhancing the side-chain density of a donor-acceptor copolymer, which is widely used for organic solar cells, improved its luminescence properties significantly, thus allowing for application in light-emitting devices (11). Appending sterically demanding groups like dendrimers (12) stiffens the backbone through steric repulsion

Significance

Conjugated polymers are promising materials for flexible electronics and photovoltaics. Recent progress in polymer design led to a rise in device efficiency. Tailoring intramolecular interactions is a central design element, which allows fine-tuning of optical and electronic properties. However, prediction and measurement of intrinsic properties of newly synthesized polymers is challenging, as they are often hidden by ensemble effects. Single-molecule spectroscopy allows revelation of the intrinsic changes upon chemical modification, here specifically a variation of the side chains. Surprisingly, a more disordered, bulky side chain leads to a higher order and better conjugation within the electronically active backbone of a single chain. This study gives detailed insights into changes in photophysical properties and suggests new ideas for synthesis.

Author contributions: L.S., P.J.R., and R.H. designed research; D.R., L.S., S.P., K.S., and F.P. performed research; S.B., D.S., R.L., M.T., and M.S. contributed new reagents/analytic tools; D.R., L.S., S.P., K.S., and R.H. analyzed data; D.R., L.S., S.P., K.S., J.K., A.K., P.J.R., and R.H. interpreted data; and D.R., L.S., and R.H. wrote the paper.

The authors declare no conflict of interest.

This article is a PNAS Direct Submission.

Published under the PNAS license.

¹Present address: Polymerchemie, Technische Universität Chemnitz, 09111 Chemnitz, Germany.

²To whom correspondence should be addressed. Email: richard.hildner@uni-bayreuth.de.

This article contains supporting information online at www.pnas.org/lookup/suppl/doi:10.1073/pnas.1719303115/-DCSupplemental.

Published online February 26, 2018.

of neighboring side chains. The resulting increase in persistence length was recently highlighted as a new design aspect to optimize optical absorption and thus solar cell performance (13). However, a high persistence length alone is not sufficient; only a concomitant backbone planarization enhances absorption due to an increase in transition dipole moment (14–16). However, more bulky side groups are usually associated with a larger torsion of the conjugated backbone, i.e., with a large distribution of interring dihedral angles (17–19), which localizes electronic excitations and gives rise to less favorable material properties.

Here, we show that, contrary to this common notion, bulky side chains can force the backbone of conjugated polymers into a more planar conformation via side-chain alignment. We combine single-molecule low-temperature photoluminescence (PL) spectroscopy with quantum-classical atomistic simulations to investigate two polythiophenes with defined molecular weight and high regioregularity but different substitution patterns (Fig. 1 *D–F*, *Insets*): First, poly(3-(2,5-dioctylphenyl)thiophene) (PDOPT) with sterically very demanding 2,5-dioctylphenylene side-chains, which prevent direct π – π interaction of neighboring backbones (20, 21). Second, the prototypical poly(3-hexylthiophene) (P3HT) with relatively short hexyl side groups. For P3HT, interchain π – π interactions play an important role and determine the transition energy, to a large extent (22). Particularly, this latter system was studied extensively by ensemble (16, 23–25) and single-molecule spectroscopy (26–28).

We find that the PDOPT single-chain PL spectra are strongly red-shifted by $>2,000\text{ cm}^{-1}$ ($>0.25\text{ eV}$) with respect to P3HT, which is not obvious from the corresponding, very similar ensemble spectra (Fig. S1). We were able to ascribe this substantial spectral shift to side-chain induced backbone planarization in PDOPT that increases the electronic coupling between repeating units. This is accompanied by a reduction in the difference between the centers of mass of the electron/hole wave functions—the electron–hole polarization (29), which is a measure for the charge transfer character of the excited state.

Results and Discussion

PL Spectroscopy of Single PDOPT Chains. We investigated two PDOPT samples, PDOPT16 and PDOPT89, with number average molecular weights of $M_n = 6.1\text{ kDa}$ (~ 16 repeating units, PDOPT16 with a dispersity of 1.07 and a regioregularity of $>93\%$), and $M_n = 33.7\text{ kDa}$ (~ 89 repeating units, PDOPT89 with a dispersity of 1.66 and a regioregularity of $>98\%$); see *Methods and Materials* and *SI Methods and Materials*. Fig. 1 *A* and *B* depicts two representative single-chain PL spectra of PDOPT16 and PDOPT89 after partial temporal averaging (see *SI Methods and Materials*). Both spectra show a prominent zero-phonon line (ZPL) at $17,022\text{ cm}^{-1}$ and $16,777\text{ cm}^{-1}$ with line widths of 33 cm^{-1} and 64 cm^{-1} (FWHM) for PDOPT16 and PDOPT89, respectively. A broad phonon-side band appears in the low-energy shoulder of the ZPLs and indicates weak electron–phonon coupling to low-energy vibrational modes of the backbone or the host matrix (30, 31). The dominating vibrational transition is offset from the ZPL by around $1,480\text{ cm}^{-1}$ to lower energies and is associated with aromatic carbon–bond stretching modes (32). The PL spectra of PDOPT16 feature only one ZPL (Fig. 1*A*), i.e., only a single emitting site per chain as expected from the effective conjugation length of approximately eight repeating units for polythiophenes (33–36). In contrast, for PDOPT89, we observe two additional weak lines at high energies (Fig. 1*B*, asterisks). The independent blinking and spectral diffusion of these weak peaks (Fig. S2) demonstrates multichromophoric behavior with several emitting sites (ZPLs) per chain.

We evaluated, in total, 88 (102) ZPLs of PDOPT16 (PDOPT89) by fitting Gaussian or Lorentzian functions to their high-energy tails. The resulting histograms of the ZPL width (Fig. 1 *D* and *E*) and ZPL energy (Fig. 1 *G* and *H*) show only a little difference between the systems. The average ZPL width (FWHM) is 70 cm^{-1} for the short and 67 cm^{-1} for the long chains. Both distributions are very broad, with maximum ZPL widths of $\sim 250\text{ cm}^{-1}$. For other conjugated polymers, such as P3HT (22) and ladder-type poly(*p*-phenylenes) (37), we showed that the ZPLs are broadened by unresolved spectral diffusion, i.e., by random jumps of the transition energy on time scales faster than the temporal resolution of our measurement (here

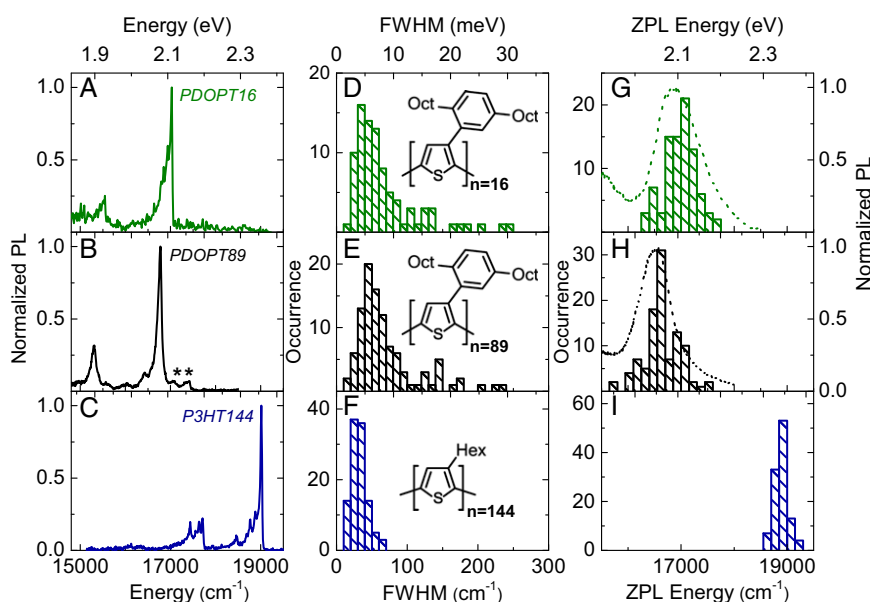


Fig. 1. Low-temperature PL spectroscopy on single polythiophene chains. (*A* and *B*) Single-chain PL spectra of poly(3-(2,5-dioctylphenyl)-thiophene), PDOPT, for two different chain lengths embedded in *n*-hexadecane. (*C*) Single-chain PL spectrum of poly(3-hexyl-thiophene), P3HT, in *n*-hexadecane. (*D–F*) Distributions of line widths (FWHM) of the ZPL. (*G–I*) Distributions of spectral positions of the ZPLs. The dashed lines in *G* and *H* are low-temperature ensemble PL spectra of the corresponding matrix-isolated PDOPT sample (in *n*-hexadecane). In *D–F*, the chemical structures are shown as *Insets*; *n* denotes the mean number of repeating units, and Oct and Hex stand for *n*-octyl and *n*-hexyl groups. The peaks in *B* marked with asterisks denote additional weak ZPLs from the same single PDOPT chain (see also Fig. S2). The data in *C*, *F*, and *I* are taken from ref. 22.

1 s to 3 s). This dynamic disorder is induced by structural fluctuations of groups of atoms or molecules in the local environment of the emitting site (31, 37–40). Accordingly, we ascribe the broad ZPLs of PDOPT to unresolved spectral diffusion processes as well.

For PDOPT16 (PDOPT89), the histograms of ZPL energies range from 16,276 cm^{-1} to 17,738 cm^{-1} (15,787 cm^{-1} to 17,480 cm^{-1}) and are centered around 16,975 cm^{-1} (16,633 cm^{-1}); see Fig. 1 *G* and *H*. The electronic transition of the corresponding low-temperature matrix-isolated ensemble spectra (dashed lines, Fig. 1 *G* and *H*) with maxima at 16,858 cm^{-1} (PDOPT16) and 16,505 cm^{-1} (PDOPT89) provide good envelopes to these histograms. We attribute the red shift of about 350 cm^{-1} from PDOPT16 to PDOPT89 in both single-chain and bulk data to intrachain downhill energy transfer within the multichromophoric PDOPT89 chains. Such energy transfer rapidly populates predominantly lower-energy emitting sites (41), whereas higher-energy sites are only weakly emitting (Fig. 1*B*, asterisks) or do not emit at all. In contrast, for PDOPT16 with only a single emitting site, the ZPL distribution is entirely determined by dispersive interactions of the emitting site with the local environment (42, 43) as well as by the degree of planarity of the polymer backbone, both of which vary for each chain (43–45).

PDOPT vs. P3HT. It is now interesting to compare our PDOPT single-chain data with those of the prototypical P3HT that we have reported recently (Fig. 1 *C*, *F*, and *I* and ref. 22). The P3HT samples investigated possess an M_n of 2.6 kDa (~ 16 repeating units, P3HT16 with a dispersity of 1.17 and a regioregularity $>93\%$) and an M_n of 24 kDa (~ 144 repeating units, P3HT144 with a dispersity of 1.15 and a regioregularity $>98\%$). For both PDOPT and P3HT, there is no difference between the corresponding spectra of short and long chains (Fig. 1 and Fig. S3), and we thus focus on the long chains (PDOPT89 and P3HT144) in the following discussion.

Dynamic and static disorder. The first obvious differences are the on average significantly broader ZPLs of PDOPT with respect to those of P3HT (mean ZPL width 67 cm^{-1} and 32 cm^{-1} , respectively, Fig. 1 *E* and *F*). These data indicate a high degree of dynamic disorder in PDOPT due to very pronounced spectral diffusion processes with large unresolved spectral jumps compared with P3HT. The magnitude of these jumps increases with decreasing distance between the thiophene backbone and the fluctuating unit in its local environment (31, 42, 46). We therefore suggest that this strong spectral diffusion in PDOPT originates from librational motions of its side-group phenyl rings (47, 48), which are directly appended to the conjugated backbone.

Furthermore, for PDOPT, the inhomogeneous width (FWHM) of the distribution of ZPL energies is larger by a factor of 2.5 (PDOPT89, 770 cm^{-1} ; P3HT144, 300 cm^{-1} ; see Fig. 1 *H* and *I*), indicating a higher static disorder in comparison with P3HT. The only difference between the samples is the more bulky side group of PDOPT, and thus steric effects induced by these groups probably play an important role (*vide infra*). These observations demonstrate that the side groups possess a strong influence on the photophysics of polythiophenes that is not obvious from ensemble PL data alone (Fig. S1).

ZPL energies. The most unexpected finding is that the ZPL energies of single PDOPT chains are red-shifted by more than 2,200 cm^{-1} (0.27 eV) in comparison with P3HT (Fig. 1 *H* and *I*). We have recently shown, by calculations on thiophene derivatives, that the transition energy of the absorbing/emitting sites red-shift by up to 4,800 cm^{-1} (0.6 eV) for increasing planarity (22, 29), in agreement with other reports (36, 44, 45, 49). Based on this work, we propose that the observed red shift between isolated PDOPT and P3HT is largely caused by backbone planarization in PDOPT, at least on length scales of an emitting site, via noncovalent interactions with the bulky side groups (7, 9). A further factor, that may in part contribute to this red shift,

is the more polarizable local environment for the emitting sites (50, 51) provided by the aromatic phenyl rings of PDOPT compared with the hexyl groups of P3HT.

Ensemble PL spectroscopy: Planarization preceding aggregation. Independent evidence for our hypothesis comes from temperature-dependent PL spectroscopy on solutions of PDOPT89 and P3HT144. This approach yields insights into the aggregation process upon cooling (16); in particular, we found that an initial backbone planarization of the disordered solution phase occurs before the transition to the aggregated phase. The signature of this initial planarization is a continuous red shift of the solution PL spectrum with decreasing temperature.

For both PDOPT and P3HT dissolved in THF, we quantified the spectral red shifts of the disordered phase by fitting the temperature-dependent PL spectra (Fig. 2, *Inset*) with Franck–Condon (FC) progressions (16) and retrieving the energies of the purely electronic (0–0) transition (Fig. 2 and *SI Franck–Condon Analysis*). A linear fit to the temperature-dependent 0–0 positions reveals an average red shift of 1.6 cm^{-1}/K for PDOPT (black) and 4.1 cm^{-1}/K for P3HT (blue). Note that the transition from disordered chains to aggregates occurs at 180 K for PDOPT and at 240 K for P3HT. Hence, the initial rate of red shift upon cooling (but before aggregation) is less pronounced for PDOPT than for P3HT, as can be expected for a more planar chain and from our single-chain data. Similar experiments on methyl-substituted ladder-type poly(*para*-phenylene) (MeLPPP) (52) result in a very small slope of about 0.60 cm^{-1}/K . Since the rigid rod-like MeLPPP represents the prototype of a highly planar system, these ensemble data provide further evidence that PDOPT possesses a rather planar conformation in solution—a conformation in which we expect PDOPT chains to exist in our single-molecule experiments as well owing to the rapid cooling procedure during sample preparation (22).

Quantum-Classical Atomistic Simulations. To gain further insight into the origin of the pronounced red shift of the ZPLs between PDOPT and P3HT, we performed quantum-classical atomistic simulations of PDOPT16 and compared with our recent results for P3HT (29). Following the same protocol as in ref. 29, we used a modified Quantum Mechanical Consistent Force Field for π -electrons (QCFF/PI) method (53, 54) to generate a thermal ensemble of single PDOPT16 at room temperature (298 K), by generating 1,000 structures and running a thermal trajectory for ~ 1 ns. We then calculated the optical and electronic properties using the semiempirical Pariser–Parr–Pople (PPP) Hamiltonian for π -electrons at the level of configuration interaction singles

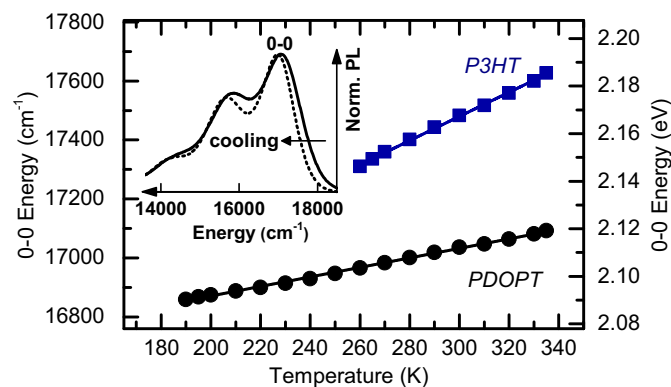


Fig. 2. Temperature-dependent solution PL spectra. Shown is evolution of the 0–0 peak position of the ensemble PL spectra of the disordered solution phase of PDOPT89 (black circles) and P3HT144 (blue squares) dissolved in THF. The solid lines are linear fits to the data points. (*Inset*) The solution PL spectra of PDOPT89 at a temperature of 300 K (solid line) and 240 K (dashed line).

(CIS). The choice of high temperature was motivated by the experimental conditions, in which the rapid cooling of the sample is expected to trap the molecules in typical high-temperature conformations. For details of the simulations, see *Methods and Materials* and *SI Simulation Protocol*.

Backbone and side-chain conformations. For PDOPT, we initialized our molecular dynamics simulations with single PDOPT16 structures similar to those in crystals (20) with all thiophene units in trans configuration (interring dihedral angle $\phi = 180^\circ$), and with the phenyl rings at 90° to the backbone. The torsional free energy, calculated as potential of mean force [PMF = $-k_B T \log P(\phi)$], shows a minimum at 180° (Fig. 3A), which reflects a stable transplanar backbone. The minimum is rather flat, and thus a large set of dihedral angles is thermally accessible, which allows for a large degree of torsional disorder—the variation around the mean angle—in agreement with our single-chain data. The *n*-octyl chains on adjacent monomers were found to form stable contacts, which lead to the emergence of helical wrapping, resembling barber's pole stripes, around the thiophene backbone (Fig. 3B). These contacts stabilize the perpendicular orientation between thiophene and phenyl units, and balance steric repulsions leading to the backbone planarization.

In contrast, in single-molecule P3HT, the backbone is more exposed, and side chains do not form an identifiable structural motif. We recently showed that the PMF of P3HT (see Fig. 3A) possesses a clear minimum around a dihedral angle of $\phi = 145^\circ$ (29), and, in consequence, the chain conformation is rather disordered, as illustrated in Fig. 3A, *Top*. This behavior is in line with other work on P3HT, in which repulsive S...H interactions between the sulfur atom and the hydrogen atoms of the closest methylene unit in the adjacent hexyl group were shown to lead to nonplanar optimal structures (27, 32, 49, 55).

Optical and electronic properties. Our simulated absorption spectra of the thermal ensembles of PDOPT and P3HT at room temperature are depicted in Fig. 3C. Notably, they exhibit a spectral shift of *ca.*

$2,000 \text{ cm}^{-1}$, in good quantitative agreement with our experiments. These results clearly show that the observed differences in backbone conformation between PDOPT and P3HT, induced by very different side groups, result in the experimentally measured, profoundly distinct optical properties.

We further calculated a coherence length L and an electron-hole displacement distance R_{e-h} . L is a measure for the size of the emitting/absorbing sites ("chromophores") and is defined as the "radius of gyration" of the exciton wave function (56). R_{e-h} is computed as the difference between the centers of mass of the electron/hole wave functions, and is a measure of electron-hole polarization, i.e., of the charge transfer character of the excited state. Interestingly, the calculated coherence lengths L are similar for both systems, ~ 6.5 repeating units; see Fig. 3D. This finding is rather surprising, as the spectral red shift would conventionally be interpreted as being due to an increase in L , or chromophore size, because of the planarization of the PDOPT backbone. Hence, we must depart from this "particle-in-a-box model" view, and notice that it is the magnitude of the electron-hole displacement, R_{e-h} , that distinguishes the two systems: The mean $\langle R_{e-h} \rangle$ is reduced in PDOPT (0.11 repeating units) with respect to P3HT (0.45 repeating units); see Fig. 3E. We recall that the transition energy of conjugated polymers does not depend only on the coherence length but also on the electronic π -overlap coupling (or conjugation) between repeating units. Given that the mean coherence lengths are similar in both materials, the reduced transition energy in single PDOPT necessarily implies a stronger electronic coupling in this system, which is witnessed by the smaller calculated R_{e-h} (29). Computationally, for the more disordered P3HT, the wave function of the lowest excited state is dominated by Slater determinants describing the promotion of an electron from HOMO to LUMO as well as from HOMO to LUMO+1. In particular, the latter results in a more pronounced charge transfer character of the excited state in

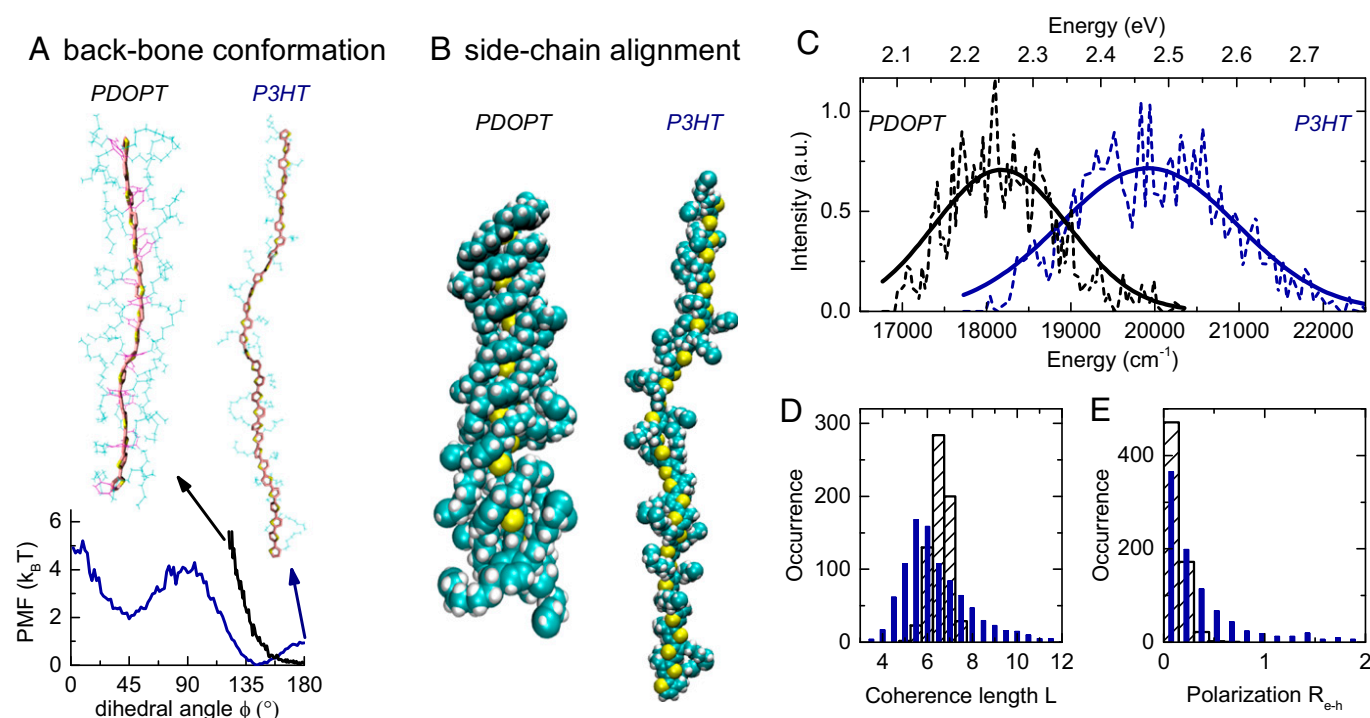


Fig. 3. Quantum-classical atomistic simulations of the conformational, optical, and electronic properties of single PDOPT and P3HT chains. (A) (*Top*) Snapshots from trajectories of PDOPT16 and P3HT30 chains highlighting the backbone conformation. (*Bottom*) Corresponding PMF as a function of the dihedral angle ϕ (blue, P3HT; black, PDOPT). (B) Snapshots showing the side-chain alignment of the two polythiophenes. (C) Dashed lines denote calculated absorption spectra from thermal ensembles of PDOPT (black) and P3HT (blue). Solid lines denote Gaussian fits to the calculated spectra. (D and E) Distribution of (D) coherence lengths L and (E) electron-hole separation distances R_{e-h} (both in number of repeating units) for P3HT (solid blue) and PDOPT (hatched black).

P3HT. For PDOPT, in contrast, the relative contribution of Slater determinants for the HOMO to LUMO+1 promotion is significantly reduced. Hence, the higher degree of planarity in PDOPT enhances conjugation, which results in more tightly bound excitons with less pronounced charge transfer character (reduced R_{e-h}), compared with P3HT. For further details, see the discussion of the polarization index parameter D in our recent work (29).

In this context, we note that, according to the simplified models of Spano, Barford, and coworkers (57, 58), the ratio between the area of the ZPL and the area of the effective vibrational mode (here around $1,480\text{ cm}^{-1}$) in the experimental spectra is usually interpreted as a measure for the coherence length L of the absorbing/emitting sites, with a relatively stronger ZPL indicating a larger L . From such analysis, we find an increase in coherence length by roughly a factor of 2 from the disordered P3HT to the more planar PDOPT (Fig. S4), in agreement with common notion, but in contrast to our results of a direct calculation. Although largely ignored in the literature, the framework developed by Spano and coworkers (57, 59) also allows for the possibility to account for different peak ratios by distinct electron–hole separations for a given coherence length. Consistent with our results, a larger electron–hole distance is predicted to give rise to a decreased peak ratio between the ZPL and the vibrational mode (*SI Coherence Length of the Emitting Site*). We conclude that the experimental ratio between ZPL and the effective vibrational mode may rather reflect the strength of the conjugation controlled by backbone conformation, but not the coherence length. Finally, we emphasize that this shifts the discussion from the comparison of coherence lengths in two materials to a discussion of a so far overlooked physical quantity affected by the conjugation, the electron–hole polarization.

Conclusion

Based on our combined experimental and theoretical investigation of the two polythiophene derivatives PDOPT and P3HT on the single-chain and bulk level, we have demonstrated that, contrary to common notion, the bulky side groups of PDOPT actually induce a stable planarization of the conjugated backbone via noncovalent interactions. This more planar backbone leads to a red shift of $>2,000\text{ cm}^{-1}$ (0.25 eV) of its electronic transition relative to that in the more conformationally disordered P3HT single chains. Intriguingly, this side-chain induced planarization does not give rise to an increase in mean coherence length (spatial extent of the absorbing/emitting sites), which is essentially identical for both polythiophenes. It is rather the conjugation, i.e., the electronic π -overlap between thiophene rings, that is stronger in PDOPT, and ultimately causes the observed red shift in transition energy and reduces the electron–hole polarization.

Our spectroscopic data strongly indicate that the bulky di-*o*-cylphenyl side groups of PDOPT have a strong impact on the static and dynamic disorder, and must be involved in planarization. According to our simulations of single chains, their phenyl rings are rotated $\sim 90^\circ$ out of the backbone plane (Fig. 3A). Recent work on arene–thiophene systems suggests that such a T-shaped arrangement is indeed a stable, energetically favorable configuration (60). In PDOPT, this orientation is arguably further stabilized by the interaction between the *n*-octyl side chains which extend across its backbone. The importance of the side groups for structural properties in PDOPT is also manifest in its crystallization behavior. Despite the absence of π – π stacking, spherulitic structures of several hundred micrometers diameter and a high degree of

crystallinity can be grown under appropriate conditions (61). The main driving forces for spherulite formation are noncovalent interactions between side groups of neighboring chains (20). In the resulting configuration, the phenyl rings and *n*-octyl chains are oriented perpendicularly to the plane of the backbones, with a dense interdigitation of adjacent *n*-octyl chains (62). Interestingly, the concept of side-chain induced stabilization of polymers' secondary and tertiary structures is also known in biological systems. Interactions of side groups, such as aromatic–aromatic interactions, routinely lead to a stabilization of the ternary structure of proteins (63, 64). Such interactions are also conceivable between adjacent phenyl rings of a PDOPT chain, with a mean distance slightly larger than $\sim 7\text{ \AA}$ in spherulites (20).

Further studies are clearly required to develop broader insight into the structural variation obtainable via side-chain manipulation. The backbone planarization in PDOPT suggests that this control may ultimately pave the road for the design of optimized structures for efficient optoelectronics applications.

Methods and Materials

Experimental Methods. Single-molecule PL experiments on PDOPT were performed employing a home-built confocal microscope, as reported recently (22). For sample preparation, PDOPT was diluted in *n*-hexadecane, shock-frozen in liquid nitrogen, and subsequently cooled down to 1.5 K in a home-built bath cryostat. For each chain, we measured up to 500 sequential spectra with an integration time of 1 s to 3 s each. Temperature-dependent ensemble PL spectra were measured in a home-built setup described in detail elsewhere (65). In brief, the polymers were dissolved in THF, and the sample was placed in an electrically heatable continuous flow cryostat. Each temperature was stabilized for 15 min before measurement to ensure a homogeneous temperature across the sample. See *SI Methods and Materials* for details.

Materials. To synthesize PDOPT with a defined molecular weight, low dispersity, and high regioregularity, a Kumada catalyst-transfer polycondensation including a nickel catalyst with a hybrid P,N ligand was used (21). P3HT was synthesized via catalyst transfer polymerization (66). Both PDOPT and P3HT contain only a single regiodefect at one end of each chain which is introduced by the synthetic route (23, 66, 67).

Simulation. To compare the optical properties of single-molecule P3HT with those of PDOPT, we repeated the calculation recently published by two of us in ref. 29. The polymers were modeled with a nonpolar environment through the alkane-like dielectric constant $\epsilon = 2.7$. The relevant properties of the lowest energy excited state, i.e., the coherence length L and the electron–hole displacement distance R_{e-h} , were derived using the CIS mixed density matrix. Importantly, since the side chains in both thiophenes are not expected to contribute to the spectrum in the relevant energy window, they were modeled via classical equations of motion with an appropriate force field. In P3HT, this is justified due to the alkyl character of the side chains, while, in PDOPT, the conjugation between the thiophene backbone and the substituted aromatic phenyl rings is broken due to steric interactions in our simulations at all times. See *SI Simulation Protocol* for details.

ACKNOWLEDGMENTS. We thank Marin van Heel (University of Leiden, Leiden, Netherlands) for providing the multivariate statistical analysis algorithm for data analysis. D.R. thanks Thiago B. de Queiroz for helpful discussions. This work was financially supported by the German Research Foundation through Projects HI1508/2 (to D.R., S.B., and R.H.), SO1213/5-1 (to D.S. and M.S.), and GRK1640 (to D.R., F.P., S.B., J.K., A.K., M.T., and R.H.). Additional funding came from the Bavarian State Ministry of Science, Research and the Arts for the collaborative research network Solar Technologies Go Hybrid (J.K., M.T., and A.K.). R.H. acknowledges support from the Elite Network of Bavaria "Macromolecular Science." P.J.R. is grateful for the support of the National Science Foundation (CHE-1362381).

- Huang Y, Kramer EJ, Heeger AJ, Bazan GC (2014) Bulk heterojunction solar cells: Morphology and performance relationships. *Chem Rev* 114:7006–7043.
- Noriega R, et al. (2013) A general relationship between disorder, aggregation and charge transport in conjugated polymers. *Nat Mater* 12:1038–1044.
- Hildner R, Köhler A, Müller-Buschbaum P, Panzer F, Thelakkat M (2017) π -conjugated donor polymers. Structure formation and morphology in solution, bulk and photovoltaic blends. *Adv Energy Mater* 7:1700314.
- Hu Z, et al. (2017) Impact of backbone fluorination on nanoscale morphology and excitonic coupling in polythiophenes. *Proc Natl Acad Sci USA* 114:5113–5118.
- Milián-Medina B, Gierschner J (2017) "Though it be but little, it is fierce": Excited state engineering of conjugated organic materials by fluorination. *J Phys Chem Lett* 8: 91–101.
- Mei J, Bao Z (2014) Side chain engineering in solution-processable conjugated polymers. *Chem Mater* 26:604–615.

- Mueller CJ, Gann E, Singh CR, Thelakkat M, McNeill CR (2016) Control of molecular orientation in polydiketopyrrolopyrrole copolymers via diffusive noncovalent interactions. *Chem Mater* 28:7088–7097.
- Himmelberger S, et al. (2015) Role of side-chain branching on thin-film structure and electronic properties of polythiophenes. *Adv Funct Mater* 25:2616–2624.
- Jackson NE, et al. (2013) Controlling conformations of conjugated polymers and small molecules: The role of nonbonding interactions. *J Am Chem Soc* 135:10475–10483.
- Mueller CJ, Singh CR, Fried M, Huettner S, Thelakkat M (2015) High bulk electron mobility diketopyrrolopyrrole copolymers with perfluorothiophene. *Adv Funct Mater* 25:2725–2736.
- Lombek F, et al. (2016) PCDTBT: From polymer photovoltaics to light-emitting diodes by side-chain-controlled luminescence. *Macromolecules* 49:9382–9387.
- Schlüter AD, Rabe JP (2000) Dendronized polymers: Synthesis, characterization, assembly at interfaces, and manipulation. *Angew Chem Int Ed Engl* 39:864–883.
- Vezie MS, et al. (2016) Exploring the origin of high optical absorption in conjugated polymers. *Nat Mater* 15:746–753.
- Strickler SJ, Berg RA (1962) Relationship between absorption intensity and fluorescence lifetime of molecules. *J Chem Phys* 37:814–822.
- Milad R, et al. (2016) Effective conjugation in conjugated polymers with strongly twisted backbones. A case study on fluorinated MEHPPV. *J Mater Chem C* 4: 6900–6906.
- Panzer F, Bässler H, Köhler A (2017) Temperature induced order-disorder transition in solutions of conjugated polymers probed by optical spectroscopy. *J Phys Chem Lett* 8: 114–125.
- Andersson MR, et al. (1999) Substituted polythiophenes designed for optoelectronic devices and conductors. *J Mater Chem* 9:1933–1940.
- Ko S, et al. (2012) Controlled conjugated backbone twisting for an increased open-circuit voltage while having a high short-circuit current in poly(hexylthiophene) derivatives. *J Am Chem Soc* 134:5222–5232.
- Kuei B, Gomez ED (2016) Chain conformations and phase behavior of conjugated polymers. *Soft Matter* 13:49–67.
- Hamidi-Sakr A, et al. (2016) Highly oriented and crystalline films of a phenyl-substituted polythiophene prepared by epitaxy. Structural model and influence of molecular weight. *Macromolecules* 49:3452–3462.
- Schiefer D, et al. (2014) Nickel catalyst with a hybrid P, N ligand for Kumada catalyst transfer polycondensation of sterically hindered thiophenes. *ACS Macro Lett* 3: 617–621.
- Raithel D, et al. (2016) Emitting species of poly(3-hexylthiophene): From single, isolated chains to bulk. *Macromolecules* 49:9553–9560.
- Kohn P, et al. (2012) On the role of single regiodefects and polydispersity in regioregular poly(3-hexylthiophene): Defect distribution, synthesis of defect-free chains, and a simple model for the determination of crystallinity. *J Am Chem Soc* 134: 4790–4805.
- Brinkmann M (2011) Structure and morphology control in thin films of regioregular poly(3-hexylthiophene). *J Polym Sci B Polym Phys* 49:1218–1233.
- Clark J, Silva C, Friend RH, Spano FC (2007) Role of intermolecular coupling in the photophysics of disordered organic semiconductors: Aggregate emission in regioregular polythiophene. *Phys Rev Lett* 98:206406.
- Thiessen A, et al. (2013) Unraveling the chromophoric disorder of poly(3-hexylthiophene). *Proc Natl Acad Sci USA* 110:E3550–E3556.
- Hu Z, et al. (2013) Effect of the side-chain-distribution density on the single-conjugated-polymer-chain conformation. *ChemPhysChem* 14:4143–4148.
- Chen P-Y, Rassamesard A, Chen H-L, Chen S-A (2013) Conformation and fluorescence property of poly(3-hexylthiophene) isolated chains studied by single molecule spectroscopy: Effects of solvent quality and regioregularity. *Macromolecules* 46: 5657–5663.
- Simine L, Rossky PJ (2017) Relating chromophoric and structural disorder in conjugated polymers. *J Phys Chem Lett* 8:1752–1756.
- Hildner R, Lemmer U, Scherf U, van Heel M, Köhler J (2007) Revealing the electron-phonon coupling in a conjugated polymer by single-molecule spectroscopy. *Adv Mater* 19:1978–1982.
- Hildner R, Winterling L, Lemmer U, Scherf U, Köhler J (2009) Single-molecule spectroscopy on a ladder-type conjugated polymer: Electron-phonon coupling and spectral diffusion. *ChemPhysChem* 10:2524–2534.
- Brambilla L, et al. (2014) Regio-regular oligo and poly(3-hexyl thiophene): Precise structural markers from the vibrational spectra of oligomer single crystals. *Macromolecules* 47:6730–6739.
- Becker RS, Seixas de Melo J, Maçanita AL, Elisei F (1996) Comprehensive evaluation of the absorption, photophysical, energy transfer, structural, and theoretical properties of α -oligothiophenes with one to seven rings. *J Phys Chem* 100:18683–18695.
- Gierschner J, Cornil J, Egelhaaf H-J (2007) Optical bandgaps of π -conjugated organic materials at the polymer limit: Experiment and theory. *Adv Mater* 19:173–191.
- Rossi G, Chance RR, Silbey R (1989) Conformational disorder in conjugated polymers. *J Chem Phys* 90:7594–7601.
- de Queiroz TB, Kümmel S (2015) Tuned range separated hybrid functionals for solvated low bandgap oligomers. *J Chem Phys* 143:034101.
- Baderschneider S, Scherf U, Köhler J, Hildner R (2016) Influence of the conjugation length on the optical spectra of single ladder-type (p-phenylene) dimers and polymers. *J Phys Chem A* 120:233–240.
- Ambrose WP, Moerner WE (1991) Fluorescence spectroscopy and spectral diffusion of single impurity molecules in a crystal. *Nature* 349:225–227.
- Feist FA, Basché T (2008) Fluorescence excitation and emission spectroscopy on single MEH-PPV chains at low temperature. *J Phys Chem B* 112:9700–9708.
- Pullerits T, Mirzov O, Scheblykin IG (2005) Conformational fluctuations and large fluorescence spectral diffusion in conjugated polymer single chains at low temperatures. *J Phys Chem B* 109:19099–19107.
- Westenhoff S, et al. (2006) Anomalous energy transfer dynamics due to torsional relaxation in a conjugated polymer. *Phys Rev Lett* 97:166804.
- Kador L (1991) Stochastic theory of inhomogeneous spectroscopic line shapes re-investigated. *J Chem Phys* 95:5574–5581.
- Hoffmann ST, Bässler H, Köhler A (2010) What determines inhomogeneous broadening of electronic transitions in conjugated polymers? *J Phys Chem B* 114: 17037–17048.
- Marcus M, Tozer OR, Barford W (2014) Theory of optical transitions in conjugated polymers. II. Real systems. *J Chem Phys* 141:164102.
- Kobayashi H, Tsuchiya K, Ogino K, Vacha M (2012) Spectral multitude and spectral dynamics reflect changing conjugation length in single molecules of oligophenylenevinyls. *Phys Chem Chem Phys* 14:10114–10118.
- Geva E, Skinner JL (1997) Theory of single-molecule optical line-shape distributions in low-temperature glasses. *J Phys Chem B* 101:8920–8932.
- Kador L, Horne DE, Moerner WE (1990) Optical detection and probing of single dopant molecules of pentacene in a p-terphenyl host crystal by means of absorption spectroscopy. *J Phys Chem* 94:1237–1248.
- Orrit M, Bernard J (1990) Single pentacene molecules detected by fluorescence excitation in a p-terphenyl crystal. *Phys Rev Lett* 65:2716–2719.
- Bhatta RS, Tsige M, Perry DS (2014) Torsionally-induced blue shift of the band gap in poly(3-hexylthiophene). *J Comput Theor Nanosci* 11:2157–2164.
- Renger T, Grundkötter B, Madjet M-A, Müh F (2008) Theory of solvatochromic shifts in nonpolar solvents reveals a new spectroscopic rule. *Proc Natl Acad Sci USA* 105: 13235–13240.
- Renge I (1992) Relationship between electron-phonon coupling and intermolecular interaction parameters in dye-doped organic glasses. *J Opt Soc Am B* 9:719–723.
- Athanasopoulos S, Hoffmann ST, Bässler H, Köhler A, Beljonne D (2013) To hop or not to hop? Understanding the temperature dependence of spectral diffusion in organic semiconductors. *J Phys Chem Lett* 4:1694–1700.
- Warshel A, Karplus M (1972) Calculation of ground and excited state potential surfaces of conjugated molecules. I. Formulation and parametrization. *J Am Chem Soc* 94:5612–5625.
- Lobaugh J, Rossky PJ (1999) Computer simulation of the excited state dynamics of betaine-30 in acetonitrile. *J Phys Chem A* 103:9432–9447.
- Darling SB, Sternberg M (2009) Importance of side chains and backbone length in defect modeling of poly(3-alkylthiophenes). *J Phys Chem B* 113:6215–6218.
- Barford W, Lidzey DG, Makhov DV, Meijer AJ (2010) Exciton localization in disordered poly(3-hexylthiophene). *J Chem Phys* 133:044504, and correction (2010) 133:119901.
- Spano FC, Silva C (2014) H- and J-aggregate behavior in polymeric semiconductors. *Annu Rev Phys Chem* 65:477–500.
- Barford W, Marcus M (2017) Perspective: Optical spectroscopy in π -conjugated polymers and how it can be used to determine multiscale polymer structures. *J Chem Phys* 146:130902.
- Hestand NJ, Spano FC (2016) Determining the spatial coherence of excitons from the photoluminescence spectrum in charge-transfer J-aggregates. *Chem Phys* 481: 262–271.
- Castellano O, Gimón R, Soscun H (2011) Theoretical study of the σ - π and π - π interactions in heteroaromatic monocyclic molecular complexes of benzene, pyridine, and thiophene dimers. Implications on the resin-asphaltene stability in crude oil. *Energy Fuels* 25:2526–2541.
- Keheze FM, et al. (2017) Signatures of melting and recrystallization of a bulky substituted poly(thiophene) identified by optical spectroscopy. *Macromolecules* 50: 6829–6839.
- Aasmundtveit KE, et al. (2000) Structural ordering in phenyl-substituted polythiophenes. *Macromolecules* 33:5481–5489.
- Burley SK, Petsko GA (1985) Aromatic-aromatic interaction: A mechanism of protein structure stabilization. *Science* 229:23–28.
- Salonen LM, Ellermann M, Diederich F (2011) Aromatic rings in chemical and biological recognition: Energetics and structures. *Angew Chem Int Ed Engl* 50: 4808–4842.
- Panzer F, et al. (2016) Reversible laser-induced amplified spontaneous emission from coexisting tetragonal and orthorhombic phases in hybrid lead halide perovskites. *Adv Opt Mater* 4:917–928.
- Lohwasser RH, Thelakkat M (2011) Toward perfect control of end groups and polydispersity in poly(3-hexylthiophene) via catalyst transfer polymerization. *Macromolecules* 44:3388–3397.
- Schiefer D, et al. (2016) Poly(3-(2,5-dioctylphenyl)thiophene) synthesized by direct arylation polycondensation. End groups, defects, and crystallinity. *Macromolecules* 49:7230–7237.

Supporting Information

Raithel et al. 10.1073/pnas.1719303115

SI Methods and Materials

Ensemble absorption and PL spectra were recorded using commercial spectrometers (Lambda 750 UV/VIS Spectrometer; Perkin-Elmer and Cary Eclipse Fluorescence Spectrophotometer; Varian) using chloroform (Fluka, $\geq 99.8\%$) for P3HT and *n*-hexadecane (Fluka, $\geq 98\%$) for PDOPT.

For low-temperature single-chain PL spectroscopy, PDOPT was dissolved and further diluted in *n*-hexadecane (Fluka, $\geq 98\%$) to a final concentration of about 0.3 nM and subsequently cooled down to liquid helium temperature (1.5 K). The experimental setup is based on a home-built confocal microscope (1, 2). To exclude preferential excitation of specific subensembles of PDOPT chains, we used excitation wavelengths between 420 nm and 460 nm using a FemtoPower1060 Supercontinuum Laser (Fianium SC 400-4) or a pulsed 450-nm diode laser (LDH-P-C-450B; PicoQuant) in combination with the Clean-Up filter BP 440/40, the dichroic beam splitter 458DCR, and the long-pass filter 467LP (all AHF). For polarization-resolved measurements, we additionally inserted a half-wave plate (Thorlabs) mounted in a motorized rotating mount (Owis) in the excitation path. The PL signal was dispersed by a spectrometer (300 lines per millimeter grating, SpectraPro-150; Acton Research Corporation) and imaged onto an electron-multiplying charge-coupled device camera (iXon DV-887; Andor). From each single chain, we typically acquired several hundred PL spectra with integration times between 1 s and 3 s.

We performed data analysis with a home-written software which allowed correction for background signals and the quantum efficiency of the detector as well as to fit the spectra. Furthermore, we employed a multivariate statistical pattern recognition algorithm (MSA) for data analysis to overcome spectral diffusion on time scales slower than the integration time for an individual spectrum (1 s to 3 s) by averaging only statistically similar spectra. For details, see ref. 1.

Temperature-dependent ensemble PL spectra were measured in a home-built setup which is described in detail elsewhere (3). In brief, the polymers were dissolved in THF and poured into fused silica cuvettes. The sample was then placed in an electrically heatable continuous flow cryostat (Oxford Instruments). It was excited using a continuous-wave diode laser with an excitation wavelength of 405 nm. The emitted light of the samples was focused into a spectrograph (Shamrock SR303i; Andor) and detected with a CCD camera (iDus; Andor). Each temperature was stabilized for 15 min before measurement to ensure a homogeneous temperature across the sample. The emission spectra were corrected for the transmission through the setup. Subsequently, the temperature-dependent 0–0 transition energy was extracted by an FC analysis, assuming that only a single effective vibrational mode with an energy of around $1,400\text{ cm}^{-1}$ (0.17 eV) couples to the electronic transition; see *SI Franck–Condon Analysis*.

SI Ensemble Spectra

Normalized absorption and PL spectra of both PDOPT and P3HT in solution are shown in Fig. S1.

SI Single-Chain Spectra and Statistics

In Fig. S2, the temporal evolution of the emission spectra of a single, isolated PDOPT89 chain is shown. In this experiment, the half-wave plate was placed in the excitation path to rotate the polarization of the excitation light by 2.75° between successively recorded spectra. The intensity of the resulting emission follows

a clear \cos^2 modulation as a function of the polarization of the excitation light, which is shown in Fig. S2, *Top Right* by the spectrally integrated intensity of the main ZPL at $16,800\text{ cm}^{-1}$ and the corresponding fit (gray line). These data lead us to the conclusion that only one absorbing unit/chromophore is excited resonantly with the linearly polarized excitation light.

On the high-energy side of the prominent ZPL, at $16,800\text{ cm}^{-1}$, two additional weak peaks are observed (marked with asterisks in Fig. S2), which follow the same polarization dependence as the main ZPL. Since the weak lines show blinking and spectral diffusion independent from each other and from the main ZPL at $16,800\text{ cm}^{-1}$, we interpret these two weak peaks as additional ZPLs on the same chain. These (weakly) emitting ZPLs are populated by downhill intrachain energy transfer from the same absorbing unit/chromophore. The long PDOPT chains are therefore multichromophoric systems. In contrast, the long P3HT144 chains showed only single-chromophoric emission; that is, we observed only a single emitting site per chain (1).

SI Coherence Length of the Emitting Sites

According to Spano, Barford, and coworkers (4–7), an increasing backbone planarization gives rise to a larger delocalization of electronic excitations (in terms of the coherence length N_{coh} , in units of monomers), and concomitantly to an increase in peak ratio $P_{em} = I_{0-0}/I_{0-1}$ between the intensity I_{0-0} of the ZPL and the intensity I_{0-1} of the effective carbon bond stretch mode around $1,400\text{ cm}^{-1}$. The peak ratio for PDOPT89 can be easily extracted from single-chain spectra (Fig. 1B) or the matrix-isolated spectra (dotted line in Fig. 1H, and Fig. S4). The resulting value of $P_{em} = I_{0-0}/I_{0-1} = 2.7$ translates into a coherence length of about $N_{coh} = P_{em} \cdot S_{mon} / \kappa = 3.8$ to 5 monomers according to Spano and Yamagata (4, 5) or $N_{coh} = 2 \cdot P_{em} \cdot S_{mon} = 7.6$ to 10 monomers according to Barford and coworkers (6, 7). Here, S_{mon} represents an effective Huang–Rhys factor for a thiophene monomer for the several vibrational lines around $1,400\text{ cm}^{-1}$, which was determined to be $S_{mon} = 1.4$ to 1.9 (8). The electron–hole distance parameter κ is usually assumed to be unity in the analysis of optical spectra of conjugated polymers using Spano’s approach.

For P3HT144, we find a peak ratio of $P_{em} = I_{0-0}/I_{0-1} \approx 1.3$ (Fig. S4), which corresponds to $N_{coh} = 2$ to 2.5 monomers (Spano) and $N_{coh} = 4$ to 5 monomers (Barford), respectively. Irrespective of the definition of the delocalization of electronic excitation and the exact value of S_{mon} , this means a nearly doubled coherence length for PDOPT in comparison with P3HT, as the ratio is defined as

$$\frac{N_{coh}^{PDOPT}}{N_{coh}^{P3HT}} = \frac{P_{em}^{PDOPT}}{P_{em}^{P3HT}} = \frac{2.7}{1.3} = 2.1.$$

This finding supports the idea of a more planar backbone in PDOPT.

Note, however, that the increase in P_{em} from P3HT to PDOPT may not necessarily reflect a larger coherence length of electronic excitations but may, in fact, be rather a consequence of the stronger electronic coupling between repeating units in the more planar PDOPT, which results in different electron–hole polarizations in these two materials; see our discussion in the main text. This is also captured in the framework of Hestand and Spano (9) by the electron–hole distance parameter κ which can be approximated in conjugated polymers as

$$\kappa \approx \frac{1}{\langle FE \rangle + 2(1 - \langle FE \rangle)} = \frac{1}{2 - \langle FE \rangle}$$

with $\langle FE \rangle$ being the Frenkel component of the lowest energy emissive eigenstate. A smaller Frenkel, and thus a higher charge transfer contribution ($1 - \langle FE \rangle$), leads to a smaller κ and thus a decreased peak ratio ($P_{em} = I_{0-0}/I_{0-1} = \kappa N_{coh}/S_{mon}$) for a given coherence length. Thus, considering this electron–hole distance parameter κ , the decreased peak ratio observed here for P3HT can be rationalized by a stronger charge transfer character of the electronic excitations in P3HT compared with PDOPT, which is consistent with our simulations.

SI Franck–Condon Analysis

The temperature-dependent PL spectra of PDOPT and P3HT dissolved in THF were analyzed following an approach based on an FC analysis, as described in previous work (3, 10). Assuming that a single effective carbon bond stretching mode with an energy of $\sim 1,400 \text{ cm}^{-1}$ couples to the 0–0 transition, the PL spectra can be satisfactorily be fitted by the FC progression

$$I_{PL}(E) \propto E^3 \sum_{i=0}^m \frac{S^m}{m!} \exp\left(-\frac{1}{2} \left[\frac{E - (E_{0-0} - mE_{vib})}{\sigma} \right]^2\right).$$

Here, E is the photon energy, E_{0-0} is the center energy of the 0–0 transition, E_{vib} represents the energy of an effective carbon bond stretching mode, S denotes the Huang–Rhys factor of this mode, m represents the vibrational quantum number, and σ is a Gaussian line width (disorder parameter). The Huang–Rhys parameter S and the vibrational energy E_{vib} were kept fixed for all temperatures at $S = 0.9$ ($S = 1.0$) and $E_{vib} = 1,346 \text{ cm}^{-1}$ ($E_{vib} = 1,411 \text{ cm}^{-1}$) for PDOPT (P3HT). From this fitting, we obtain the temperature-dependent evolution of the inhomogeneous line width σ and the peak energy E_{0-0} , with the latter one being displayed in Fig. 2.

SI Simulation Protocol

As mentioned in the main text, we use the modified QCFF/PI method (11, 12), with thermalizing stochastic Langevin dynamics to generate a thermal ensemble of 16-poly(3-(2,5-diocetylphenyl) thiophene) (PDOPT16) at room temperature (298 K). The absorption spectra are computed at the level of CIS, and the properties of the exciton, i.e., the centers of mass of the electron, and, separately, of the hole, and their localization lengths are derived using a reduced description starting from the CIS mixed density matrix,

$$\rho = \sum_i p_i |\Phi_i\rangle \langle \Phi_i| = \sum_{i,a,r,b,s} c_a^r c_b^{s*} |\Psi_a^r\rangle_i \langle \Psi_b^s|_i \quad [\text{S1}]$$

where the index i runs over all accessible nuclear configurations in the thermal ensemble, the weight p_i represents the probability of the i th nuclear configuration, and the wave function $|\Phi_i\rangle$ is given by the configuration interaction series with coefficients c_a^r, c_b^s and the Slater determinants $|\Psi_{a,b}^{r,s}\rangle_i$ for which the indices a, b run over the ground state orbitals and r, s run over the virtual orbitals.

The reduced density matrix is constructed for the excited electron by tracing out the contributions from all but one relevant MO and is given in the space of virtual MOs by

$$\rho_e = \sum_{a,r,s} c_a^r c_a^{s*} |\phi_r^v\rangle \langle \phi_s^v|. \quad [\text{S2}]$$

Analogously, by tracing out all of the states occupied by electrons, we arrive at the reduced density matrix for the hole,

$$\rho_h = \sum_{a,r} |c_a^r|^2 |\phi_a^{oc}\rangle \langle \phi_a^{oc}|. \quad [\text{S3}]$$

The superscripts v and oc emphasize that the orbital is virtual or occupied.

The mapping from MO basis to atomic basis is achieved by the usual unitary matrix of MO coefficients. The observables (O) are computed for the excited electron and for the hole separately as

$$\langle O_{e/h} \rangle = \text{Tr}(O \rho_{e/h}).$$

Following Barford et al. (13), the electron/hole localization length $L_{e/h}$ is defined as the “radius of gyration” of the exciton wave function

$$L_{e/h} = 2\sqrt{\langle n^2 \rangle_{e/h} - \langle n \rangle_{e/h}^2}, \quad [\text{S4}]$$

where $n = [1, 2, \dots, 80]$ is a discrete coordinate corresponding to the position of the π atoms within the polymer, and the averages are performed using the density matrix $\rho_{e/h}$ as $\langle n_{e/h} \rangle = \text{Tr}(n \rho_{e/h})$ and $\langle n_{e/h}^2 \rangle = \text{Tr}(n^2 \rho_{e/h})$.

QCFF/PI. Here we provide the minimal details of the method, described previously in ref. 11, necessary for the discussion. The ground state potential is divided into the classical V_σ and quantum V_π parts,

$$V_{TOT} = V_\sigma + V_\pi. \quad [\text{S5}]$$

The classical part captures the dynamics of the nuclei, while the quantum part represents the π electrons and includes the interaction between electrons and nuclei via electrostatic potential. The dynamics were integrated using a generalization of the Velocity Verlet algorithm (14), known as OVRVO, with the Mersenne Twister pseudorandom number generator (15). At each temperature, the ensemble was constructed by picking configurations from a 1-ns-long trajectory at 1-ps intervals. The trajectory was seeded with an initial structure, taken from a separate room-temperature trajectory.

Molecular Mechanics Force Field. An empirical force field describes the mechanical interactions between all atoms in the simulated system. The classical potential V_σ is composed of bonded (B) and nonbonded (NB) interactions

$$V_\sigma = V_{\sigma,conj}^B + V_{\sigma,conj-sat}^B + V_{\sigma,UD}^B + V_{\sigma}^{NB} \quad [\text{S6}]$$

where the subscript *conj* stands for the subset of atoms in the systems which contribute electrons to the π network, *sat* refers to saturated atoms, which are electronically inert, and *UD* stands for the unique dihedral potential for the intermonomer torsions. The bonded potential between conjugated atoms is given by

$$\begin{aligned} V_{\sigma,conj}^B = & \sum_i e^{2\alpha(b_i - b_0)} - 2e^{\alpha(b_i - b_0)} \\ & + 1/2 \sum_i K_\theta (\theta_i - \theta_0)^2 + F(q_i - q_0)^2 \\ & + 1/2 \sum_i K_\phi^{(1)} \cos \phi_i + K_\phi^{(2)} \cos 2\phi_i \\ & + \sum_i K_{\theta,\theta'} (\theta_i - \theta_0) (\theta_{i'} - \theta_0) \cos \phi_i \end{aligned} \quad [\text{S7}]$$

where the first term is a Morse potential, which captures the bond stretching between two adjacent π atoms, with b_i as the position coordinate and b_0 as an equilibrium bond length;

the second term captures the angular bending with θ_i —the angle defined by three directly bonded atoms—and q_i —the distance between the first and the third atoms with the force constants K_θ, F , respectively. The torsional potential in the third term describes the torsional angles ϕ_i formed by three consecutive bonds, with one-fold $K_\phi^{(1)}$ and twofold $K_\phi^{(2)}$ force constants. The last term adds a contribution from the interaction of pairs of two bending angles and the dihedral angle, sharing a common bond.

The bonded potential is given by

$$V_{\sigma, \text{conj-sat}}^B = 1/2 \sum_i K_b (b_i - b_0)^2 + 2D_b + 1/2 \sum_i K_\theta (\theta_i - \theta_0)^2 + F(q_i - q_0)^2 + 1/2 K_\phi^{(2)} \cos 2\phi_i, \quad \text{[S8]}$$

where K_b, D_b are harmonic force constants, and K_θ, F and $K_\phi^{(2)}$ are as before.

Finally, the uniquely defined torsional potential for the torsional angles ϕ_j^T between the thiophene monomers is given by

$$V_{UD}^B = \sum_j K_1^{UD} \cos(\phi_j^T) + K_2^{UD} \cos(2\phi_j^T) \quad \text{[S9]}$$

with the index j running over all intermonomer bonds.

The nonbonded term is given by

$$V_\sigma^{NB} = \sum_{ij} A_{ij} e^{-\mu_{ij} r_{ij}} - B_{ij} r_{ij}^{-6} \quad \text{[S10]}$$

where r_{ij} is the distance between two nonbonded atoms, and parameters A_{ij}, B_{ij} , and μ_{ij} determine the shape of interaction. Most of the parameters for the classical force field were taken from ref. 16, with the exception of the force constants associated with the intermonomer dihedrals, for which the following values were adopted: $K_1^{UD} = 5.725$ and $K_2^{UD} = 0.11$.

PPP Hamiltonian. The electronic part of the potential is given by

$$V_\pi = \sum_{\mu\nu} P_{\mu\nu} (H_{\mu\nu} + F_{\mu\nu}) \quad \text{[S11]}$$

where $P_{\mu\nu}, H_{\mu\nu}$, and $F_{\mu\nu}$ are the elements of the bond-order matrix \mathbf{P} , the one-electron Core matrix \mathbf{H} , and the Fock matrix \mathbf{F} , respectively, with the indices μ, ν running over the π atoms. The bond-order matrix

$$P_{\mu\nu} = 2 \sum_i c_\mu^i c_\nu^i \quad \text{[S12]}$$

represents the electronic overlaps between all pairs of π atoms, with the index i running over the occupied molecular orbitals (MOs), and c_μ^i, c_ν^i are the MO coefficients at atoms μ and ν . Fock matrix elements are described by

$$F_{\mu\nu} = H_{\mu\nu} - 1/2 P_{\mu\nu} \gamma_{\mu,\nu} + \sum_{\rho \neq \mu} P_{\rho\rho} \gamma_{\mu,\rho} \quad \text{[S13]}$$

where the electron–electron Coulomb repulsion matrix elements $\gamma_{\mu\nu}$ are given by

$$\begin{aligned} \gamma_{\mu,\mu} &= \gamma_{\mu,\mu}^0 + G_s e^{-2\mu_\beta (R_{\mu,\mu+1} - R_{\mu,\mu+1}^{eq})} \cos^2(\phi_{\mu,\mu+1}) \\ &\quad + G_s e^{-2\mu_\beta (R_{\mu,\mu-1} - R_{\mu,\mu-1}^{eq})} \cos^2(\phi_{\mu,\mu-1}) \\ \gamma_{\mu,\mu+1} &= \frac{e^2}{\varepsilon (R_{\mu,\mu\pm 1} + a_{\mu,\mu\pm 1})} + G_s e^{-2\mu_\beta (R_{\mu,\mu\pm 1} - R_{\mu,\mu\pm 1}^{eq})} \cos^2(\phi_{\mu,\mu\pm 1}) \\ \gamma_{\mu,\mu\pm 1} &= \frac{e^2}{\varepsilon (R_{\mu,\mu\pm m} + a_{\mu,\mu\pm m})}, m > 1 \end{aligned} \quad \text{[S14]}$$

with

$$a_{\mu,\nu} = \frac{e^2}{\gamma_{\mu,\mu}^0 + \gamma_{\nu,\nu}^0}. \quad \text{[S15]}$$

In the above, e is the charge of the electron, $R_{\mu\nu}$ is the interatomic distance between two π atoms, and $\phi_{\mu,\nu}$ is the torsional angle used to parametrize the disruption in π conjugation between π orbitals of atoms μ and ν due to misalignment of π orbitals for a particular arrangement of the nuclei. Furthermore, G_s is the Slater orbital overlap matrix parameter (16) renormalized by the dielectric constant $\varepsilon = 2.7$; $\gamma_{\mu,\mu}^0 = I - A/\varepsilon$ is calculated as the ratio of the difference between the valence ionization potential I and the electron affinity A , and the dielectric constant of the medium, ε .

The off-diagonal elements of the one-electron core matrix \mathbf{H} are treated at the level of Hückel theory

$$H_{\mu\nu} = \beta_{\mu\nu}^0 \cos(\phi_{\mu,\nu}), \quad \text{[S16]}$$

where μ, ν are restricted to the nearest neighbors and $\beta_{\mu\nu}^0$ is the electronic resonance parameter. The Hückel parameters at perfect conjugation are given by

$$\beta_{\mu\nu}^0 = \frac{\hbar^2}{m_e R_{\mu\nu}} \frac{dS_{\mu\nu}}{dR_{\mu\nu}}, \quad \text{[S17]}$$

where \hbar is the reduced Planck's constant, m_e is the electron mass, and $S_{\mu\nu}$ is the overlap integral of the p_z orbitals for atoms μ and ν . These are approximated by the Linderberg expression

$$\beta_{\mu\nu}^0 = e^{-\zeta_{\mu\nu} (R_{\mu\nu} - R_{\mu\nu}^{eq})} \left(\beta_1^{\mu\nu} + \beta_2^{\mu\nu} (R_{\mu\nu} - R_{\mu\nu}^{eq}) \right) \quad \text{[S18]}$$

fitting Eq. S16 using $\zeta_{\mu\nu}, \beta_1^{\mu\nu}$, and $\beta_2^{\mu\nu}$ parameters.

The diagonal elements of \mathbf{H} are given by

$$H_{\mu\mu} = \alpha_\mu - \sum_{\rho \neq \mu} Z_\rho \gamma_{\mu\rho}, \quad \text{[S19]}$$

where α_μ represents the valence ionization parameter at the atom μ , while the electron–core repulsion is given by the second term, with Z_ρ —the nuclear charge on atom ρ (equal to the number of π electrons this atom contributes). The MO coefficients then follow from the self-consistent field calculation.

The parametrization of the PPP Hamiltonian was adopted from previous work by the Rossky group; for a complete list of parameters, see the supplementary materials in refs. 17 and 18, with the exception of S (Sulfur), for which the following parameters were used: $\gamma_{\mu\mu}^0 = 9.79/\varepsilon eV$, $\alpha_\mu^0 = -20.0 eV$, $G_s = 8.16/\varepsilon$, $\mu_\beta = \zeta_{CS} = 1.54 \text{ \AA}^{-1}$, $R_{CS}^{eq} = 1.41 \text{ \AA}$, $\beta_1^{CS} = -2.12 eV$, $\beta_2^{CS} = 1.31 eV/\text{ \AA}$.

- Raithel D, et al. (2016) Emitting species of poly(3-hexylthiophene): From single, isolated chains to bulk. *Macromolecules* 49:9553–9560.
- Baderschneider S, Scherf U, Köhler J, Hildner R (2016) Influence of the conjugation length on the optical spectra of single ladder-type (p-phenylene) dimers and polymers. *J Phys Chem A* 120:233–240.
- Panzer F, et al. (2016) Reversible laser-induced amplified spontaneous emission from coexisting tetragonal and orthorhombic phases in hybrid lead halide perovskites. *Adv Opt Mater* 4:917–928.
- Spano FC, Yamagata H (2011) Vibronic coupling in J-aggregates and beyond: A direct means of determining the exciton coherence length from the photoluminescence spectrum. *J Phys Chem B* 115:5133–5143.
- Yamagata H, Spano FC (2014) Strong photophysical similarities between conjugated polymers and J-aggregates. *J Phys Chem Lett* 5:622–632.
- Marcus M, Tozer OR, Barford W (2014) Theory of optical transitions in conjugated polymers. II. Real systems. *J Chem Phys* 141:164102.
- Barford W, Marcus M (2014) Theory of optical transitions in conjugated polymers. I. Ideal systems. *J Chem Phys* 141:164101.
- Yamagata H, Spano FC (2012) Interplay between intrachain and interchain interactions in semiconducting polymer assemblies: The HJ-aggregate model. *J Chem Phys* 136:184901.
- Hestand NJ, Spano FC (2016) Determining the spatial coherence of excitons from the photoluminescence spectrum in charge-transfer J-aggregates. *Chem Phys* 481:262–271.
- Panzer F, Sommer M, Bässler H, Thelakkat M, Köhler A (2015) Spectroscopic signature of two distinct H-aggregate species in poly(3-hexylthiophene). *Macromolecules* 48:1543–1553.
- Warshel A, Karplus M (1972) Calculation of ground and excited state potential surfaces of conjugated molecules. I. Formulation and parametrization. *J Am Chem Soc* 94:5612–5625.
- Lobaugh J, Rossky PJ (1999) Computer simulation of the excited state dynamics of betaine-30 in acetonitrile. *J Phys Chem A* 103:9432–9447.
- Barford W, Lidzey DG, Makhov DV, Meijer AJ (2010) Exciton localization in disordered poly(3-hexylthiophene). *J Chem Phys* 133:044504.
- Di Pierro M, Elber R, Leimkuhler B (2015) A stochastic algorithm for the isobaric-isothermal ensemble with Ewald summations for all long range forces. *J Chem Theory Comput* 11:5624–5637.
- Matsumoto M, Nishimura T (1998) Mersenne twister: A 623-dimensionally equidistributed uniform pseudo-random number generator. *ACM Trans Model Comput Simul* 8:3–30.
- Barford W, Bittner ER, Ward A (2012) Exciton dynamics in disordered poly(p-phenylenevinylene). 2. Exciton diffusion. *J Phys Chem A* 116:10319–10327.
- Sterpone F, Rossky PJ (2008) Molecular modeling and simulation of conjugated polymer oligomers: Ground and excited state chain dynamics of PPV in the gas phase. *J Phys Chem B* 112:4983–4993.
- Jailaubekov AE, et al. (2013) Hot charge-transfer excitons set the time limit for charge separation at donor/acceptor interfaces in organic photovoltaics. *Nat Mater* 12:66–73.

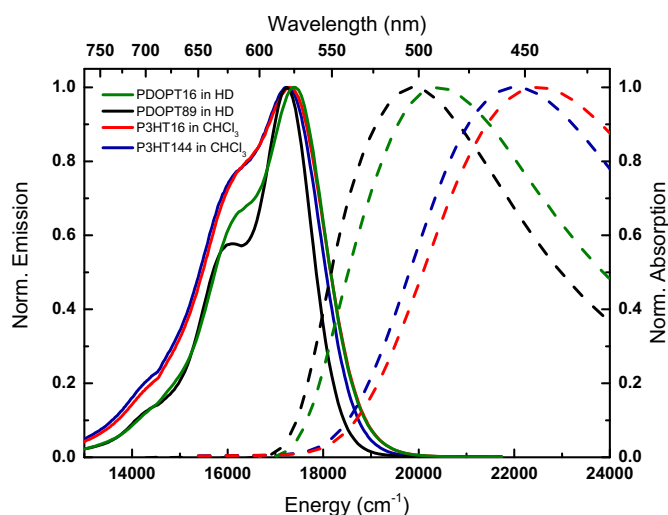


Fig. S1. Normalized absorption (dashed lines) and PL spectra (solid lines) of P3HT16 (red) and P3HT144 (blue) dissolved in chloroform in comparison with PDOPT16 (green) and PDOPT89 (black) dissolved in *n*-hexadecane. All spectra were measured at room temperature. The concentrations were 5 μM for P3HT16, 0.5 μM for P3HT144, 3 μM for PDOPT16, and 0.3 μM for PDOPT89. In absorption, the redshift of around 2,000 cm^{-1} between the maxima of P3HT and PDOPT already indicates a more planar ground state conformation of PDOPT in solution.

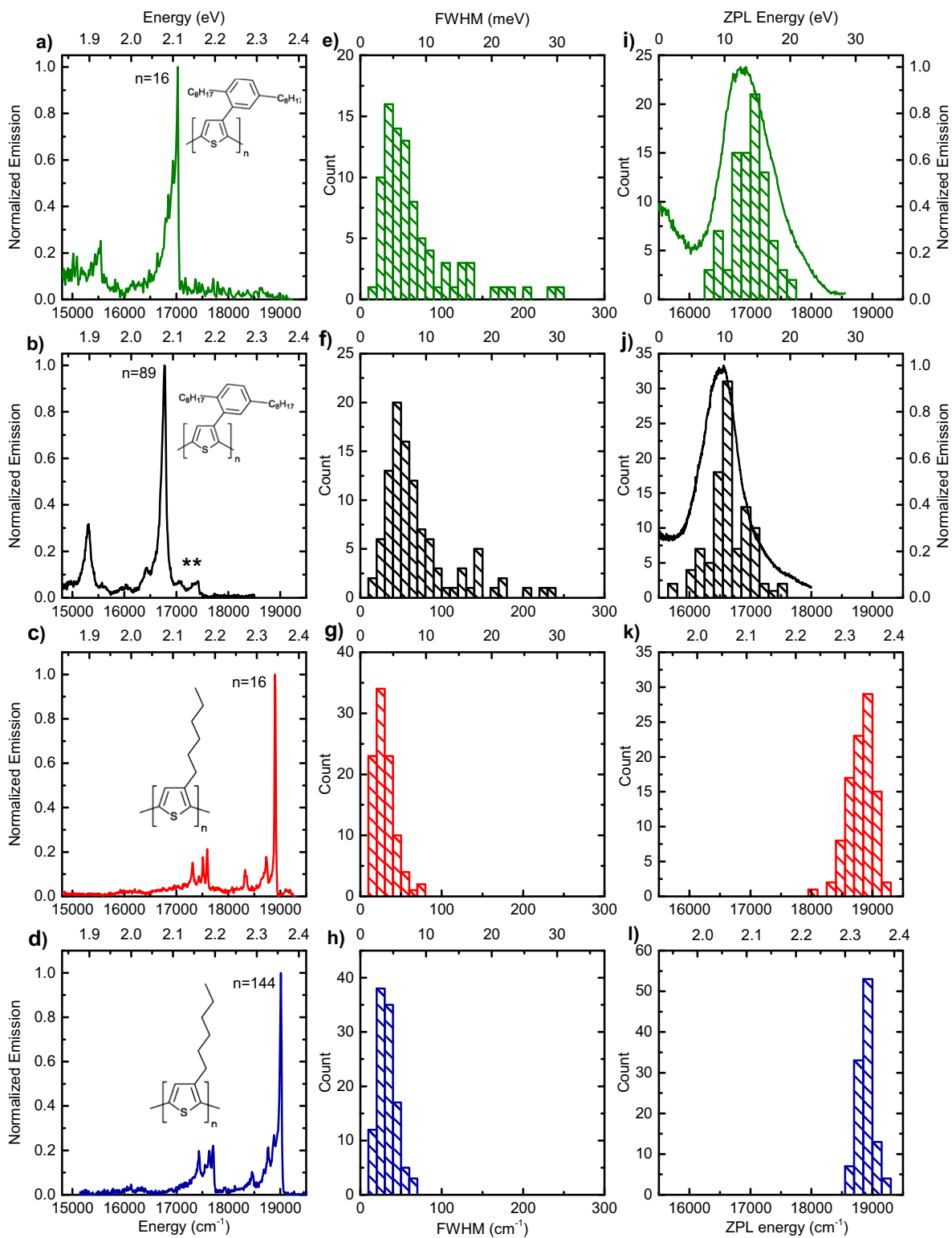


Fig. S3. Low-temperature single-chain PL spectra and ZPL statistics of *A*, *E*, and *I*) PDOPT16 (green), (*B*, *F*, and *J*) PDOPT89 (black), (*C*, *G*, and *K*) P3HT16 (red), and (*D*, *H*, and *L*) P3HT144 (blue). (*A–D*) Representative single-molecule spectra, (*E–H*) distributions of ZPL widths (FWHM), and (*I–L*) distributions of spectral positions of the ZPLs. In *A–D*, the chemical structures are shown as *Insets*. Data for P3HT were taken from ref. 1. *n*, mean number of repeating units.

1. Raithel D, et al. (2016) Emitting species of poly(3-hexylthiophene): From single, isolated chains to bulk. *Macromolecules* 49:9553–9560.

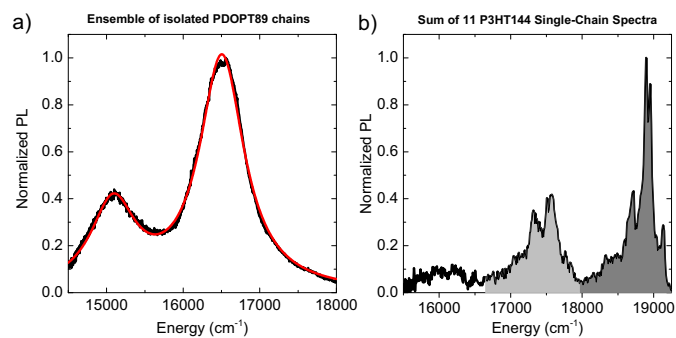
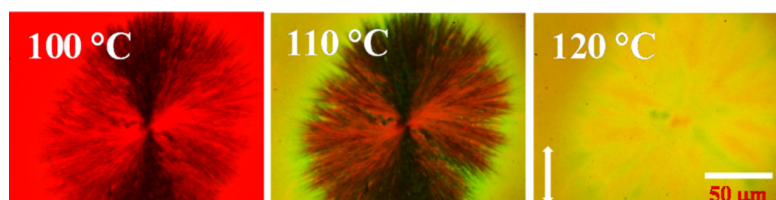


Fig. S4. Extracting the Huang–Rhys parameter from (sub)ensembles of matrix-isolated polythiophene chains embedded in *n*-hexadecane at $T = 1.5$ K. Both spectra are corrected for the photon density of states; thus the Huang–Rhys parameters can be determined from the ratios of peak areas. (A) PL of matrix isolated PDOPT89 (black), fitted with a sum of two Lorentzian functions (red). We find $I_{0-1}/I_{0-0} = S = 1/R_{em} = 0.37$ and thus $R_{em} = 2.7$. (B) PL of a subensemble of P3HT144, i.e., the sum of 11 single-chain spectra, yields a Huang–Rhys factor of $S = 0.77 \pm 0.03$ and thus a peak ratio of $R_{em} = 1.3 (\pm 0.05)$. The error stems from the choice of the integration areas for the effective 0–0 peak (dark gray) and 0–1 peak (light gray).

4.3 Publication 3: Signatures of Melting and Recrystallization of a Bulky Substituted Poly(thiophene) Identified by Optical Spectroscopy



Fanuel Keheze, Dominic Raithel, Tianyu Wu, Daniel Schiefer, Michael Sommer,
Richard Hildner, Günter Reiter

Published in
Macromolecules
DOI: 10.1021/acs.macromol.7b01080

Reproduced with permission from Macromolecules 50 (2017) 6829
Copyright © 2017 American Chemical Society

Signatures of Melting and Recrystallization of a Bulky Substituted Poly(thiophene) Identified by Optical Spectroscopy

Fanuel M. Keheze,[†] Dominic Raithel,[‡] Tianyu Wu,[†] Daniel Schiefer,[§] Michael Sommer,^{§,||,⊥,♯} Richard Hildner,[‡] and Günter Reiter^{*,†,||,⊥}

[†]Physikalisches Institut, Universität Freiburg, Hermann-Herder-Straße 3, 79104 Freiburg, Germany

[‡]Experimentalphysik IV, University of Bayreuth, 95440 Bayreuth, Germany

[§]Institut für Makromolekulare Chemie, Universität Freiburg, Stefan-Meier-Straße 31, 79104 Freiburg, Germany

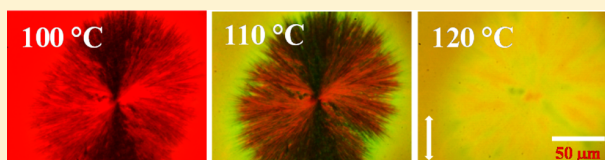
^{||}Freiburger Materialforschungszentrum FMF, Stefan-Meier-Straße 21, 79104 Freiburg, Germany

[⊥]Freiburger Institut für interaktive Materialien und bioinspirierte Technologien FIT, Georges-Köhler-Allee 105, 79110 Freiburg, Germany

[♯]Polymerchemie, Technische Universität Chemnitz, Strasse der Nationen 62, 09111 Chemnitz, Germany

Supporting Information

ABSTRACT: As-cast and slowly crystallized films of conjugated polymers can contain (partially) ordered and less ordered (amorphous) regions with structural defects. Crystallization allows to generate chains with highly planarized backbones, embedded in structures exhibiting long-range order. In the present study, we used spatially resolved optical spectroscopy to quantify differences in the degree of order of a bulky substituted poly(3-(2,5-dioctylphenyl)thiophene) (PDOPT). In particular, we compared absorption and photoluminescence (PL) measurements from large spherulitic crystals, and the same region rapidly recrystallized after melting, which allowed to identify characteristic features of ordered and less ordered regions. In addition, on the basis of temperature-dependent absorbance and PL measurements, we followed *in situ* melting and recrystallization processes, i.e., transitions between ordered and disordered phases. A multipeak analysis of absorption and PL spectra based on a modified Franck–Condon progression showed changes in for example the relative intensities of each peak, the excitonic bandwidth, and the vibronic energy as a function of temperature. Most importantly, at the phase transition temperature, a clear change in the positions of the peaks (i.e., their wavelengths, corresponding to the energy of the emitted photons) was detected. In particular, the relative absorption and PL intensities depended sensitively on the extent of order within PDOPT samples. Furthermore, on the basis of a comparison with calorimetric measurements, we have confirmed correlations between changes in the relative absorbance and PL intensities with variations in order/disorder occurring during melting and recrystallization.



INTRODUCTION

In order to understand optoelectronic properties of conjugated polymer systems and to establish ways for enhancing their performance in optoelectronic applications, previous studies have measured absorption and emission spectra as a function of packing and order in thin films.^{1–7} To a large extent, optical properties of conjugated systems are determined by intra- and interchain interactions,^{8,9} which also strongly influence energy and charge transfer. A conjugated polymer chain can be viewed as a system of many coupled chromophores. Although the contour length of a polymer chain may be more than 100 nm, the presence of disorder of different kinds leads to localization of the exciton wave function on a smaller sequence of the polymer chain, to the ultimate extent that each individual chromophore along a polymer chain may act as an (independent) emitter. For instance, in a solution of poly(phenylenevinylene) (PPV), excitons are localized on segments with a size range of 5–10 monomer units, corresponding to a typical length of ca. 3–6 nm.¹⁰ Hence, because of variations in

the degree of delocalization of the exciton along the chain, emission from a long polymer chain will generally have a broad spectrum resulting from a superposition of individual spectral lines.¹⁰ Depending on the extent of delocalization, emission ranges from rather short (blue) to long (red) wavelengths. In addition, the wavelength of emitted photons detected in a photoluminescence (PL) experiment is influenced by the nature of the morphology, solvent, concentration, and temperature.^{11–14} In particular, the formation of highly ordered structures is meant to planarize the chains and to reduce the number of defects, e.g., due to twisting of the backbone, and hence to increase the conjugation length.^{15,16} In addition, crystallization may cause a change of intermolecular distances and thus may affect the electronic and vibrational coupling of chromophores. Hence, crystallization may give rise to changes

Received: May 29, 2017

Revised: July 3, 2017

Published: August 16, 2017

in the energy levels and energy transfer processes and thus in the optical properties of the conjugated polymer.

Having said that, large intermolecular spacing and correspondingly weaker intermolecular interactions may also have a significant influence on molecular ordering. Bulky side chains attached to conjugated polymers may separate the polymer backbones from each other, and this can lead to changes of the final optoelectronic properties of these materials. Except for a few recent reports,^{6,14,17–20} a clear understanding of the relationship between ordering of molecules with bulky side chains, the resulting morphology, and optoelectronic properties of conjugated systems having a large interchain separation distance (>1 nm), and thus no π – π interactions, has yet to emerge. Recently, large spherulites of poly(3-(2,5-dioctylphenyl)thiophene) (PDOPT) were reported.^{1,19} According to previous studies, the bulky dioctylphenyl side groups separate the thiophene backbones of PDOPT by ca. 1.47 nm.^{1,6,17,19} Hence, π – π interactions do not play an important role in PDOPT.^{1,12,14} Moreover, the weakened interchain interactions in PDOPT lead to a much lower melting temperature as compared to poly(3-hexylthiophene) (P3HT)¹⁶ and most other polythiophenes.¹⁶ Large interchain separation can also strongly affect the photoluminescence quantum efficiency (PLQE), i.e., the ratio of the number of emitted photons to the number of absorbed photons, of conjugated systems.^{6,17,21,22} Polythiophenes for which the electronic energy gap is increased by steric hindrance show low PLQE, in both film and solution. This low PLQE originates from a nonradiative decay of excited states.^{17,22}

Morphology-induced thermochromism is a frequently encountered phenomenon in conjugated polymers. It was first observed when studying the fluorescence from polydiacetylene in solution.¹¹ In polydiacetylene, depending on temperature, the relative emission intensity was high either from a high-energy state (blue phase) or from a lower-energy state (red phase). Temperature-dependent PLQE of poly(9,9-dioctylfluorene) (PFO) films with different morphologies showed that PLQE depended on morphology.²

In most theoretical treatments of the electronic properties of polymer aggregates, it is assumed that every noninteracting chromophore can be represented by individual, well-defined ($S_0 \rightarrow S_1$) electronic transitions.²³ Vibronic progression peaks, observed in both absorption and PL spectra, accompany these electronic transitions. These vibronic progression peaks result from coupling to vibronic wave functions of the ground state and excited states. Often, the most intense peak is represented by the transition which takes place between the lowest energy level in the excited state and the zero vibronic level in the ground state for both emission and absorption (the so-called 0–0 transition).

If crystallites of conjugated polymers are formed, and thus interchain interactions (between chromophores) are considered, electronic excitations become delocalized over several chromophores; i.e., exciton manifolds form. As a consequence, both the absorption and emission spectra shift and the vibronic progression become distorted with respect to that of the spectra of the noninteracting chromophores.^{24–27} In the resulting emission spectra, the change of the 0–0/0–1 ratio characterizes the degree of order in the crystallites. In the absorption spectra, the corresponding peak ratio is a measure for the strength of the interchain interactions. Hence, the energy distribution in the excited state is a fundamental property of an ensemble of chromophores constituting an organic semi-

conductor, which is controlled by interactions between chromophores. Manifestations of the latter are changes in the optical spectra as well as modified charge and energy transfer rates that are of paramount importance to the operation of optoelectronic devices.²⁸

In this study, we performed temperature-dependent optical spectroscopy on as-cast thin films and spherulitic crystals of PDOPT in order to understand, in particular, the relationship between emission probability and changes in morphology from ordered crystalline regions to disordered molten chains. Specifically, we focused on properties of highly ordered polymer chains resulting from crystallization and the changes induced by melting. Crystallization of PDOPT is expected to planarize the backbone, thereby increasing the effective conjugation length. In our system, we observed distinct differences in optical spectra obtained from slowly formed spherulitic crystals and the same molecules after melting. In addition, we correlated PL spectra with calorimetric data in order to establish a relation between thermal and optical properties.

EXPERIMENTAL DETAILS

Materials and Preparation. Poly(3-(2,5-dioctyl phenyl)thiophene) (PDOPT) (Figure 1) was synthesized through Kumada

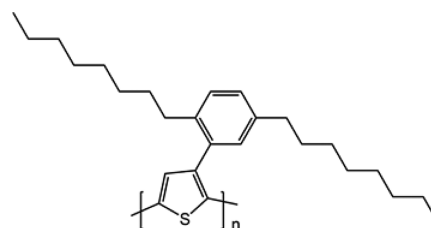


Figure 1. Schematic representation of the chemical structure of poly(3-(2,5-dioctylphenyl)thiophene) (PDOPT).

catalyst transfer polycondensation.¹ The weight-average molecular weight (M_w) of the PDOPT sample used was 28 kg/mol with a dispersity $D = 1.86$. All studied samples were prepared from a 3.3 mg/mL PDOPT solution in toluene. To ensure complete dissolution, the vial was placed in an oil thermostat at an elevated temperature of 60 °C for 10 h. A thin film of thickness 200 nm was made by casting approximately 10 μ L of this hot solution of PDOPT on 1 cm² glass or silicon substrates, which earlier were carefully cleaned in an ultrasonic bath at 45 °C for 15 min using acetone, followed by a 30 min treatment in a UV-ozone chamber.

Isothermal Crystallization of Pristine PDOPT Films. Large spherulitic crystals were grown via isothermal crystallization from molten films. First, to erase memory effects, films were brought to a temperature well above the nominal melting temperature T_m of PDOPT ($T_m \approx 115$ °C), i.e., to 150 °C for ca. 2 min.¹ Sample temperature was controlled to a precision of ca. 0.1 °C by a hot stage purged with nitrogen (Linkam Scientific Instruments, UK). Then, the sample was cooled to selected crystallization temperatures T_c (e.g., to $T_c = 100$ °C) at a rate of 10 °C/min and isothermally crystallized for up to 50 h. Highly birefringent large spherulitic crystals (Figure 2a) were formed. The size of the spherulites varied from 10 μ m to more than 250 μ m in diameter, depending on when nucleation occurred during the crystallization process (see Figure S1a).

Optical Microscopy and Spectroscopy. To characterize the morphology of the spherulitic crystals formed, optical micrographs were taken using a Zeiss Axio 100 microscope. In order to gain insight into the origin of the optical properties, spatially resolved (with a diameter of 10 μ m for the detected area) absorption and PL spectra were recorded on different regions in as-cast films and spherulitic

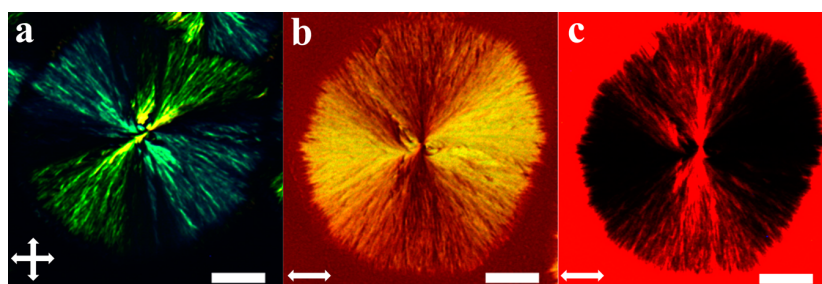


Figure 2. Optical micrographs (a) under crossed polarizers (indicated by the white arrows) showing strong birefringence and (b) of absorption and (c) of emission upon excitation with polarized light (polarization direction is indicated by the horizontal white arrows) for a spherulitic crystal grown at 100 °C for 50 h in a molten thin film (ca. 200 nm) of PDOPT. All micrographs were taken after the sample was quenched to room temperature; i.e., the surrounding molten film was rapidly crystallized. The scale bar indicates a length of 50 μm .

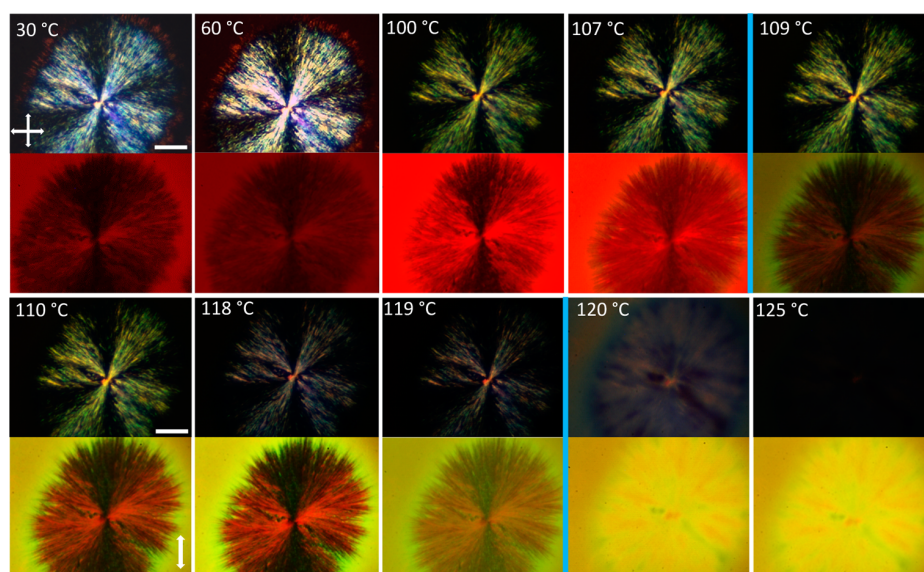


Figure 3. First and third rows show the birefringence from a spherulitic crystal during heating from 30 to 125 °C. The second and fourth rows show the corresponding PL images, when the spherulite was excited by light polarized in the direction indicated by the white arrows. The crystal was grown at 100 °C for 50 h. The scale bar indicates a length of 20 μm .

crystals, enabling the identification of contributions from different regions of order and different morphologies to optical spectra. Absorption measurements with a USB 2000 Ocean Optics spectrometer and Ocean Optics optical fibers were performed in combination with the Zeiss Axio 100 microscope, allowing for such localized measurements. *In situ* photoluminescence spectra were taken as a function of temperature in order to gain insight into how a change from an ordered crystalline phase (spherulitic crystal) to a disordered molten phase is reflected in optical properties. As light source for PL measurements, we used an Ocean Optics TS-LED light source combined with a filter set having a band-pass for the incident light ranging from 450–500 nm, a long pass starting at 500 nm for the emitted light, and a beam splitter with 99% transmission above 500 nm (all filters were purchased from AHF analysentechnik AG, Tübingen, Germany). In this study, while absorption spectra were collected in transmission mode, PL spectra were collected in reflection mode using an optical fiber of diameter 200 μm and a 20 \times objective of the Zeiss Axio 100 microscope (see also Figure S7).

RESULTS AND DISCUSSION

Morphology of PDOPT Crystals. When observed under crossed polarizers at room temperature, the spherulitic crystals showed the characteristic Maltese cross,²⁹ indicating a pattern of radially oriented crystalline lamellae (Figure 2a). The high

molecular order within the lamellae resulted in strong birefringence. The edges of the spherulitic crystals were not sharp but rather diffuse, indicating that lamellae grew in parallel but with some lag time. The absorption image (Figure 2b) clearly showed that only lamellae in the direction orthogonal to the polarization direction of the incoming light were strongly absorbing. Accordingly, emission was only observed in regions where absorption was occurring (Figure 2c). Interestingly, emission from the spherulitic crystal was less than from the surrounding quenched and thus rapidly crystallized film.

Melting: A Phase Transition from Order to Disorder. *Optical Microscopy.* PDOPT spherulites exhibited a clear anisotropy (see Figure 2), demonstrating that the transition dipole moment of PDOPT (along the chain, i.e., *c*-axis) in spherulitic crystals was perpendicular to the radius. Optical micrographs with crossed polarizers (i.e., birefringence images) taken during the heating process (Figure 3) also showed this anisotropy. However, the birefringence intensity from the spherulitic crystals decreased with increasing temperature and disappeared upon melting of the spherulitic crystal. The corresponding PL images in Figure 3 from the central spherulite showed an analogous behavior. Interestingly, at 30 °C, PL emission was more intense in the film surrounding the

spherulitic crystal. However, the relative intensity of emission from the spherulitic crystal increased with increasing temperature until it matched the intensity of the surrounding film at around 125 °C, when the spherulite was molten completely. This temperature-dependent change of optical properties, i.e., the thermochromic behavior observed in PL, can be directly mapped to melting of the spherulite, i.e., a change in morphology. Interestingly, fully consistent with the well-known Hoffman–Weeks relation of polymer crystals, i.e., the dependence of melting temperature of a polymer crystal on its crystallization temperature,³⁰ the film surrounding the spherulite (which crystallized upon quenching the sample to room temperature) showed the thermochromic change in the PL spectrum reflecting the melting process at a ca. 11° lower temperature.

Temperature-Dependent Absorption Spectra. To gain further insight into the influence of molecular conformation and order on the photophysical properties of PDOPT spherulites, we studied *in situ* changes in absorption spectra while heating the PDOPT spherulites from 30 to 150 °C and subsequently cooling of the melt back to 30 °C, both at a rate of 2 °C/min. The corresponding absorption spectra measured with 10 μm spatial resolution at the position of a spherulite are shown in Figure 4a for the heating process and in Figure 4c for the cooling process from the melt.

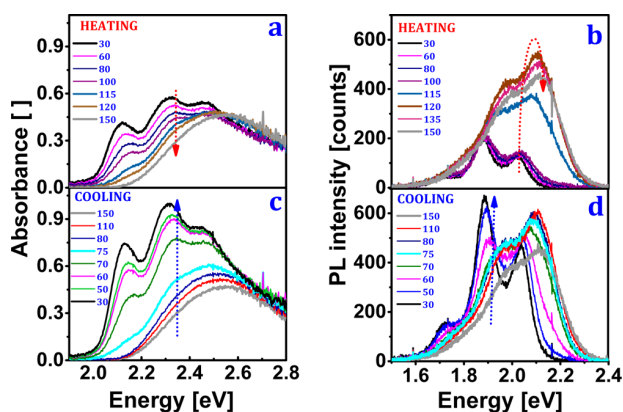


Figure 4. Optical absorption and PL spectra of a spherulitic crystal showing (a, c) absorbance and (b, d) emitted photons during (a, b) heating and (c, d) cooling at a rate of 2 °C/min. The numbers in blue represent temperature in °C (for curves measured at additional temperatures, see Figures S8 and S9). Note that during these measurements the number of molecules interacting with light was always constant.

The absorption spectrum of the spherulite at 30 °C (Figure 4a, black) showed three distinct peaks between 2.12 and 2.5 eV and a broad shoulder at higher energies around 2.6 eV. Upon heating the sample, the intensity of the lower-energy peaks dropped and peak positions shifted to higher energies. Above the nominal melting temperature of around 120 °C (see also Figure 3), only the higher-energy contribution survived. In the subsequent cooling process, absorption at higher energy prevailed down to about 75 °C. Below 75 °C, structured absorption features started to dominate once more at lower energies. The spectrum of the sample cooled back to 30 °C looked qualitatively very similar to the initial 30 °C spectrum before heating, but with significantly higher absorbance.

It should be noted that the spherulites were grown by slow isothermal crystallization of PDOPT and grew in the radial direction. The PDOPT chains arranged in a well-ordered fashion into radially growing lamellar crystals, with the polymer backbones being oriented perpendicular to the growth direction,^{6,19} giving rise to clearly observed anisotropy under crossed polarizers (see Figures 2 and 3). The space in between these lamellar crystals contained disordered chain segments (or chain ends).³¹ Both the shape of the 30 °C absorption spectrum of the PDOPT spherulite and the sample morphology (crystalline lamellae intertwined with disordered regions) were similar to that found for semicrystalline films of the prototypical poly(3-hexylthiophene).^{32–34} Hence, we attribute the 30 °C spectrum from a PDOPT spherulite to a superposition of absorption from a lower-energy (2.12–2.5 eV) crystalline phase with reasonable interchain interactions that features a distorted vibronic progression with a peak spacing of about 170 meV and a broad unstructured absorption from a disordered phase, dominating at higher energies around 2.6 eV. Upon heating, the spherulitic structure of PDOPT disappeared above ca. 120 °C. At higher temperatures, exclusively the spectrum from the disordered melt prevailed, which closely resembled that of a dilute solution (see later, Figure 9), suggesting a loss of significant interaction between PDOPT chains. After rapid cooling from the melt, PDOPT recrystallized at around 75 °C, as evidenced by the reappearance of the corresponding peaks at lower energies in the absorption spectrum. Yet, formation of macroscopic spherulites did not occur, as demonstrated under polarized illumination (see Figure S1c), where no significant anisotropy in PL was observed. Hence, a semicrystalline film was formed containing randomly oriented nanometer-sized crystallites embedded in a matrix of disordered polymers.

The similarity between PDOPT and P3HT with respect to the spectral shape and position of the crystalline absorption (relative to that of the disordered contribution) suggested that PDOPT crystallites form H-type aggregates both in isothermally grown spherulites and in semicrystalline films after rapid cooling from the melt. At first glance, this observation might be surprising as in contrast to P3HT, there is no π – π stacking in PDOPT, suggesting that crystallization was driven by side-chain interactions.^{6,19} The crystal structure of PDOPT features a distance of 1.47 nm between backbones in π – π stacking direction, while the smallest backbone–backbone distance is about 0.55 nm, measured perpendicular to the stacking direction of backbone planes.^{6,19} However, it is important to realize that the appearance of H-type spectra does not require π – π stacking. The transition dipole moments that are oriented along the PDOPT backbone only have to be arranged in a parallel fashion with respect to each other to give rise to a positive interchain interaction characteristic of H-type structures.³⁵ For PDOPT, the interchain coupling is therefore almost exclusively determined by the smallest backbone–backbone distance perpendicular to the π – π stacking direction. Hence, using the framework for H-type spectra put forward by Spano and co-workers,^{36,37} an analysis of the contribution to the absorption resulting exclusively from crystalline regions was possible (see also Figure S4).

Such quantitative analysis of the absorption spectra required a “deconvolution” of the contributions from disordered and crystalline regions. In short, we assumed that absorption at 125 °C (or at higher temperatures T) stemmed solely from disordered chains in the melt. Scaling this contribution to the

absorption spectrum to the high-energy tails of the spectra measured for $T < 120$ °C (for a heating run) and $T < 70$ °C (for a cooling run), and subtracting this so-adjusted contribution, allowed us to extract the part of the absorption spectrum resulting from the crystalline regions, as illustrated in Figure 5.^{32–34}

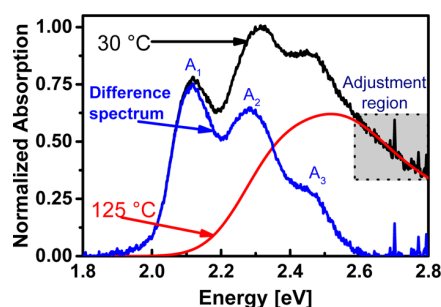


Figure 5. Extraction of the contribution to the measured spectrum (black) resulting from the aggregated phase of PDOPT at 30 °C. The spectrum of the disordered, molten film at 125 °C (red) was scaled to the high-energy tail of the 30 °C spectrum (black). The difference curve (blue) is taken for further fitting.

To comply with Spano's notation, the peaks of this latter spectrum were labeled A_i ($i = 1, 2, 3, \dots$) in order of increasing energy. The crystalline absorption was then fitted by a modified Franck–Condon (FC) progression (see eq 1) put forward by Spano and co-workers.^{36,37}

$$\begin{aligned} \frac{A(E)}{nE} &\sim \left(1 - \frac{We^{-S}}{2E_d} \left(\sum_{n \neq m} \frac{S^n}{n!(n-m)} \right) \right)^2 \\ &\times \exp \left(-\frac{(E - E_{A_1})^2}{2\sigma_{A_1}^2} \right) \\ &+ \sum_{m=1} \frac{S^m}{m!} \left(1 - \frac{We^{-S}}{2E_d} \left(\sum_{n \neq m} \frac{S^n}{n!(n-m)} \right) \right)^2 \\ &\times \exp \left(-\frac{(E - E_{A_1} - mE_d)^2}{2\sigma^2} \right) \end{aligned} \quad (1)$$

Here, $A(E)$ is the intensity of absorption, S is the Huang–Rhys parameter of disordered chains ($S = 0.7$), and the vibrational energy $E_d = 167$ meV (1350 cm^{-1}) of the effective carbon-stretching mode was extracted from solution spectra with a standard FC progression (see Figure S3). The remaining free parameters are the vibrational quantum number m , the free exciton bandwidth W (related to the interchain electronic coupling J by $W = 4J$), the transition energy E_{A_1} of the lowest-energy peak A_1 , and the width σ_{A_1} of the Gaussian line shape functions. Note that we used a modified version of the fitting function proposed by Spano et al. in order to allow for a different (narrower) Gaussian line width σ_{A_1} of the absorption peak A_1 compared to the line width σ of the absorption peaks A_i ($i > 1$). As shown in detail in Figure S4, this modification significantly enhanced the quality of the fits. This modified Franck–Condon progression was fitted to all deconvoluted crystalline absorption spectra, for both heating and cooling runs. The resulting temperature-dependent evolution of the

relevant fitted parameters is displayed in Figure 6a–c, i.e., the free exciton bandwidth W , the center energy E_{A_1} and width σ_{A_1} of the A_1 peak versus temperature (red symbols: heating; blue symbols: subsequent cooling).

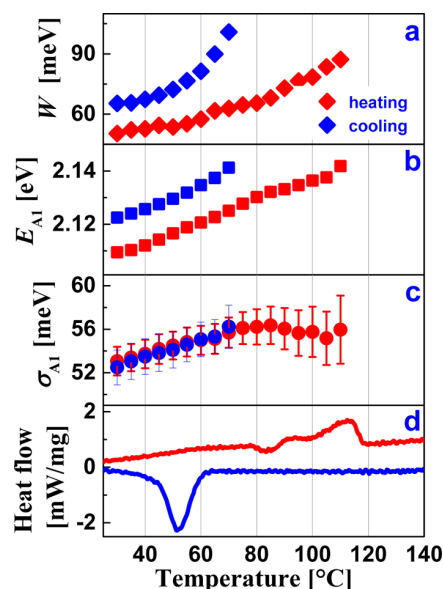


Figure 6. Results of the fits to the temperature-dependent contribution of crystalline domains to the absorption spectra: (a) Free exciton bandwidth W , (b) energy E_{A_1} and (c) line width σ_{A_1} of the A_1 peak, evaluated for 30–120 °C for heating (red symbols) and for 30–70 °C for cooling (blue symbols). (d) Heat flow curve for heating and cooling spherulitic crystals at a rate of 2 °C/min, prepared in an aluminum cap by crystallizing the molten polymers at $T_c = 100$ °C for 50 h (see Figure S6). The red and the blue curves represent heating and cooling, respectively.

During the process of heating PDOPT spherulites, the free exciton bandwidth W , the A_1 peak position E_{A_1} , and its line width σ_{A_1} increased rather steadily from 50 to 87 meV (W), from 2.109 to 2.142 eV (E_{A_1}), and from 53 to 56 meV (σ_{A_1}), respectively. These changes in absorption from the crystalline regions clearly indicated an increasing degree of structural and electronic disorder up to the melting temperature (reached at ca. 120 °C, for the spherulite).⁶ It has been shown that the backbones of PDOPT chains in crystallites are fully planar at room temperature.⁶ Increasing temperature activates torsional degrees of freedom of the backbone, and thus deviations from planarity become more and more evident. For an isolated and disordered chain, this effect gives rise to a localization of the wave function of intrachain electronic excitations. In an H-type crystalline arrangement, this temperature-activated localization results in a stronger interchain electronic interaction and thus in a larger free exciton bandwidth (W).^{38,39} Upon heating, thermal expansion of the crystalline lamellae in the spherulite gives rise to an increasing interchain distance and thus a decreasing W . In a previous work, upon heating the interchain distance was found to increase by $\approx 3\%$.¹⁷ Hence, this effect can be neglected. Importantly, our value for the free exciton bandwidth W of around 50 meV at 30 °C is substantially smaller than the value found for crystalline P3HT at room temperature, which is up to 120 meV, depending on processing

conditions.^{4,33,37} This substantially larger value of W for P3HT is related to the smaller backbone–backbone distance as compared to PDOPT (0.38 nm for π – π stacked P3HT and 0.55 nm for PDOPT).

The blue-shift in the A_1 peak position E_{A_1} was partly caused by the increase in W from 50 to 87 meV (from 30 to 110 °C) because the upper (absorbing) exciton state in the lowest energy exciton band shifts to higher energy with larger W . However, this effect was not large enough to account for the observed peak shift of 32 meV (from 2.109 to 2.141 eV) because the width of the lowest exciton band is given by $W \cdot e^{-S}$,²⁶ with the Huang–Rhys factor $S = 0.7$ for an isolated, disordered chain. A further contribution to the blue-shift of E_{A_1} arises from the increasing localization of intrachain wave functions due to increasing structural disorder, as discussed above. Moreover, upon heating the sublattice of the dioctyl-phenylene side groups will eventually melt as well and thus lose its perfect order. As a consequence, the local dielectric environment for the polymer backbones changes. The resulting different local polarization energy may contribute to the shift of E_{A_1} to higher energies (similar to a recent observation for P3HT³⁴).

In addition to this increasing intrachain (and thus intracrystallite) disorder that modified W and E_{A_1} as a function of temperature, the line width σ_{A_1} of the A_1 peak increased continuously up to 70–80 °C and then reached a plateau. This inhomogeneous width σ_{A_1} is determined by disorder between different crystallites probed in our measurement, implying that intercrystallite disorder did not change anymore above ca. 80 °C (despite high spatial resolution of 10 μm , we still probe many crystalline lamellae within the detected area inside the spherulite).

The temperature-dependent absorption spectra upon heating suggested that the melting of a spherulite—or more precisely of the crystalline lamellae arranged within the spherulite—is a rather continuous process over a wide temperature range, in which the structural and thus electronic order is being continuously reduced until it is lost completely at the melting temperature of ca. 120 °C.

Upon cooling from the melt, signs of absorption from crystalline regions reappeared at around 75 °C. However, no (macroscopic) spherulites but many randomly arranged small crystallites were formed. Below 75 °C, both W and E_{A_1} were consistently higher with respect to the corresponding values at the same temperatures upon heating the spherulite. This difference suggests that the crystallites formed upon cooling from the melt did not possess the same degree of structural perfection as the crystalline lamellae in the initial spherulite, slowly grown at 100 °C for 50 h. Caused by the rather fast cooling process, chains did not have enough time to re-form the better ordered macroscopic spherulitic structure. In fact, the higher energy E_{A_1} after cooling is consistent with the recent observation of a more blue-shifted absorption of as-cast semicrystalline (rapidly quenched) PDOPT films as compared to the spherulite absorption,¹⁹ which further supports our interpretation of the formation of less perfectly crystalline films upon rapid cooling and recrystallization. The inhomogeneous line width σ_{A_1} is identical before and after melting, implying that disordered segments between lamellar crystals in a spherulite

are not differing much from disordered segments between lamellar crystals in rapidly crystallized films.

It is now interesting to compare the changes in these spectra with the corresponding variations in thermal properties as determined by differential scanning calorimetry (DSC) (Figure 6d). Upon heating (red curve), a cold crystallization peak appeared around 80 °C. This peak indicates that even after 50 h at $T_c = 100$ °C not all parts of the sample were completely crystallized (see also Figures 2 and 3, where the spherulites are surrounded by regions which only crystallized upon quenching the sample to room temperature). Alternatively, some reorganization of molecules, which may not have been aligned appropriately in the spherulite structure, may have occurred. Such reorganization is consistent with the observed plateau in the σ_{A_1} line width (i.e., the constant intercrystallite disorder) above 70 °C. At around 115 °C, DSC indicated the melting of the spherulites. The melting peak from DSC agreed with the disappearance of the crystalline absorption; i.e., any long-range order and thus electronic interchain interactions were lost upon melting. Upon cooling, the DSC curve (Figure 6d, blue line) showed the recrystallization peak at around 50 °C. This low temperature may appear to be in conflict with the higher recrystallization temperature of ≈ 70 °C observed in the absorption spectra (appearance of a low-energy peak at around 2.14 eV). Tentatively, this difference may be attributed to a higher (re)nucleation probability in the region of molten spherulites, as randomization of chain conformations requires time and some polymers may “remember” their ordered states for times longer than the characteristic relaxation time.^{40,41} Correlations between thermal and optical properties in crystalline regions are probably related to the rather long-range nature of electronic interchain interactions between thiophene backbones, as demonstrated recently,^{38,42} that have a strong impact on the shape and position of optical spectra. Hence, spatially resolved optical spectroscopy can be used to study melting and recrystallization of polythiophenes.

Temperature-Dependent Photoluminescence Spectra. To gain further insight into the influence of molecular conformation and order, we additionally studied *in situ* changes in emission spectra when increasing or decreasing temperature at a rate of 2 °C/min, focusing in particular on the processes of melting of spherulites grown via isothermal crystallization at 100 °C (Figures 2 and 3) and their subsequent recrystallization. The emission spectra from a PDOPT spherulite measured with nonpolarized light in reflection mode with a spatial resolution of 10 μm are shown in Figures 4b and 4d. During heating and cooling, a spectrum was recorded after typically a temperature change of 5 °C. At room temperature, the emission spectra allowed to identify clearly three peaks,^{4,34} with a suppressed 0–0 emission peak which is characteristic for PL of H-type crystallites that could be associated with a distorted single Franck–Condon progression.⁴³ With temperature increasing up to 120 °C, we observed a significant increase of the overall intensity, followed by a (small) decrease in intensity and the emergence of new peaks in higher energy regions at higher temperatures. These high-temperature spectra closely resemble PL from solution (see later, Figure 9) with its dominating 0–0 emission, in agreement with the loss of order in the melt. Furthermore, from Figures 4b and 4d, we can observe a significant broadening of the PL peaks at elevated temperatures.

Melting of the spherulitic crystal led to a significant increase of emission intensity of the PDOPT structures (Figure 4b).

Above 120 °C, there is increased PLQE due to increasing disorder (decreasing H-type character). It should be noted that disorder breaks the symmetry of (weakly) interacting molecules, allowing for 0–0 emission.²⁵ For ideal H-aggregates at 0 K, 0–0 emission is forbidden by symmetry rules of emission.^{25–27,44} Increasing disorder (e.g., by increasing temperature) allows for 0–0 emission and thus gives rise to an overall increase in PL intensity. The spectra of Figure 4b showed that for increasing temperature the emission intensity increased, with a bias toward higher energies, a signature which we tentatively attribute to increasing disorder,^{14,18,45,46} in agreement with the absorption data presented above.

In order to determine more quantitatively the corresponding changes in the PL spectra with temperature and to identify the origin of the PL peaks, in an approach fully consistent with the discussion on absorption data, we used the framework of analysis developed by Spano and co-workers.⁴ In the deconvolution of absorption spectra, it was argued that analysis of the contributions from crystalline regions (aggregates) in PDOPT was only possible using the H-aggregate type spectra. For the analysis of the emission spectra, we therefore also adopted the H-type model. The peaks of the emission spectra were labeled from highest energy to the lowest energy as L_i ($i = 1, 2, \dots$). Each emission spectrum was therefore fitted with the modified Franck–Condon progression (see eq 2) as suggested by Spano and co-workers.⁴

$$L(\omega) \sim (\hbar\omega)^3 n_f^3 e^{-S} \left\{ \alpha \Gamma(\hbar\omega - E_{L_1}) + \sum_{m=0}^{\infty} \frac{S^m}{m!} \Gamma(\hbar\omega - (E_{L_1} - mE_d)) \right\} \quad (2)$$

where n_f is the real part of the refractive index, $\hbar\omega$ is the photon energy, $L(\omega)$ is the intensity of emission, m denotes the vibrational quantum number, S is the Huang–Rhys factor for the dominant carbon bond stretch mode of disordered chains ($S = 0.70$), E_{L_1} is the 0–0 transition energy, $E_d (= E_{L_1} - E_{L_2})$ is the C=C symmetric stretching vibration coupling of electronic transition (ca. 0.16 eV), Γ is the line shape function (Gaussian with constant width), and α gives the “suppression” factor for the 0–0 emission peak. Note that for simplicity we used eq 2 also to fit the high-temperature PL spectra above 120 °C, although there was no emission from H-type crystallites anymore. In this situation α approaches 1, yielding a nearly undistorted vibronic progression as expected for the emission of a disordered ensemble.

Based on eq 2, the modified Franck–Condon progression was fitted to all PL spectra for both heating and subsequent cooling (see Figure S5). Figures 7a–d represent the resulting temperature-dependent evolution of some of the fitted parameters, i.e., the peak position E_{L_1} and the width σ_{L_1} of the L_1 peak, the variation of the vibronic energy E_d (C–C stretching mode), and amplitude I_{L_1} of the L_1 peak during the heating and cooling cycle.

A closer look at the evolution of these parameters with temperature (E_{L_1} , σ_{L_1} , E_d and amplitude of I_{L_1}) showed a steady increase from 2.024 to 2.117 eV (E_{L_1}), from 47 to 83 meV (σ_{L_1}), from 0.154 to 0.1705 eV (E_d), and from 0.314 to 0.66 (I_{L_1}), as temperature increased from 30 to 150 °C (Figure 7a–

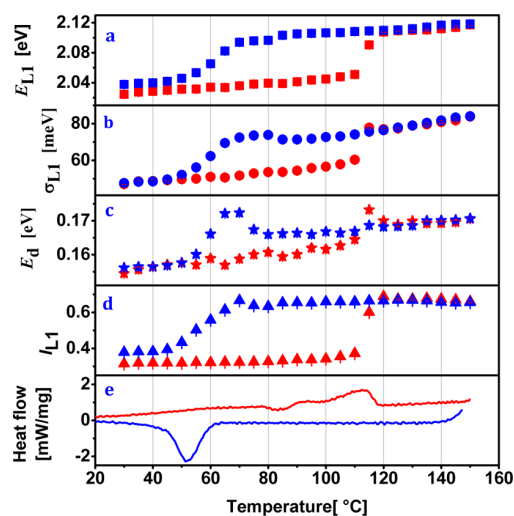


Figure 7. Results of the fits to the temperature-dependent PL spectra. (a) Peak position E_{L_1} and (b) line width σ_{L_1} of the L_1 peak, (c) vibronic energy E_d , (d) relative amplitude I_{L_1} of the L_1 peak for the heating (red symbols) and cooling (blue symbols) cycle, respectively, and (e) heat flow curve for heating (red) and cooling (blue) spherulitic crystal (see also Figure 6d and Figure S6).

d). Figure 7d revealed a steady increase of the intensity I_{L_1} up to around the nominal melting temperature of PDOPT. This could be attributed to an increasing degree of thermally induced structural disorder, in line with the absorption data.⁴⁷ The peak position E_{L_1} (Figure 7a) increased steadily and changed only by 20 meV up to ca. 110 °C, where a steep increase was observed, shifting the peak by ca. +70 meV, which reflects the transition from crystalline H-type to amorphous (solution-like) PL spectra. Likewise, during the cooling process (Figure 7a), a reverse transition could be observed at ca. 70 °C, where the peak positions also changed by ca. –70 meV. It should be noted that the observed transitions at ca. 110 °C and ca. 70 °C were at temperatures close to the nominal melting and crystallization temperatures, in agreement with absorption data (Figure 6). The variations in vibronic energy E_d during heating and cooling cycles could be associated with the varying degree of order of the emitting crystalline lamellae.^{48,49} The relative increase in emission intensity of the 0–0 peak L_1 with temperature is a typical characteristic of disorder in H-aggregates systems.²⁵ The line width σ_{L_1} (Figure 7b) increased steadily with temperature increasing from 30 to 150 °C and followed a reverse trend during the cooling cycle. The increasing (decreasing) line width σ_{L_1} during heating (cooling) is a signature of increasing (decreasing) disorder. Interestingly, at room temperature, both before the heating and after the cooling cycle, E_d and σ_{L_1} were quite similar, indicating that the degree of disorder of the emitting crystallites is very similar in both situations, as explained above.

A comparison of peak positions and maximum intensity of all the peaks L_1 , L_2 , L_3 , and L_4 showed that at temperatures below the melting transition all peaks hardly changed their position (only a rather small increase by about 20 meV could be observed). However, at temperatures above ca. 120 °C, there was a clear change in position by over +70 meV (Figure 8a,b). This confirms that the energy of a peak is a function of

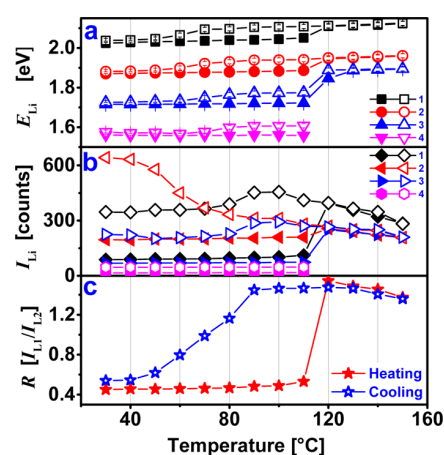


Figure 8. Results of the fits to the temperature-dependent PL spectra. (a) Peak positions (E_{L_i}), (b) maximum intensities of peaks (I_{L_i}), and (c) peak intensity ratio $R = I_{L_1}/I_{L_2}$ for the heating (full symbols) and cooling (open symbols) cycle.

temperature. The maximum peak intensity of L_2 dropped relative to L_1 , with the peak intensity ratio $R = I_{L_1}/I_{L_2}$ changing from $R < 1$ for temperatures less than ca. 110 °C to $R > 1$ for temperatures above ca. 120 °C during the heating cycle (Figure 8b,c).

Comparing Optical Properties of PDOPT As-Cast Thin Films and Spherulitic Crystals. Figure 9 compares spatially

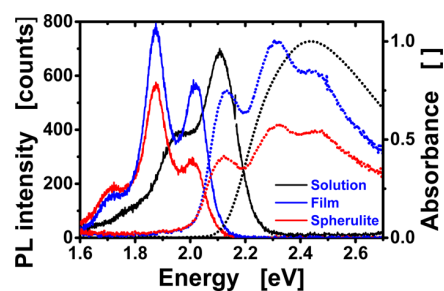


Figure 9. Absorbance (dotted curves) and photoluminescence spectra (solid curves) of PDOPT from solution (black), an as-cast film (blue), and a spherulitic crystal (red) grown at 100 °C for 50 h in a molten thin film (ca. 200 nm), taken at room temperature at an area of a diameter of 10 μm and an integration time of 5 s, measured with nonpolarized light. For comparison, we also added results for a dilute PDOPT solution in toluene.

resolved (detecting a small circular area having a diameter of 10 μm) absorption and PL spectra, collected at room temperature from an as-cast film and from a region within a spherulite. We observed qualitatively similar spectra for both samples, characterized by broad peaks and a small red-shift of ca. 0.02 eV in absorbance spectra for the spherulite with respect to the as-cast film. Interestingly, this shift was similar to that between the spectra acquired from a spherulite before heating and from the same area taken in the semicrystalline film obtained after cooling the molten spherulite down to 30 °C (see Figure 6b). Hence, the small shift in absorption spectra indicated that the crystalline structures formed in as-cast films did not possess the high structural order observed for the crystalline lamellae grown during slow isothermal crystallization in spherulites, as discussed above. Yet, the structured low-energy contribution

to the absorbance spectra still indicates the formation of excitons delocalized over several chromophores in the crystalline regions of the as-cast film. From the same data, it was observed that the spherulite had lower absorption and emission relative to the film. This could be attributed to the interdigitation of side chains during slow crystallization of the spherulites, reducing the intermolecular distance and hence reducing the quantum yield.¹⁷ At room temperature, emission from the spherulitic crystal showed a number of vibronic peaks. It was interesting to note that at room temperature the emission intensity from the film was almost a factor of 2 higher than from the spherulitic crystal. Besides low emission from the spherulitic crystal, we observed a small red-shift (ca. 0.02 eV), just like in absorption spectra.

At room temperature, owing to thermally induced structural disorder, vibronic peaks were rather broad. In the PL spectra taken at room temperature, three clearly identifiable peaks were observed at 2.02 ± 0.02 , 1.87 ± 0.02 , and at 1.76 ± 0.02 eV for both the as-cast film and the spherulitic crystal. The solution of PDOPT in toluene also had two peaks and a big blue-shift relative to the spherulitic crystal. We attribute the first two peaks to the 0–0 (L_1) and 0–1 (L_2) transitions.³⁹ To precisely identify the vibronic peaks due to contributions from more ordered spherulitic crystal and less ordered as cast film and to quantify differences in the spectra, we used a set of four Gaussian functions for a deconvolution of the spectra (Figures 10a and 10b) without imposing any constraints on the fit

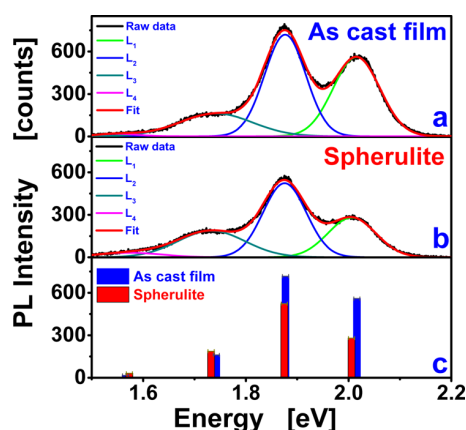


Figure 10. PL spectra measured at room temperature (same as in Figure 3), decomposed into four Gaussian functions, for (a) an as-cast film and (b) a spherulitic crystal. (c) Bar chart of the intensity of the individual Gaussians for the film and the spherulitic crystal. The energy E of the emitted photons is decreasing from peak L_1 to peak L_4 , as can be seen also in (a) and (b).

parameters. In addition to three clearly visible peaks, a fourth but very small Gaussian peak close to 1.6 eV was included in the fitting procedure to ensure that the width of the peak at ca. 1.75 eV was comparable to the width of the other peaks. From Figure 10a–c, we can find the energy gap between E_1 and E_2 to be ca. 0.145 eV, which is within a margin of error for the typically observed energy for C–C stretching modes in substituted polythiophenes (0.16 ± 0.02 eV).³⁹

In the following discussion, we rely on the sensitivity of photoluminescence spectra with respect to changes in order and morphology.^{5,14,23} By using a series of four Gaussian functions, we simulated the vibronic progressions of the 0–0,

0–1, 0–2, and 0–3 peaks. Energy gaps of most conjugated systems show a vibronic progression as a result of symmetric vinyl stretching modes.^{14,23,25,39,45} Fourier transform infrared spectroscopy results for PDOPT have shown that electronic transitions couple strongly to the aromatic carbon-bond stretching of the thiophene ring within an energy range from 0.148 to 0.20 eV and a strong peak at 0.18 eV (Figure S2). Absorption and emission spectra of virtually all phenyl- and thiophene-based conjugated molecules reveal vibronic progressions, mainly due to symmetric ring breathing stretching modes or a group of such modes.²⁷

The comparison of results (Figures 9 and 10) from such a spectral analysis of the emission spectra for as-cast films and spherulitic crystals at room temperature showed that the positions of the four peaks (in terms of their emission energy) were (almost) independent of morphology (Figure 10a–c). Interestingly, while peak positions matched, intensities clearly differed. For the highly ordered structures within spherulitic crystals, the relative emission intensities were higher in the low-energy region while for the less ordered PDOPT molecules in as-cast thin films intensities were more pronounced in the high-energy region (Figure 10c). This observation is corroborated by the fact that in crystalline regions PDOPT chains are better ordered. Crystallization of the bulky 2,5-dioctylphenyl side groups of PDOPT could assist in planarizing the polymer backbone. Local molecular order and changes in conformation also affect the exciton radiative recombination probability and thus the resulting photoluminescence intensity.² Relative changes in PL intensity of the emitting species, taken at a given wavelength, for different morphologies may differ due to changes in intermolecular and intramolecular interactions.^{14,50} Tentatively, the difference in spectral PL intensity between as-cast film and spherulitic crystal may be attributed to an improved planarized thiophene backbone induced by crystallization,⁵ i.e., due to different degrees of order and hence differences in quantum efficiency as seen in temperature-dependent experiments above.

CONCLUSIONS

We have demonstrated that crystallization and melting of poly(3-(2,5-dioctylphenyl)thiophene) (PDOPT) were accompanied by significant changes in optical properties. The change in morphology, i.e., changing from an ordered to a disordered state, induced by melting of a spherulitic crystal was accompanied by particular changes in emission and absorption spectra, reflecting a change in color and an increase of emission intensity. Furthermore, upon melting, birefringence was completely lost due to a loss of preferential orientation of the transition dipole moments within the crystalline structure. We observed that well-ordered spherulitic crystals emit less than the same polymers when rapidly recrystallized after being molten. Moreover, molten polymers showed a significantly higher emission probability although the absorbance rather decreased. Thus, characteristic changes in absorption and emission spectroscopy on samples of substituted polythiophenes allow to follow melting and recrystallization processes and to establish relations between optical properties and the corresponding changes in molecular conformations and order.

ASSOCIATED CONTENT

Supporting Information

The Supporting Information is available free of charge on the ACS Publications website at DOI: 10.1021/acs.macromol.7b01080.

Figures S1–S9 (PDF)

AUTHOR INFORMATION

Corresponding Author

*E-mail guenter.reiter@physik.uni-freiburg.de (G.R.).

ORCID

Michael Sommer: 0000-0002-2377-5998

Richard Hildner: 0000-0002-7282-3730

Günter Reiter: 0000-0003-4578-8316

Notes

The authors declare no competing financial interest.

ACKNOWLEDGMENTS

The authors are very grateful for the funding from DAAD-Kenya government partnership, Pwani University, and from the Deutsche Forschungsgemeinschaft (International Research Training group IRTG-1642 “Soft Matter Science”, Research Training Group 1640 “Photophysics of Synthetic and Biological Multichromophoric Systems”, projects SO 1213/5-1, RE 2273/10-1, and HI1508/2). R.H. is supported by the Elite Network of Bavaria (ENB) within the programme Macromolecular Sciences. The authors acknowledge the fruitful discussions with members of the IRTG. We also thank Silvia Siegenführ for performing the DSC measurements.

REFERENCES

- (1) Schiefer, D.; Wen, T.; Wang, Y.; Goursot, P.; Komber, H.; Hanselmann, R.; Braunstein, P.; Reiter, G.; Sommer, M. Nickel Catalyst with a Hybrid P, N Ligand for Kumada Catalyst Transfer Polycondensation of Sterically Hindered Thiophenes. *ACS Macro Lett.* **2014**, *3* (7), 617–621.
- (2) Ariu, M.; Lidzey, D.; Sims, M.; Cadby, A.; Lane, P. A.; Bradley, D. D. C. The Effect of Morphology on the Temperature-Dependent Photoluminescence. *J. Phys.: Condens. Matter* **2002**, *14* (42), 9975–9986.
- (3) Bjorklund, T. G.; Lim, S. H.; Bardeen, C. J. The Optical Spectroscopy of Poly(p-Phenylene Vinylene)/polyvinyl Alcohol Blends: From Aggregates to Isolated Chromophores. *Synth. Met.* **2004**, *142* (1–3), 195–200.
- (4) Clark, J.; Silva, C.; Friend, R. H.; Spano, F. C. Role of Intermolecular Coupling in the Photophysics of Disordered Organic Semiconductors: Aggregate Emission in Regioregular Polythiophene. *Phys. Rev. Lett.* **2007**, *98* (20), 206406.
- (5) Granlund, T.; Pettersson, L. A. A.; Andersson, M. R.; Inganäs, O. Luminescence Probing of Crystallization in a Polymer Film. *J. Appl. Phys.* **2000**, *87* (12), 8549–8556.
- (6) Hamidi-Sakr, A.; Schiefer, D.; Covindarassou, S.; Biniek, L.; Sommer, M.; Brinkmann, M. Highly Oriented and Crystalline Films of a Phenyl-Substituted Polythiophene Prepared by Epitaxy: Structural Model and Influence of Molecular Weight. *Macromolecules* **2016**, *49* (9), 3452–3462.
- (7) Eslamibidgoli, M. J.; Lagowski, J. B. The Effect of Side-Chain Length on the Solid-State Structure and Optoelectronic Properties of Fluorene-Alt-Benzothiadiazole Based Conjugated Polymers-A DFT Study. *J. Phys. Chem. A* **2012**, *116* (43), 10597–10606.
- (8) Schwartz, B. J.; Nguyen, T. Q.; Wu, J.; Tolbert, S. H. Interchain and Intrachain Exciton Transport in Conjugated Polymers: Ultrafast Studies of Energy Migration in Aligned MEH-PPV/mesoporous Silica Composites. *Synth. Met.* **2001**, *116* (1–3), 35–40.

- (9) Shirakawa, H.; Louis, E. J.; MacDiarmid, A. G.; Chiang, C. K.; Heeger, A. J. Synthesis of Electrically Conducting Organic Polymers: Halogen Derivatives of Polyacetylene, (CH) X. *J. Chem. Soc., Chem. Commun.* **1977**, 578–580.
- (10) Forster, M.; Thomsson, D.; Hania, P. R.; Scheblykin, I. G. Redistribution of Emitting State Population in Conjugated Polymers Probed by Single-Molecule Fluorescence Polarization Spectroscopy. *Phys. Chem. Chem. Phys.* **2007**, *9* (6), 761–766.
- (11) Rughooputh, S. D. D. V.; Bloor, D.; Phillips, D.; Jankowiak, R.; Schütz, L.; Bässler, H. Fluorescence Studies of Polydiacetylenes in 2-Methyltetrahydrofuran Vitreous Glasses at Low Temperatures. *Chem. Phys.* **1988**, *125* (2–3), 355–373.
- (12) Patel, G. N.; Chance, R. R.; Witt, J. D. A Planar–nonplanar Conformational Transition in Conjugated Polymer Solutions A Planar-Nonplanar Conformational Transition in Conjugated Polymer Solutions. *J. Chem. Phys.* **1979**, *70* (4387), 4387–4392.
- (13) Chance, R. R.; Patel, G. N.; Witt, J. D. Thermal Effects on the Optical Properties of Single Crystals and Solution-Cast Films of Urethane Substituted Polydiacetylenes Thermal-Effects on the Optical Properties of Single Crystals and Solution-Cast Films of Urethane Substituted Polydiacetylenes. *J. Chem. Phys.* **1979**, *71* (1), 206–211.
- (14) Köhler, A.; Hoffmann, S. T.; Bässler, H. An Order-Disorder Transition in the Conjugated Polymer MEH-PPV. *J. Am. Chem. Soc.* **2012**, *134* (28), 11594–11601.
- (15) Schiefer, D.; Komber, H.; Mugwanga Kezeze, F.; Kunz, S.; Hanselmann, R.; Reiter, N.; Sommer, M. Poly(3-(2,5-Dioctylphenyl)-thiophene) Synthesized by Direct Arylation Polycondensation: End Groups, Defects, and Crystallinity. *Macromolecules* **2016**, *49*, 7230–7237.
- (16) Kohn, P.; Huettner, S.; Komber, H.; Senkovskyy, V.; Tkachov, R.; Kiri, A.; Friend, R. H.; Steiner, U.; Huck, W. T. S.; Sommer, J. U.; Sommer, M. On the Role of Single Regiodefects and Polydispersity in Regioregular poly(3-Hexylthiophene): Defect Distribution, Synthesis of Defect-Free Chains, and a Simple Model for the Determination of Crystallinity. *J. Am. Chem. Soc.* **2012**, *134*, 4790–4805.
- (17) Aasmundtveit, K. E.; Samuelsen, E. J.; Mammo, W.; Svensson, M.; Andersson, M. R.; Pettersson, L. A. A.; Inganäs, O. Structural Ordering in Phenyl-Substituted Polythiophenes. *Macromolecules* **2000**, *33* (15), 5481–5489.
- (18) Li, N.; Shi, T.; Chen, J.; Han, M.; Li, X.; Zhou, B.; Duan, H.; Wang, Y. An Abnormal Melting Behavior from the in Situ Photoluminescence Spectral in Poly (3-Hexylthiophene) Thin Films Annealed at High Temperature. *Chem. Phys. Lett.* **2015**, *623*, 89–92.
- (19) Wang, Y.; Heck, B.; Schiefer, D.; Agumba, J. O.; Sommer, M.; Wen, T.; Reiter, G. Anisotropic Photophysical Properties of Highly Aligned Crystalline Structures of a Bulky Substituted Poly(thiophene). *ACS Macro Lett.* **2014**, *3* (9), 881–885.
- (20) Guha, S.; Rice, J. D.; Yau, Y. T.; Martin, C. M.; Chandrasekhar, M.; Chandrasekhar, H. R.; Guentner, R.; Scanduicci de Freitas, P.; Scherf, U. Temperature Dependent Photoluminescence of Organic Semiconductors with Varying Backbone Conformation. *Phys. Rev. B: Condens. Matter Mater. Phys.* **2003**, *67*, 8.
- (21) McQuade, D. T.; Kim, J.; Swager, T. M. Two-Dimensional Conjugated Polymer Assemblies: Interchain Spacing for Control of Photophysics [5]. *J. Am. Chem. Soc.* **2000**, *122* (14), 5885–5886.
- (22) Theander, M.; Inganäs, O.; Mammo, W.; Olinga, T.; Svensson, M.; Andersson, M. R. Photophysics of Substituted Polythiophenes. *J. Phys. Chem. B* **1999**, *103*, 7771–7780.
- (23) Yamagata, H.; Spano, F. C. Interplay between Intrachain and Interchain Interactions in Semiconducting Polymer Assemblies: The HJ-Aggregate Model. *J. Chem. Phys.* **2012**, *136* (18), 184901.
- (24) Yamagata, H.; Spano, F. C. Strong Photophysical Similarities between Conjugated Polymers and J-Aggregates. *J. Phys. Chem. Lett.* **2014**, *5* (3), 622–632.
- (25) Spano, F. C. The Spectral Signatures of Frenkel Polarons in H- and J-Aggregates. *Acc. Chem. Res.* **2010**, *43* (3), 429–439.
- (26) Spano, F. C. Modeling Disorder in Polymer Aggregates: The Optical Spectroscopy of Regioregular poly(3-Hexylthiophene) Thin Films. *J. Chem. Phys.* **2005**, *122* (23), 234701.
- (27) Spano, F. C.; Clark, J.; Silva, C.; Friend, R. H. Determining Exciton Coherence from the Photoluminescence Spectral Line Shape in poly(3-Hexylthiophene) Thin Films. *J. Chem. Phys.* **2009**, *130* (7), 074904.
- (28) Hoffmann, S. T.; Bässler, H.; Köhler, A. What Determines Inhomogeneous Broadening of Electronic Transitions in Conjugated Polymers? *J. Phys. Chem. B* **2010**, *114* (51), 17037–17048.
- (29) Shtukenberg, A. G.; Punin, Y. O.; Gunn, E.; Kahr, B. *Chem. Rev.* **2012**, *112*, 1805–1838.
- (30) Hoffman, J. D.; Lauritzen, J. I. Crystallization of Bulk Polymers With Chain Folding: Theory of Growth of Lamellar Spherulites. *J. Res. Natl. Bur. Stand., Sect. A* **1962**, *66A* (13), 13–28.
- (31) Brinkmann, M. Structure and Morphology Control in Thin Films of Regioregular poly(3-Hexylthiophene). *J. Polym. Sci., Part B: Polym. Phys.* **2011**, *49* (17), 1218–1233.
- (32) Reichenberger, M.; Baderschneider, S.; Kroh, D.; Grauf, S.; Köhler, J.; Hildner, R.; Köhler, A. Watching Paint Dry: The Impact of Diiodooctane on the Kinetics of Aggregate Formation in Thin Films of Poly(3-Hexylthiophene). *Macromolecules* **2016**, *49* (17), 6420–6430.
- (33) Scharf, C.; Lohwasser, R. H.; Sommer, M.; Asawapirom, U.; Scherf, U.; Thelakkat, M.; Neher, D.; Köhler, A. Control of Aggregate Formation in poly(3-Hexylthiophene) by Solvent, Molecular Weight, and Synthetic Method. *J. Polym. Sci., Part B: Polym. Phys.* **2012**, *50* (6), 442–453.
- (34) Panzer, F.; Sommer, M.; Bässler, H.; Thelakkat, M.; Köhler, A. Spectroscopic Signature of Two Distinct H-Aggregate Species in Poly(3-Hexylthiophene). *Macromolecules* **2015**, *48* (5), 1543–1553.
- (35) Kasha, M.; Rawls, H.; El-Bayoumi, M. The Exciton Model in Molecular Spectroscopy. *Pure Appl. Chem.* **1965**, *11* (3–4), 371–392.
- (36) Spano, F. C. Absorption in Regio-Regular poly(3-Hexyl)-thiophene Thin Films: Fermi Resonances, Interband Coupling and Disorder. *Chem. Phys.* **2006**, *325* (1), 22–35.
- (37) Clark, J.; Chang, J. F.; Spano, F. C.; Friend, R. H.; Silva, C. Determining Exciton Bandwidth and Film Microstructure in Polythiophene Films Using Linear Absorption Spectroscopy. *Appl. Phys. Lett.* **2009**, *94* (16), 163306.
- (38) Gierschner, J.; Huang, Y. S.; Van Averbeke, B.; Cornil, J.; Friend, R. H.; Beljonne, D. Excitonic versus Electronic Couplings in Molecular Assemblies: The Importance of Non-Nearest Neighbor Interactions. *J. Chem. Phys.* **2009**, *130* (4), 044105.
- (39) Spano, F. C.; Silva, C. H- and J-Aggregate Behavior in Polymeric Semiconductors. *Annu. Rev. Phys. Chem.* **2014**, *65*, 477–500.
- (40) Chandran, S.; Reiter, G. Transient Cooperative Processes in Dewetting Polymer Melts. *Phys. Rev. Lett.* **2016**, *116* (8), 88301.
- (41) Rastogi, S.; Lippits, D. R.; Peters, G. W. M.; Graf, R.; Yao, Y.; Spiess, H. W. Heterogeneity in Polymer Melts from Melting of Polymer Crystals. *Nat. Mater.* **2005**, *4* (8), 635–641.
- (42) Raitchel, D.; Baderschneider, S.; de Queiroz, T. B.; Lohwasser, R.; Köhler, J.; Thelakkat, M.; Kümmel, S.; Hildner, R. Emitting Species of Poly(3-Hexylthiophene): From Single, Isolated Chains to Bulk. *Macromolecules* **2016**, *49* (24), 9553–9560.
- (43) In the fitting procedure, a fourth but very small Gaussian peak close to 1.6 eV was included to assure that the width of the peak at ca. 1.75 eV was comparable to the width of the other peaks.
- (44) Brown, P.; Thomas, D.; Köhler, A.; Wilson, J.; Kim, J.-S.; Ramsdale, C.; Siringhaus, H.; Friend, R. Effect of Interchain Interactions on the Absorption and Emission of poly(3-Hexylthiophene). *Phys. Rev. B: Condens. Matter Mater. Phys.* **2003**, *67* (6), 1–16.
- (45) Martin, T. P.; Wise, A. J.; Busby, E.; Gao, J.; Roehling, J. D.; Ford, M. J.; Larsen, D. S.; Moule, A. J.; Grey, J. K. Packing Dependent Electronic Coupling in Single Poly(3-Hexylthiophene) H- and J-Aggregate Nanofibers. *J. Phys. Chem. B* **2013**, *117*, 4478–4487.
- (46) Son, S.; Dodabalapur, A.; Lovinger, A. J.; Galvin, M. E. Luminescence Enhancement By the Introduction of Disorder Into Poly(P-Phenylene Vinylene). *Science* **1995**, *269* (5222), 376–378.
- (47) Callis, P. R.; Scott, T. W.; Albrecht, A. C. Perturbation Selection Rules for Multiphoton Electronic Spectroscopy of Neutral Alternating Hydrocarbons Perturbation Selection Rules for Multiphoton Elec-

tronic Spectroscopy of Neutral Alternant Hydrocarbons a. *J. Chem. Phys.* **1983**, *78*, 16–22.

(48) Wise, A.; Grey, J. Understanding the Structural Evolution of Single Conjugated Polymer Chain Conformers. *Polymers (Basel, Switz.)* **2016**, *8* (11), 388.

(49) Gao, Y.; Grey, J. K. Resonance Chemical Imaging of Polythiophene/Fullerene Photovoltaic Thin Films: Mapping Morphology-Dependent Aggregated and Unaggregated CdC Species. *J. Am. Chem. Soc.* **2009**, *131*, 9654–9662.

(50) Kuo, C. C.; Lin, C. H.; Chen, W. C. Morphology and Photophysical Properties of Light-Emitting Electrospun Nanofibers Prepared from Poly(fluorene) derivative/PMMA Blends. *Macromolecules* **2007**, *40* (19), 6959–6966.

Supporting Information for:

Signatures of Melting and Recrystallization of a Bulky Substituted Poly(thiophene)

Identified by Optical Spectroscopy

Fanuel M. Keheze¹, Dominic Raithe², Tianyu Wu¹, Daniel Schiefer³, Michael Sommer^{3,4,5,6}, Richard Hildner² and Günter Reiter^{1,4,5}*

¹Physikalisches Institut, Universität Freiburg, Hermann-Herder-Straße 3, 79104 Freiburg, Germany

²Experimentalphysik IV, University of Bayreuth, 95440 Bayreuth, Germany

³Institute für Makromolekulare Chemie, Universität Freiburg, Stefan-Meier-Straße 31, 79104 Freiburg, Germany

⁴Freiburger Materialforschungszentrum FMF, Stefan-Meier-Straße 21, 79104 Freiburg, Germany

⁵Freiburger Institut für interaktive Materialien und bioinspirierte Technologien FIT, Georges-Köhler-Allee 105, 79110 Freiburg, Germany

⁶Polymerchemie, Technische Universität Chemnitz, Strasse der Nationen 62, 09111 Chemnitz

Optical microscopy measurements:

Large spherulitic crystals were grown via isothermal crystallization from molten films. The size of the spherulites varied from 10 μm to more than 150 μm in diameter, depending on when nucleation occurred during the crystallization process.¹ in the melt state, i.e., at 150 $^{\circ}\text{C}$, there is complete loss of birefringence and the cooled film does not show birefringence either.

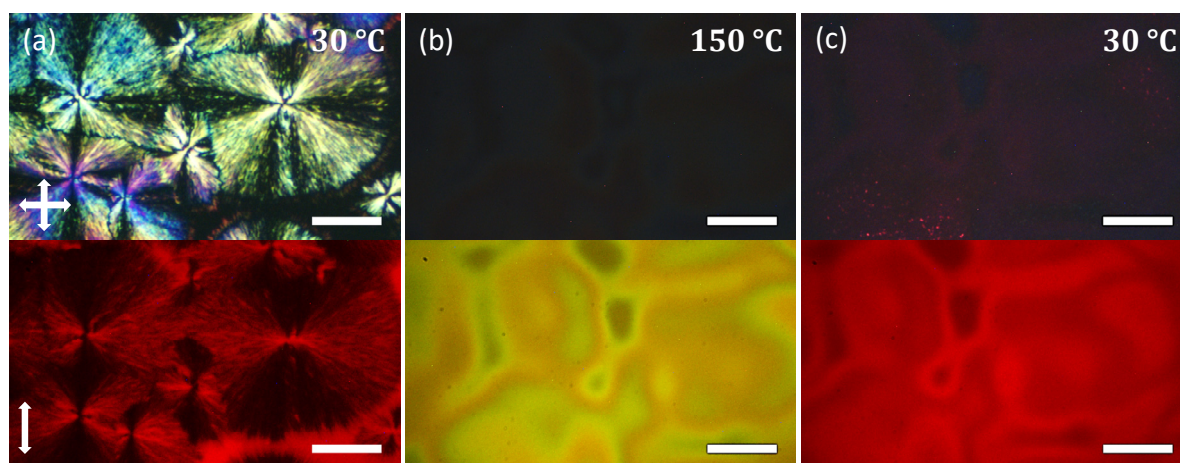


Figure S1: Birefringence (first row) and PL (second row, the light used for excitation was polarized in the direction indicated by the white arrows) images of (a) PDOPT spherulites grown on a silicon substrate for 50 hours at crystallization temperature of 100 $^{\circ}\text{C}$. (a) Images were measured after crystallization at 100 $^{\circ}\text{C}$ and cooling to 30 $^{\circ}\text{C}$, (b) after heating the spherulitic crystals up to 150 $^{\circ}\text{C}$ and (c) after cooling the molten spherulites back to 30 $^{\circ}\text{C}$. Heating and cooling rates were 2 $^{\circ}\text{C}/\text{min}$. The scale bar represents a length of 50 μm .

Rapid recrystallization that occurred when the molten PDOPT spherulites (see Figure S1b) were cooled from 150 $^{\circ}\text{C}$ to 30 $^{\circ}\text{C}$ (see Figure S1c). Such crystallization was accompanied by the formation of many small and randomly oriented crystallites, which did not become visible under crossed polarizers, i.e., birefringence was absent. Crystallization leads to a homogeneous change in color as observed in PL spectra.

FTIR measurements:

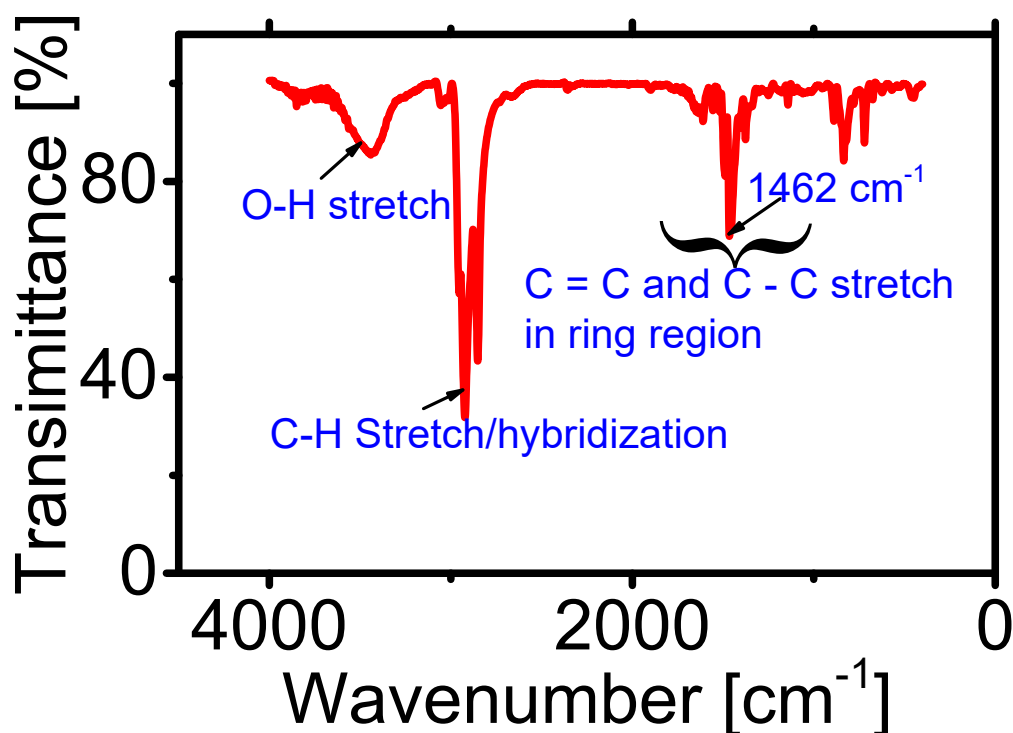


Figure S2: PDOPT FTIR Spectra for poly (3-(2, 5-dioctyl-phenyl) - thiophene) (PDOPT) showing various stretching modes.

Figure S2 shows that the electronic transitions couples strongly to stretching phonon mode (C-C stretching of the phenyl ring) with a peak ranging from 1200 cm^{-1} (148 meV) to 1611 cm^{-1} (200 meV), most strongly absorbing at 1462 cm^{-1} (180 meV). The C-C stretching mode can be used to estimate the separation between peaks in a Franck-Condon progression.

Franck-Condon -Fit to solution spectrum of PDOPT:

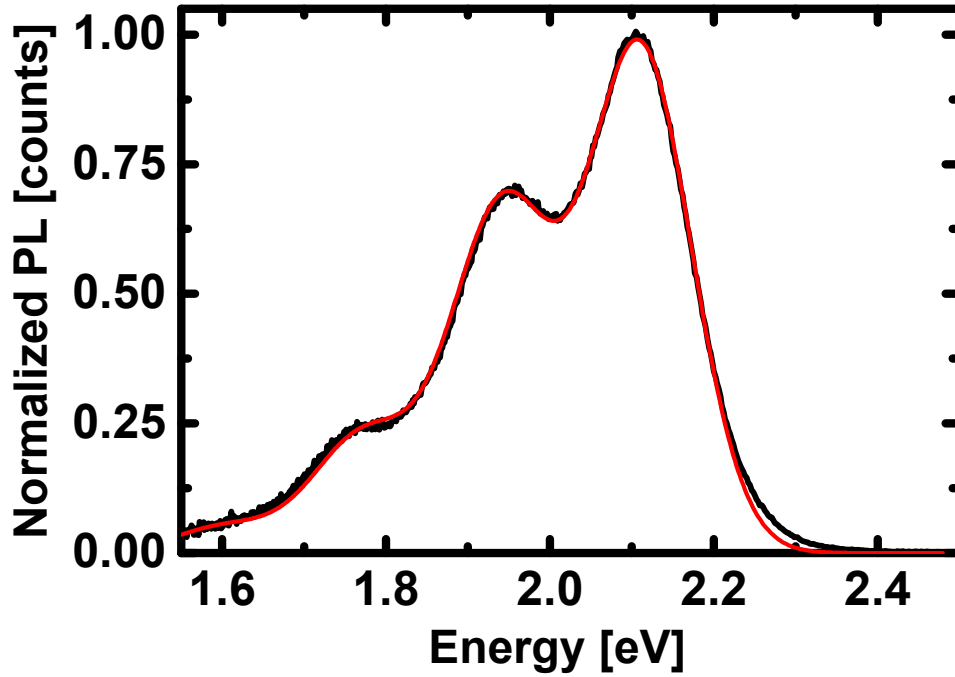


Figure S3: The PL spectra of PDOPT dissolved in toluene solution (black) is fitted with a Franck-Condon progression (red). The resulting Huang-Rhys parameter $S=0.7$ and the vibronic Energy $E_d = 167$ meV is used for fitting the absorption spectra. The 0-0 transition energy is $E_0 = 2.12$ eV. The spectrum is corrected for the photon density of states.

Fitting Absorption

For fitting the remaining aggregate absorption the progression developed by Spano and coworkers.^{2,3}

$$\frac{A(E)}{nE} \sim \sum_{m=0} \frac{S^m}{m!} \left(1 - \frac{We^{-S}}{2E_d} \left(\sum_{n \neq m} \frac{S^n}{n!(n-m)} \right) \right)^2 \cdot \exp \left(- \frac{(\hbar\omega - E_{A1} - mE_d)^2}{2\sigma^2} \right) \quad (1)$$

The Huang-Rhys parameter $S=0.7$ and the vibronic energy $E_d=167$ meV of the effective carbon-stretching mode are extracted from solution spectra with a standard FC progression (see above).

The remaining free parameters are the free exciton bandwidth W , the transition energy E_{A1} of the lowest-energy crystalline absorption peak and the line width σ of the absorption peaks.

In Figure S4a, the spectra of absorption at 30° C (after subtraction of the disordered contribution) is fitted by equation (1). The fit did not systematically match the positions and widths of the peaks. A closer look at the peaks shows that, the A_1 peak is narrower than the A_i ($i>1$) peaks. The above discrepancy could be explained by the possible existence of two or several different species within the spherulite which contribute to the total absorption spectra. However, from single-molecule spectroscopy on polythiophenes⁴ we know that the A_i ($i>1$) peaks consist of several vibrational modes and not just a single one what leads to broader A_i ($i>1$) peaks (“effective vibronic mode”) in bulk measurements. A further possibility is the formation of Fermi-resonances between the excitons and further dark states which also broadens the A_i ($i>1$) peaks with respect to the A_1 peak.² Usually this effect is only resolvable in a regime where the disorder is small in comparison to the excitonic coupling between the chains. (This may apply for the spherulites). Consequently, a different (fitting) model has to be applied, in which we introduced the line width of the A_1 peak as additional parameter σ_{A1} (with $\sigma_{A1} < \sigma$):

$$\begin{aligned} \frac{A(E)}{nE} \sim & \left(1 - \frac{We^{-S}}{2E_d} \left(\sum_{n \neq m} \frac{S^n}{n!(n-m)} \right) \right)^2 \cdot \exp \left(- \frac{(E - E_{A1})^2}{2\sigma_{A1}^2} \right) \\ & + \sum_{m=1} \frac{S^m}{m!} \left(1 - \frac{We^{-S}}{2E_d} \left(\sum_{n \neq m} \frac{S^n}{n!(n-m)} \right) \right)^2 \cdot \exp \left(- \frac{(E - E_{A1} - mE_d)^2}{2\sigma^2} \right) \end{aligned} \quad (2)$$

The resulting fit is shown in Figure S4 b. Compared to the fit with formula (1) (see Fig. S4 a), the fit reproduced the experimental data much better over the entire energy range.

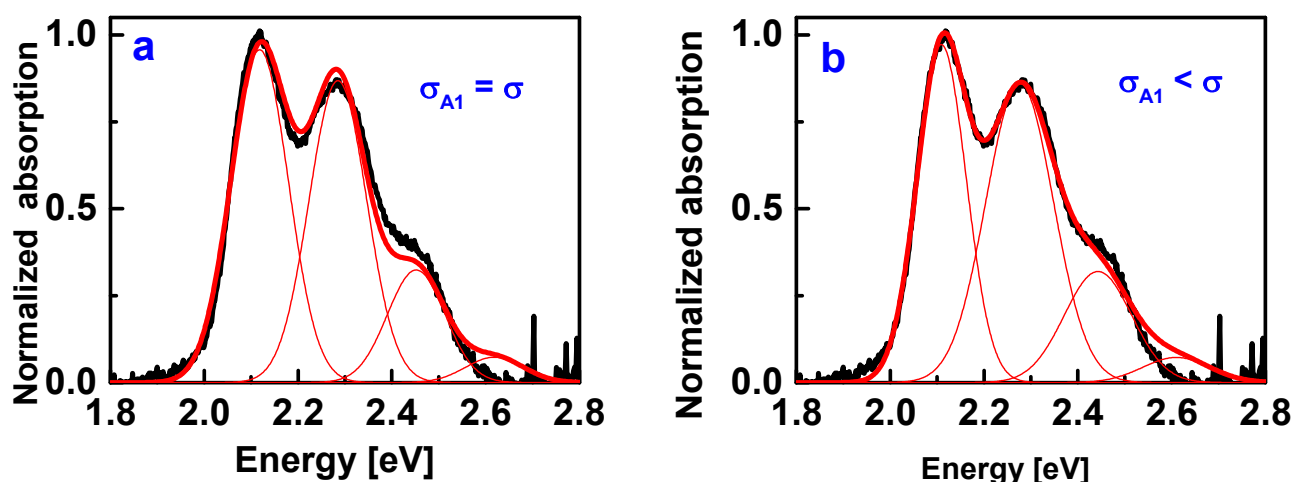


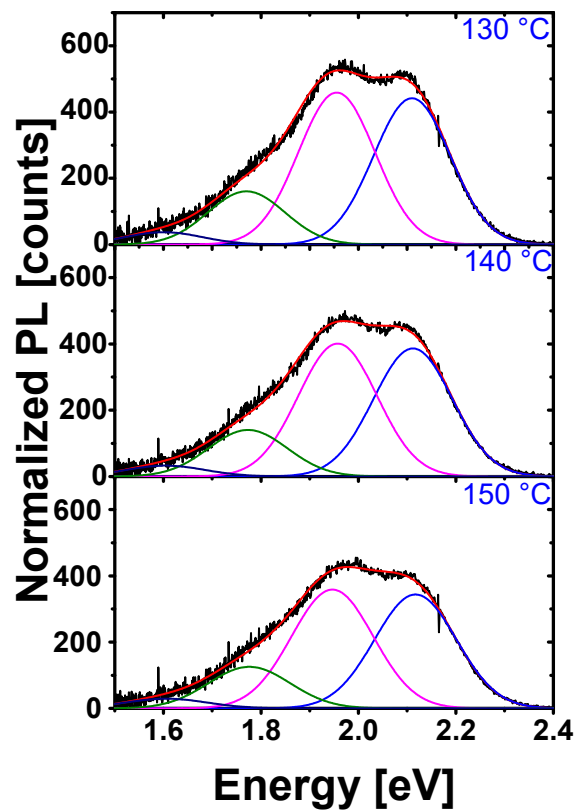
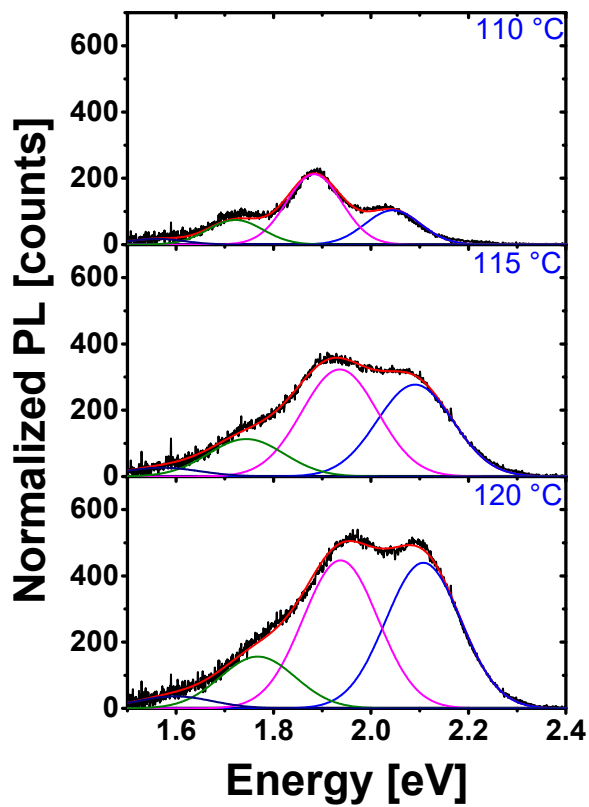
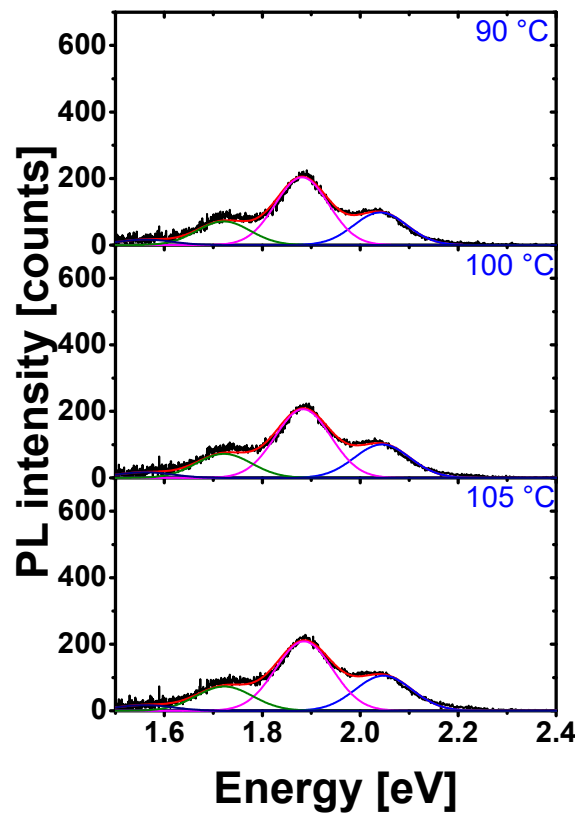
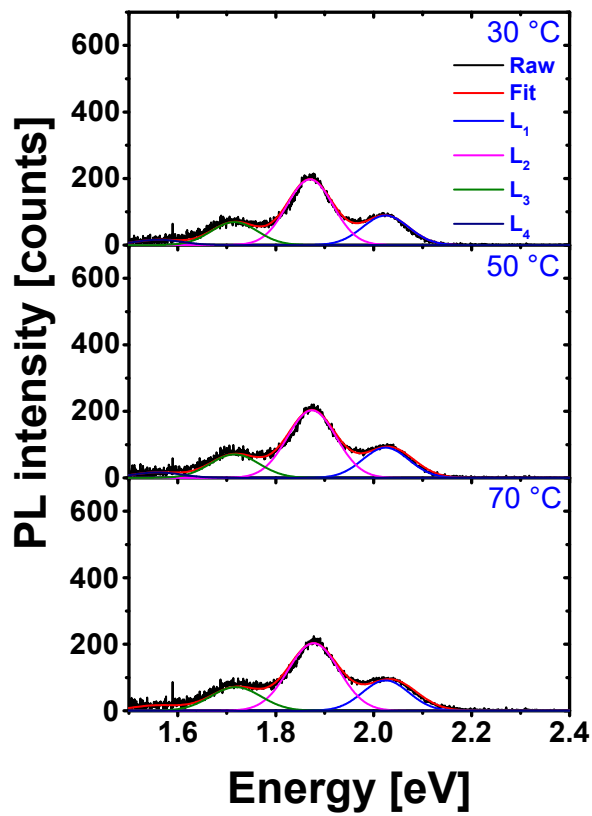
Figure S4: Fitting the absorption spectra of the spherulitic crystal at 30°C after subtraction of the disordered high-energy contribution with (a) equation (1) and (b) equation (2).

Fitting photoluminescence (PL) spectra:

For fitting the emission spectra, the progression developed by Spano and coworkers⁵ was used (equation 2 in the main paper). The intensity of the spectra were first normalized by dividing by energy (E^3) to correct for photon the density of states. Thereafter, the intensities were normalized to between 0 and 1. Lastly, the normalized Spectra were then fitted with a single FC progression with Huang-Rhys parameter $S=0.7$ and a vibronic energy of around *ca.* 1350 cm^{-1} (167 meV), as measured in solution and used for fitting absorption spectra (Figure S3). The vibronic energy E_d , line the width σ_{A1} and amplitudes of peaks were set as a free parameters of the emission peaks. The peaks were labelled as L_i ($i > 1$) starting with highest energy. In Figure S5, intensity of the various fits were multiplied by the normalizing factors to rescale to the absolute intensities

Finally, we note that reproducing the temperature-dependent changes of the absorption and PL spectra with a variable Huang-Rhys parameter is not possible. There is always non-zero inter-chain interaction (or free exciton bandwidth W) required, which further shows the importance of this inter-chain interaction in PDOPT crystalline lamellae despite the absence of π - π -stacking.

Heating series:



Cooling series:

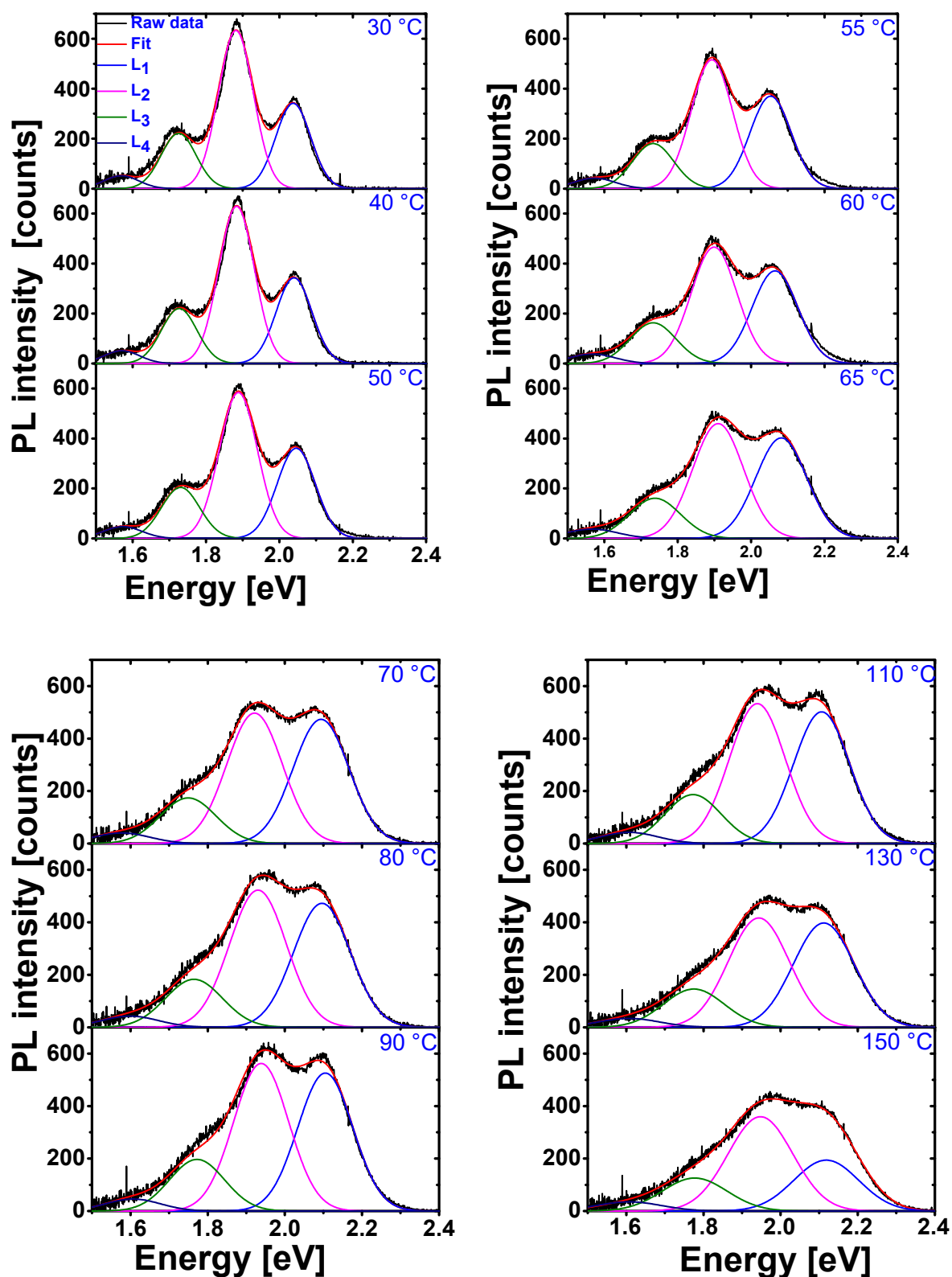


Figure S5: Sample fits for the PL spectra of the spherulitic crystal during heating and cooling cycles between 30°C and 150 °C according to equation 2 of the main text.

DSC measurements on spherulitic crystals:

Spherulitic crystals were prepared in a DSC pan in order to correlate thermal and optical properties of spherulitic crystals. First, the mass of an empty DSC pan was measured, followed by drop casting a solution of PDOPT in toluene into the pan. The DSC pan was then placed in a vacuum chamber at 50 °C and left there for 24 hours to dry completely. The total mass of DSC pan with the resulting thin PDOPT film was also measured. This film was then molten at 150 °C for 3 minutes and crystallized isothermally at 100 °C for 50 hours in a Linkam TMS 94 device purged with nitrogen. Optical images of the spherulitic crystals formed were taken (Figure S6). This sample was then used for DSC measurements.

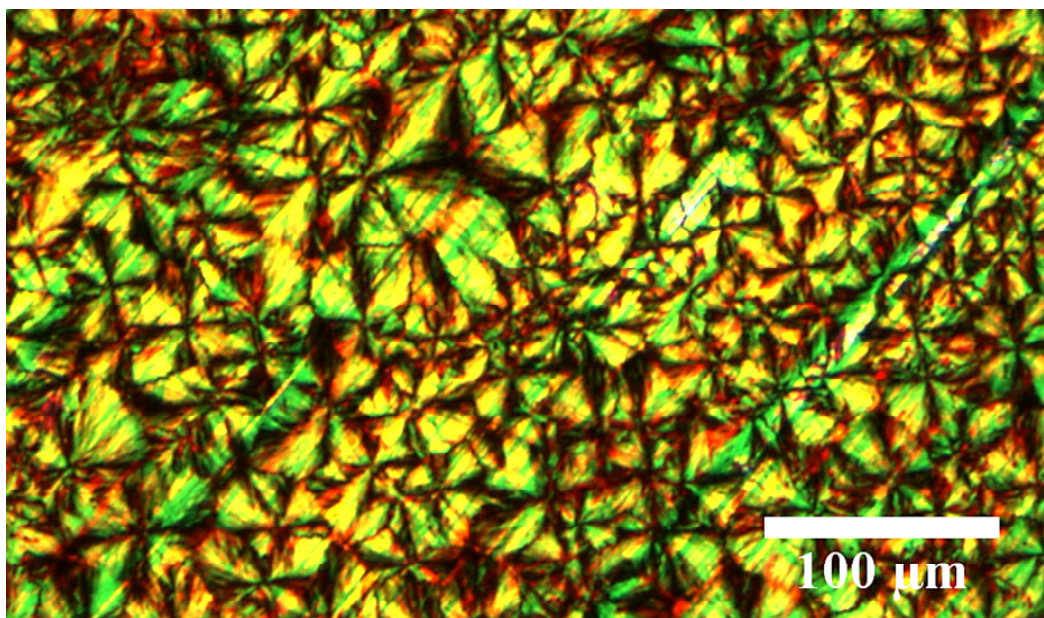


Figure S6: Birefringence image of PDOPT spherulites grown on a DSC pan for 50 hours at $T_c = 100$ °C. The spherulitic crystals varied in sizes, a consequence of variations in the local nucleation density.

In-situ temperature –dependent absorption and photoluminescence measurements

Temperature-dependent absorption and PL spectroscopy measurements were performed using the USB2000 Ocean Optics spectrophotometer, Ocean Optics optical fibers of 400 μm diameter and the Zeiss Axio 100 microscope combinations allowing for spatially resolved measurements. Ocean Optics TS-LED light sources were used for excitation and PL measurements. For these latter measurements an excitation filter transmitting between 450 and 500 nm was used as well as a 500 nm long-pass filter (both AHF) in front of the detector. Glass and silicon (100) wafers were used as substrates. Si-wafers were supplied by Silchem Handelsgesellschaft mbH, D-09599, Freiberg, Germany. The heating and cooling of the samples was achieved with a hot stage purged with nitrogen and controlled by a Linkam TMS 94 device (Linkam Scientific instruments, Surrey, Kt20 5HT, UK).

The sample temperature was increased or decreased at a rate of 2 $^{\circ}\text{C}/\text{minute}$. Figure S7 shows the setups used for absorption and for photoluminescence experiments while Figures S8 and S9 show the corresponding spectra obtained with these set-ups for absorption and PL measurements, respectively.

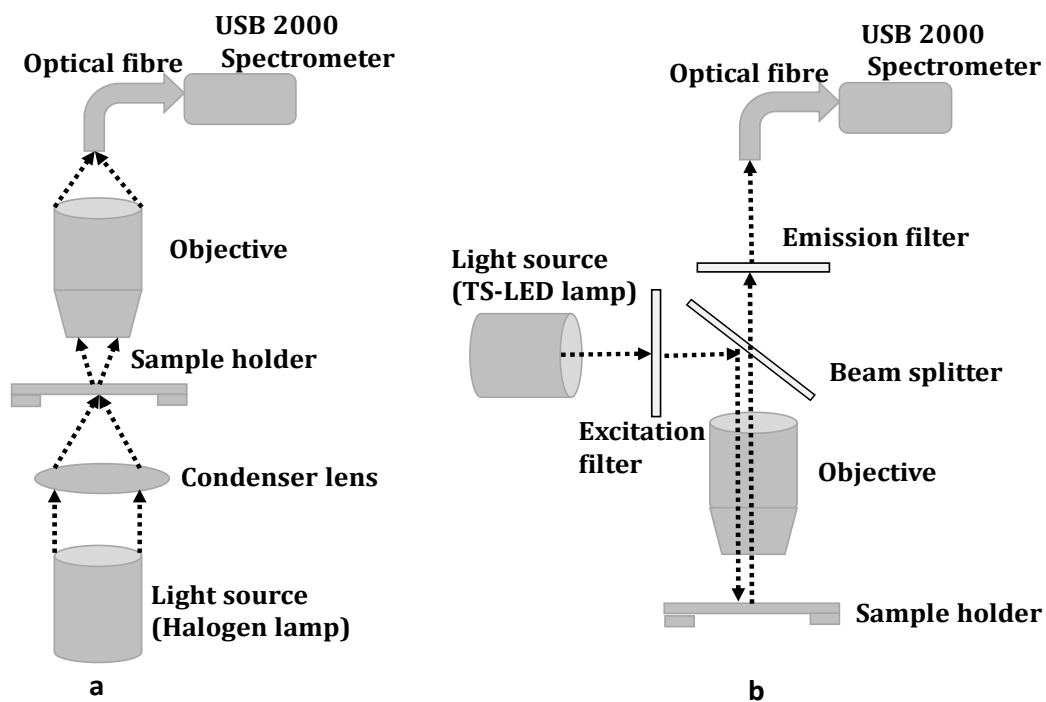


Figure S7: Schematic illustration of set-up used to measure (a) absorption and (b) photoluminescence of spherulitic crystals.

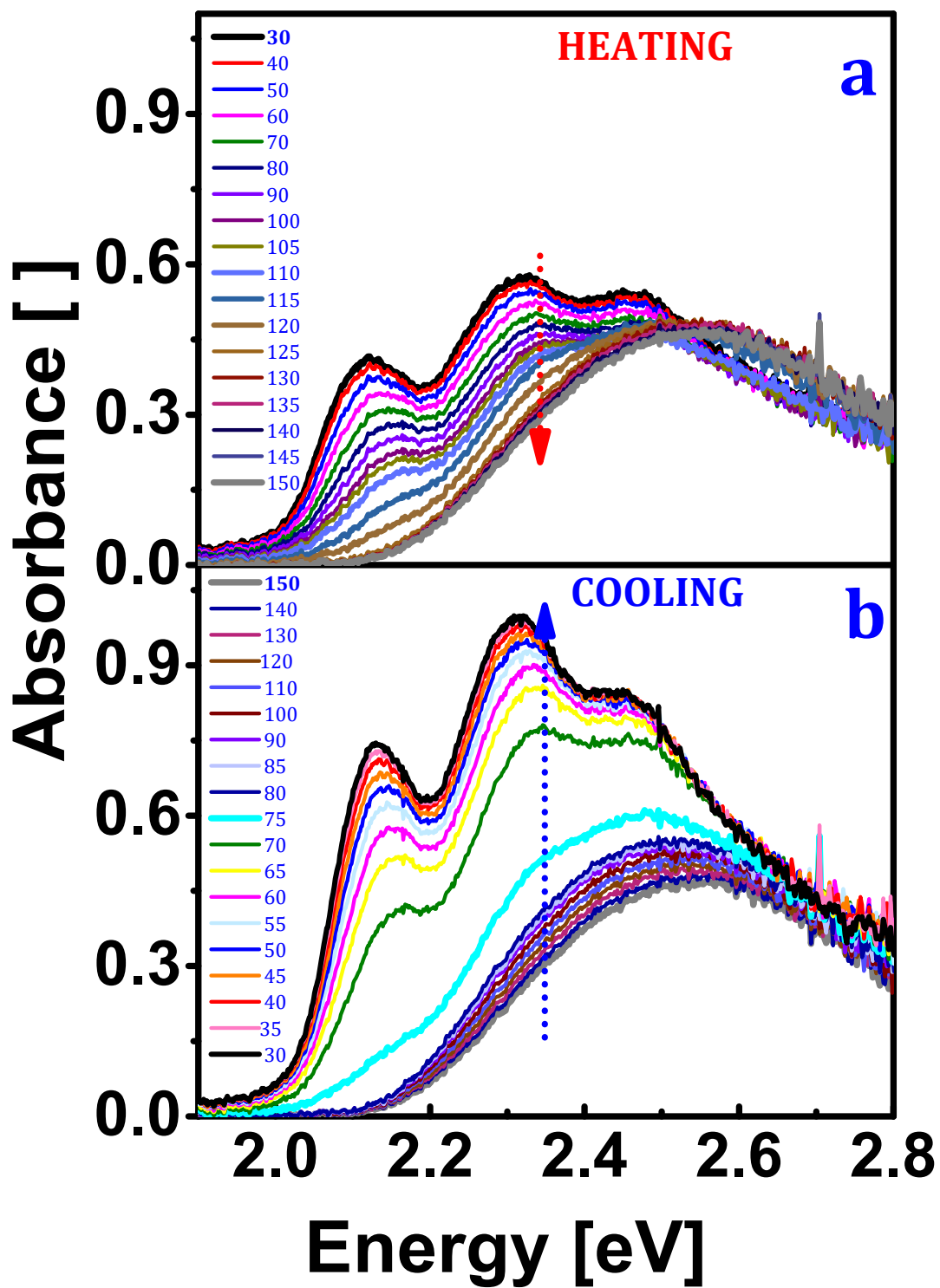


Figure S8: A series of absorption spectra during the heating (a) and cooling (b) cycles between 30°C and 150 °C. The heating rate was 2 °C / min for a spherulitic crystal grown at 100 °C for 50 hours.

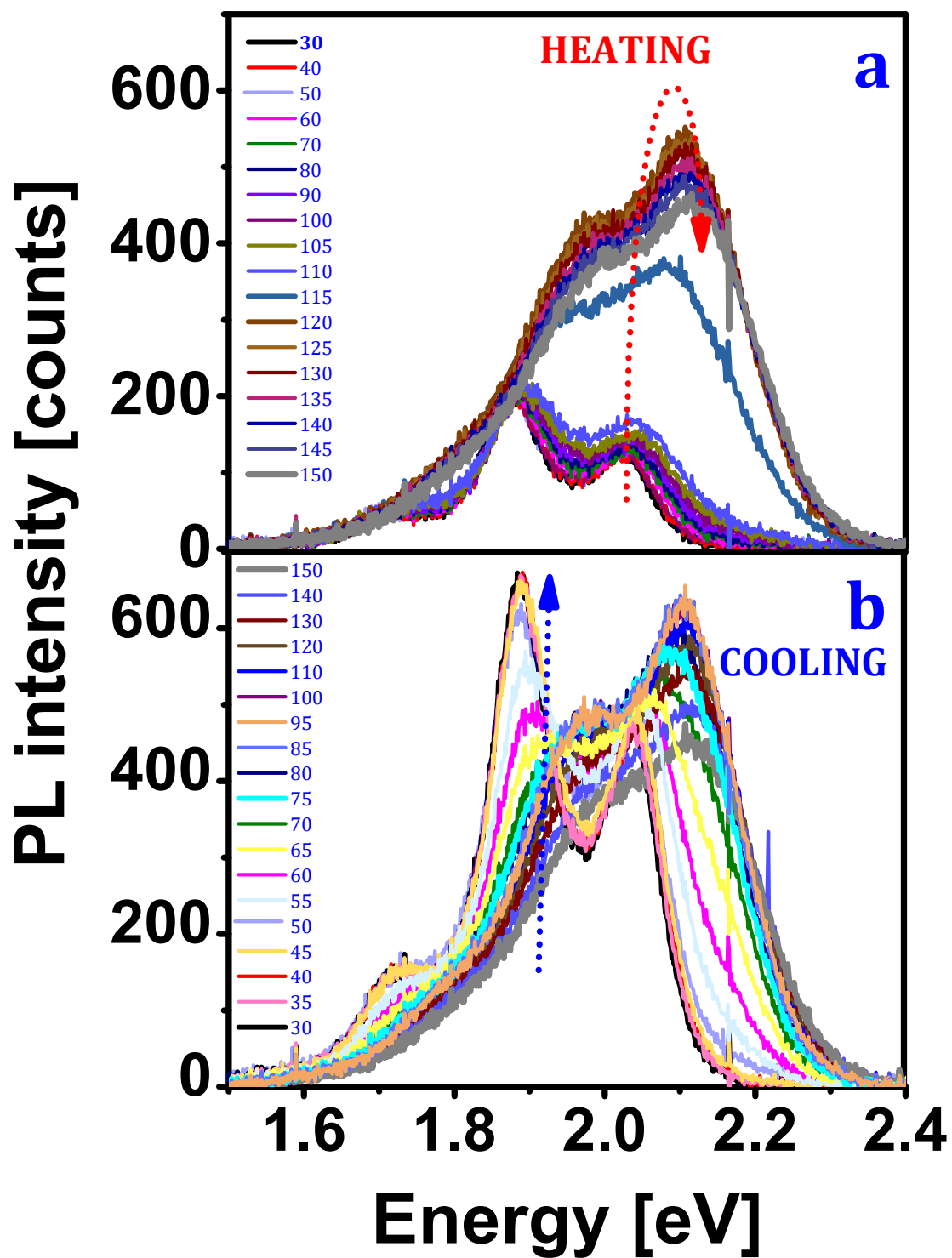
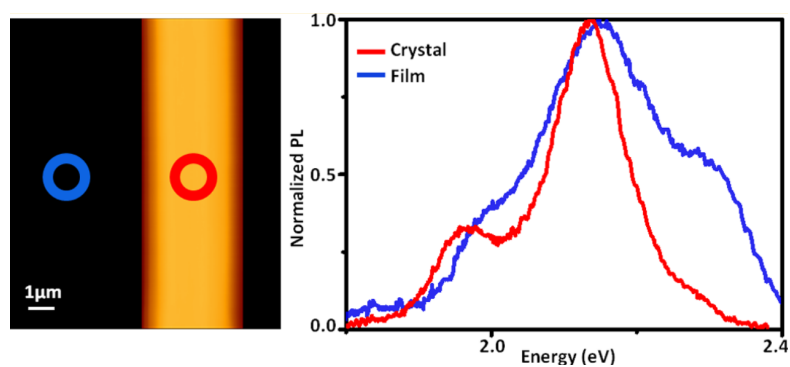


Figure S9: A series of photoluminescence spectra during the heating (a) and cooling (b) cycles between 30°C and 150 °C. The heating rate was 2 °C / min for a spherulitic crystal grown at 100 °C for 50 hours.

References:

- (1) Wang, Y.; Heck, B.; Schiefer, D.; Agumba, J. O.; Sommer, M.; Wen, T.; Reiter, G. Anisotropic Photophysical Properties of Highly Aligned Crystalline Structures of a Bulky Substituted Poly(thiophene). *ACS Macro Lett.* **2014**, *3* (9), 881–885.
- (2) Spano, F. C. Absorption in Regio-Regular poly(3-Hexyl)thiophene Thin Films: Fermi Resonances, Interband Coupling and Disorder. *Chem. Phys.* **2006**, *325* (1), 22–35.
- (3) Clark, J.; Chang, J. F.; Spano, F. C.; Friend, R. H.; Silva, C. Determining Exciton Bandwidth and Film Microstructure in Polythiophene Films Using Linear Absorption Spectroscopy. *Appl. Phys. Lett.* **2009**, *94* (16), 1–4.
- (4) Raithel, D.; Baderschneider, S.; de Queiroz, T. B.; Lohwasser, R.; Köhler, J.; Thelakkat, M.; Kümmel, S.; Hildner, R. Emitting Species of Poly(3-Hexylthiophene): From Single, Isolated Chains to Bulk. *Macromolecules* **2016**, *49* (24), 9553–9560.
- (5) Clark, J.; Silva, C.; Friend, R. H.; Spano, F. C. Role of Intermolecular Coupling in the Photophysics of Disordered Organic Semiconductors: Aggregate Emission in Regioregular Polythiophene. *Phys. Rev. Lett.* **2007**, *98* (20), 206406.

4.4 Publication 4: Revealing order and disorder in films and single crystals of a thiophene-based oligomer by optical spectroscopy



Sajedeh Motamen, Dominic Raithel, Richard Hildner, Khosrow Rahimi, Jarrosson Thibaut, Françoise Serein-Spirau, Lauren Simon, Günter Reiter Published in

ACS Photonics

DOI: 10.1021/acsp Photonics.6b00473

Reproduced with permission from ACS Photonics 3 (2016) 2315

Copyright © 2016 American Chemical Society

Revealing Order and Disorder in Films and Single Crystals of a Thiophene-Based Oligomer by Optical Spectroscopy

Sajedeh Motamen,[†] Dominic Raithel,[‡] Richard Hildner,[‡] Khosrow Rahimi,[§] Thibaut Jarrosson,^{||} Françoise Serein-Spirau,^{||} Laurent Simon,[⊥] and Günter Reiter^{*,†,Ⓢ}

[†]Physikalisches Institut, Albert-Ludwigs-Universität, 79104 Freiburg, Germany

[‡]Experimentalphysik IV, University of Bayreuth, 95440 Bayreuth, Germany

[§]DWI-Leibniz Institute for Interactive Materials, Forckenbeckstr. 50, 52056 Aachen, Germany

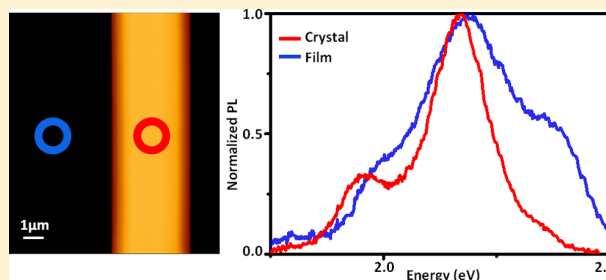
^{||}Institut Charles Gerhardt de Montpellier, UMR 5353-CNRS Equipe Architectures Moleculaires et Matériaux Nanostructurés (AM2N), Ecole Nationale Supérieure de Chimie de Montpellier, 8 Rue de l'École Normale, 34296 Montpellier cedex 05, France

[⊥]Institut de Sciences des Matériaux de Mulhouse IS2M, UMR7361 CNRS-UHA, 3 bis rue Alfred Werner, 68093 Mulhouse, France

Supporting Information

ABSTRACT: Depending on processing conditions, ordered microstructures of conjugated oligomers or polymers exhibit variable amounts of grain boundaries, lattice disorder, and amorphous (disordered) regions. These structural details can be determined very precisely. Their correlations with optical or electronic properties, however, are very difficult to establish, because, for example, optical spectra are usually averaged over regions with different degrees of disorder. In an attempt to facilitate the interpretation of optical spectra, we performed systematic studies on thin films and μm -sized single crystals of thiophene-based conjugated molecules, which allowed identifying the relative contributions of ordered and disordered regions in optical emission spectra. A detailed multippeak analysis of the emission spectra showed that the peak positions, the energies of the emitted photons, showed only minor changes, independent if highly ordered or rather disordered samples were examined. However, the relative emission intensity changed significantly between samples. In particular, for highly ordered single crystals the purely electronic 0–0 transition nearly vanished, that is, it was essentially optically forbidden as theoretically predicted. Thus, changes in emission probability are correlated with the degree of structural order in semiconducting conjugated systems and provide a possibility to quantify structural order.

KEYWORDS: single crystal, local spectroscopy, anisotropic behavior, degree of structural order, organic conjugated oligomers



Triggered by their tunable photophysical and electronic properties, organic semiconducting materials have been widely studied, mainly in view of various optoelectronic applications.^{1–6} Currently, strong efforts are undertaken for improving our understanding of the relation between morphology and electronic structure. Detailed knowledge of this relation may help to improve the performance of devices such as field effect transistors and organic photovoltaics,^{7,8} in which various organic materials with ordered nano/microstructures have been used as the active layer.⁹ Triggered by the observation of high charge-carrier mobilities and of long-range energy transport in highly ordered (supramolecular) structures, much effort was invested on the improvement of structural order in organic conjugated materials.^{10–12} However, in most of the studied devices the active layer possessed a complex morphology with a large amount of ordered and disordered regions, and grain boundaries, which depended on processing conditions. The simultaneous existence of highly ordered (crystalline) and structurally more disordered regions make it difficult to interpret electronic behavior unambiguously and to establish a clear

relation between structural features and electronic properties. Structural disorder implies a reduction of overall intrachain (planarity), reduced conjugation length and low interchain order, which give rise to energetic disorder, that is, variations in energy levels across the material.¹³ By controlling processing conditions, we can achieve samples of variable degrees of order and thus investigate the impact of regions of variable degrees of order on electronic features. This may help to identify pathways, allowing to tune optoelectronic properties of conjugated nanostructures.

In this work, we systematically control molecular order using different processing methods (growth of single crystals vs spin-coated films of a thiophene-based conjugated oligomer) and quantify the degree of structural order from optical properties by performing spectroscopy measurements. By controlling the nucleation stage, we have grown millimeter-long needle-like single crystals of thiophene-benzene-thiophene (3TBT) oligomers. 3TBT is a trimer with each monomer having two

Received: July 8, 2016

Published: November 8, 2016

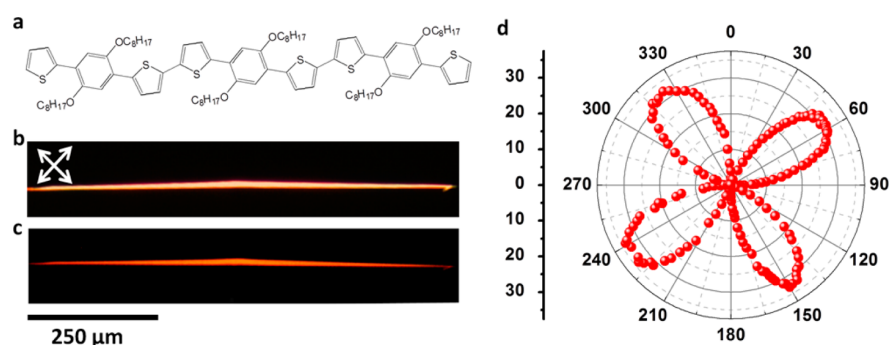


Figure 1. (a) Chemical structure of 3TBT. (b) Optical micrograph ($800\ \mu\text{m} \times 160\ \mu\text{m}$) under crossed polarizers of a 3TBT single crystal on a silicon substrate, crystallized from a $0.1\ \text{g/L}$ solution in dodecane at $60\ ^\circ\text{C}$ for 1 week. (c) Photoluminescence microscopy image ($800\ \mu\text{m} \times 160\ \mu\text{m}$) of a single crystal excited with blue light in the range from $450\text{--}490\ \text{nm}$. (d) Polar plot of the birefringence intensity measured for a 3TBT crystal as a function of its orientation angle with respect to the analyzer.

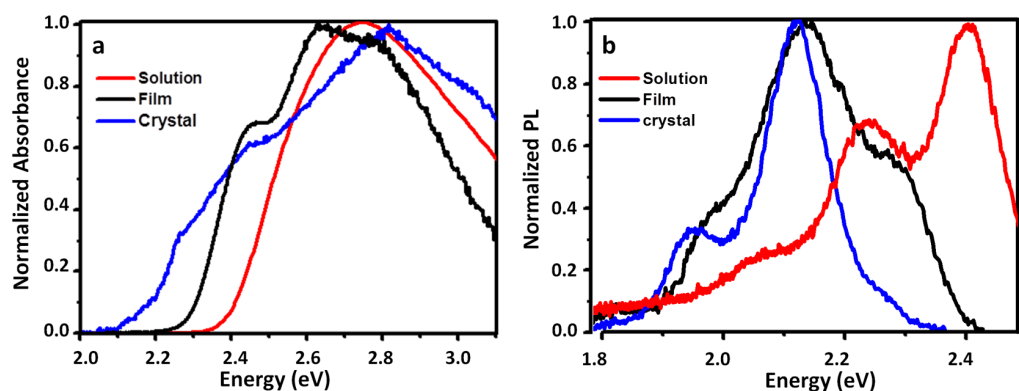


Figure 2. Normalized (a) UV–visible absorption (of nonpolarized light) and (b) photoluminescence spectra of a homogeneous 3TBT solution, a spin-coated film, and a single crystal.

thiophene (T) units separated by one dialkoxybenzene (B) unit. Compared to molecules composed of only thiophene units, 3TBT exhibits better photostability at ambient conditions.^{14,15} The well-defined molecular order of single crystals over macroscopic dimensions results in high anisotropy in structure as well as in optical properties. However, depositing these crystals from solution leads to the coexistence of randomly oriented crystalline fibers and amorphous molecules around these crystals. Local spectroscopic measurements allow to spatially distinguish disordered and ordered regions and thus to identify the contribution of these regions in emission spectra.

EXPERIMENTAL SECTION

Material and Film Preparation. The studied 3TBT molecules consisted of a sequence of three TBT monomers, each having a central dialkoxybenzene unit (denoted by B), with two octyl side groups attached orthogonally to the main axis of the molecule, and sandwiched by two thiophene rings (denoted by T; Figure 1a).¹⁵ The molecule was 100% regioregular, with a number-average molecular weight $M_n = 1492.32\ \text{g/mol}$ and a contour length of $3.6\ \text{nm}$. 3TBT molecules were dissolved in dodecane at a concentration of $10^{-6}\ \text{M}$. Thin films of 3TBT were prepared by spin coating this solution onto a solid substrate (glass or Si-wafer).

Crystallization from Solution. A $0.1\ \text{g/L}$ solution of 3TBT in dodecane was prepared at room temperature. 3TBT molecules were homogeneously dissolved by heating the solution to $100\ ^\circ\text{C}$ for 3 min. Subsequently, this solution was cooled to the

crystallization temperature ($60\ ^\circ\text{C}$), where it was kept for 1 week. At this relatively high crystallization temperature, the nucleation density was low and the crystal growth rate was slow, allowing for the formation of large and perfect single crystals. Subsequently, $10\ \mu\text{L}$ of this solution containing large crystals was spin-cast at $500\ \text{rpm}$ onto a UV-ozone cleaned silicon substrate. Under such conditions, the resulting sample contained crystals embedded in a comparatively disordered polycrystalline film (Figure S1).

Optical Microscopy and Spectroscopy. Single crystals on glass substrates were characterized with an optical microscope (Zeiss A1). Spatially resolved absorption spectra of these crystals were obtained in transmission mode by using a UV–vis spectrometer (USB2000 from Ocean Optics) connected to the microscope (Zeiss A1) by means of an optical fiber. Photoluminescence spectroscopy was performed under nitrogen (N_2) atmosphere with the same setup in reflection mode, employing a light emitting diode (LED) as an excitation source. For photoluminescence spectroscopy, we used a narrow wavelength range ($450\ \text{nm}\text{--}490\ \text{nm}$) for excitation, employing the filter set 09 installed in Zeiss microscope. This filter set allowed that emitted light at wavelengths above $515\ \text{nm}$ ($2.40\ \text{eV}$) passed to the detector. Using this microscopy setup, we were able to focus on areas within the single crystals at a lateral resolution of some micrometers. Such local spectra allowed for the determination of the optical properties of single crystals without significant contributions from surrounding less-ordered, polycrystalline structures.

RESULTS

Morphology and Structure of 3TBT Single Crystals. The large 3TBT single crystals grown from solution exhibited needle-like morphology having a length of several hundred micrometers and a much smaller width of several micrometers. The thickness, as measured by atomic force microscopy (AFM), of most crystals ranged from 2 to 6 μm .

As expected for materials of high molecular order, 3TBT crystals were birefringent. Under crossed polarizers, these crystals exhibited a uniform intensity (birefringence; Figure 1b) that varied when the crystals were rotated within the plane of observation. Moreover, when excited by light in the wavelength range from 450 to 490 nm, 3TBT single crystals exhibited strong yellow to red photoluminescence (PL), as shown in Figure 1c for a 3TBT single crystal on a glass substrate.

Analyzing the birefringence intensity as a function of the orientation angle (the angle between the long axis of the crystal and the polarization direction of the polarizer) yielded the expected periodic minima and maxima every 45° , as shown in Figure 1d.

Photophysical Properties of 3TBT Single Crystals and Films. Normalized absorption and photoluminescence (PL) spectra were obtained from a dilute homogeneous 3TBT/dodecane solution, from a spin-coated film, and from a needle-like single crystal, as shown in Figure 2 (see Figure S8 for absolute absorption coefficients). The absorption spectrum of the solution exhibited a single broad absorption peak with a maximum around 2.74 eV (Figure 2a), arising from intrachain states of isolated molecules.¹⁶ Compared to 1TBT, a molecule with only one TBT monomer, this peak has been red-shifted by about 70 meV,¹⁷ indicating a substantially larger π -electron delocalization in 3TBT. In fact, quantum mechanical calculations¹⁷ revealed an almost planar arrangement for 3TBT molecules induced by noncovalent S \cdots O interactions. Hence, the π electrons can be expected to be delocalized over nearly the whole 3TBT molecule.¹⁸

Compared to the solution absorption, the spectrum of the spin-coated film was substantially different, with clear peaks at 2.72, 2.64, and 2.44 eV, respectively. The broad peak at 2.72 eV resembles the absorption of 3TBT in dilute solution, and absorption at this energy can therefore be attributed to isolated 3TBT molecules in the film. The more red-shifted features in the film absorption at 2.64 and 2.44 eV indicate the presence of aggregated 3TBT molecules. In particular, the smaller intensity of the lowest-energy peak at 2.44 eV with respect to the 2.64 eV peak is characteristic for H-type aggregation, with the molecules being arranged in a cofacial fashion.^{19,20} During spin-coating, 3TBT molecules were distributed randomly on the substrate. Due to fast evaporation of the solvent, these molecules did not have enough time to arrange themselves into large scale ordered structures. Thus, a large number of only small fiber-like objects with an ordered, cofacial arrangement of 3TBT molecules could be formed, as revealed by AFM measurements (see Figure S2).

By contrast, micrometer-sized crystals possessed long-range order of an enormous number of molecules. Crystals were deposited on solid substrates and all these crystals showed similar absorption spectra, which typically exhibited three peaks at about 2.76, 2.45, and 2.26 eV, respectively. The first peak centered around 2.76 eV was again similar to the absorption peak for the dilute 3TBT dodecane solution and probably reflects isolated nonaggregated 3TBT molecules, for example, adsorbed on the crystal surface.²¹ The two low-energy peaks centered at 2.45 and

2.26 eV, respectively, showed the same trend in their intensity ratio with respect to the film spectrum. Hence, the 3TBT molecules in the crystal are also arranged in a cofacial, H-type fashion.

However, there are clear differences between the absorption spectra of the crystal and film, which indicate differences in their electronic and structural properties. First, the intensity ratio between the two lowest-energy peaks appears to be smaller in the crystal spectrum than in the film spectrum, which points toward a stronger electronic interaction between the transition dipole moments of 3TBT molecules in the single crystal with respect to the interaction within the aggregates in spin-coated films.^{22,23} Indeed, a detailed analysis based on a framework put forward by Spano and co-workers^{20,23} shows that the nearest-neighbor interaction between 3TBT molecules substantially decreases from 41 meV in single crystals to 11 meV in films (see Supporting Information, Figure S3). This stronger interaction in crystals can be attributed to a more dense and ordered H-type packing of the 3TBT molecules, which is probably related to the much slower crystallization rate, allowing for more time for the molecules to arrange properly. Second, the absorption of the 3TBT crystal was red-shifted by 187 meV with respect to the film spectrum, which can be explained by a slight change in the dielectric environment of the 3TBT molecules. The observation of a more dense packing in crystals indicates increased nonresonant dispersive interactions between molecules, which typically give rise to a red-shift compared to the situation with less dense packing in film aggregates. Furthermore, in crystals the slow crystallization process (week) allows for a perfect arrangement of the entire 3TBT molecule (i.e., backbone and side chain), whereas in spin-coated films the molecules rapidly crystallize (seconds) and thus some degree of disorder also in the side-chain arrangement of 3TBT may be present. These different side chain arrangements provide then a different dielectric environment that further contributes to the shift of the absorption between crystals and films, similar to a recent finding on poly(3-hexyl-thiophene) aggregates.²⁴ The observed changes in the absorption spectra therefore suggest that the order (or H-type packing) of the 3TBT molecules in crystals is significantly improved compared to aggregates in spin-coated films.

Similar characteristic differences were observed in the photoluminescence spectra of 3TBT molecules in solution, as-cast film, and single crystalline state (Figure 2b). For a 3TBT solution, a peak around 2.42 and shoulders at 2.24 and 2.08 eV were found. This vibronic structure is due to coupling to predominantly aromatic carbon-bond stretch modes. Together with a large Stokes shift between absorption and PL spectra, these observations are typical for thiophene-based systems. Compared to the solution, the PL spectra of the single crystal and the polycrystalline film showed large red shifts of about 120 meV and a strongly reduced intensity of the highest energy peak, which is characteristic of the emission of H-type aggregates. The substantially decreased intensity of the highest energy PL peak at ~ 2.3 eV in crystals is again indicative of an improved structural order of 3TBT molecules in crystals with respect to aggregates in films, as discussed above. This higher structural order gives rise to stronger interchain interactions in crystals, that is, to a larger exciton bandwidth, and to a different dielectric environment, which, in total, shifts the PL of the crystal to lower energies with respect to the PL of the film, as observed in Figure 2b. Notably, the PL spectra of both crystal and film do not exhibit emission features that can be associated with disordered, nonaggregated 3TBT molecules, although the corresponding absorption spectra

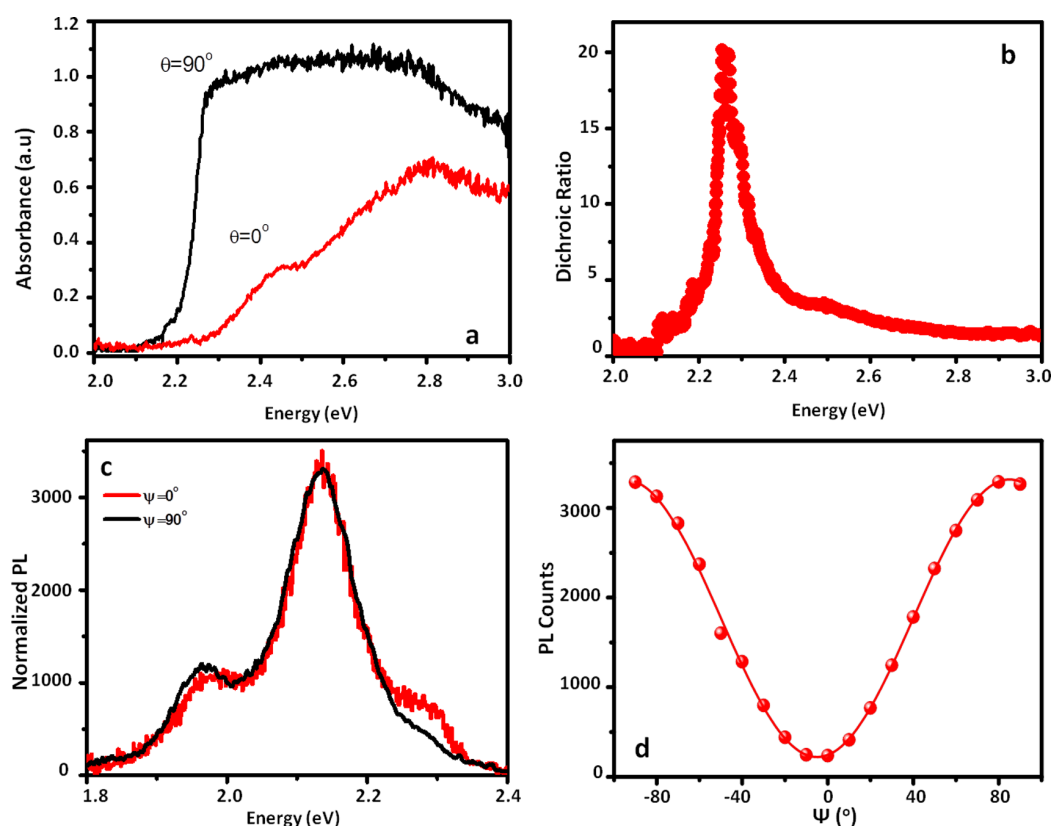


Figure 3. (a) Absorption spectra of a 3TBT single crystal measured at normal incidence with polarized light, where θ is the angle between the long axis of single crystal and the polarizer. (b) Dichroic ratio of the 3TBT crystal as a function of energy of absorbed light. (c) Photoluminescence spectra of a 3TBT single crystal measured at normal incidence with an analyzer, where ψ is the angle between the long axis of single crystal and analyzer (whole crystal excited by visible LED; spectra at $\psi = 0^\circ$ scaled up by a factor of 15). (d) Photoluminescence intensity measured at the maximum peak at 2.13 eV as a function of ψ . The solid line shows a $\cos^2 \psi$ -fit of the intensity.

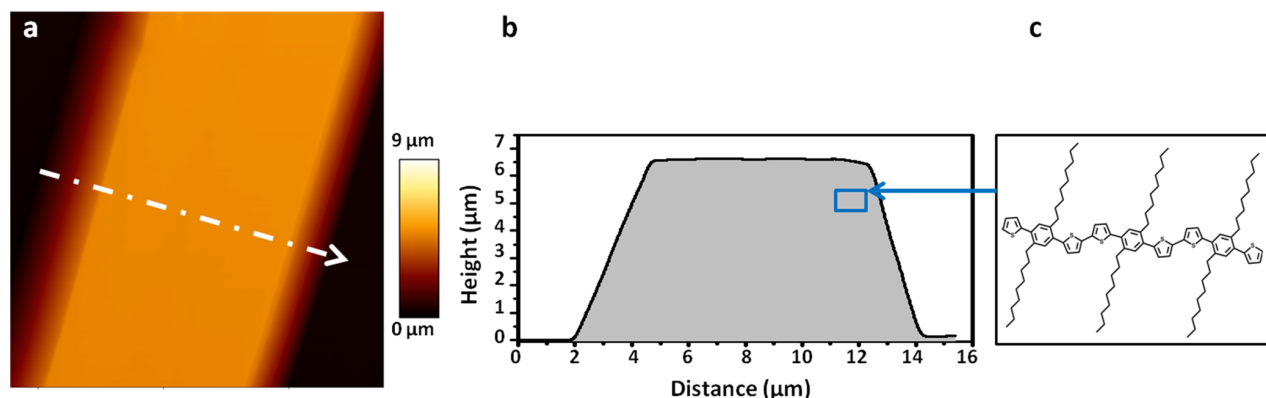


Figure 4. (a) AFM height image of 3TBT single crystal obtained by crystallization at 60°C from a 0.1 g/L solution in dodecane and spin-coated onto a silicon substrate ($15\ \mu\text{m} \times 15\ \mu\text{m}$). (b) Corresponding height profile along the dashed line shown in (a). (c) Scheme indicating the orientation of 3TBT molecules within the single crystal.

clearly show the presence of isolated molecules in both samples. This observation shows that energy transfer is highly efficient from the disordered regions to the crystal, implying that the two regions are separated by no more than the exciton diffusion length which is expected to be $\sim 10\text{--}20\ \text{nm}$.

Anisotropic Absorption and Photoluminescence Spectra of 3TBT Single Crystal. In ordered structures, the unique orientation of all molecules influences directly various optical properties such as refractive index, polarization state of the

absorbed and emitted light and nonlinear optical activity.²⁵ To measure the optical anisotropy caused by the regular molecular orientation in the crystal, we carried out optical spectroscopy with polarized light, as shown in Figure 3, to reveal the orientation of 3TBT molecules within the single crystal.

As shown in Figure 3a, the absorption spectra depended on the polarization direction of the exciting linearly polarized light with respect to the long axis of the single crystal, characterized by the angle θ . Both, intensity and shape of the absorption spectra

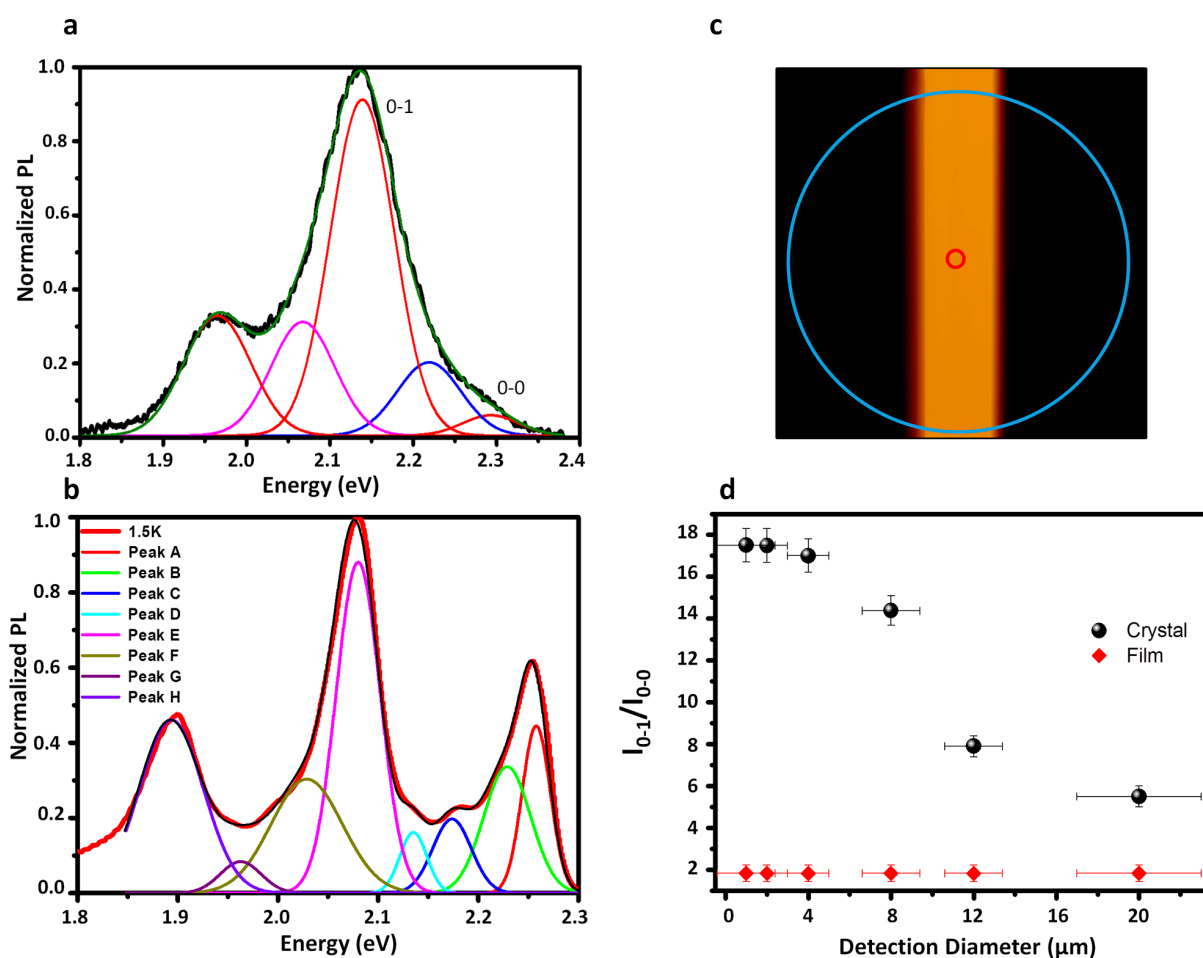


Figure 5. (a) Normalized PL spectrum (black curve) of a 3TBT crystal at room temperature, together with a fit (green curve) of five Gaussian peaks to reproduce the vibronic structure. This PL spectrum was acquired from a single crystal with a width of 4 μm using a detection area of 1 μm . (b) Normalized PL spectrum (red curve) of a 3TBT crystal at 1.5 K, together with a fit (black curve) of eight Gaussian peaks to reproduce the vibronic structure. This 1.5 K PL spectrum was recorded from a single crystal with a width of about 1 μm using a detection area of ~ 600 nm. (c) Superposed on an AFM topography image (size $16.5 \times 16.5 \mu\text{m}^2$), schematic representation of the change in detection area centered on the crystal. The width of the crystal is 4 μm . (d) 0–1/0–0 intensity ratio of the room-temperature PL spectrum of the single crystal shown in (c) as a function of detection diameter, together with the corresponding values measured for a spin-coated film.

changed with θ . We observed the strongest absorption when the exciting light was polarized in the plane perpendicular to the long axis of the crystal, that is, $\theta = 90^\circ$. Lowest absorption, especially in the range from about 2.48 to 2.29 eV, where H-aggregate absorption prevailed (Figure 3a), was observed when the long axis of the crystal was parallel to the polarization plane, that is, $\theta = 0^\circ$. Under the latter conditions, the shoulder around 2.29 eV nearly disappeared. This indicates that the electronic transition at energies less than about 2.29 eV was only possible for light polarized perpendicular to the long axis of the crystal. In other words, the transition dipole moments of the absorbing aggregates are oriented almost exclusively perpendicular to the long crystal axis. The dichroic ratio, $R = A_{\text{max}}/A_{\text{min}}$ ²⁶ at 2.29 eV, shown in Figure 3b, was found to be about 20. The dependence of the absorption behavior of 3TBT crystals on polarization direction was highly reproducible. Thus, the crystalline structure contained well-aligned molecules absorbing light only when polarized appropriately. The small dichroic ratio R at higher energies (around 2.8 eV) suggests a more isotropic distribution of transition dipole moments, which can be related to the

presence of randomly oriented, nonaggregated 3TBT molecules on the crystal surface.

The most prominent driving force for crystallization is provided by π – π interactions between coplanar molecules. Thus, the fastest growth direction is expected to be along this π – π stacking direction. Considering that the transition dipole moment of 3TBT molecules is along the long axis of the molecule,¹⁷ the results of Figure 3 indicate that within the crystals the long axis of 3TBT molecules was orthogonal to the long axis of the crystal (Figure 4). This orientation is consistent with the assumption that the fast growth rate induced by π – π stacking of molecules is responsible for the length of the crystal.

A similar understanding concerning the orientation of the 3TBT molecule within the single crystal can be derived by determining the polarization direction of the light emitted from a single crystal (Figure 3c). As expected, the intensity varied when the analyzer direction was changed. The highest and lowest emission intensity (I_{max} and I_{min} , respectively) were found when the direction of the analyzer, characterized by the angle ψ , was perpendicular ($\psi = 90^\circ$) and parallel ($\psi = 0^\circ$), respectively, to the long axis of the single crystal (differences in emission spectra

taken at $\psi = 90^\circ$ and $\psi = 0^\circ$ is related to the different absorptions for light polarized perpendicular ($\psi = 90^\circ$) and parallel ($\psi = 0^\circ$) to the long axis of the crystal, see also Figure S9). The emission dichroic ratio, defined by $R_d = I_{\max}/I_{\min}$, was about 15 ± 1.5 for maximum emission at 2.13 eV, and the corresponding anisotropy value $r = (R_d - 1)/(R_d + 1)$ was 0.87 ± 0.01 . This anisotropy value is among the highest values reported so far for both, inorganic and organic materials: $r = 0.6$ for nanowires of a conjugated polymer;²⁷ $r = 0.7$ – 0.86 for single-crystalline CdSe nanorods;²⁸ $r = 0.80$ for organic crystals based on ionic perylenemonoimide;²⁹ $r = 0.82$ single-crystalline organic nanobelts of perylene-carboxylic diimides (PTCDI);³⁰ and $r = 0.71$ for organic microbelts generated by hydrogen bonding between guanidinium cations and stilbene-based sulfonate anions.³¹ In addition, the ψ -dependent photoluminescence intensity at 2.13 eV fitted by a $\cos^2 \psi$ -function (shown in Figure 3d) is supporting our conclusion of perfectly aligned 3TBT molecules within the single crystal.

Spectroscopic Signature of Transition from Disorder to Order. As discussed in the previous sections, large 3TBT single crystals grown in solution exhibited a high degree of molecular order. However, during the deposition of the crystals by spin-coating the solution onto the substrate also dissolved molecules were adsorbed on both the crystal and the surrounding substrate, which, after rapid evaporation of the solvent, generated nanoscopic randomly oriented fiber-like aggregates and isolated molecules around the crystals, contributing to the PL spectra. Comparing PL spectra of single crystals with those of spin-coated films enables us to establish a relation between molecular order and specific features of the emission spectra. Thus, the emission spectra can be calibrated to provide a measure of the contribution of ordered and disordered regions in the PL spectra.

In order to quantitatively investigate differences in the spectroscopic features between disordered and ordered 3TBT structures, we analyzed the emission spectra in terms of decomposition into Gaussian functions (Figure 5a). PL spectra of 3TBT crystals and films taken at room temperature showed three dominating peaks. Because their relative energy differences are about 170 meV (1400 cm^{-1}), we associate this structure with the purely electronic transition, the aromatic carbon-bond stretch mode with an energy of about 170 meV (1400 cm^{-1}) and its overtone. In the following, we will refer to these peaks as $0 - n$ ($n = 0, 1, 2$) peaks in order of decreasing energy. Unfortunately, a simple decomposition of the PL spectra using three Gaussian functions did not yield satisfactory results. We had to use five Gaussian functions in total, for which their full widths at half-maximum (fwhm) and their areas were adjustable parameters, to give the best fit to the experimental data (see Tables S1 and S2 and Figures S4 and S5 for an illustration of this decomposition procedure). The energies of the Gaussian peaks were approximately the same for films and single crystals, but the relative intensities of the various peaks changed (Figure S6). In order to justify the use of five Gaussian functions and to reveal the origin of the additional peaks between the $0 - n$ transitions, we performed PL spectroscopy on single crystals at 1.5 K (for the experimental setup, see Supporting Information and our previous paper³²). When reducing the temperature, the line widths of electronic/vibronic transitions are typically strongly reduced and therefore subtle features can be resolved in optical spectra that are blurred out at room temperature (see Supporting Information, Figure S7). As depicted in Figure 5b, in the PL spectrum of the crystal at 1.5 K, the three dominating peaks due to the aromatic carbon-bond stretch mode are still present, yet,

several shoulders and smaller maxima between those main peaks are clearly identified. This rich structure of the low temperature spectrum can only be reproduced accurately by, in total, eight Gaussian functions. The lowest-energy peak A is ascribed to the purely electronic $0 - 0$ transition of the 3TBT crystal and peaks E and H represent the $0 - 1$ and $0 - 2$ transitions of the aromatic carbon-bond stretch. The remaining peaks can be attributed to various intramolecular vibrational modes, which are discussed in the Supporting Information, Figure S7).

Notably, the inhomogeneous line width of the $0 - 0$ transition of the crystal was only 33 meV (fwhm) at 1.5 K, which again demonstrates the extraordinarily high degree of order within single crystals. At room temperature, the line width (fwhm) of all peaks became much broader, so that neighboring lines separated by less than about 60 meV cannot be resolved in the spectra any more. Consequently, the use of five Gaussian functions to fit the room temperature PL is certainly justified, with some peaks actually representing superpositions of two vibronic transitions (see Supporting Information for details).

Contributions to the room temperature PL spectra from ordered and disordered regions in crystals were evaluated by analyzing the peak intensity ratios between the purely electronic $0 - 0$ and the $0 - 1$ vibrational transition of the carbon-bond stretch mode, following the approach put forward by Spano and co-workers. We note that although we are neglecting all other vibronic modes that are visible in the PL spectra, this approach still yields qualitatively correct insight into PL from ordered/disordered regions (see Supporting Information). In a first experiment, we studied a single crystal with a width of $4 \mu\text{m}$, and we progressively increased the detection area for the PL, ranging from a small spot with a diameter of $1 \mu\text{m}$, which was exclusively within a single crystal, up to a large area with a diameter of $20 \mu\text{m}$, which covered crystal and surrounding matrix of less-ordered 3TBT molecules (Figure 5c). In this experiment, the whole sample was excited with a visible LED. As a reference, we performed the same measurements on a homogeneous spin-coated film.

As shown in Figure 5d, we found that the $0 - 1/0 - 0$ intensity ratio of the PL from the crystal decreased with increasing detection diameter. The ratio changed from 18, when exclusively detected from within the crystal, to about 5–6, when PL from both crystal and surrounding matrix was recorded. In contrast, for a spin-coated film the $0 - 1/0 - 0$ intensity ratio was about 2 and independent of the detection area. For determining the error bar of these values, we took into account uncertainties in determining the peak position ($\pm 10 \text{ meV}$) and the optical resolution of the microscope for the detection diameter.

For a detection area fully within the crystal, we measured the emission only from the single crystal and probably a few molecules underneath and on top of the crystal, which were deposited there during spin-coating. In this situation, the very high $0 - 1/0 - 0$ intensity ratio, or in other words, the strongly suppressed $0 - 0$ transition reflects the extraordinary structural order of the crystal. For a detection area bigger than the crystal, we obtained simultaneously contributions from ordered (single crystal) and less ordered regions (randomly oriented) nanometer-sized aggregates with lower degree of order and smaller electronic interactions in the surrounding of the crystal). This yields in total a reduced $0 - 1/0 - 0$ ratio with increasing detection area. The film PL was always averaged over many, randomly oriented nanoscale aggregates (see Figure S2), which renders the $0 - 1/0 - 0$ peak ratio independent of the detection area. Moreover, the lower degree of order in these aggregates

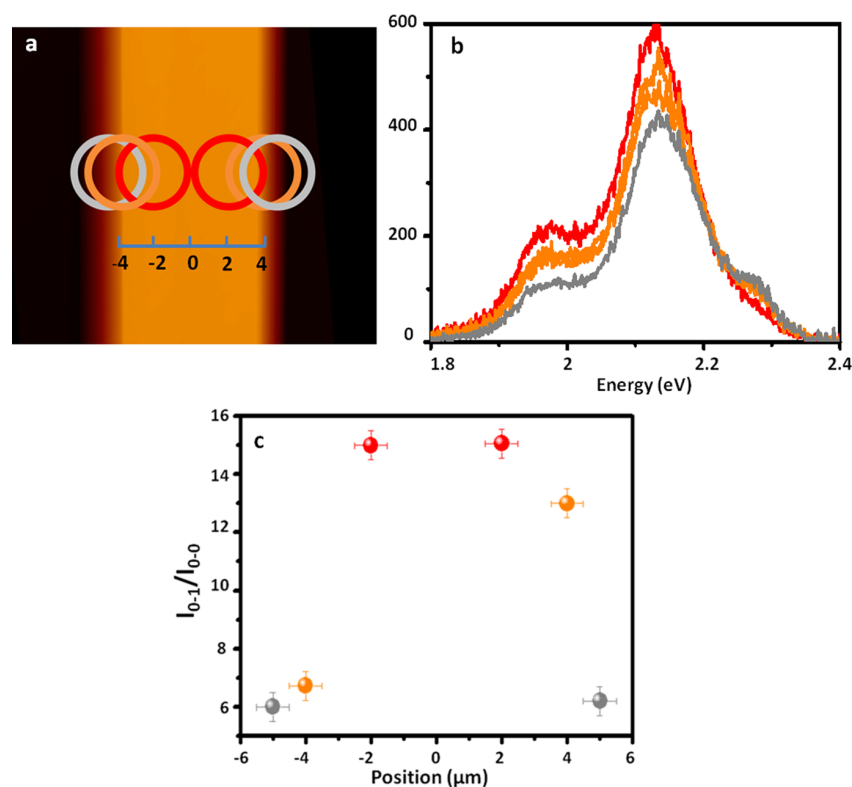


Figure 6. (a) Schematic representation of all measured areas with a diameter of 4 μm , scanned across a crystal having a width of 8 μm . (b) PL spectra from the single crystal when the detection area was moved across the width of the crystal. The color of the curves corresponds to the color of the circles shown in (a). (c) Corresponding 0–1/0–0 intensity ratio as a function of the distance to the center of the crystal, reflecting that less ordered molecules surrounded the single crystal.

compared to single crystals is reflected in the smaller 0–1/0–0 peak ratio in the spin-coated film.

Further evidence for distinct contributions from ordered and less ordered regions to the emission spectra of crystals was obtained by a second experiment, in which a small detection area (diameter 4 μm) was scanned across a crystal having a width of 8 μm , as schematically shown in Figure 6a. By moving the detection area from the disordered to the ordered (crystalline) region, the 0–1/0–0 intensity ratio increased as expected (Figure 6b,c, see also Figure S9).

When chromophores arranged in a cofacial π -stacked fashion interact electronically, the relative peak intensities of the optical spectra of an ideal disorder-free crystal are changed relative to those of an isolated chromophore. In particular, the electronic 0–0 transition is entirely forbidden but becomes (weakly) allowed when the symmetry is broken by the presence of structural and electronic disorder. In contrast, the intensities of the 0–1, 0–2 peaks of the dominating carbon–carbon bond stretch are largely unaffected by the electronic interaction. As a consequence, the ratio of the oscillator strength of the first two vibronic peaks in the PL spectra (0–1/0–0) decreases with increasing disorder.^{20,23} The intermolecular interaction-induced changes in the vibronic line strengths therefore reveal information about the exciton bandwidth (the magnitude of the electronic interaction), the degree of disorder, and the exciton coherence lengths.^{33–35} Our results show that an increase of the contribution from the ordered region (single crystal) led to an increase in the 0–1/0–0 intensity ratio. Thus, the relative intensities of vibronic peaks in emission spectra can indeed be considered as signatures of disorder and order.

CONCLUSIONS

In summary, we identified and controlled the contribution of ordered and disordered regions in emission spectra by performing local spectroscopic measurements. Our results show that the characteristic energies of the emitted photons were almost the same, independent if highly ordered or rather disordered samples were examined. However, the relative emission intensities changed significantly between ordered and disordered samples. Thus, by investigating these changes we quantified the degree of structural order in our samples of a semiconducting molecule.

ASSOCIATED CONTENT

Supporting Information

The Supporting Information is available free of charge on the ACS Publications website at DOI: 10.1021/acsp Photonics.6b00473.

AFM images of spin coated film and top surface of the crystal and detailed analysis of absorbance and PL spectra of spin coated film and crystal at 1.5K and room temperature (PDF).

AUTHOR INFORMATION

Corresponding Author

*E-mail: guenter.reiter@physik.uni-freiburg.de.

ORCID

Günter Reiter: 0000-0003-4578-8316

Author Contributions

The manuscript was written through contributions of all authors. All authors have given approval to the final version of the manuscript.

Notes

The authors declare no competing financial interest.

ACKNOWLEDGMENTS

This work is supported by the German Research Foundation (DFG, RE 2273/6-1 and IRTG Soft Matter Science (IGRK 1642)). Authors are thankful to Roozbeh Shokri and Yingying Wang for fruitful discussions. Dominic Raithel and Richard Hildner acknowledge funding from the German Research Foundation DFG (HI1508/2 and GRK1640) and thank S. Pickel and C. Schörner for their assistance during data analysis.

REFERENCES

- (1) Friend, R. H.; Gymer, R. W.; Holmes, a. B.; Burroughes, J. H.; Marks, R. N.; Taliani, C.; Bradley, D. D. C.; Dos Santos, D. a.; Bredas, J. L.; Logdlund, M.; Salaneck, W. R. Electroluminescence in Conjugated Polymers. *Nature* **1999**, *397*, 121–128.
- (2) Arias, A. C.; MacKenzie, J. D.; McCulloch, I.; Rivnay, J.; Salleo, A. Materials and Applications for Large Area Electronics: Solution-Based Approaches. *Chem. Rev.* **2010**, *110*, 3–24.
- (3) Dimitrakopoulos, C. D.; Malenfant, P. R. L. Organic Thin Film Transistors for Large Area Electronics. *Adv. Mater.* **2002**, *14*, 99–117.
- (4) Halls, J. J. M.; Walsh, C. a.; Greenham, N. C.; Marseglia, E. a.; Friend, R. H.; Moratti, S. C.; Holmes, a. B. Efficient Photodiodes From Interpenetrating Polymer Networks. *Nature* **1995**, *376*, 498–500.
- (5) Yu, G.; Gao, J.; Hummelen, J. C.; Wudl, F.; Heeger, a. J. Device Structure Consisted Polymer Photovoltaic Cells: Enhanced Efficiencies via a Network of Internal Donor-Acceptor Heterojunctions. *Science* **1995**, *270*, 1789–1791.
- (6) Murphy, A. R.; Fréchet, J. M. J. Organic Semiconducting Oligomers for Use in Thin Film Transistors. *Chem. Rev.* **2007**, *107*, 1066–1096.
- (7) Siringhaus, H.; Brown, P. J.; Friend, R. H.; Nielsen, M. M.; Bechgaard, K.; Langeveld-Voss, B. M. W.; Spiering, a. J. H.; Janssen, R. a. J.; Meijer, E. W.; Herwig, P.; de Leeuw, D. M. Two-Dimensional Charge Transport in Self-Organized, High-Mobility Conjugated Polymers. *Nature* **1999**, *401*, 685–688.
- (8) Salleo, A.; Kline, R. J.; DeLongchamp, D. M.; Chabincyn, M. L. Microstructural Characterization and Charge Transport in Thin Films of Conjugated Polymers. *Adv. Mater.* **2010**, *22*, 3812–3838.
- (9) Reese, C.; Bao, Z. Organic Single-Crystal Field-Effect Transistors. *Mater. Today* **2007**, *10*, 20–27.
- (10) Crossland, E. J. W.; Tremel, K.; Fischer, F.; Rahimi, K.; Reiter, G.; Steiner, U.; Ludwigs, S. Anisotropic Charge Transport in Spherulitic Poly(3-Hexylthiophene) Films. *Adv. Mater.* **2012**, *24*, 839–844.
- (11) Rahimi, K.; Botiz, I.; Stingelin, N.; Kayunkid, N.; Sommer, M.; Koch, F. P. V.; Nguyen, H.; Coulembier, O.; Dubois, P.; Brinkmann, M.; Reiter, G. Controllable Processes for Generating Large Single Crystals of poly(3-Hexylthiophene). *Angew. Chem., Int. Ed.* **2012**, *51*, 11131–11135.
- (12) Haedler, A. T.; Kreger, K.; Issac, A.; Wittmann, B.; Kivala, M.; Hammer, N.; Köhler, J.; Schmidt, H.-W.; Hildner, R. Long-Range Energy Transport in Single Supramolecular Nanofibres at Room Temperature. *Nature* **2015**, *523*, 196–199.
- (13) Noriega, R.; Rivnay, J.; Vandewal, K.; Koch, F. P. V.; Stingelin, N.; Smith, P.; Toney, M. F.; Salleo, A. A General Relationship between Disorder, Aggregation and Charge Transport in Conjugated Polymers. *Nat. Mater.* **2013**, *12*, 1038–1044.
- (14) Jiménez, Á. J.; Lin, M.-J.; Burschka, C.; Becker, J.; Settels, V.; Engels, B.; Würthner, F. Structure–property Relationships for 1,7-Diphenoxy-Perylene Bisimides in Solution and in the Solid State. *Chem. Sci.* **2014**, *5*, 608.
- (15) Silva, R. A.; Bouachrine, M.; Le, J.; Moreau, J. E. Synthesis and Characterization of Thienylene – Phenylene Copolymers with Oligo (Ethylene Oxide) Side Chains. *J. Mater. Chem.* **2004**, *14*, 3043–3050.
- (16) Lois, S.; Florès, J. C.; Lère-Porte, J. P.; Serein-Spirau, F.; Moreau, J. J. E.; Miqueu, K.; Sotiropoulos, J. M.; Baylère, P.; Tillard, M.; Belin, C. How to Build Fully Π -Conjugated Architectures with Thienylene and Phenylene Fragments. *Eur. J. Org. Chem.* **2007**, *2007*, 4019–4031.
- (17) Narayanan Nair, M.; Hobeika, N.; Calard, F.; Malval, J. P.; Aloise, S.; Spangenberg, a.; Simon, L.; Cranney, M.; Vonau, F.; Aubel, D.; Serein-Spirau, F.; Lère-Porte, J. P.; Lacour, M. a.; Jarrosson, T. One- and Two-Photon Absorption and Emission Properties of an Oligo-(phenylenethienylene)s Series. *Phys. Chem. Chem. Phys.* **2014**, *16*, 12826–12837.
- (18) Shokri, R.; Lacour, M. A.; Jarrosson, T.; Serein-spirau, F.; Miqueu, K.; Sotiropoulos, J.; Aubel, D.; Cranney, M.; Reiter, G.; Simon, L. Generating Long Supramolecular Pathways with a Continuous Density of States by Physically Linking Conjugated Molecules via Their End Groups. *J. Am. Chem. Soc.* **2013**, *135*, 5693.
- (19) Gierschner, J.; Park, S. Y. Luminescent Distyrylbenzenes: Tailoring Molecular Structure and Crystalline Morphology. *J. Mater. Chem. C* **2013**, *1*, 5818.
- (20) Spano, F. C.; Silva, C. H- and J-Aggregate Behavior in Polymeric Semiconductors. *Annu. Rev. Phys. Chem.* **2014**, *65*, 477–500.
- (21) Rahimi, K.; Botiz, I.; Agumba, J. O.; Motamen, S.; Stingelin, N.; Reiter, G. Light Absorption of poly(3-Hexylthiophene) Single Crystals. *RSC Adv.* **2014**, *4*, 11121.
- (22) Gierschner, J.; Oelkrug, D.; Egelhaaf, H. Highly Emissive H Aggregates or Aggregation-Induced Emission Quenching? The Photo-physics of All-trans para-Distyrylbenzene. *J. Phys. Chem. Lett.* **2013**, *4*, 2686–2697.
- (23) Spano, F. C. The Spectral Signatures of Frenkel Polarons in H- And J-Aggregates. *Acc. Chem. Res.* **2010**, *43*, 429–439.
- (24) Panzer, F.; Sommer, M.; Bässler, H.; Thelakkat, M.; Köhler, A. Spectroscopic Signature of Two Distinct H-Aggregate Species in poly(3-Hexylthiophene). *Macromolecules* **2015**, *48*, 1543–1553.
- (25) O'Carroll, D.; Redmond, G. Highly Anisotropic Luminescence from Poly(9,9-dioctylfluorene) Nanowires Doped with Orientationally Ordered-Phase Polymer Chains. *Chem. Mater.* **2008**, *20*, 6501–6508.
- (26) Montali, A.; Bastiaansen, C.; Smith, P.; Weder, C. Polarizing Energy Transfer in Photoluminescent Materials for Display Applications. *Nature* **1998**, *392*, 261–264.
- (27) Movnihan, S.; Lovera, P.; O'Carroll, D.; Iacopino, D.; Redmond, G. Alignment and Dynamic Manipulation of Conjugated Polymer Nanowires in Nematic Liquid Crystal Hosts. *Adv. Mater.* **2008**, *20*, 2497–2502.
- (28) Hu, J. Linearly Polarized Emission from Colloidal Semiconductor Quantum Rods. *Science* **2001**, *292*, 2060–2064.
- (29) Huang, L.; Tam-Chang, S. W.; Seo, W.; Rove, K. Microfabrication of Anisotropic Organic Materials via Self-Organization of an Ionic Perylenemonoimide. *Adv. Mater.* **2007**, *19*, 4149–4152.
- (30) Che, Y.; Yang, X.; Balakrishnan, K.; Zuo, J.; Zang, L. Highly Polarized and Self-Waveguided Emission from Single-Crystalline Organic Nanobelts. *Chem. Mater.* **2009**, *21*, 2930–2934.
- (31) Yan, D.; Jones, W.; Fan, G.; Wei, M.; Evans, D. G. Organic Microbelt Array Based on Hydrogen-Bond Architecture Showing Polarized Fluorescence and Two-Photon Emission. *J. Mater. Chem. C* **2013**, *1*, 4138–4145.
- (32) Baderschneider, S.; Scherf, U.; Köhler, J.; Hildner, R. Influence of the Conjugation Length on the Optical Spectra of Single Ladder-Type (p-Phenylene) Dimers and Polymers. *J. Phys. Chem. A* **2016**, *120*, 233–240.
- (33) Spano, F. C. Modeling Disorder in Polymer Aggregates: The Optical Spectroscopy of Regioregular Poly(3-hexylthiophene) Thin Films. *J. Chem. Phys.* **2005**, *122*, 234701.
- (34) Spano, F. C. Absorption in Regio-Regular poly(3-Hexyl)-thiophene Thin Films: Fermi Resonances, Interband Coupling and Disorder. *Chem. Phys.* **2006**, *325*, 22–35.
- (35) Spano, F. C.; Yamagata, H. Vibronic Coupling in J-Aggregates and beyond: A Direct Means of Determining the Exciton Coherence Length

from the Photoluminescence Spectrum. *J. Phys. Chem. B* **2011**, *115*, 5133–5143.

Supporting Information

Revealing Order and Disorder in Films and Single Crystals of a Thiophene-Based Oligomer by Optical Spectroscopy

Sajedeh Motamen¹, Dominic Raithe², Richard Hildner², Khosrow Rahimi³, Thibaut Jarrosson⁴,
Françoise Serein-Spirau⁴, Laurent Simon⁵, Günter Reiter¹

¹Physikalisches Institut, Albert-Ludwigs-Universität, 79104 Freiburg, Germany

²Experimentalphysik IV, University of Bayreuth, 95440 Bayreuth, Germany

³DWI-Leibniz Institute for Interactive Materials, Forckenbeckstr. 50, 52056 Aachen, Germany

⁴Institut Charles Gerhardt de Montpellier, UMR 5353-CNRS Equipe Architectures Moleculaires et Matériaux Nanostructurés (AM2N), Ecole Nationale Supérieure de Chimie de Montpellier, 8 Rue de l'Ecole Normale, 34296 Montpellier cedex 05, France

⁵Institut de Sciences des Matériaux de Mulhouse IS2M, UMR7361 CNRS-UHA, 3 bis rue Alfred Werner, 68093 Mulhouse, France.

AFM Measurements:

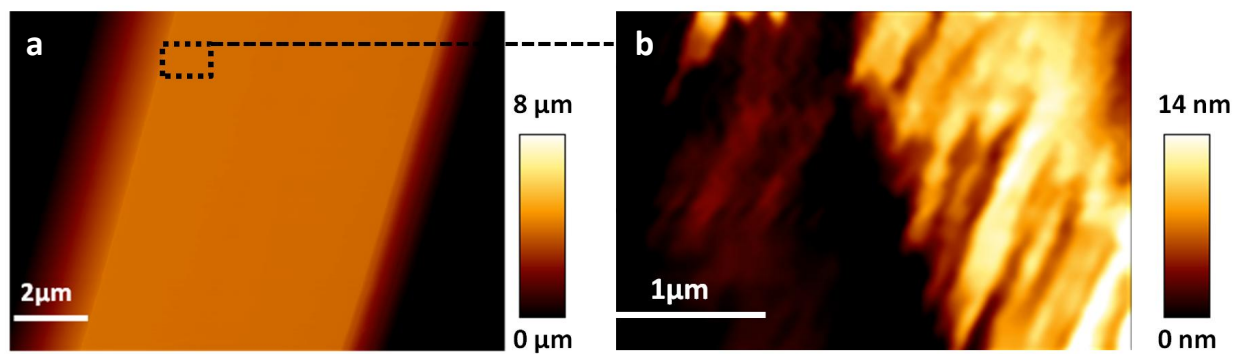


Figure S1: a) AFM height image of a 3TBT single crystal obtained by crystallization at 60 °C from a 0.1 g/L solution in dodecane and spin-coated onto a solid substrate. b) AFM height image of the area within the dashed box in a) showing fluctuations of height on the surface of the crystal.

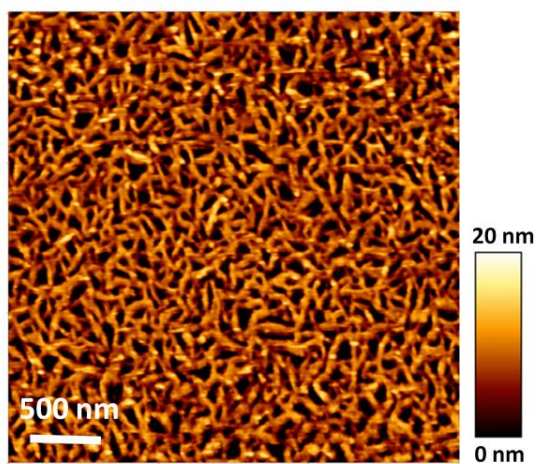


Figure S2: AFM height image of a 3TBT thin film (15 ± 3 nm) spin coated from solution onto a solid substrate (2 g/L in dodecane).

Absorbance Measurements:

In order to determine the electronic interaction between nearest-neighbor 3TBT molecules in single crystals and in nanoscale aggregates in spin-coated films, we analyzed the corresponding room temperature absorption spectra. The absorption from both samples exhibits a pronounced peak around 2.7 – 2.8 eV (see Figure 2a and S3), which indicates the presence of a non-negligible fraction of non-aggregated (“amorphous”) 3TBT molecules. To correct the measured film and crystal spectra for the absorption of non-aggregated molecules, we scaled and shifted the solution absorption (Figure. 2a, red spectrum), such that we obtain the best fit to the highest-energy part of both the film and crystal absorption. The best agreement is achieved with a blue shifted solution spectrum by 120 meV (see Figure S3); this spectral shift represents a polarization energy and accounts for different dielectric environments for the non-aggregated 3TBT molecules (solution: solvent; film/crystal: 3TBT). Note that especially the film spectrum is not perfectly reproduced at high energies, which may be due to scattering on the nanoscale crystallites (see Figure S2). Subsequently, we subtracted the scaled and shifted “solution” spectrum to obtain the absorption spectrum exclusively of interacting 3TBT molecules in crystals/films.

This latter spectrum is then numerically simulated based on the framework developed by Spano and co-workers^{1,2}, which allows to retrieve the nearest-neighbor electronic interaction between 3TBT molecules.

These simulations required as input parameters the Huang-Rhys factor S and the vibrational energy E_{vib} of the dominating aromatic carbon-bond stretch mode of isolated, non-interacting 3TBT molecules, which we determined from the PL spectrum of molecularly dissolved 3TBT in dodecane (see Figure. 2b of the main text) to $S = 0.85$ and $E_{vib} = 170$ meV. Moreover, we limited the number of interacting 3TBT molecules to 20, which is a compromise between size of the system and computational time. The best agreement between experiment and simulations was obtained using a free exciton bandwidth W of 164 meV for the crystal and 43 meV for the film (Figure S3). Because W is related to the nearest-neighbor interaction J by $W = 4J$, we finally get $J = 41$ meV (crystal) and $J = 11$ meV (film).

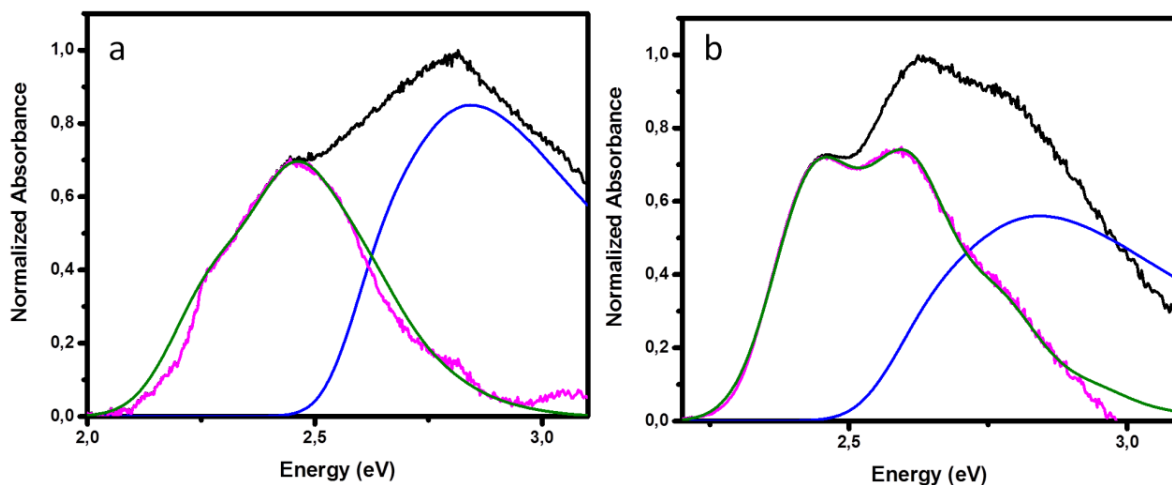


Figure S3: a) Normalized absorbance spectrum of a 3TBT single crystal (black), the scaled and spectrally shifted solution absorption (blue), the difference spectrum (pink), and the simulated spectra (green). (b) Normalized absorbance spectrum of a spin-coated 3TBT film (black), the scaled and spectrally shifted solution absorption (blue), the difference spectrum (pink), and the simulated spectra (green).

In principle, the data in Figure S3 allow to retrieve the fraction of non-interacting 3TBT molecules in both samples from the relative areas under the scaled and shifted solution absorption and the difference spectrum (weighted by the different oscillator strengths for aggregates and non-interacting molecules). For the spectrum of the spin-coated film the relative areas are 45 % for the solution contribution and 55 % for the remaining aggregate spectrum. Hence, there is still a substantial fraction of non-interacting molecules, which is expected as a result of very fast evaporation of the solvent. For the measured crystal spectrum, we obtain a similar ratio of areas: 55 % for solution and 45 % for the crystal contribution. This large fraction of non-interacting molecules in the crystal spectrum is clearly a strong overestimation, because in the measured crystal spectrum also the absorption of a fraction of nanoscale aggregates (as in spin-coated films) will contribute (see AFM image in Figure S1b). We note that a deconvolution of the total crystal absorption spectrum into “true” crystal, nanoscale aggregate and solution contribution to obtain the relative areas, was not possible (in fact such deconvolution would require prior knowledge of the relative areas and exact

polarization energies of all contributions, which is not available). From the AFM data (Figure S1), we can estimate a non-crystalline contribution of about 10 %. Also from the sharply peaked dichroic ratio of the crystal (Figure 3b) the contribution of both the nanoscale aggregate and solution contribution to the measured crystal absorption is visible. The nanoscale aggregates absorb at 2.4 eV and higher energies (Figure S3b), yet their orientations on the crystal are not unique as for the crystal orientation itself (see Figure S1b), and hence, absorption of the aggregates will not show a strong polarization dependence. This explains why the dichroic ratio is strongly peaked only around 2.25 eV, where exclusively the crystal with its strongly polarization-dependent absorption contributes.

PL Measurements:

The room-temperature PL spectra of a 3TBT film and a single crystal exhibit three peaks/shoulders with an energy spacing of approximately 170 meV (1400 cm^{-1}), representing the purely electronic transition, a vibronic transition into the aromatic carbon-bond stretch and its overtones (0-0, 0-1, 0-n) (Figure S4 and S5). However, fitting of these spectra with three Gaussian functions was not possible, only a fit with five Gaussians yielded satisfactory results. The full width at half maximum (fwhm) and the area of the Gaussians were treated as adjustable parameters to give the best fit to the experimental data. We attempted to represent the data by the smallest as possible number of different vibronic families. In the fits in Figure S4 and S5 the red curves represent the carbon-carbon bond stretch vibration with energy of 170 meV (1400 cm^{-1}), while the blue and pink curves can be attributed to (superpositions of) other intra-molecular vibrations of 3TBT based on low-temperature spectra (see Figure S7).

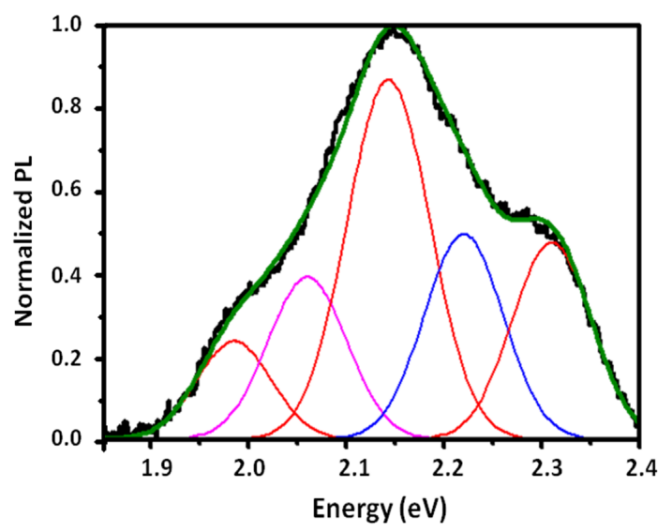


Figure S4: Normalized PL spectrum (black curve) of 3TBT **film** at room temperature, together with a fit (green curve) of five Gaussian peaks.

Gaussian	Peak Position [eV]	Integrated Area	Full Width at Half Maximum FWHM [eV]	Intensity at Peak Position [Counts]	Relative Integrated Area [%]
Peak 1	2.31	0.047	0.095	0.475	18.89
Peak 2	2.22	0.050	0.095	0.496	19.84
Peak 3	2.143	0.092	0.1	0.869	36.62
Peak 4	2.06	0.039	0.095	0.391	15.67
Peak 5	1.985	0.022	0.09	0.236	8.95

TableS1. Fitting parameters used for the decomposition of photoluminescence spectra of the film.

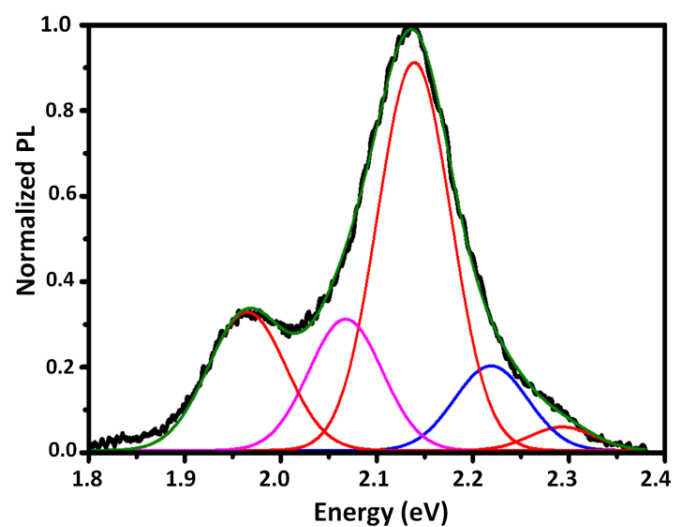


Figure S5: Normalized PL spectrum (black curve) of a 3TBT **crystal** at room temperature, together with a fit (green curve) of five Gaussian peaks to reproduce the vibronic structure. The diameter of the detection area was 1 μm and the width of crystal was 4 μm .

Gaussian	Peak position [eV]	Integrated Area	Full Width at Half Maximum FWHM [eV]	Intensity at Peak Position [Counts]	Relative Integrated Area [%]
Peak 1	2.293	0.004	0.08	0.05	2.70
Peak 2	2.22	0.019	0.09	0.20	10.97
Peak 3	2.14	0.087	0.09	0.90	50.33
Peak 4	2.064	0.029	0.09	0.30	17.03
Peak 5	1.965	0.033	0.095	0.32	18.95

TableS2. Fitting parameters used for the decomposition of photoluminescence spectra of the crystal.

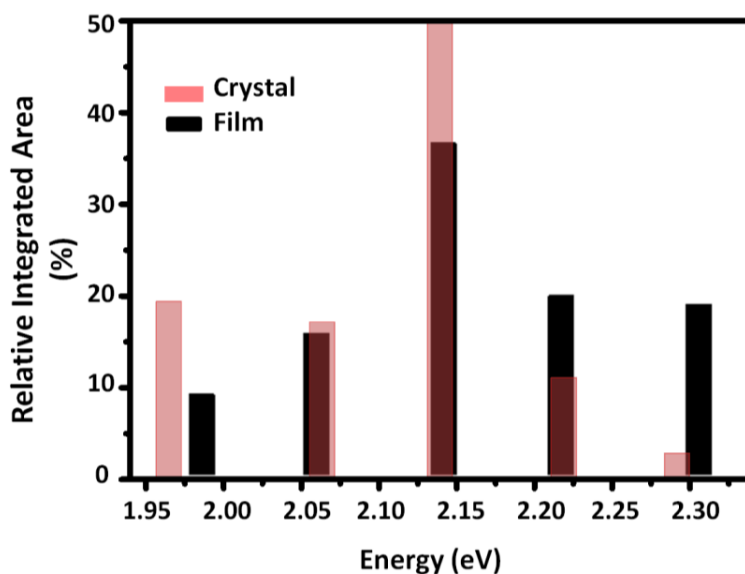


Figure S6: Relative integrated area of five Gaussian peaks fit to the PL spectra of a 3TBT crystal and film at room temperature a function of emitting energy. Width of errors was chosen 0.02 eV.

Low temperature measurements were done using a home-built confocal microscope with a spot size of ~ 600 nm diameter and a pulsed 450 nm diode-laser for excitation. The sample was placed inside of a helium bath-cryostat and cooled to 1.5 K. Low temperature PL spectra from a single crystal exhibited three dominating peaks and a rich sub-structure with minor peaks and shoulders (Figure S7 and table S3). Hence, a decomposition required eight Gaussian peaks. Peak A can be ascribed to the purely electronic 0-0 transition of the PL of the 3TBT crystal. The peaks B – H are attributed to intra-molecular vibrations coupling to the electronic transition based on literature data³⁻⁵: Peak B (29 meV or 232 cm^{-1} relative to the 0-0 transition) is attributed to a superposition of a stretching vibration of the 3TBT backbone, a libration motion of the rings within the 3TBT backbone, and in- and out-of-plane bending. Peaks C (84 meV , 670 cm^{-1}) and D (122 meV , 976 cm^{-1}) stem from ring breathing/deformation modes of thiophene and benzene as well as from CCH-bending and COC- and CS-stretch modes. In most thiophene-based molecules, the aromatic carbon bond stretch with energies around 170 meV (1400 cm^{-1}) couple strongly to the electronic transition, which corresponds to peak E. Consequently, peak H (364

meV, 2910 cm^{-1}) represents the overtone of the aromatic carbon-bond stretch mode E. Peak F (229 meV , 1832 cm^{-1}) may be caused by a carbon-carbon double-bond stretching mode. Peak G (295 meV , 2360 cm^{-1}) is probably a combination vibration, e.g. from peak D and peak E. From this assignment it is clear that most of the eight peaks that are resolved in the low temperature PL spectrum are in fact a superposition of several unresolvable vibrational modes, i.e. vibrational modes with energy separations smaller than the inhomogeneous width. Hence, the use of different line widths for the different peaks is justified. We note that a fit using the same width for all vibronic lines requires in total 10 to 12 Gaussian functions to reproduce the low temperature PL spectrum with the same quality and over the same spectral range. Yet, in this spectrum we can not identify that many peaks and shoulders, and we therefore did limit ourselves to 8 Gaussians only.

The appearance of this rich vibrational structure in the 1.5 K PL spectrum compared to the room temperature PL can be traced back to the strong reduction of the homogeneous line width upon cooling down. Typically, for large organic molecules, such as conjugated polymers and oligomers, the homogeneous line width is below 0.13 meV (1 cm^{-1}) at 1.5 K^{6-8} . Hence, line broadening is dominated by inhomogeneous broadening and all (groups of) vibrational modes with energy separations larger than the inhomogeneous width can be discriminated as distinct peaks/shoulders in the low temperature PL. From the width of the 0-0 transition (peak A, Figure S7 and table S3) the inhomogeneous line width at 1.5 K can be estimated to about 33 meV . In contrast, at room temperature the homogeneous line width is up to 60 meV ($\sim 500\text{ cm}^{-1}$). Consequently, neighboring lines separated by less than ca. 60 meV cannot be resolved as distinct lines any more (neglecting a possible increase in the inhomogeneous line width with increasing temperature due to increasing thermal disorder). This means that peaks A and B of the low temperature spectrum with an energy separation of only 29 meV appear as a single broad line (peak 1) in the room temperature PL; similarly peaks C and D merge into peak 2; finally, peaks F and G give peak 4. Only the strong aromatic carbon-bond stretch (peaks E and H at 1.5 K) still appears as clearly distinct peaks at room temperature as well (peaks 3 and 5).

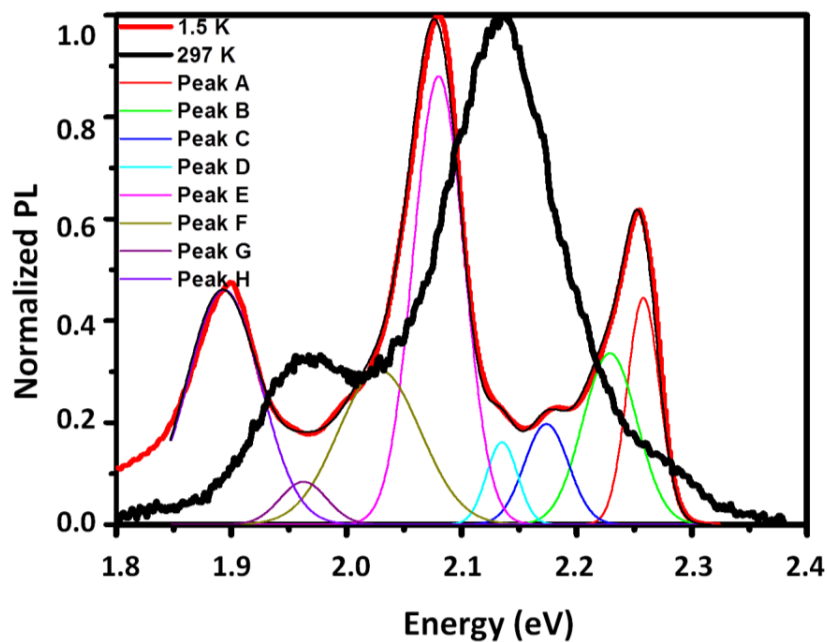


Figure S7: Normalized PL spectra of 3TBT crystal at 1.5 K (red curve) and at room temperature (black curve) were fit to families of Gaussian functions to reproduce the vibronic structure.

Gaussian	Peak Position [eV]	Full Width at Half Maximum FWHM [eV]	Integrated Area
Peak A	2.257	0.033	10.19
Peak B	2.228	0.055	11.33
Peak C	2.173	0.045	4.71
Peak D	2.135	0.0318	2.52
Peak E	2.080	0.051	32.19
Peak F	2.028	0.083	15.73
Peak G	1.962	0.048	1.22
Peak H	1.893	0.075	22.07

TableS3. Fitting parameters used for the decomposition of photoluminescence spectra of the single crystal at 1.5K.

Finally, we note that the relative 0-0 peak intensity decreases from 1.5 K to room temperature and thus shows an unusual temperature-dependence. This behavior cannot be explained in a straightforward way with Spano's approach, because upon heating up the thermal disorder in the crystal increases which is expected to increase the relative 0-0 peak intensity^{9,10}. However, in an perturbative ansatz Spano showed that the 0-0/0-1 intensity ratio is inversely proportional to the square of the free exciton bandwidth W in a regime where energy disorder is not too large^{9,10}. If we then assume that at 1.5 K the 3TBT molecules in the crystal are nearly perfectly arranged and planar, i.e. electronic excitations are fully delocalized over a molecule, whereas at higher temperatures thermal energy allows for small torsional degrees of freedom of 3TBT, which slightly localizes electronic excitations. Owing to this reduction in delocalization, the nearest-neighbor interaction between 3TBT molecules increases with increasing temperature, and thus the 0-0/0-1 intensity ratio decreases (again: if disorder does not increase too strongly). Since it is very difficult, however, to unambiguously determine the energy disorder from our data, we do not wish to make any quantitative statements as to the temperature-dependence of the 0-0/0-1 intensity ratio. The 1.5 K PL spectrum is only meant to justify the use of 5 Gaussian peaks for the fitting of the room temperature data.

Moreover, there are some limitations of Spano's theory: only a single effective vibrational mode is included, whereas we clearly do see a rich vibronic structure; especially low energy vibrational modes exhibit a strong temperature dependence, which is also not included in this theoretical framework; only nearest-neighbor interactions are considered, which is a rather strong approximation for a densely packed system as represented by a 3TBT crystal. Probably, a combined quantum chemistry/molecular mechanics approach as used by Beljonne, Gierschner et al. might be more suited to reproduce the temperature-dependence of our PL spectra¹¹.

An alternative interpretation for this unusual temperature-dependence of the relative 0-0 peak intensity are temperature-dependent energy transfer rates between disordered and ordered regions of the samples. In our PL experiments we predominantly excite disordered regions (excitation energy ~ 2.66 eV, compare Figures 2a, 3b, and S3), from where ordered regions are populated by incoherent hopping processes prior to emission. The transfer rate for incoherent hopping, however, increases with increasing temperature¹², i.e. this transfer is slower at 1.5 K

than at room temperature. Consequently, at low temperatures we may expect emission also from more disordered regions due to incomplete energy transfer to ordered regions. This results in PL spectra with a larger relative 0-0 peak intensity. In contrast, at room temperature this energy transfer is fast and thus highly efficient, which results in emission from nearly exclusively highly ordered regions with a small relative 0-0 peak intensity. Since we cannot deduce the energy transfer rates from our PL measurements, we unfortunately cannot tell which mechanism is responsible for the unusual temperature-dependence of the relative 0-0 peak intensity.

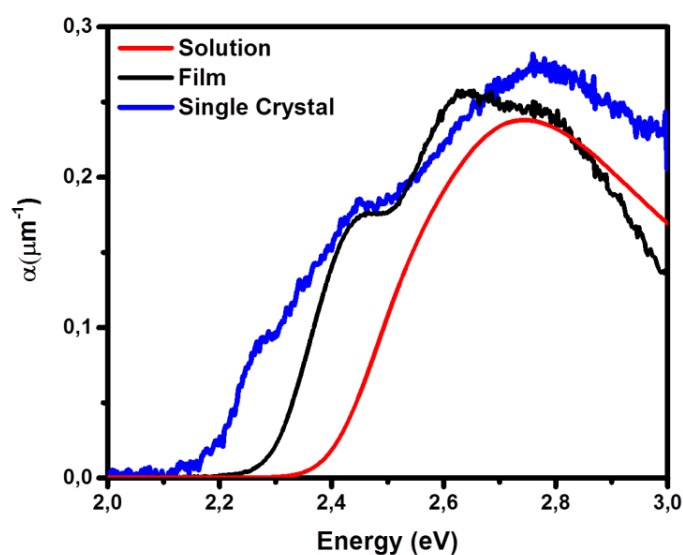


Figure S8: Absorption coefficient of solution (red), film (black) and crystal (blue).

Optical Density of Solution, Film and Single Crystal:

We calculated the absorption coefficient (α) for the film and the single crystal according to the Beer-Lambert law: $A = -\log T = -\frac{1}{\ln 10} \ln T$ with A being the absorbance. The transmittance (T) is defined by: $T = \exp(-\alpha z)$.

Then $A = \frac{\alpha z}{\ln 10} \approx 0.4343 \alpha z$, where z is the thickness of the crystal. The extinction coefficient (ϵ) for the solution was calculated by using: $A = \epsilon c l$, where c is the concentration of the solution and l is the length of the optical path (thickness of the solution).

Figure S8 shows the absorption coefficient of the solution (measuring the absorption of light for an optical path of $1\mu\text{m}$ in the solution), film and crystal. All values are of the same order of magnitude, consistent with results obtained for P3HT by Clark et al¹³.

Comparison of PL spectra of Crystal Measured at Different Polarization Direction:

In Figure S9a, we scaled up the emission spectrum at $\psi = 0^\circ$ (i.e., emitted light is polarized in the direction of the long axis of the crystal). As seen in Figure S9, the intensity ratio I_{0-1}/I_{0-0} decreased by changing the angle between the long axis of the crystal and the analyzer from 90° to 0° . This is related to the different absorptions for light polarized perpendicular ($\psi = 90^\circ$) and parallel ($\psi = 0^\circ$) to the long axis of the crystal. For PL in the energy range 2.3 eV with polarization parallel ($\psi = 0^\circ$) to the long axis the overlap with the absorption is negligible, as evident from the corresponding absorption spectrum (Figure 3a, red line). Hence, reabsorption does not take place. For light polarized perpendicularly, there is some overlap between absorption and emission, and some reabsorption takes place. These data provide further evidence that reabsorption is only a minor effect in our PL spectra of crystals, and cannot account for the difference between film and crystal PL.

Figure S9b, shows normalized PL spectra taken at the center and the edge of the crystal. By moving the detection area (diameter of $4\mu\text{m}$) from the ordered (crystalline) to the disordered (film) region, the intensity ratio I_{0-1}/I_{0-0} changed from 17 to 5. When changing the angle between the long axis of the crystal and the analyzer from 90° to 0° , the intensity ratio I_{0-1}/I_{0-0} decreased from 12 to 6.5 (Figure S9a). In other words, although reabsorption probably contributes in the change of this I_{0-1}/I_{0-0} ratio, reabsorption certainly cannot account for observed change in this ratio when going from the centre to the edge of the crystal.

Furthermore, we have measured dichroic ratio at the center, edge and far outside of the crystal. Figure S9c clearly shows that the dichroic ratio decreased by moving the detection area from the ordered (crystalline) to the disordered (film) region. These results confirm that changing the contribution of ordered region in the detection area influences the emission spectra with respect to the dichroic ratio and the intensity ratio I_{0-1}/I_{0-0} .

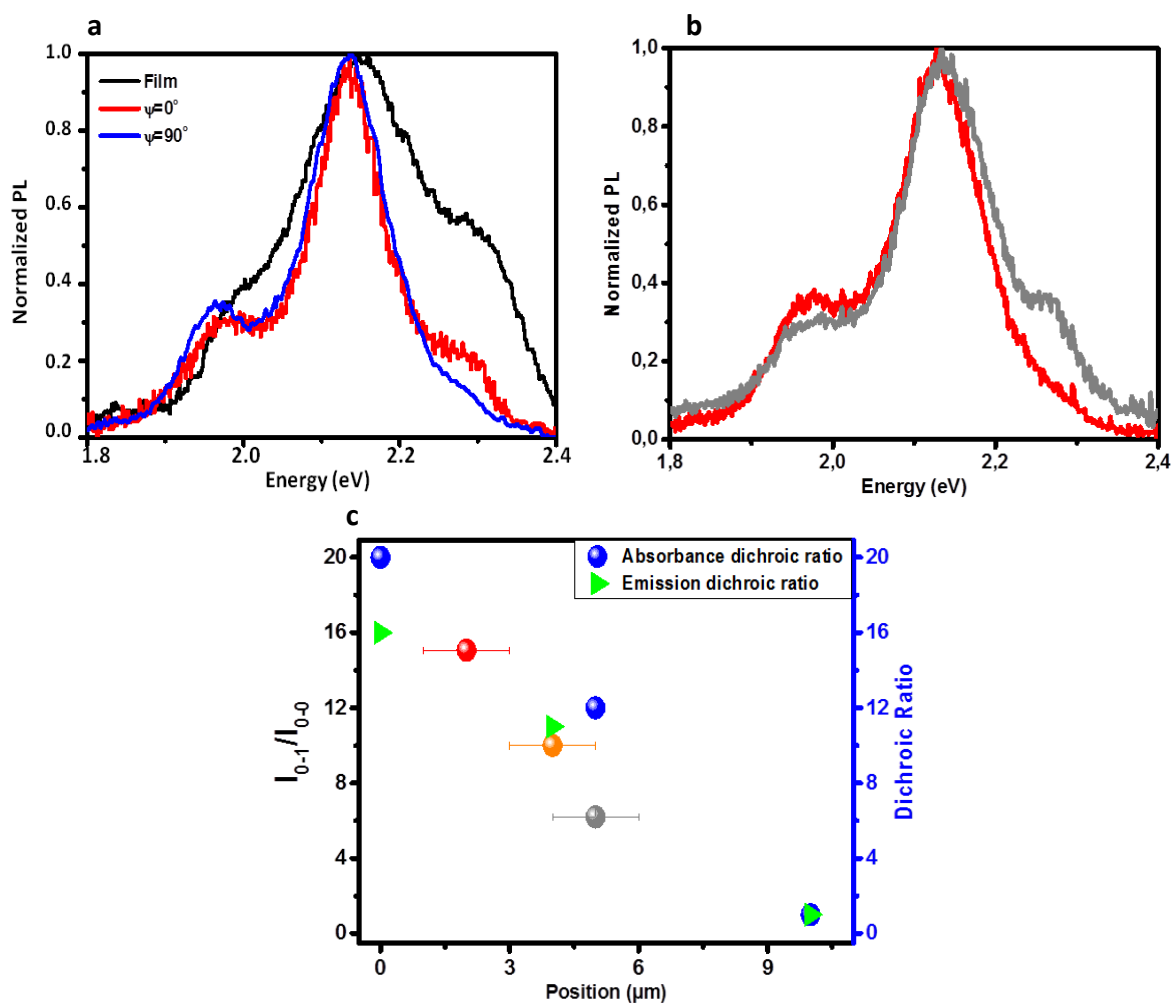


Figure S9: a) Normalized PL spectra of a 3TBT single crystal measured at the center of the crystal at normal incidence (dichroic ratio is 15), where ψ is the angle between the long axis of the crystal and analyzer together with the normalized PL spectrum from an as-cast 3TBT film. b) Normalized PL spectra taken at the edge (gray) and center of the crystal (red). c) Intensity ratio I_{0-1}/I_{0-0} as a function of the distance to the center of the crystal, compared with the corresponding dichroic ratio (blue and green).

References:

- (1) Spano, F. C. The Spectral Signatures of Frenkel Polarons in H- And J-Aggregates. *Acc. Chem. Res.* **2010**, *43*, 429–439.
- (2) Spano, F. C. Modeling Disorder in Polymer Aggregates: The Optical Spectroscopy of Regioregular poly(3-Hexylthiophene) Thin Films. *J. Chem. Phys.* **2005**, *122*.
- (3) Degli Esposti, a; Moze, O.; Taliani, C.; Tomkinson, J. T.; Zamboni, R.; Zerbetto, F. The Intramolecular Vibrations of Prototypical Polythiophenes. *J. Chem. Phys.* **1996**, *104*, 9704–9716.
- (4) Bouachrine, M.; Bouzakraoui, S.; Hamidi, M.; Ayachi, S.; Alimi, K.; Lère-Porte, J. P.; Moreau, J. Synthesis and Characterization of Co-Polymers Involving Various Thiophene and Phenylene Monomers. *Synth. Met.* **2004**, *145*, 237–243.
- (5) Hermet, P.; Lois-Sierra, S.; Bantignies, J. L.; Rols, S.; Sauvajol, J. L.; Serein-Spirau, F.; Lère-Porte, J. P.; Moreau, J. J. E. Lattice Dynamics of Oligo(phenylenethienylene)s: A Far-Infrared and Inelastic Neutron Scattering Study. *J. Phys. Chem. B* **2009**, *113*, 4197–4202.
- (6) Baderschneider, S.; Scherf, U.; Köhler, J.; Hildner, R. Influence of the Conjugation Length on the Optical Spectra of Single Ladder-Type (p-Phenylene) Dimers and Polymers. *J. Phys. Chem. A* **2016**, *120*, 233–240.
- (7) Lang, E.; Hildner, R.; Engelke, H.; Osswald, P.; Würthner, F.; Köhler, J. Comparison of the Photophysical Parameters for Three Perylene Bisimide Derivatives by Single-Molecule Spectroscopy. *ChemPhysChem* **2007**, *8*, 1487–1496.
- (8) Feist, F. a.; Tommaseo, G.; Basché, T. Observation of Very Narrow Linewidths in the Fluorescence Excitation Spectra of Single Conjugated Polymer Chains at 1.2 K. *Phys. Rev. Lett.* **2007**, *98*, 1–4.
- (9) Spano, F. C.; Clark, J.; Silva, C.; Friend, R. H. Determining Exciton Coherence from the Photoluminescence Spectral Line Shape in poly(3-Hexylthiophene) Thin Films. *J. Chem. Phys.* **2009**, *130*, 1–16.
- (10) Spano, F. C. Modeling Disorder in Polymer Aggregates: The Optical Spectroscopy of Regioregular poly(3-Hexylthiophene) Thin Films. *J. Chem. Phys.* **2005**, *122*.
- (11) Wykes, M.; Parambil, R.; Beljonne, D.; Gierschner, J. Vibronic Coupling in Molecular Crystals: A Franck-Condon Herzberg-Teller Model of H-Aggregate Fluorescence Based on Quantum Chemical Cluster Calculations. *J. Chem. Phys.* **2015**, *143*.

- (12) Scholes, G. D. L Scholes, G. D. L Long-Range Resonance Energy Transfer in Molecular Systems. *Annu. Rev. Phys. Chem.* **2003**, *54* (1), 57–87.
- (13) Clark, J.; Chang, J. F.; Spano, F. C.; Friend, R. H.; Silva, C. Determining Exciton Bandwidth and Film Microstructure in Polythiophene Films Using Linear Absorption Spectroscopy. *Appl. Phys. Lett.* **2009**, *94*, 2007–2010.

Danksagung

Am Ende dieser Arbeit möchte ich mich bei allen bedanken, die zum Entstehen und Gelingen dieser Arbeit beigetragen und mich die letzten Jahre unterstützt haben.

Mein größter Dank gilt meinem “Doktorvater” PD Dr. Richard Hildner für die Möglichkeit, dieses spannende Thema bearbeiten zu können, für die sowohl menschlich als auch fachlich fantastische Betreuung und dafür, dass er immer ein offenes Ohr für Anliegen aller Art hatte.

Prof. Dr. Jürgen Köhler möchte ich für das gute Arbeitsklima am Lehrstuhl und die fachliche Unterstützung danken. Prof. Dr. Anna Köhler danke ich für die fachlichen Diskussionen über konjugierte Polymere und die Übernahme der Zweitkorrektur, wofür ich mich ebenfalls bei Prof. Dr. Markus Lippitz bedanken möchte. Außerdem danke ich Prof. Dr. Stephan Kümmel für die Unterstützung von theoretischer Seite und als Mentor.

Allen Professoren des Graduiertenkollegs 1640 möchte ich dafür danken, das Grako mit viel Einsatz überhaupt erst nach Bayreuth geholt zu haben. Der interdisziplinäre Austausch, aber auch die Softskill-Seminare sowie die Möglichkeit internationale Konferenzen und Workshops zu besuchen, haben meine Promotion wahrlich bereichert.

Many thanks go to Prof. Dr. Thiago B. de Queiroz and Dr. Lena Simine: Thank you for the patient replies to the questions of an experimental physicist and of course for the fruitful collaboration and your ingenious simulations!

Sebastian Baderschneider möchte ich für die Einführung in die Einzelmolekül-Spektroskopie und für das umfangreiche Auswertungsprogramm danken, dass er mir ebenfalls zur Verfügung gestellt hat. Inga und Sebastian sei natürlich noch für die entspannte Büroatmosphäre gedankt.

Sebastian Pickel, Stephan Wiesneth und Patrick Beer: Danke, dass Ihr Euch darauf eingelassen habt, Euch von mir betreuen zu lassen. Die Zusammenarbeit im Labor und das gemeinsame Grübeln über Sinn und Unsinn der Daten hat wirklich Spaß gemacht.

Ein großer Dank für Bereitstellung der einzigartigen Proben an die Arbeitsgruppen von Prof. Dr. Mukundan Thelakkat und Prof. Dr. Michael Sommer. Insbesondere möchte ich Paul Reichstein, Dr. Daniel Schiefer und Johannes Welz für die Unterstützung und Beratung in chemischen Fragen danken. Für die angenehme und spannende Zusammenarbeit an den Veröffentlichungen ein großes Danke an Dr. Sajedah Motamen, Fanuel Keheze, Dr. Fabian Panzer und Konstantin Schötz.

Ohne die Technikabteilung am Lehrstuhl ginge wohl gar nichts mehr: Stefan Schlicht und Werner Reichstein kann man nicht oft genug für die schnelle und unkomplizierte Hilfe danken, die leider öfter nötig war als erhofft (Stichwort Kryo).

Ein großes Dankeschön auch an Frank Neumann und das gesamte Team der Mechanik-Werkstatt des NW2. Eure schnelle Hilfe in Notfällen war Gold wert! Für die reibungslose Heliumversorgung natürlich auch ein Dankeschön an Michael Heimler, Harald Heindl und das Team der Heliumwerkstatt.

Vielen Dank auch an das Sekretariat, allen voran Evelyn Hülsmann und Claudia Geier, die in verwaltungstechnischen Fragen immer weiterhelfen konnten und den Lehrstuhl am Laufen halten.

Als PC-Beauftragter auch ein großes Dankeschön an Rainer Noack und seine “virtualisierten” Kenntnisse und vor allem dafür, dass er uns auch außerplanmäßig stets geholfen hat! Auch ein Dankeschön an Peter Hagen, der die IT-Abteilung nun übernommen hat.

Dem ganzen Haufen des (ehemaligen) EPIV: Ich habe die Zeit am Lehrstuhl mit Euch sehr genossen und hoffe, Ihr seid nicht böse, dass ich Euch nicht einzeln aufzähle. Es war eine sehr schöne Zeit, vor allem die Kaffeepausen, inkl. Strafkuchen, blödem Gelaber aber auch fachlichen Diskussionen!

Was wäre das Leben ohne gute Freunde. Ein fettes Dankeschön an alle für die geile Zeit während des Studiums und der Promotion, ob in der Fachschaft, auf dem Boltzplatz oder anderswo.

Ganz herzlich möchte ich meinen Eltern und meiner Familie danken, die mir ein sorgenfreies Studium ermöglicht und mir stets vollen Rückhalt gegeben haben. Ganz besonders möchte ich Jessica danken, welche mein Leben die letzten Jahre auf vielfältige Weise bereichert und mich in allen Belangen unterstützt hat. Danke.

Eidesstattliche Versicherung

Hiermit versichere ich an Eides statt, dass ich die vorliegende Arbeit selbstständig verfasst und keine anderen als die von mir angegebenen Quellen und Hilfsmittel verwendet habe.

Zusätzlich erkläre ich hiermit, dass ich keinerlei frühere Promotionsversuche unternommen habe.

Weiterhin erkläre ich, dass ich keine Hilfe von gewerblichen Promotionsberatern bzw. -vermittlern oder ähnlichen Dienstleistern weder bisher in Anspruch genommen habe, noch künftig in Anspruch nehmen werde.

Außerdem erkläre ich mich einverstanden, dass die elektronische Fassung meiner Dissertation unter Wahrung meiner Urheberrechte und des Datenschutzes einer gesonderten Prüfung unterzogen werden kann.

Des Weiteren erkläre ich mich einverstanden, dass bei Verdacht wissenschaftlichen Fehlverhaltens Ermittlungen durch universitätsinterne Organe der wissenschaftlichen Selbstkontrolle stattfinden können.

Bayreuth, den 05.02.2018